2013-03-18

Resorcinarene-Based Cavitands: From Structural Design and Synthesis to Separations Applications

Na Li
Brigham Young University - Provo

Resorcinarene-Based Cavitands: From Structural Design and Synthesis to Separations Applications

Na Li

A dissertation submitted to the faculty of
Brigham Young University
in partial fulfillment of the requirements for the degree of

Doctor of Philosophy

John D. Lamb, Chair
Roger G. Harrison
Matthew R. Linford
David V. Dearden
Richard K. Watt

Department of Chemistry and Biochemistry

Brigham Young University

March 2013

ABSTRACT

Resorcinarene-Based Cavitands: From Structural Design and Synthesis to Separations Applications

Na Li
Department of Chemistry and Biochemistry, BYU
Doctor of Philosophy

Resorcinarenes are cyclic tetramers that are synthesized by the condensation of resorcinol and various aldehydes. The upper and lower rims can be modified with substituents that provide specific selectivity and other chemical features. In this work, resorcinarene-based macrocyclic ligands with specific selectivities have been designed, synthesized and applied to chiral amine discrimination and transition metal ion separations.

These resorcinarenes fall into two categories. In the first type, the upper rims of resorcinarenes were modified with amino acid groups, including chiral alanine groups. The lower rims were modified with $–CH_3$, or $–C_{11}H_{23}$ groups. The structures were studied by nuclear magnetic resonance (NMR), mass spectrometry (MS), dynamic light scattering (DLS), and sustained *off*-resonance irradiation collision induced dissociation (SORI-CID) techniques in Fourier transform ion cyclotron resonance mass spectrometry (FTICR-MS). The binding strength between the resorcinarenes with amines was studied by ^1H NMR titration. Among these new resorcinarenes, the chiral alanine undecyl resorcinarenes acid (AUA) showed chiral discrimination among chiral secondary amines. The AUA ligands were adsorbed onto 55% cross-linked styrene-divinylbenzene resin and used as cation-exchangers in ion chromatography (IC) for transition metal ion separations. The AUA IC column showed selectivity for Cu^{2+} when no chelating eluent was used in the eluent, a selectivity which was not observed with a commercial column containing standard cation-exchangers. Six metal ions (Cu^{2+}, Mn^{2+}, Co^{2+}, Ni^{2+}, Cd^{2+}, and Zn^{2+}) were separated on the AUA column within a reasonable time with a simple oxalic acid gradient eluent. The second type of resorcinarene-based ligand, cyclenbowl, contains four cyclen units on the upper rim and four $–C_{11}H_{23}$ chains on the lower rim. The column packed with cyclenbowl adsorbed onto polystyrene showed selectivity for Cu^{2+} over five other transition metal ions including Mn^{2+}, Co^{2+}, Ni^{2+}, Cd^{2+}, and Zn^{2+} ions. The preconcentration of Cu^{2+} at the parts per billion level from a high concentration matrix of Mn^{2+}, Co^{2+}, Ni^{2+}, Cd^{2+}, and Zn^{2+} ions was achieved using HNO_3 eluent. Recovery of Cu^{2+} was greater than 98%. Furthermore, the other five transition metal ions were well separated on the cyclenbowl column with an oxalic acid eluent gradient.

Keywords: resorcinarene, chiral recognition, ion chromatography, selectivity, transition metal ions, preconcentration, macrocyclic ligands, separations

ACKNOWLEDGEMENTS

I have been supported and inspired by my family, friends, supervisor Dr. John D. Lamb, and my committee members during my Ph. D. study. When looking back the way that I have passed, I have enormous appreciation for those individuals and Brigham Young University. The great educational opportunity that BYU offered me not only taught me knowledge, but also taught me love and faith. The study and research experience in a different culture not only increased my professional knowledge, but also opened my eyes, inspired my thoughts and made me reflect on the values that I believed before. This unique experience at BYU will benefit my whole life.

While working with Dr. Lamb, I have appreciated his mentorship and the research opportunity that he provided me. His keen insights always enlightened me. Every experimental result and every paper that I have published were finished under his zealous help and instruction. I would like to thank Dr. Roger Harrison for the valuable discussions in my synthesis and NMR work. He was always patient to me and willing to give me suggestions both in work and life. I also would like to express my gratitude to my Ph.D. committee members, Dr. David V. Dearden, Dr. Richard K. Watt, and Dr. Matthew R. Linford for their good advice and guidance through my research. Their advice in my yearly progress report always gave me inspiration in my research.

Finally, I would like to give my special thanks to my dear sister Qing who accompanied me through all the ups and downs in my life. I dedicate this book to my mother Aiqin Gao and father Senlin Li for their support, sacrifice, understanding, and love throughout my life.

TABLE OF CONTENTS

ABSTRACT ii

ACKNOWLEDGEMENTS iii

TABLE OF CONTENTS iv

Chapter 1 Ion Chromatography and Membrane Separations Using Macrocyclic Ligands 1

1. Introduction 2

2. Selective binding by macrocyclic ligands 3

2.1 Structures of macrocycles used in ion chromatography and membrane separations 4

2.2 Macrocyclic ligand characteristics which influence selectivity 6

2.2.1 Size-fit and conformational changes 6

2.2.2 Donor type, number, and position 11

2.2.3 Substitution effects on complexation selectivity 14

2.3 Ion effect on macrocycle selectivity 15

2.4 Solvent 16

3. Ion chromatography (IC) 19

3.1 Principles of suppressed IC 19

3.2 New perspectives of IC 23

4. Application of macrocycles to ion chromatography 25

4.1 Macrocyclic ligands in the stationary phase 26

4.1.1 Crown ethers 26

4.1.2 Crown ethers in the mobile phase 32

4.1.3 Crown ethers in detection systems 36

4.2 Cryptands in ion chromatography 36

4.3 Calixarenes in ion chromatography 43

4.4 Cyclodextrins 45

5. Liquid membranes 49

5.1 Facilitated transport mechanism and membrane types 49

5.2 Macrocyclic carriers in liquid membranes 52

6. Conclusions 64

Chapter 2 Application of Resorcinarene Derivatives in Chemical Separations 77

1. Introduction 77

2. High Performance Liquid Chromatography (HPLC) 82

3. Gas Chromatography (GC) 93

4. Electrokinetic Chromatography (EKC) and Capillary Electrophoresis (CE) 99

5. Membrane separations 114

6. Ion chromatography (IC) 119

Chapter 3 Resorcinarene-based Cavitands with Chiral Amino Acid Substituents for Chiral Amine Recognition 127

1. Introduction 128

2. Experimental 130

2.1 General methods 130

2.2 Synthesis 131

2.3 NMR and 1H NMR titrations 137

2.4 Mass spectrometry 137

2.5 Dynamic Light Scattering 137

3. Results and Discussion 138

3.1 NMR Characterization 140

3.2 Particle Size Analysis 144

3.3 Mass Spectrometry Characterization 146

3.4 Interaction with amines 153

3.4.1 The effect of solvent 159

3.4.2 The effect of guest size 161

3.4.3 The effect of substituent group type, position, and number 162

3.4.4 Chirality 167

4. Conclusions 171

Chapter 4 Cation Separation and Preconcentration Using Columns Containing Cyclen and Cyclen-Resorcinarene Derivatives 177

1. Introduction 178

2. Materials and methods 181

2.1 Reagents 181

2.2 Column preparation 181

2.3 Instrumentation 182

3. Results and discussion 182

3.1 Effect of HNO_3 concentration 184

3.2 Preconcentration of Cu^{2+} with cyclenbowl column 185

3.3 Transition metal cation separations: Effect of chelating ligand oxalic acid in the eluent 187

3.4 Oxalic acid gradient separation of transition metal ions 191

3.5 Separation of transition metal ions on N-cyclen column 192

3.6 Unsubstituted resin column 195

3.7 Effect of chelating ligand iminodiacetic acid (IDA) in the eluent 196

3.8 Effect of post column reagent composition 197

4. Conclusions 198

Chapter 5 Transition Metal Cation Separations with a Resorcinarene-based Amino Acid

Stationary Phase 203

1. Introduction 204

2. Experimental 207

2.1 Reagents 207

2.2 The pKa value of the AUA ligand 208

2.3 Synthesis and column preparation 208

2.4 Instrumentation 209

3. Results and discussion 209

3.1 Separation of transition metal ions with the AUA column 210

3.1.1 Effect of HNO_3 concentration 210

3.1.2 Effect of chelating ligand – oxalic acid in the eluent 213

3.1.3 Effect of chelating ligand – succinic acid in the eluent 216

3.1.4 Effect of chelating ligand – citric acid in the eluent 217

3.1.5 Effect of chelating ligand – dipicolinic acid (PDCA) in the eluent 217

3.2 Separation of transition metal ions with the IonPac CS12 column 219

3.2.1 Effect of HNO_3 concentration with Ionpac CS12 column 219

3.2.2 Effect of chelating ligand – oxalic acid in the eluent 221

3.2.3 Effect of chelating ligand – dipicolinic acid (PDCA) in the eluent 221

4. Conclusions 224

Chapter 6 Summary and Perspective 229

Appendix 232

Chapter 1 Ion Chromatography and Membrane Separations Using Macrocyclic Ligands

Abstract[1]

The selectivity of macrocyclic ligand hosts in binding ionic and neutral guests was recognized early and has been applied to separations science in a number of ways. Prominent among these applications are ion chromatography and liquid membranes. This chapter summarizes the various ways that macrocyclic ligands have been incorporated into these two separations techniques. It begins with a description of the intrinsic selectivities of the macrocyclic hosts used in these applications to date. The next section describes the basic elements of ion chromatography and the chemical features of standard ion chromatographic separations. It then proceeds to describe how macrocycles such as crown ethers, cryptands, resorcinarenes, and others have been incorporated into both the mobile and stationary phases of ion chromatographic systems to effect novel separations of both cations and anions. The development of capacity gradient chromatography of anions, unique to macrocycle-based ion chromatography, is described. The application to both analytical separations and preconcentration/matrix elimination is also included. The next section introduces the various types of liquid membranes, including bulk liquid membranes, solid supported liquid membranes, emulsion liquid membranes and polymer inclusion membranes. This section then proceeds to

[1]This chapter has been published.

Lamb, J. D.; Li, N. Supramolecular chemistry: from molecules to nanomaterials. Edited by Philip A. Gale and Jonathan W. Steed. **2012,** 563-587

describe the various studies done to characterize the use of macrocyclic ligands as selective carriers of cations, anions and neutral species across these membranes for separations purposes.

1. Introduction

One of the most intriguing characteristics of macrocyclic ligands is their binding selectivity for specific guest species. From the inception of studies of synthetic macrocycles in the late 1960s and early 1970s, researchers from various chemical fields were investigating this selectivity and how it might be applied to separations science. Indeed, the 1987 Nobel Prize for chemistry was awarded to Cram, Lehn, and Pedersen for their development and use of molecules with structure-specific interactions of high selectivity.[1] Investigation into macrocycle selectivity and its applications has gained increasing momentum during the past 40 years; and from 2004 to 2009, more than 800 papers relating to macrocyclic chemistry have been published each year.[2] Separations and other practical analytical chemistry applications for these compounds include liquid membrane separations, chromatography of various types, capillary electrophoresis (CE), luminescent sensors, and ion selective electrodes,[3] among others. And beyond these, other applications have been made in macrocycle–metal complexes, such as magnetic resonance imaging (MRI) contrast agent sensors[4] and catalysts.[5]

This chapter focuses specifically on the application of macrocyclic ligands to ion chromatography (IC) and liquid membrane separations. It begins with a brief description of the intrinsic selectivities of the macrocyclic hosts used to date in these applications. Since the majority of applications involve the separation of metal cations, the discussion focuses primarily

on these species, with some attention being given to the separation of anions and neutral species. The chapter then proceeds to describe the basic elements and chemical features of IC and how macrocycles such as crown ethers, cryptands, resorcinarenes, and cyclodextrins (CDs) have been incorporated into both the mobile and stationary phases of IC to effect novel separations of both cations and anions. The development of capacity gradient chromatography of anions, unique to macrocycle-based IC, is described. The application to both analytical separations and preconcentration/ matrix elimination is included. The final section introduces the various types of liquid membranes, including bulk liquid membranes (BLMs), solid supported liquid membranes (SLMs), emulsion liquid membranes (ELMs), and polymer inclusion membranes (PLMs). It then proceeds to describe the various studies done to characterize the use of macrocyclic ligands as selective carriers of cations, anions, and neutral species across these membranes for separations purposes. The chapter does not endeavor to branch out into the expansive field of biomembranes and biomembrane mimics.

2. Selective binding by macrocyclic ligands

The separations chemist relies on the selectivity of chemical systems to achieve the desired separations outcome. As chemists search the literature to find selective molecules for such applications among known macrocyclic structures, it is important that they be attuned to the structural and system parameters that can affect this selectivity, especially if the macrocycle must be modified structurally to meet the needs of the desired separation. The selectivity of macrocyclic ligands is determined by various characteristics of the host, guest, and reaction

medium. In this section, we discuss parameters that affect selectivity in some detail inasmuch as this selectivity lies at the heart of separations that may be achieved. We begin with a discussion of host characteristics.

2.1 Structures of macrocycles used in ion chromatography and membrane separations

Macrocyclic ligands used in IC and liquid membrane separations can be divided into four classes according to ligand heteroatom: O-donor macrocycles, N-donor macrocycles, S-donor macrocycles, and mixed donor macrocycles. Figure 1.1 shows the structures of the representative members of these groups. Typically, the O-donor macrocycles are crown ethers and their substituted analogs, as well as CDs. The typical N-donor macrocycles are, in increasing ring size and number of nitrogen atoms: tacn (L_1), cyclen (L_2), and cyclam (L_3) and their analogs. The S-donor macrocycles are typically sulfur-substituted crown ethers. The mixed donor macrocycles include those with N/S, S/O, N/O, and N/S/O combinations. Calixarenes and resorcinarenes are most often O-donors, but may contain various functional groups and thus be classified here as mixed donor macrocycles. The macrocycles most widely used in IC and liquid membrane separations have been the crown ethers, nitrogen-substituted crown ethers, cyclen, cyclam, cryptands, calixarenes, resorcinarenes, and CDs.

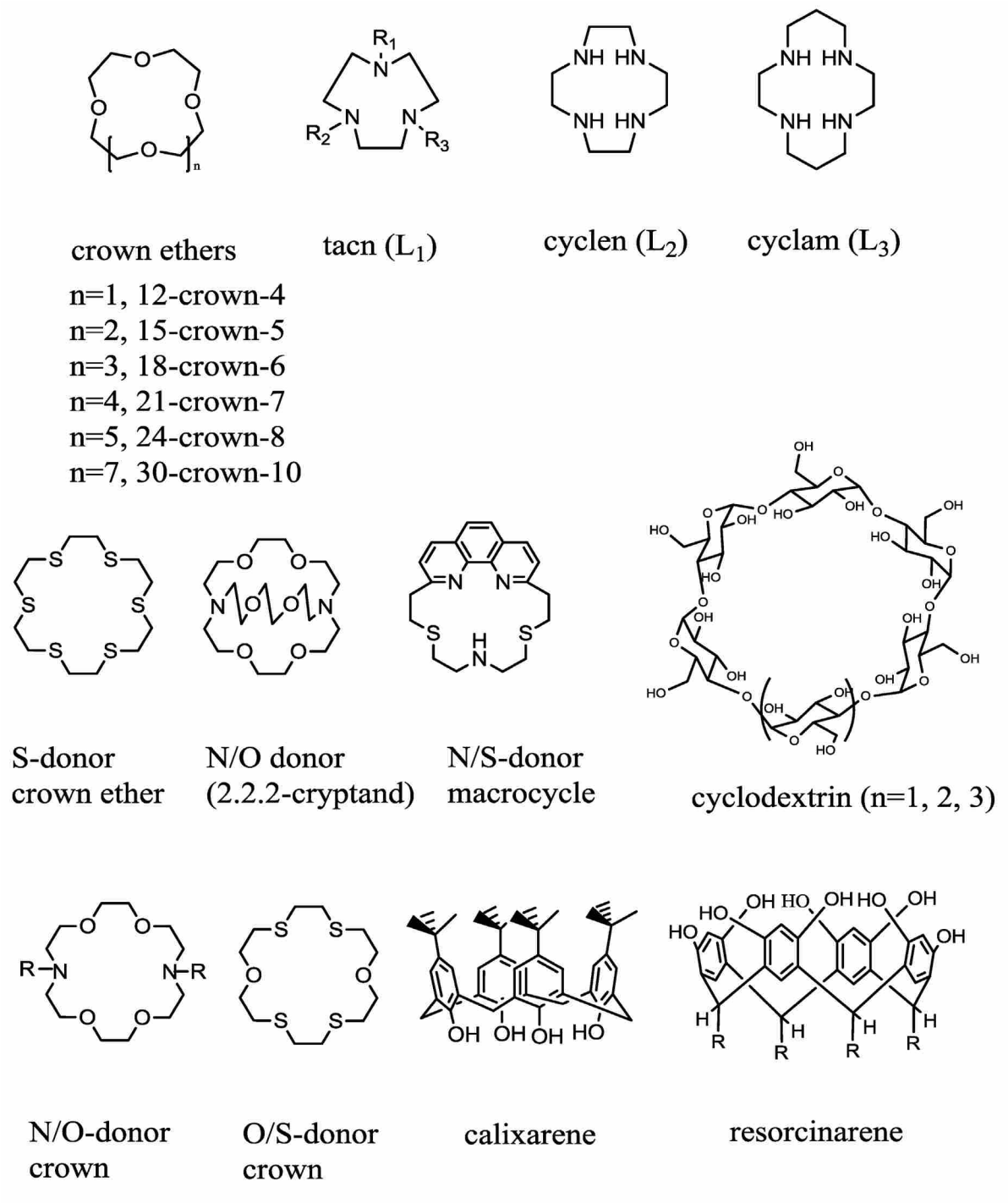

Figure 1.1 Basic structures of macrocyclic ligands used in IC and liquid membrane separations.

2.2 Macrocyclic ligand characteristics which influence selectivity

2.2.1 Size-fit and conformational changes

It is important for the designer of separations systems, based on macrocycle selectivity, to be familiar with the ligand design features that influence that selectivity. Macrocyclic hosts typically bind guests by sequestering them in the host cavity. For example, the binding of alkali and alkaline earth metal ions to crown ethers involves a guest–ion interaction with the crown cavity, and is considered to be electrostatic in nature. It follows, therefore, that one important contributor to selectivity is the relative sizes of guest ion and host cavity, since this influences the distances and orientation between the ligand dipoles and ion charge. In general, this kind of host–guest interaction has been likened to that of a "key" and a "lock";[6] and in the particular case of metal cations and crown ethers, when the ionic radius of the metal matches the cavity size of the crown ether, this particular contribution to complex stability is maximized. Experimental results not only confirmed this point early in macrocyclic chemistry research but also made it clear that other contributions could be equally important, as is described below. For example, Lamb *et al*.[7] summarized the binding stability of 18-crown-6 with alkali and alkaline earth metal ions in water. K^+ and Ba^{2+} form the most stable metal ion complexes in their respective groups, and this can be explained in part because their ionic radii closely match the cavity size of 18-crown-6.[7] From the X-ray crystallographic data, the cavity radius of 18-crown-6 is determined to be between 1.34 and 1.43 Å. The sizes of K^+ and Ba^{2+} closely match the size of this ligand cavity (Table 1.1).

Table 1.1 Radii of mono- and divalent cations and their stability constants with 18-crown-6 in methanol at 25 ^{o}C[8]

Cation	Radius (Å)[a]	log *K*	Cation	Radius (Å)[a]	log *K*
Li^{+}	0.76	b	Be^{2+}		b
Na^{+}	1.02	4.36±0.02	Mg^{2+}	0.72	b
K^{+}	1.38	6.06±0.03	Ca^{2+}	1.00	3.86±0.02
Rb^{+}	1.52	5.32±0.11	Sr^{2+}	1.18	>5.5
Cs^{+}	1.67	4.79±0.05	Ba^{2+}	1.49	7.04±0.08

[a] ionic radii of metals when coordination number is 6. [b] No measurable heat.

This size-fit selectivity among metal cations is also applicable to cryptands. Zhang *et al*.[9] summarized size–match relationship between cryptands and alkali and alkaline metal ions. The smaller cryptand [2.1.1], with a cavity size of 0.8 Å, formed the most stable complex with Li^{+} (ionic radius: 0.76 Å) among the alkali metal cations. Cryptand [2.2.1], with a cavity size 1.1 Å, matches the size of Na^{+} (ionic radius 1.02 Å), and showed the highest selectivity for Na^{+}. Large cryptands like [3.3.2] and [3.3.3] form more stable complexes with larger cations such as Rb^{+} and Cs^{+}. Figure 1.2 shows the dramatic correspondence between cation selectivity and ligand cavity size among the alkali metal cations for a sequence of cryptands.[7, 10] Although this size-fit principle is only one of the several factors that come into play, it remains a significant contributor to all host–guest interactions to the degree that it influences the energy associated with the proximity of attracting charges (sometimes in the form of dipoles or H-bonds) between species.

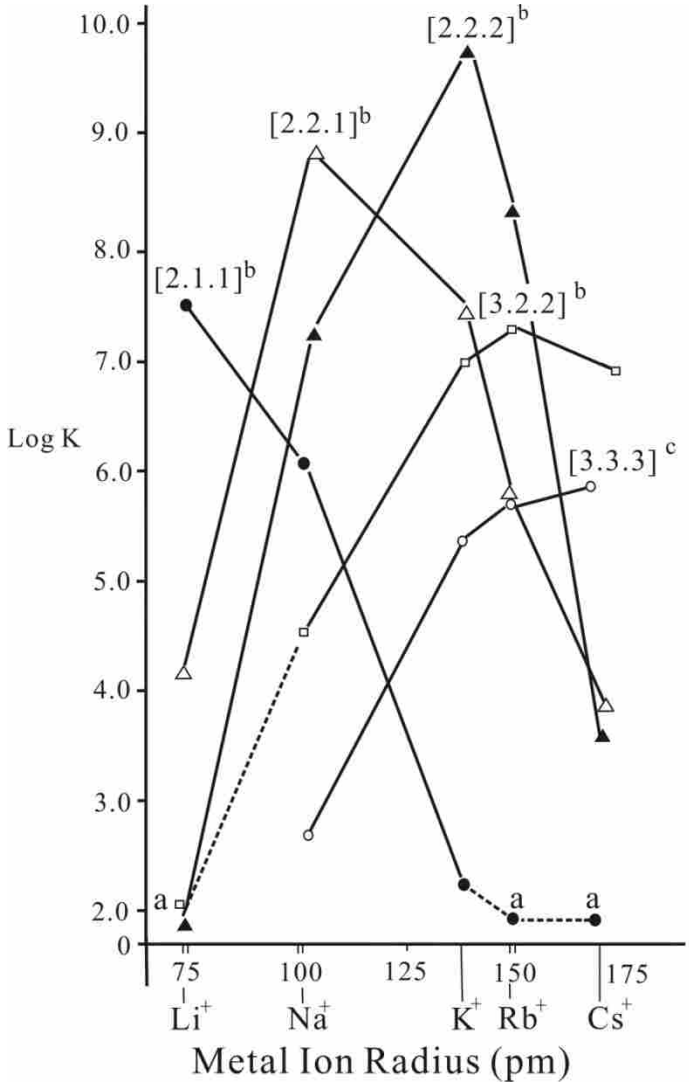

Figure 1.2 Selectivity of cryptands among alkali metal cations (a-value reported < 2.0; b- in 95% MeOH; c- in methanol).[7]

As macrocyclic chemistry developed, the influence of ligand flexibility and the associated conformational energies was appreciated. For example, large crown ethers like 30-crown-10 can form complexes with metals in a variety of conformations, and in general, the greater the flexibility of the ligand, the less appropriate it becomes to consider the cavity as preorganized to accommodate the host. X-ray diffraction techniques have vividly illustrated this

principle, as shown in Figure 1.3, in which the 30-crown-10 molecule wraps itself around the K^+ ion.[11]

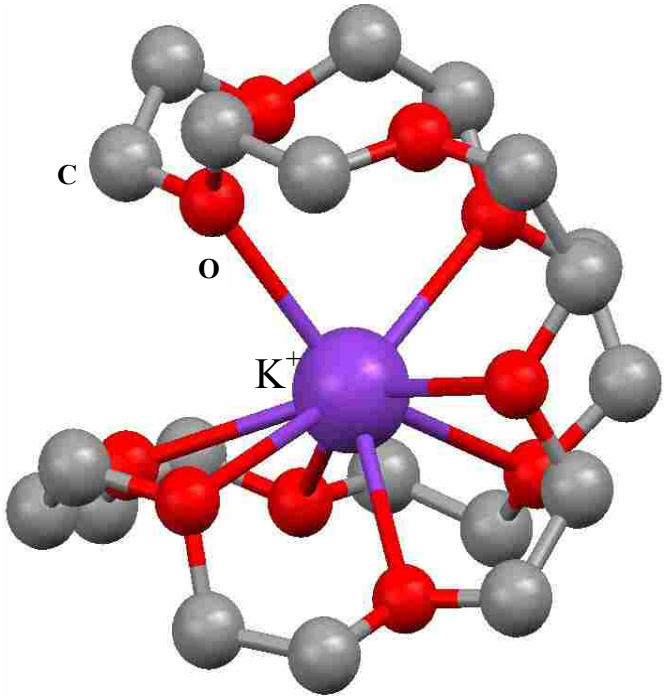

Figure 1.3 Crystal structure of KI(dibenzo-30-crown-10).[11]

It is also possible for stoichiometries other than 1:1 to form between host and guest, so that even rigid hosts may bind guests in unusual arrangements. For example, the smallest alkali metal ion, Li^+, with an ionic radius of 0.76 Å, is much smaller than the cavity of the smallest crown ether, 12-crown-4 (1.20–1.50 Å). Yet this ligand can form a sandwich-like complex with two 12-crown-4 molecules.[12] When speaking of ligand selectivity, it is important to keep in mind the possibility of such alternative stoichiometries.

In many cases, the host does not entirely satisfy the coordination/solvation needs of the guest, and this feature can be exploited in making separations. For instance, in [K(18-crown-6)NO_3], K^+ is coordinated by six oxygen atoms of 18-crown-6 in an equatorial-like arrangement,

and the oxygen atoms of a nitrate ion satisfy the need for charge balance above the plane of the complex in the crystal. In this case, K^+ actually lifts slightly above the crown ether plane to provide a more accessible surface for nitrate.[6]

Often a particular conformation of a macrocyclic ligand is more selective and therefore more desirable for separations applications. If this conformation can be selectively stabilized over less desirable conformations, the ligand is rendered much more effective. A good example comes from the work of Ungaro and coworkers, who introduced crown ether units to calixarene platforms in order to control and regulate the selectivity of these calixcrowns to alkali metals.[13] The selectivity of these calixcrowns not only depends on the number and nature of the donor atoms but also on the conformations of the calixcrown ligand. Take calix[4]arene as an example (Figure 1.1). The four repeating aromatic units in the ring are flexible: they can flop sideways and vertically to display several conformations such as cone, partial cone, 1,2-alternate, and 1,3-alternate, as shown in Figure 1.4(a). In 1,3-dialkoxycalix[4]arene-crown-6, which Ungaro's group synthesized, an 18-crown-6 unit was bridged to the 1,3-phenolic hydroxyl groups (Figure 1.4b). By introducing bulkier alkyl substituents to the upper rim of the ligand on the 2,4-phenolic hydroxyl groups, such as *i*-propyl (**3**), *n*-propyl (**5**), and *n*-octyl (**4**), the 1,3-alternate conformation (Figure 1.4c) is significantly stabilized; and this modification makes the ligand much more selective for separations applications. This conformation showed great selectivity toward Cs^+ versus other metal cations. The selectivity coefficient of Cs^+/Na^+ was higher than 33,000 with *n*-octyl substituents, which made it an excellent candidate for removing the short-lived ^{137}Cs from nuclear waste. The high selectivity toward Cs^+ is enhanced by the interaction

between the metal cation and the π-electrons of the raised aromatic rings.

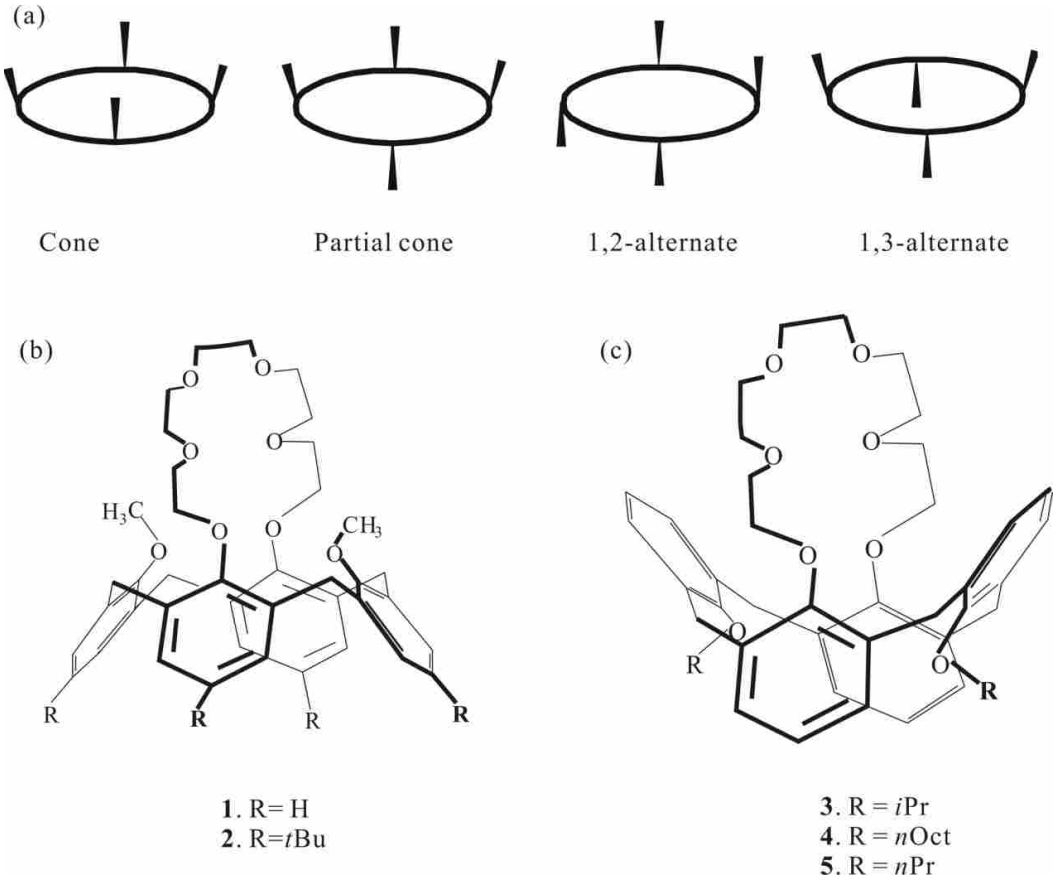

Figure 1.4 (a) simplified possible conformations of calix[4]arene; (b) structure of calixcrown, cone conformation; (c) 1,3-alternate enhanced calixcrown.[13]

2.2.2 Donor type, number, and position

In addition to size and ligand conformation, donor type and number are also important factors that affect the binding selectivity of macrocycles. As an example, Solov'ev *et al*.[14] reported that with an increasing number of nitrogen atoms on the 18-crown-6 ring, the binding stability constants for the 1 : 1 complexes with K+ and Na+ decrease in the following order: 18-crown-6 > monoaza-18-crown-6 > 1,10-diaza-18-crown-6. Thaler *et al*.[15] compared the stability

constants of Ag+ with several crown ethers to corresponding monoaza- and diaza- analogs in CH_3OH and propylene carbonate (PC) solutions. When oxygen atoms were replaced by nitrogen atoms, the cavity sizes changed only slightly since the van der Waals radii of oxygen and nitrogen are quite similar. For the four classes of crown ethers studied (12-crown-4, 15-crown-5, 18-crown-6, and 21-crown-7), they reported that the replacement of oxygen atoms by nitrogen atoms caused the stability constants of the Ag^+ complex to increase in the following order: crown ether < monoaza-crown < diaza-crown. Furthermore, Kodama *et al*.[16] reported that when the six oxygen atoms of 18-crown-6 were totally replaced by nitrogen, the stability constants of the resulting macrocycle with transition metal ions are significantly higher than with alkali and alkaline earth metal ions. For instance, the stability constant of hexaaza-18-crown-6 with Ca^{2+} is 2.5 ± 0.2, while that with Co^{2+} is 18.9 ± 0.2.

The relationship of ligand selectivity to donor atom type can be understood from hard–soft acid–base theory. O-donor macrocycles can bind alkali, alkaline, and rare earth metals predominantly by electrostatic forces. By contrast, N-donor macrocycles can bind softer Lewis acids like transition metals, and in this particular case, the interactions are predominantly coordinate in nature. Thia-substituted ligands are much softer than O- and N-donor macrocycles and can selectively bind softer Lewis acids like Ag^+ and Hg^{2+}.

In addition to donor atom type and number, the position of the donor atoms has a noticeable effect on the stability constants with metal cations. Solov'ev *et al*.[14] studied the stability constants of K^+ with two isomers of diaza-18-crown-6 in which nitrogen atoms occupied different positions. The structures of the two ligands are shown in Figure 1.5 and the

stability constants and thermodynamic parameters are shown in Table 1.2. Clearly, not only the number of heteroatoms but also their positions in the ring, has a significant effect on ligand selectivity.

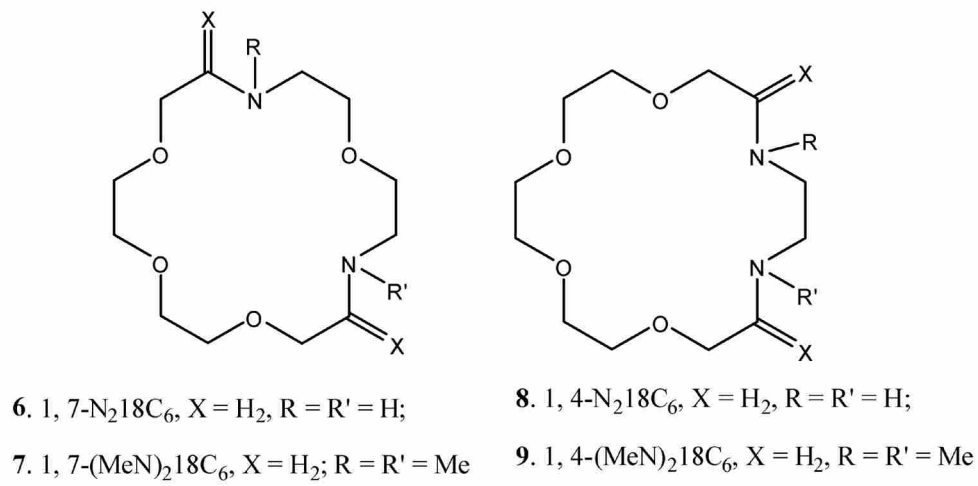

6. 1, 7-$N_2$18C_6, X = H_2, R = R' = H;

7. 1, 7-$(MeN)_2$18C_6, X = H_2; R = R' = Me

8. 1, 4-$N_2$18C_6, X = H_2, R = R' = H;

9. 1, 4-$(MeN)_2$18C_6, X = H_2, R = R' = Me

Figure 1.5 Structures of macrocycle isomers with nitrogen donors at different positions.[14]

Table 1.2 Stability constant (log β) and thermodynamic data (kJ/mol) for diazacrown-K^+ complexes in methanol at 298 K.[14] (Structures from Figure 1.5)

	M:L	Log β	-ΔG	-ΔH	+$T\Delta S$
1, 7-$N_2$18C_6	1:1	4.17(0.42)	23.8(2.4)	1.4(0.1)	22.4(2.4)
	1:2	5.97(0.44)	34.1(2.5)	6.1(0.6)	28.0(2.6)
1, 4- $N_2$18C_6	1:1	2.6(0.4)	14.8(2.3)	13(6)	2(6)
	1:2	5.5(0.2)	31.4(1.1)	11(1)	20(1)
1, 7-$(MeN)_2$18C_6	1:1	4.92(0.58)	28.1(3.3)	28.5(1.8)	-0.4(3.8)
	1:2	8.60(0.73)	49.1(4.2)	44.6(1.3)	4.5(4.4)
1, 4-$(MeN)_2$18C_6	1:1	4.71(0.54)	26.9(3.1)	19.8(0.8)	7.1(3.2)
	1:2	8.44(0.54)	48.2(3.1)	37.1(0.2)	11.1(3.1)

2.2.3 Substitution effects on complexation selectivity

Often in separations applications of macrocycles, it is necessary to add substituents to the ligand to adjust its solubility or phase partitioning. In such cases, however, the user must be aware of potential alterations these substituents might make to the very ligand selectivity that is being applied to the separations objective. As an example, Monsef *et al*.[17] studied the stability constants of aza-18-crown-6 and dibenzopyridino-18-crown-6 with three different metal ions, Tl^{+}, Pb^{2+}, and Cd^{2+}, using direct current and differential pulse polarographic techniques (DPP). The stability constants were determined in some binary mixed solutions of dimethylformamide (DMF) and other solvents such as methanol, *n*-propanol, nitromethane, and acetonitrile at 22 °C. In all of the solvent systems they studied, aza-18-crown-6 showed stronger binding than dibenzopyridino-18-crown-6 for 1:1 complexes. Aza-18-crown-6 and dibenzopyridino-18-crown-6 have the same ligand donor atoms and arrangement, but dibenzopyridino-18-crown-6 has two phenyl rings as well as the pyridine ring. These electron-withdrawing benzyl groups reduce the electron-donating character of the oxygen atoms on the 18-crown-6 ring. Furthermore, they reduce the flexibility of the crown ether ring that can weaken the binding with metal ions if this preorganized arrangement does not suit. Finally, the nitrogen atom in the 18-crown-6 ring is part of the pyridine unit, so the electron-donating power of the nitrogen atom is reduced by the resonance inherent in the pyridine ring. Thus, when designing ligands for use in separations, all such factors must be considered as the hydrophilicity of the ligand is adjusted by substitution.

Another example of this principle is illustrated in the work of Shchori and Jagur-Grodzinski *et al*.[7, 18] who studied the effect of substituent groups on the selectivity of dibenzo-

18-crown-6 for Na^+ in DMF. When the electron withdrawing group $-NO_2$ was added to the phenyl ring, the stability constant with Na+ decreased from 2.69 to 1.99. Yet, when the electron-donating group $-NH_2$ was added, the stability constant with Na+ increased from 2.69 to 2.76. In addition, the positions of substitutions can also have a noticeable effect on the selectivity of host–guest association. As an example, Chi *et al*.[19] studied the stability constants of alkali metals with two isomers of diaza-18-crown-6 derivatives. In one isomer, two 2,6- difluorobenzyl groups substituted two protons on two nitrogen atoms on the crown ether ring; in the other isomer, 3,5-difluorobenzyl was the substituent group. For the four alkali metal ions Na^+, K^+, Rb^+, and Cs^+ that they studied, 2,6-difluorobenzyl substituted aza- crown ether showed higher binding stability than the 3,5-difluorobenzyl substituted azacrown.

2.3 Ion effect on macrocycle selectivity

Since the binding of macrocyclic ligands to alkali and alkaline metals is electrostatic in nature, the binding between them has no real stereochemical requirements. Such metal ions can bind to macrocyclic ligands with various coordination numbers and conformations. For example, Li^+ can form a 1:2 sandwich complex with the smallest crown ether, 12-crown-4. Li^+ is coordinated to eight oxygen atoms of the two 12-crown-4 molecules.[12] With the larger 15-crown-5, Li^+ is six-coordinated with five oxygen atoms of 15-crown-5 and one Cl^- from the counter ion in the inner sphere. In this case, Li^+ fits well in the crown ether cavity, and only a slight displacement from the crown ring was observed for this 1:1 complex.[20] For the much larger 18-crown-6, 1:2 complexes have been reported. Watson *et al*.[21] reported that two Li^+ cations can be

encapsulated in the ring, and are coplanar with the six oxygen atoms. Also, 18-crown-6 can dramatically distort to coordinate with two Li^+ ions.[22] Steed[6] has reviewed the coordination chemistry of alkali metal cations with crown ether ligands in detail.

Size fit was described above as one of the primary reasons for the selectivity of macrocyclic ligands among cations. But cations of like size may exhibit significantly different binding constants with metal cations of different charge. For example, Ba^{2+} exhibits stronger binding to 18-crown-6 than singly charged K^+ of very similar size. However, the role of cation charge in selectivity is complex, because charge affects not only the energy of association with the ligand but also the energy that must be expended in the desolvation of the cation, as described below. For example, Ca^{2+} is similar in size to Na^+; yet the experimental results show that 18-crown-6 prefers Na^+ over Ca^{2+}. This selectivity can be manifested in both the enthalpy and the entropy of the complexation reaction as described by Lamb *et al*.[8]

Cation polarizability is also a factor in selectivity. Kodama *et al*.[16] studied the complexation of aza-18-crown-6 with alkali, alkaline earth, and some d-block metals. This ligand showed higher selectivity toward the more polarizable, soft d-block metal ions than the hard, nonpolarizable alkali and alkaline earth metal cations.

2.4 Solvent

Selectivity of the macrocyclic ligand is significantly affected by the reaction medium, specifically the nature of the solvent. The stability constants of alkali metals with 18-crown-6 have been reported in several solvents, such as water, methanol, acetonitrile, benzonitrile, and

propylene carbonate (PC). Table 1.3 lists example stability constants to illustrate the wide range of stabilities that can be achieved.[8, 23–25] The effect on selectivity is thus illustrated in Figure 1.6. Specifically, in all of the solvents shown, the relative binding strengths, which are at the root of selectivity, are often maintained even though the strength of complexation can vary dramatically with solvent. In this case, not only is the order of selectivity maintained but the degree of selectivity of 18-crown-6 for K^+ over other cations in the same group is also largely conserved. The difference in absolute binding strengths can be understood in terms of the smaller ion desolvation energy for the nonaqueous solvents than for water. In this sense, the dielectric constant of the solvent plays an important role. Water has a high dielectric constant compared to many nonaqueous solvents, and this parameter is often a good predictor of the relative energy required to desolvate cations. Moreover, the energy of desolvation of the ligand must be taken into account. This energy is especially high for O-donor and N-donor ligands that can hydrogen bond to water or to other hydrogen-bonding solvents.

Table 1.3 Stability constants of 18-crown-6 with alkali metals in several solvents[8, 23-25]

	H_2O[23]	MeCN[24]	Benzonitrile[25]	PC[24,a]	MeOH[8]
Li^+			4.74±0.02		
Na^+	0.80±0.10	4.75±0.11	4.89±0.09	5.26±0.06	4.36±0.02
K^+	2.03±0.10	5.76±0.13	6.11±0.11	6.12±0.08	6.06+0.03
Rb^+	1.56±0.02	4.89±0.09	5.84±0.08	5.34±0.07	5.32±0.11
Cs^+	0.99±0.07	4.36±0.08		4.50±0.04	4.79±0.05

[a]PC is propylene carbonate.

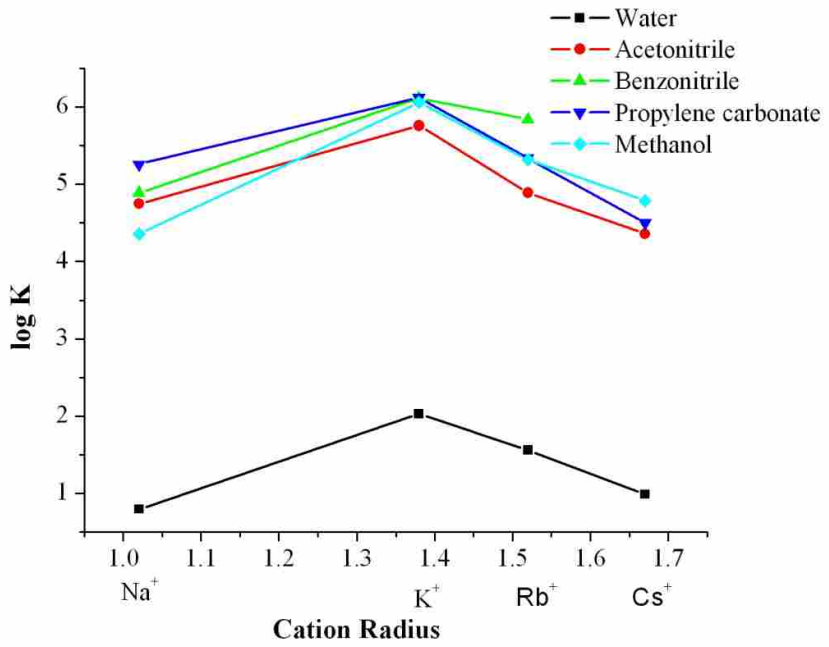

Figure 1.6 Selectivity of 18-crown-6 to alkali metals in different solvents.[8, 23-25]

When multiple factors come into play, it is not always easy to extrapolate selectivity in one solvent to predict that in another. Katsuta *et al*.[26] studied the stability of complexes formed by alkali metals with dibenzo-18-crown-6 (DB18C6) and dibenzo-24-crown-8 (DB24C8) in different solvents. They found that, as would be predicted, the complexes were much less stable in water than in any of the nonaqueous solvents they chose such as methanol, DMF, PC, and acetonitrile. However, the degree of selectivity for K^+ over Na^+ in water and methanol is reduced for DB18C6 and actually reversed for DB24C8 in PC and acetonitrile. They rationalize these results in terms of the transfer activity coefficients of the respective species, alkali metal ions, ligands, and, in particular, the complexes formed. In effect, the solvation of any resulting complex is partly governed by the conformation of the ligand surrounding the metal ion, which in turn affects the degree of association of solvent with the complexed metal ion. This effect is

more pronounced as ligand flexibility increases. The same is true when mixed stoichiometries are present or when the cation is not well sequestered in the ligand cavity. This latter point is underscored in the work of Arnett and Moriarity[27] on the complexation of dicyclohexano-18-crown-6 in various solvents. In strongly solvating solvents, a greater affinity is observed for larger cations. The net result for the separations chemist is that, in general, complex stability is higher in nonaqueous solvents, and because there are so many parameters affecting selectivity, direct measurement is really required when a new solvent system is employed.

3. Ion chromatography (IC)

3.1 Principles of suppressed IC

In the early 1970s, new discoveries led to the development of the analytical method now called "ion chromatography." This name applies specifically to modern high performance liquid chromatographic determination of ionic species, and is distinct from other chromatographic ion separations that are not carried out in high performance mode. While some applications of non-HPLC (high performance liquid chromatography) employing macrocyclic ligands have been studied, this chapter focuses specifically on the analytical method defined narrowly as IC.

A sensitive, universal detector for inorganic cations and anions in chromatography was the principle unsolved problem that delayed the development of IC. Although these ions could be separated efficiently by ion-exchange, sensitive direct detection could not be achieved by any spectrophotometric detector because most common ions do not absorb in the visible or UV ranges.[28] Conductance is a universal property of ions in solution and is directly dependent on

concentration. Yet, while the most direct method to detect inorganic ions would be to use a conductivity detector, the background conductance of the ionic mobile phase (eluent) constituents makes the sensitive detection of inorganic ions difficult. Specifically, the analyst is faced with measuring a very small signal atop a very large background.

In 1975, Small *et al*.[29] published a method that laid the foundation for modern IC. A conventional liquid chromatographic system consists of four parts: a pump that pumps the flowing mobile phase, a sample injector, an ion exchange column, and a detector. The new instrumental setup that Small *et al*. reported contained a second column that was added between the separator column and the detector known as a suppressor. Take anion separation as an example: when the analyte KCl passes through the anion separator column, Cl^- ions exchange with the anion exchange sites on the resin, typically quaternary amines. The mobile phase NaOH then elutes the analyte from this column in the form of NaCl as shown in (Equation 1.1). The newly added suppressor column is a strong cation-exchanger, so when eluent and analyte pass through this column, reactions (1.2) and (1.3) occur. The background conductance of the eluent NaOH is converted to H_2O, which has a much lower conductance than NaOH. In addition, after the suppressor column, the detected signal is the conductance of HCl, which has much higher conductance than NaCl. (Equivalent conductances H^+ 34.96, Na^+ 5.01$mS \cdot m^2 \cdot mol^{-1}$).[30] In this way, not only is the background conductance of eluent reduced but also the detection sensitivity is significantly improved.

$$\text{Resin}^{+}\text{Cl}^{-} + \text{OH}^{-} \rightarrow \text{Resin}^{+}\text{OH}^{-} + \text{Cl}^{-} \quad (1.1)$$

$$\text{Resin}^{-}\text{H}^{+} + \text{NaOH} \rightarrow \text{Resin}^{-}\text{Na}^{+} + \text{H}_2\text{O} \quad (1.2)$$

$$\text{Resin}^{-}\text{H}^{+} + \text{NaCl} \rightarrow \text{Resin}^{-}\text{Na}^{+} + \text{H}^{+} + \text{Cl}^{-} \quad (1.3)$$

Over more than 30 years of development, this suppressor concept has been modified and improved significantly and the previously used packed column suppressors have evolved into membrane-based self-regenerating suppressors. Dionex Corporation markets different suppressors for cation and anion determination based on specific ion-exchange membranes. For the anion suppressor, two cation-exchange membranes divide the unit into three compartments, that is, two regenerant chambers and one eluent chamber. Water in the regenerant channels is electrolyzed when an electrical potential is applied. The resulting H^+ ions in one regenerant chamber pass through the cation-exchange membrane to neutralize the OH^- ions in the eluent, yielding a reaction similar to equation 1.2. The counter ions of the eluent pass through the other cation-exchange membrane into the other regenerant chamber and flow to waste.

In contrast to anion separations, cation separations are typically carried out using sulfonate-based stationary phases for alkali and alkaline earth metal cations, or chelating groups such as iminodiacetate for transition metal ions. In such cases, conductimetric detection can be achieved with a suppressor that contains an anion-exchange membrane to neutralize, in this case, an acidic eluent by the introduction of hydroxide ion.

IC sometimes employs methods of detection other than conductivity. For transition metal cations, UV–vis detection is used after post separator reaction with a chelating agent. Electrochemical detectors such as pulsed amperometric detectors have also been employed,

especially for organic ions. We focus here mainly on conductimetric detection since the vast majority of published work with macrocycles uses this method.[31, 32]

In recent years, it has become clear that it is possible to carry out some aspects of IC without a suppressor. Nonsuppressed and indirect conductimetric detection methods have played a minor role in IC over the past 30 years. The stationary and the mobile phases of nonsuppressed IC are quite different from those with suppressed IC. First, sensitive detection in nonsuppressed IC is achieved by carefully selecting the eluent composition. The mobile phases used are usually aromatic carboxylates[33] such as benzoate and phthalate, which have much lower conductance than the analytes of interest due to their large size and concomitant low conductivity. Second, there is a marked difference in the stationary phases used. Specifically, agglomerated ion-exchange resins are the main type of anion stationary phase for suppressed IC.[34, 35] For anion separation, these resins are comprised of sulfonated polymer cores such as polysterene-divinylbenzene (PS-DVB) coated with a monolayer of substituted latex particles coated on the surface.[36] These latex particles have various compositions and functionalities (usually quaternary amines), which can regulate the separation selectivity. By contrast, the stationary phases made for nonsuppressed IC are based primarily on the approach taken by Fritz's group,[37] which involves the functionalization of polymer beads by reacting them with sulfuric acid or aminating reagents. Third, suppressed IC uses a conductivity detector since it is universal in its response to ions. In nonsuppressed IC, however, while conductivity detectors are sometimes used,[38] other detection methods like spectrophotometric[39] and electrochemical[40] detection are more common. In such cases, indirect detection of an analyte may be achieved when a detected eluent ion is

"missing" as an analyte ion moves through, taking its place and yielding a negative peak.

3.2 New perspectives of IC

As for most current chromatographic techniques, simple, fast, and sensitive separations are the aim of IC. There are three principle areas of research for the improvement of IC methods, including the design of new ion-exchange stationary phases, the development of more effective mobile phases for specific applications, and the development of new detection techniques. With reference to stationary phase design, in a 2002 review Sarzanini[35] described the underlying principles and development strategies of stationary phases used in several IC columns. Shortly after that, Weiss and Jensen[34] summarized the various modern stationary phases used in IC. They also introduced the detailed chemical exchange processes involved in the common stationary phases in anion- and cation-exchange columns. Furthermore, Paull *et al*.[41] have detailed the specific stationary phases designed for cation and anion separations in the analysis of complex sample matrices, a common and difficult problem for the analyst.

One of the most intriguing recent developments in the stationary phases of IC is the design of monolithic stationary phases for ion separations. A monolithic stationary phase consists of a single piece of porous stationary phase material that has about 15% higher porosity than packed columns consisting of individual beads. It is also less compressible than packed beads.[42] As a result, low back pressures and high mass transfer efficiencies can be maintained with monolithic columns even while using high flow rates. For example, Lucy's group[42] used didodecyldimethylammonium bromide (DDAB) to coat a reversed-phase monolithic column and

thereby generate an ion-exchanger to separate seven anions. As is noted below, this strategy of adsorbing a hydrophobically substituted ion exchange molecule to an inert column substrate has also been a common approach to applying macrocycles to IC. The column prepared by Lucy could separate anions in ultra-short time (30 s) because the sturdy, noncompressible monolithic design allows eluent flow rates as high as 10 mL/min. In another example, Haddad's group prepared a monolithic column that was *in situ* polymerized by butyl methacrylate, ethylene dimethacrylate, and 2-acrylamido-2-methyl-1-propanesulfonic acid within fused-silica capillaries; it was then coated by Dionex AS10 or AS18 quaternary ammonium functionalized latex particles.[43] In this case, seven anions could be separated in less than 2 min using high flow rates without sacrificing separation efficiency. Several review papers about the application of monolithic columns for fast IC separations have been published.[44, 45] Most recently, in 2009, Nordborg and Hilder[45] reviewed the advances in polymer monoliths for IC between the years 2003 and 2008. Materials and methods to coat the surface of monoliths and copolymerization of the functional groups were introduced.

Developments have also occurred in the area of eluent composition. Bicarbonate was the mainstay IC eluent for anions for many years, largely because the preferable eluent, NaOH, can react with CO_2 in the atmosphere forming carbonate, which results in unpredictable concentration changes of NaOH and unstable baselines. The development of the air-isolated electrolytic eluent generator for hydroxide eluents now keeps the eluent in a closed system impeding the reaction of NaOH with CO_2 so that hydroxide is becoming the eluent of choice for anion IC.[46] Beyond these considerations, various eluents are commonly used for other

applications, depending on the specific separation objectives.[47, 48] For example, the chelating agent EDTA can be added to the mobile phase to retain Cu^{2+}, Zn^{2+}, and Pb^{2+} as complex anions in the presence of inorganic anions such as Cl^- , NO_2^-, Br^-, and NO_3^-.[48] In similar fashion, macrocyclic ligands, particularly crown ethers, can also be used as the mobile phase in IC, as described below.

In the area of detection, several interesting innovations have been developed over the years. However, most of these are targeted at specific applications, leaving conductivity detection as the prime detection method for inorganic ions, both cations and anions. Among recent developments, we find hyphenated detection methods that can not only achieve sensitive detection but also expand the analyte range of IC.[36] For example, inductively coupled plasma spectrometry-mass spectrometry (ICP-MS) is one of the attractive detection methods for IC because of its low detection limits and wide dynamic linear range. Divjak *et al*.[49] reported the detection of halogen and oxyhalogen anions, sulfate, phosphate, selenite, selenate, and arsenate by ICP-MS. With a 50 μl injection sample, the detection limit for BrO_3^- and Br^- is 1.0μg L^{-1} using this method.

4. Application of macrocycles to ion chromatography

Since the early days of macrocyclic ligand studies, these molecules have been incorporated into separation systems including chromatography. In the 1970s, Cram's group pioneered the application of an optically pure macrocycle for chiral chromatographic separations by liquid chromatography. (R', R)-tetranaphthyl-22-crown-6 was attached to macroreticular

cross-linked polystyrene *p*-divinylbenzene resin as the stationary phase for chiral separations of amino acids and ester salts.[50] Since then, macrocyclic ligands have been introduced into IC either as mobile phase or as stationary phase components. In this section, we introduce several typical types of macrocyclic ligands that have been applied to IC.

4.1 Macrocyclic ligands in the stationary phase

Macrocyclic ligands can be applied to a stationary phase in three different ways: adsorbed to the stationary phase, covalently bonded to the stationary phase, or polymerized into the stationary phase.

4.1.1 Crown ethers

The most obvious and first explored application of crown ethers and similar macrocycles to IC is in the separation of metal cations, specifically of the alkali and alkaline earth series. Kimura's group[51] pioneered the adsorption of hydrophobic crown ethers onto silica-based columns to effect cation separations, a technique labeled dynamic coating. This was accomplished by passing the coating solution of hydrophobically substituted crown ethers in a mixture of methanol and water through an octadecylsilylsilica (ODS)-packed column, so that the crown ether functional group was strongly retained on the ODS particles by hydrophobic effects.[51] The structures of the crown ethers (**10**) used are shown in Figure 1.7. These columns were then applied to the separation of alkali and alkaline metal ions in water. Unlike conventional cation-exchange materials that separate these ions according to hydrated ionic size and charge, these crown ether-coated columns displayed selectivity for certain alkali metals

related to the previously known selectivities of crown ethers measured in homogeneous solution (described above). For instance, the 18-crown-6 and 15-crown-5 based columns showed the highest selectivity for K^+, and the elution order was $Li^+ < Na^+ < Cs^+ < Rb^+ < K^+$. Smaller 12-crown-4 derivatives showed higher selectivity for Na+ with the elution order $Li^+ < Cs^+ < Rb^+ < K^+ < Na^+$. Clearly, the choice of an aliphatic substituent to add hydrophobicity (which minimizes any influence on the electron density of the oxygen donors) did little to alter the inherent selectivity of 18-crown-6, even in such a two-phase system. Yet this minimal substitution made a difference to the selectivity of 15-crown-5, an effect which is enhanced by the greater hydration energy of Na^+ over K^+. This energy must be added to partially dehydrate the metal ion as it passes from the aqueous mobile phase to be retained in the much lower dielectric environment of the stationary phase.

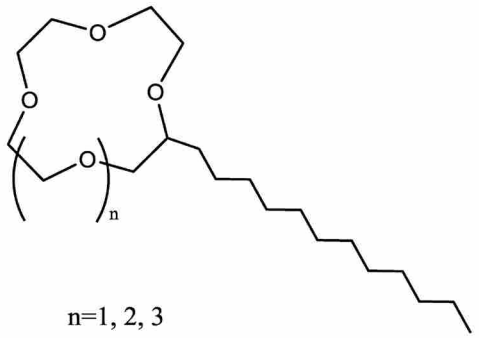

10

Figure 1.7 Structures of crown ethers coated on ODS.[51]

Using a more robust chromatographic substrate, Lamb and coworkers[52, 53] adsorbed *n*-tetradecyl-18-crown-6 (TD18C6) onto nonpolar polystyrene-divinylbenzene beads. Compared with the silica substrate, this column has the distinct advantage of being stable in basic eluents. Thus, both anion and cation separations can be accomplished on the same column based on the

cation- macrocycle interaction. Cations can be separated due to the selectivity of the macrocycle among cations, whereas anion separations result from the affinities of anions for the positively charged cation–macrocycle complex. The capacity of the column can be modified by changing the cation in the mobile phase, the temperature, and the concentration of organic modifier (e.g., methanol). By choosing an eluent cation with a low affinity for the stationary phase macrocycle, the capacity of the column can be adjusted downward. In addition, the complexation reactions between cations and macrocycles are generally quite exothermic, so increasing temperature leads to weaker complexation, thus decreasing the capacity of the column for anions. And since the stability of the cation–macrocycle complex is greatly affected by the solvent, nonaqueous solvents can be used to adjust the column capacity for anions upwards. The length of the aliphatic side-chain on the macrocycle was found to have a strong influence on the stability of the adsorbed column. Specifically, a column prepared with decyl-18-crown-6 was not as stable to mixed organic/water eluents as that prepared with the more hydrophobic TD18C6. An example separation of anions with the TD18C6 column is shown in Figure 1.8.[52] The TD18C6 column was also used to separate three alkaline earth metal cations, five alkali metal cations, and the ammonium ion.[53]

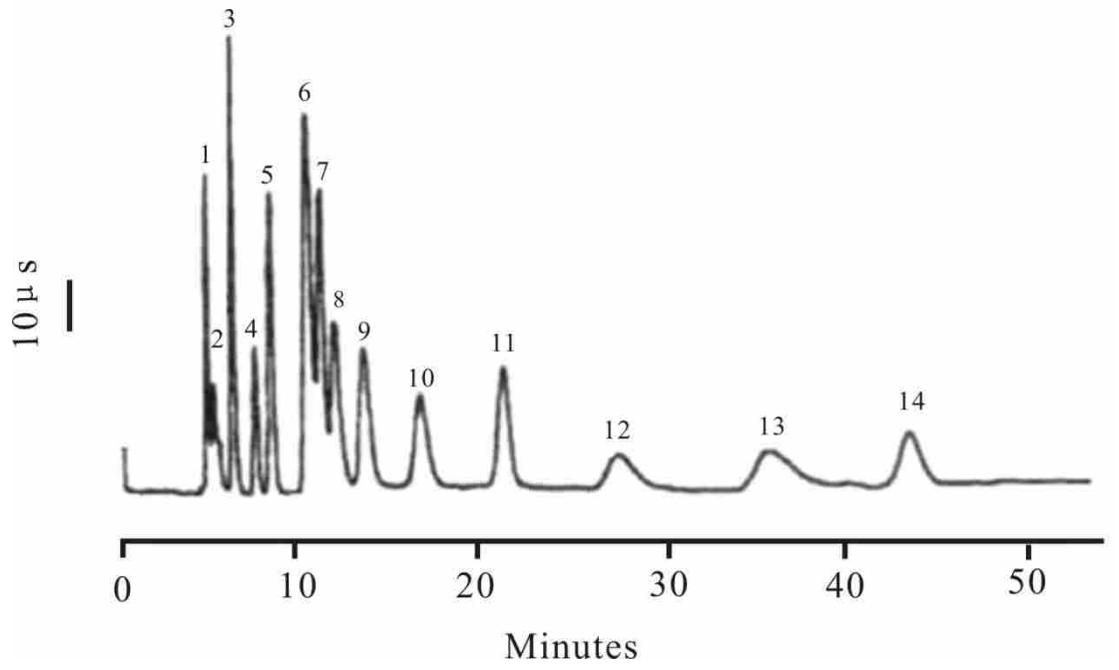

Figure 1.8 Anion separation by a n-tetradecyl-18-crown-6 (TD18C6) column, 1 = F^-, 2 = $CH_3CO_2^-$, 3 = Cl^-, 4 = NO_2^-, 5 = Br^-, 6 = SO_4^{2-}, 7 = NO_3^-, 8 = $C_2O_4^{2-}$, 9 = CrO_4^-, 10 = phthalate, 11 = I^-, 12 = PO_4^{3-}, 13 = citrate, 14 = SCN^-, eluent : 50 mM aqueous KOH-acetonitrile (80:20, v/v).[52]

Another approach to applying macrocycle selectivity to cation separations is illustrated in the work of Xu *et al*.[54] who dynamically coated a C30-substituted silica column with both dodecylsulfate and 18-crown-6 adsorbents to separate mixtures of cations containing H^+, NH_4^+, alkali, and alkaline earth metal ions. They compared the separation efficiency of this column to that coated only with the common ion-exchanger dodecylsulfate. Without the adsorbed 18-crown-6, NH_4^+ and K^+ eluted together because of their similar ionic radii and charge, but with the added 18-crown-6 coating, the column exhibited high selectivity for K^+, so that NH_4^+ and K^+ were well separated. The selectivity here is due in part to the different mode of complexation of 18- crown-6 for these two ions: K^+ is sequestered in the cavity, whereas NH_4^+ sits atop the cavity forming hydrogen bonds to alternate ligand oxygen atoms.[7] In this chromatographic example, the

macrocycle served not as the primary column active site but as a secondary feature that adjusted the selectivity of the column.

Although a crown ether-coated column can effectively separate cations and its anion capacity can be adjusted by controlling the amount of adsorbed crown ether, it is susceptible to loss of the macrocyclic active site. When water eluents are used, this is generally not a problem, but if mixed mobile phase solvents are used (e.g., water/methanol), the coated crown ether can be washed off the column resulting in a loss of capacity.[34]

To avoid this problem, macrocycles can also be covalently bonded to the stationary phase in IC. For example, the stationary phase of the Dionex IonPac CS15 cation separator column contains carboxylic acid groups, phosphonate groups, and 18-crown-6 ether groups permanently bonded to the polystyrene-divinylbenzene macroporous beads.[3] Compared to the CS12 cation separator column, which is similar to the CS15 column except that it has no crown ether on the stationary phase, the CS15 column shows better resolution for ammonium and sodium ions, which are typically difficult to quantify together because of their similar selectivity by sulfonic acid or carboxylic acid cation-exchangers.[55] In addition, in a 4000-to-1 concentration ratio of sodium to ammonium ion and a 10 000-to-1 ratio of ammonium to sodium ions, ammonium and sodium ions can be well separated isocratically (i.e., with a single eluent) using a CS15 column.[55]

Copolymerization of polymeric crown ether with silica gel or other support materials is another way to incorporate crown ether into stationary phases. Blasius and coworkers thoroughly studied methods for polymerizing cyclic polyethers with various polymeric matrices and applied

them in ion separations.[56] An example polymer structure (**11**) is shown in Figure 1.9(a).[56]

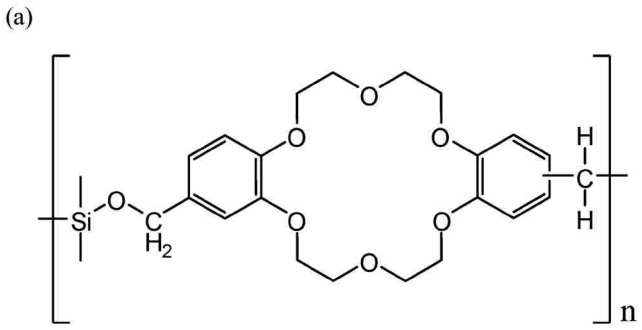

11

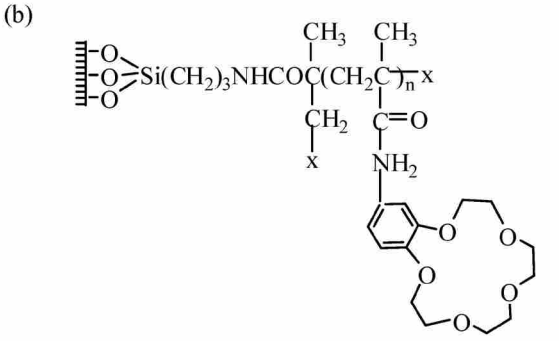

x = an end group of initiator or poly crown ether

12

Figure 1.9 (a) A polymeric crown ether stationary phase (from ref. 56); (b) Structure of the polyether modified silica stationary phase.[57]

Nakajima *et al*.[57] also explored stationary phases in which the macrocycle is covalently bonded to silica. Figure 1.9(b) shows the structure of the polyether modified silica. These stationary phases have several obvious advantages over adsorbed systems: first, by adding crown ether to the stationary phase, these columns have specific selectivity for certain ions; second, they are compatible with organic solvents like methanol that cannot be used in stationary phases made by adsorbing crown ether to support material. This provides another degree of freedom to the analyst, namely, changing the percentage of organic solvents in the mobile phase. As we

discussed previously, the stability constants of crown ethers and the selectivities among metal cations can change with solvent. Third, they have shown high capacity and chemical and thermal stability.

Unfortunately, the approaches described above have some inherent disadvantages. First, for columns of the type in Figure 1.9(a), the flow rate is usually low (0.05-0.1mLmin^{-1}) because of the low mechanical rigidity, needed to withstand high pressure, of polymeric crown ether resins. This results in long analysis times. Second, columns like those based on **12** suffer from poor hydrolytic stability due to the potential for acid or base hydrolysis; furthermore, the underlying silica structure can be ionized and thus tends to concentrate eluent as well as analyte ions, resulting in a loss of selectivity. Third, the separation efficiencies of both types of column material have not been found to be high, likely caused by irregularities in particle size and shape.

4.1.2 Crown ethers in the mobile phase

To use crown ethers in the mobile phase is more convenient than in the stationary phase since it avoids the cumbersome work of design, synthesis, and column packing, and the possibility that the macrocyclic analogs used will not display the same selectivity as expected from the parent compound. The main reason for including crown ethers in the mobile phase is their cation selectivity.[58–60] By selectively binding one of the analytes, a higher resolution for two analytes having similar selectivities with a traditional ion-exchanger can be achieved. For example, traditional cation-exchangers containing sulfonic or carboxylic functional groups have similar selectivities for NH_4^+ and Na^+, and thus the resolution between these two peaks is usually low, making quantification difficult. Indeed, in real-world samples, NH_4^+ and Na^+ are typically

quite disproportionate, either one or the other having a much higher concentration. By adding a crown ether to the mobile phase, this problem can be overcome.[58] Figure 1.10 compares the separation of cations with and without 18-crown-6 in the eluent using a standard cation-exchange separator column. The stability constants (1:1 complex) of 18-crown-6 with NH_4^+ and Na^+ in aqueous solution at 25 ^oC are 1.23 and 0.80, respectively. After adding crown ether, the retention time of NH_4^+ increased dramatically, enhancing the resolution between NH_4^+ and Na^+ peaks. In this same study, Bruzzoniti and coworkers[58] reported the separation of a large number of cations: NH_4^+, alkali (Li^+, Na+, K^+), and alkaline earth (Ca^{2+}, Mg^{2+}, Ba^{2+}, Sr^{2+}) metal cations. Both monovalent and divalent cations were separated in the same analytical run. The influence of 18-crown-6 on the retention of cations was in the following order: $K^+ >> Ba^{2+} > NH_4^+ > Sr^{2+}$, as shown in Figure 1.10. This order is in keeping with the relative stability constants of 18-crown-6 with these cations and illustrates the advantage of using the unsubstituted macrocycle in a well-characterized medium like water: namely, one can be fairly confident that the thermodynamic selectivity will be carried over into the separation.

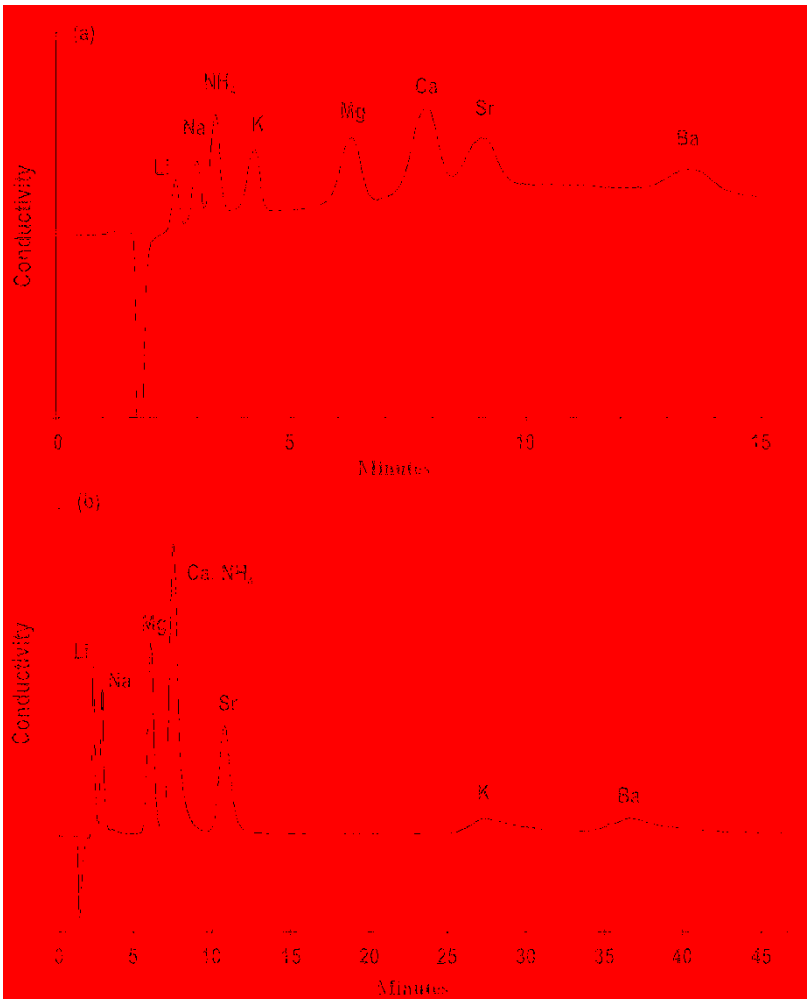

Figure 1.10 Separation of cations (a) without and (b) with the addition of 18-crown-6 ether in the eluent. Column: IonPac CS12 cation exchange.[58]

As discussed in the early part of this chapter, macrocyclic complexes are generally more stable in nonaqueous solvents than in aqueous solution. Therefore, it is expected that adding 18-crown-6 to a nonaqueous mobile phase would increase the retention time of cations to be separated. Fritz's group added 18-crown-6 to a nonaqueous IC mobile phase to study the retention of alkali metal cations and ammonium ion on a sulfonic acid cation-exchange resin.[59] The retention factors of all the ions increased with increasing concentration of 18-crown-6 in acetonitrile eluent containing 1mM methanesulfonic acid. Most notably, the separation factor of

Li^+/Na^+ increased from 2.6 without 18-crown-6 to 3.8 when including 18-crown-6 in the mobile phase, which made the separation of 1 ppm of Li^+ from 500 ppm Na^+ possible.

One interesting study incorporated a crown ether in both the mobile and stationary phases. Specifically, the Dionex Ionpac CS15 column contains covalently bonded 18-crown-6 in the stationary phase and can give good resolution at a 4000:1 concentration ratio of Na^+ to NH_4^+.[55] Lamb's group found that the addition of 18-crown-6 to a mobile phase can improve peak resolution between NH_4^+ and Na^+ even further, so that accurate analysis can be performed at a concentration ratio of as much as 60000-to-1 using this same column. Figure 1.11 shows the separation of NH_4^+ and Na^+ at a concentration ratio of 1:60000.[60] This kind of resolution is very helpful in the analysis of biological or environmental samples, where sodium ion is commonly present at very high concentrations and can make the analysis of other ions like ammonium ion extremely difficult.

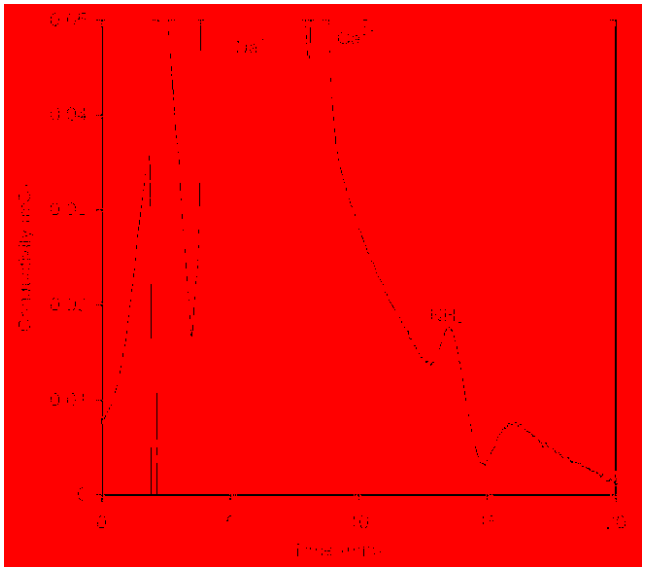

Figure 1.11 Separation of Na^+ (600 mg/L) and NH_4^+ (0.010 mg/L) at the concentration ratio of 60,000:1; Column: CG15 and CS15; Eluent: 10.80 mM H_2SO_4 and 10.0mM 18-crown-6.[60]

Possible concerns over the use of crown ethers in the mobile phase are effects on the suppressor, cost, and toxicity. The ligand indeed has an effect on suppressor performance after days of use, but this can be overcome easily with a simple rinse.[60] In terms of toxicity and cost, this ligand is less toxic than some solvents and additives commonly used in chromatography and CE[60] and no more costly.

4.1.3 Crown ethers in detection systems

Crown ethers have undergone limited investigation as components in ion chromatographic detection systems. One example is the work of Jane and Shih,[61] who coated a piezoelectric quartz crystal with dibenzo-16-crown-5-oxydodecanoic acid. The detector was used for cation and anion detection after separation on a diaza-18-crown-6-based separator column with nonionic eluents. The frequency response of this detector for both cations and anions, due to cation complexation and anion association with the resulting complex, was as reproducible and sensitive as standard conductimetric detection, but peak broadening resulted from a relatively large cell volume.

4.2 Cryptands in ion chromatography

Modified cryptand structures can be used in the stationary phases of IC either by adsorption to or covalent bonding to hydrophobic resins. Lamb and coworkers introduced the use of decyl-[2,2,2] (D222) in IC stationary phases by adsorbing D222 onto polystyrene-based resin beads and thereby developed the concept of "capacity gradient elution" of anions.[62] When an eluent containing cations like Li^+, Na^+, or K^+ passes through the D222-coated stationary phase,

the resulting cation complex serves as a positively charged functional site for anion exchange. Since [2,2,2] complexes with Li^+, Na^+, and K^+ cations to significantly varying degrees, the capacity of the column is adjusted by changing the cation present in the mobile phase. In chromatography, gradients are applied in order to shorten the retention times of highly retained species. This is typically achieved by gradually increasing the strength of the eluent. On the other hand, a capacity gradient can be achieved using macrocycle-based columns by switching from one cation with a higher affinity for the macrocycle to another with a lower affinity. In this way, the capacity of the column drops rapidly and late-eluting anions emerge much sooner. Figure 1.12 compares the elution of a series of anions from a D222 column under both isocratic and capacity gradient conditions.

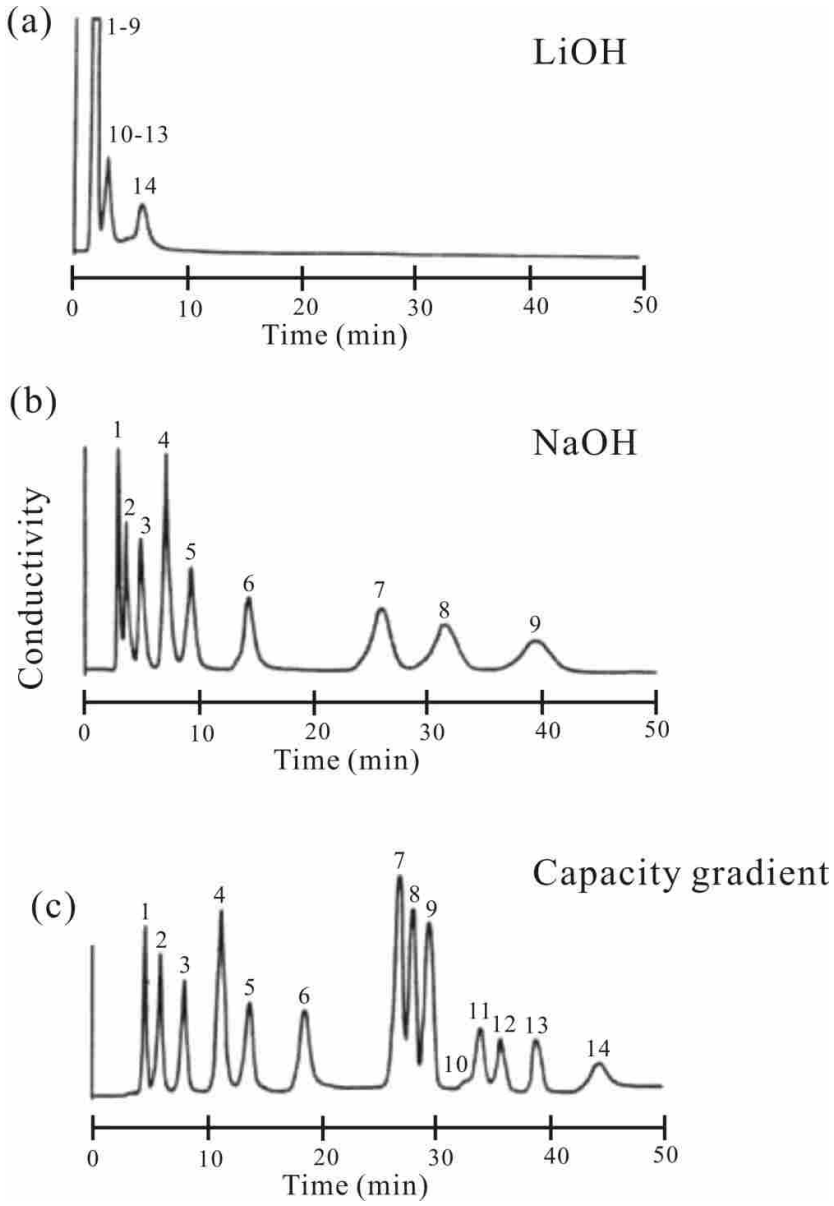

Figure 1.12 Separation of 14 common anions under isocratic and capacity gradient conditions: (a) with 20 mM LiOH as eluent (isocratic); (b) with 20 mM NaOH as eluent (isocratic); (c) with a 20 mM NaOH-20 mM LiOH gradient. Peaks: 1 = F^-, 2 = $CH_3CO_2^-$, 3 = Cl^-, 4 = NO_2^-, 5 = Br^-, 6 = NO_3^-, 7 = SO_4^{2-}, 8 = $C_2O_4^{2-}$, 9 = CrO_4^-, 10 = I^-, 11 = PO_4^{3-}, 12 = phthalate, 13 = citrate, 14 = SCN^-.[62]

One of the primary advantages of capacity gradients over traditional eluent gradients is that with capacity gradients the ionic strength of the eluent need not change, that is, only the

identity of the eluent metal cation need be changed, whereas with traditional gradients changes in eluent ionic strength can cause major disturbances in the chromatographic baseline.

As mentioned previously, columns prepared by adsorbing macrocyclic ligands to resin beads have obvious drawbacks such as limited eluent choice and potential loss of capacity because the macrocyclic active sites can gradually bleed off. Pohl, Woodruff, and coworkers[63] succeeded in overcoming these problems by covalently bonding the [2,2,2] ligand to polystyrene chromatographic beads (**13**). The baseline separation of polarizable and nonpolarizable anions in the same run by capacity gradient was demonstrated.

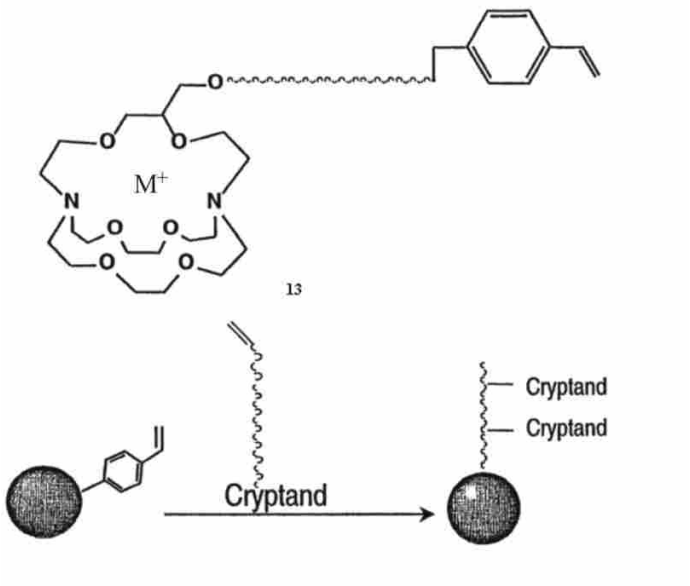

Figure 1.13 The monomer of cryptand [2,2,2] used to graft to stationary phase.[63]

Figure 1.13 shows the monomer of cryptand [2,2,2] used to graft to the polystyrene stationary phase. In one application of this method, Sarzanini and coworkers reported the separation of haloacetic acids (HAAs), a class of disinfection by-products.[64] The separation of HAAs was traditionally achieved through conventional anion-exchange columns with a fixed

capacity using an eluent gradient, from weak to strong eluents. With the cryptand column, a NaOH–LiOH step gradient was used to adjust the column capacity so that the separation of nine HAAs was achieved in 25 min with good resolution (Figure 1.14).

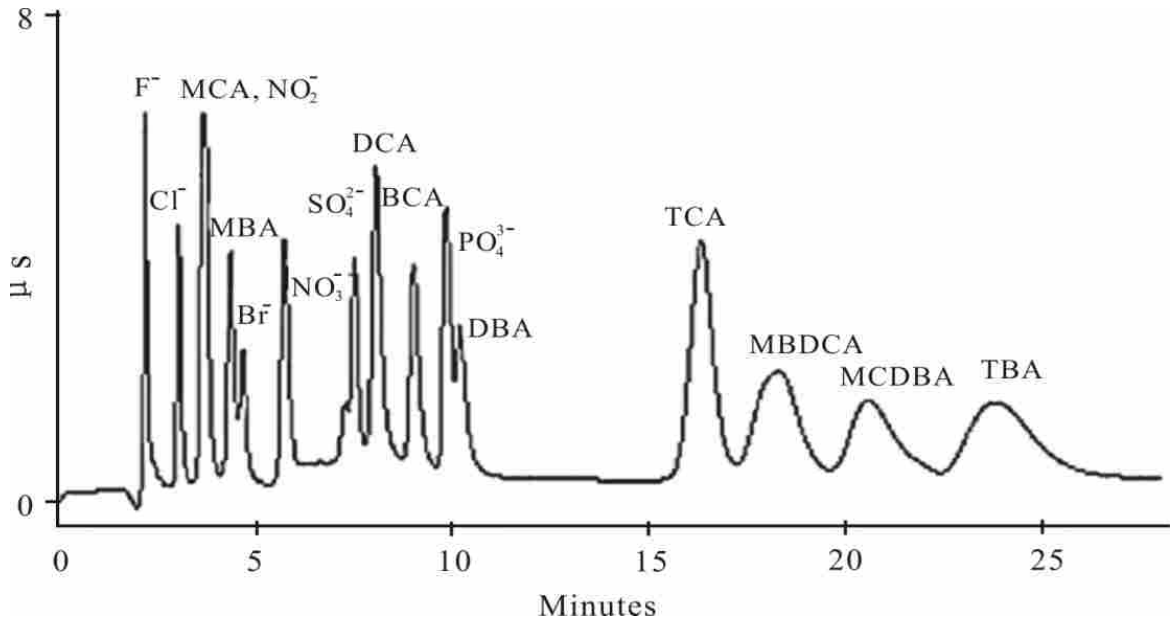

Figure 1.14 Separation of haloacetic acids and inorganic anions. Column: Cryptand A1 5 micron (150mm×3 mm); eluent gradient: −8 to 3 min 10mM NaOH; *t* = 3 min 10mM LiOH. Monochlorocacetic (MCA); Monobromoacetic (MBA); Dichloroacetic (DCA); Bromochloroacetic (BCA); Dibromoacetic (DBA), Trichloroacetic (TCA), Monobromodichloroacetic (MBDCA), Monochlorodibromoacetic (MCDBA), and Tribromoacetic (TBA) acids.[64]

The cryptand column has also been used for quantification of low molecular weight heparins (LMWHs) in bio-samples. Heparin is a highly negatively charged, sulfated glucosaminoglycan, which is an anticoagulant used to prevent thromboembolic diseases, and during kidney dialysis and cardiac surgery. LMWHs are negatively charged fractionation or

depolymerization products of heparin with molecular weight of less than 8 kDa on average.[65] Abballe *et al*.[66] illustrated the separation of LMWHs by the cryptand column using a NaOH–LiOH step gradient. LMWHs were eluted as a unique peak, making their quantification easy and fast (Figure 1.15).

Figure 1.15 Separation of heparins using a cryptand-based column.[66]

In recent years, analysts have investigated the use of cryptand columns for preconcentrating trace amounts of anions in complex matrices.[67–69] The general principle of preconcentration and matrix elimination is to use a concentrator column to trap and enrich the trace ions of interest while eliminating all or most of the matrix ions that would interfere in the chromatographic analysis. Following this pretreatment step, chromatography would be carried out as usual.[70] This approach is amenable to automation and therefore desirable in the laboratory. Haddad *et al*.[70] have reviewed the instrumentation requirements for preconcentration, including

use of the cryptand-based column.

Many recent studies have focused on determining trace amounts of perchlorate in drinking water because perchlorate ion can interfere with iodine uptake in humans, resulting in thyroid dysfunction.[69] Pohl and coworkers68 have used a cryptand [2.2.2] column to concentrate perchlorate and remove drinking water matrix anions from a large sample by a weak base eluent. Figure 1.16(b) shows the separation of 10μg L^{-1} of perchlorate from 1000 mg L^{-1} matrix ions using this concentration method followed by a standard anion chromatographic separation and suppressed conductivity detection. This is to be compared to Figure 1.16(a), in which no concentrator column was used and the perchlorate peak is not properly separated from the huge background matrix ion peak.

The US Environmental Protection Agency (EPA) has published accepted methods for perchlorate analysis in drinking water in which these approaches have been carefully optimized[69] to allow for reliable determination down to <1μg L^{-1}. Other work by Lamb *et al*.[67] using macrocycle-based IC for perchlorate ion determination has used not only the cryptand-based concentrator column but also an 18-crown-6-based mobile phase separation scheme to analyze perchlorate to concentrations of <1μg L^{-1}.

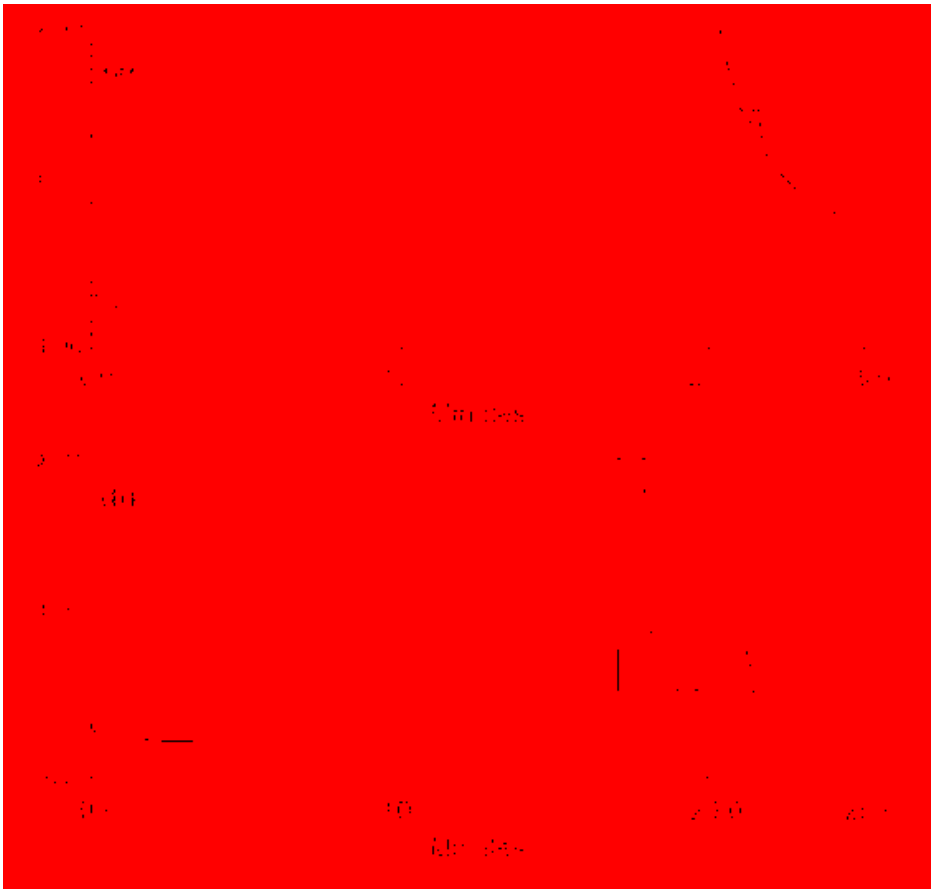

Figure 1.16 Separation of 10 μg L^{-1} of perchlorate (peak labeled 1) in the presence of 1000 mg L^{-1} of matrix ions. (a) No concentrator column was used; (b) improved peak efficiency and recovery showed when the concentrator column was used.[68]

4.3 Calixarenes in ion chromatography

Calixarenes have been extensively studied as solvent extractants for inorganic ions, stationary phases for capillary gas chromatography (GC), selectivity modifiers in CE, and as components of HPLC. The calixarene structure is quite versatile in that the lower rim can be modified to adjust solubility and the phenol groups on the upper rim are suitable for many chemical modifications that may introduce specific selectivity. Here, we describe the application

of modified calixarenes to ion chromatographic separations.

Arena and colleagues modified calixarenes with crown ethers and covalently bonded them to silica gel to serve as an IC stationary phase.[71] These calix-crown phases showed satisfactory separations among Na^+, K^+, and Cs^+. However, the columns were operated at a rather low flow rate, so the separation time was long (about 20 min) when using mixed methanol/water eluents.

Resorcinarenes, a type of calixarene, are cyclic tetramers synthesized from the condensation of resorcinol and various aldehydes. Lamb's group recently reported anion separations using a stationary phase coated with a cyclen-modified resorcinarene[72] shown in Figure 1.17(a) (cyclenbowl, **14**). The performance of the cyclenbowl tetramer stationary phase was compared to that of a column prepared with the monomer analog *N*-undecyl cyclen. Both macrocyclic ligands were successfully adsorbed to polystyrene resin beads. The capacity of this cyclenbowl column was adjustable according to the pH of the eluent. Given that the first protonation constant (p*K*a) of cyclen is 10.6, at low pH, the cyclen unit is protonated and serves as an anion-exchange site. However, at higher pH, anions are not retained by the neutral macrocycles. A step gradient from 10mM $NaHCO_3$ (pH 7.6–8.0) to 10mM NaOH (pH 12) was used to accomplish the separation. Figure 1.17(b) shows the separation of perrhenate ion from six other anions using the cyclenbowl column and illustrates the potential of this column for use in preconcentration of perrhenate. The cyclenbowl column provided better anion retention and selectivity than the monomer column.

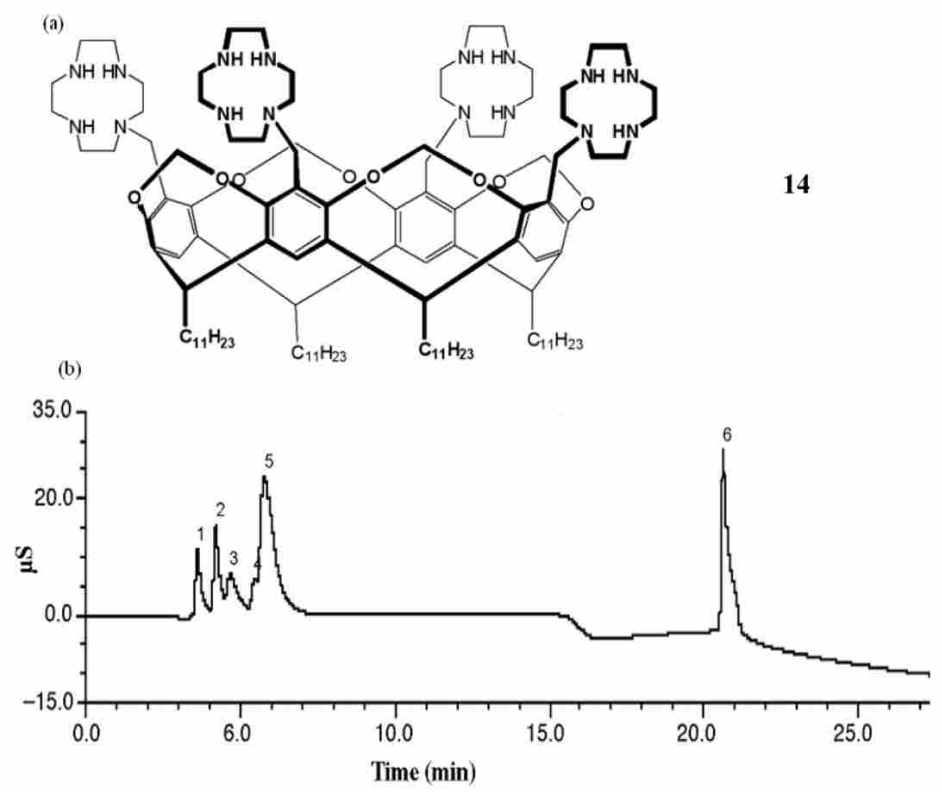

Figure 1.17 (a) Structure of cyclenbowl (b) Preconcentration of perrhenate on cyclenbowl column by step gradient. Peaks: 1 = F^-, 2 = Cl^-, 3 = NO_2^- , 4 = NO_3^-, 5 = SO_4^{2-} & PO_4^{3-}, 6 = ReO_4^-.[72]

4.4 Cyclodextrins

CDs are water soluble macrocycles containing 1,4-linked α-D-glucose units. CDs containing six, seven, and eight α-Dglucose units are labeled α-, β-, and γ - CDs, respectively. The primary and secondary hydroxyl groups of CDs make them sufficiently hydrophilic to dissolve in water, whereas the toroidal cavities are more hydrophobic. Thus, CDs can recognize guest molecules not only by strong noncovalent interactions such as hydrogen bonding but also by forming inclusion complexes with guest molecules of suitable sizes. In addition, CDs are good chiral discriminating agents for enantiomers. CDs have been applied to separations systems such as liquid chromatography (including ion-exclusion chromatography and ion-exchange

chromatography), GC, CE, and micellar electrokinetic chromatography.

In chromatography, CDs have been used in both stationary and mobile phase methods. In HPLC applications, CDs can be incorporated into stationary phases either by adsorption or bonding onto silica. As an example of the adsorption method, Thuaud *et al*.[73] first grafted a *β*-CD derivative onto a polyvinyl-imidazole (**15**) that was then absorbed onto silica and used to separate racemic mixtures of amino acid derivatives, among other species, using UV detection. The structure of one *β*-CD-containing polymer is shown in Figure 1.18.

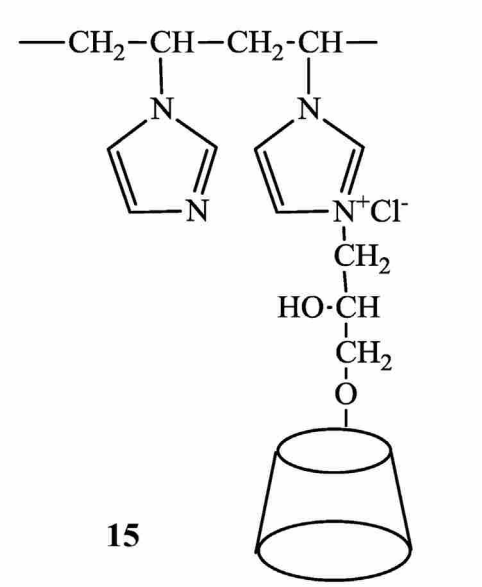

Figure 1.18 Structure of β-CD-PVI polymer.[73]

Different methods are used for covalently bonding CDs to silica. For example, Wössner *et al*.[74] prepared a *β*-cyclodextrin stationary phase (**16**) for normal-phase HPLC separation of organic nitrates. The synthetic route is shown in Figure 1.19.

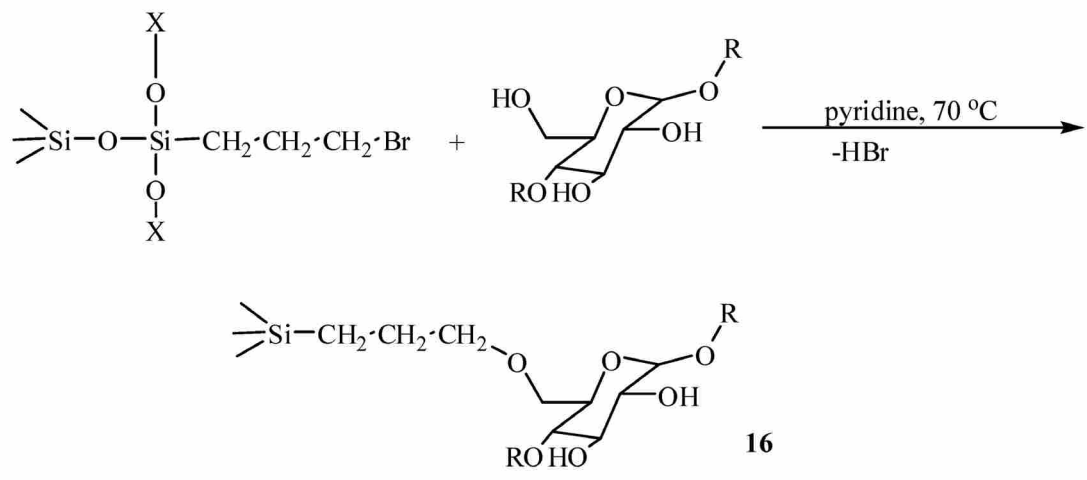

Figure 1.19 Synthesis of β-cyclodextrin-silica.[74]

Because of their good solubility in aqueous solution, low toxicity, and low UV absorbance, CDs are also easily incorporated into the chromatographic mobile phase. Ion chromatographic separations using CDs in the mobile phase are rather rare. In one example, Pullen *et al*.[75] used *β*-CD as a chiral mobile phase additive to separate racemic cycloheptaindole derivatives using an ionized silica stationary phase. Enantiomer pairs could be resolved with a mobile phase containing sodium phosphate, *β*-CD, and 2-methyl-2-propanol (*t*-BuOH).

One interesting application of CDs in IC involves its use in the detection of oxohalide ions like bromate. Bromate ion is a carcinogenic disinfection byproduct regulated by the US EPA at a maximum contamination level of 10μg L^{-1}. Kitamaki *et al*.[76] developed a simplified IC method to detect low concentrations of bromate in drinking water. *α*-CD was incorporated into a postcolumn reagent solution (introduced into the eluent stream between the separator column and the detector) to improve the sensitivity of detection. Bromate undergoes the following reactions under acidic (HBr) conditions:

$$BrO_3^- + 5Br^- + 6H^+ \longrightarrow 3Br_2 + 3H_2O \quad (1.4)$$

$$Br_2 + Br^- \rightleftharpoons Br_3^- \quad (1.5)$$

$$Br_3- + \text{a-CD} \rightleftharpoons Br_3^-/\text{a-CD} \quad (1.6)$$

The resulting Br_3^-/α-CD complex is subject to UV detection at 265 nm. Using this system, the concentration of bromate in a bottled water sample was determined at 6 μgL^{-1} and the calibration had a linear-regression coefficient of 0.996. A similar method was also used to determine trace amounts of separated iodate and nitrite ions in drinking water.[77] Iodate and nitrite in their individual chromatographic peaks form iodine when HI is introduced, after which iodine reacts with excess I^- to form I_3^-, which in turn forms an inclusion complex with CD. In this process (1.7–1.10), CD shifts the equilibrium in (1.9) to the right, the total concentration of triiodide ion is increased, and therefore, the sensitivity of detection is improved. Among α-CD, β-CD, and γ-CD, α-CD was the most effective for this application.

$$IO_3^- + 5I^- + 6H^+ \longrightarrow 3I_2 + 3H_2O \quad (1.7)$$

$$2NO_2^- + 2I^- + 4H^+ \longrightarrow I_2 + 2NO + 2H_2O \quad (1.8)$$

$$I_2 + I^- \rightleftharpoons I_3^- \quad (1.9)$$

$$I_3^- + \alpha\text{-CD} \rightleftharpoons I_3^-/\alpha\text{-CD} \quad (1.10)$$

5. Liquid membranes

5.1 Facilitated transport mechanism and membrane types

The facilitated transport mechanism of liquid membranes has been the subject of considerable research[79] and has been reviewed previously.[7] In summary, facilitated transport of this type can be broken down into the following steps: the macrocyclic ligand carrier selectively extracts ions (or neutrals) from the source phase into the membrane medium; the resulting complex then diffuses across the membrane; and finally, the guest is released from the membrane complex into the receiving phase. Dynamic equilibria come into play at every step, and rates of diffusion of species, not only through the bulk phase of the membrane but also through interfacial boundary layers at each interface, must be considered as important factors affecting membrane flux. The effectiveness of a liquid membrane is defined by two important outcomes: (i) the selectivity between species and (ii) the rate at which species pass through the membrane (expressed as membrane *flux*, i.e., moles/time/membrane area, or membrane *permeability*, i.e., flux/source phase concentration).

The rate of facilitated transport is governed ultimately by the rate of movement of the guest species through the boundary layers at the membrane–water interfaces and across the membrane itself. If the carrier–guest complex is not labile, the latter term is governed by the rate of diffusion of the complexed (guest) species, which in turn is governed according to Fick's Law in part by the concentration gradient across the membrane. The concentration of the complex on the source side of the membrane is determined by the extraction coefficient of the guest species

with the carrier. This coefficient is typically related, at least in terms of selectivity, to the thermodynamic binding constant between host and guest, and subject to all the structural and solvent considerations described in the early part of this chapter. The concentration of the complex on the receiving side of the membrane is again determined by the extraction coefficient under those chemical conditions. The winning strategy for the separations chemist is to adjust the chemical conditions on the source and receiving sides of the membrane to maximize this concentration gradient. If the host–guest complex is quite labile, transfer of guest from host to host molecule may also contribute to the overall membrane flux. Membrane flux is enhanced when chemical species are kept small (increasing diffusion coefficients) and the viscosity and tortuosity of the liquid membrane medium are kept to a minimum. Typically, rates of complexation and release of guests by macrocyclic carriers are fast compared to diffusion, so diffusion steps in the membrane transport process are rate-limiting.

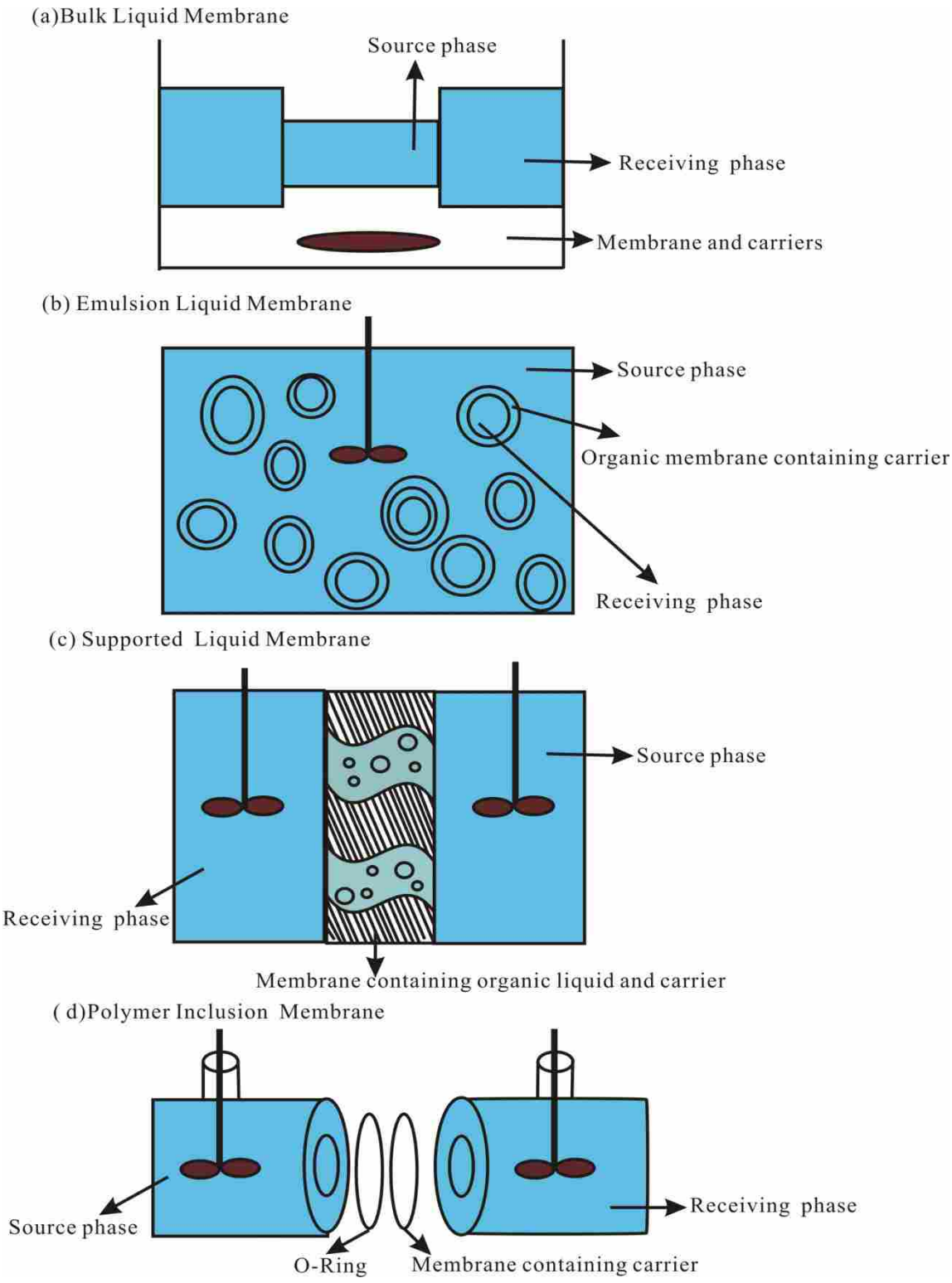

Figure 1.20 Types of liquid membranes (a) Bulk liquid membrane; (b) Emulsion liquid membrane[80]; (c) Supported liquid membrane[80]; and (d) Polymer inclusion membrane.

Macrocyclic ligands have been incorporated as carriers into four liquid membrane types, namely, bulk liquid membrane (BLMs), emulsion liquid membrane (ELMs), supported liquid membrane (SLMs), and polyer inclusion membrane (PIMs). The structures of these various membrane types are shown in Figure 1.20. As described in previous reviews,[7, 80] a BLM is simply a stirred organic layer (the membrane) that separates two water phases; an ELM is a double emulsion, usually water in oil in water (the oil being the membrane); an SLM is an organic liquid suspended in the pores of a porous amorphous polymer sheet separating two water phases; and a PIM is a gel-like suspension of a hydrophobic organic liquid in a polymer matrix (usually cellulose triacetate, CTA), forming a plastic sheet that separates two water phases. The BLM is the only one of these various types, which is not scalable for practical separations - it is used largely for screening the selectivity of carrier candidates.

5.2 Macrocyclic carriers in liquid membranes

Early experiments using synthetic macrocyclic carriers in liquid membranes were inspired by the performance of naturally occurring macrocycles such as valinomycin in transporting cations like K^+ through biological membranes. The majority of membrane separations work done using macrocyclic ligands focuses on the separation of metal cations and exploiting the inherent selectivity of macrocycles among these species. It was recognized in the work of Lamb and coworkers[81] that when neutral macrocycles are used as membrane carriers for metal cations, anions must accompany the charged metal ion complex through the membrane and thus the extractability of the coanion exerts a significant influence on cation flux. In fact, the co-

transport of anions through the membrane can be exploited to enhance separations in a number of ways. First, if a common cation is transported, anionic species (even negatively charged metal ion complexes) can be separated this way based simply on the degree to which anions are extracted into the membrane. Second, to enhance cation transport, one strategy is to increase the concentration of extractable anion in the source phase, thus providing an additional chemical potential in favor of extraction of cation into the membrane.Third, to enhance cation transport, one may add a component to the receiving phase that effectively extracts anion into the receiving phase or reduces the effective concentration of the anion in the receiving phase, keeping in mind that if the anion leaves the membrane, the cation must accompany it. Finally, it may be possible to add a hydrophobic anion to reside in the membrane itself to promote easier extraction of cations into the membrane.

In one example, Lamb and Arena's groups explored the possible application of calixarene-based carriers in PIMs to remove radioactive elements such as ^{137}Cs and ^{90}Sr from nuclear waste.[82] Figure 1.21 shows the structures of the calixarene-based carriers used. The membranes were made by combining CTA, 2-nitrophenyloctyl ether (NPOE), calixarenes, and dinonylnaphtalenesulfonic acid (DNNS) as counter ion residing in the membrane. DNNS had no effect on the selectivity of the calixarene carriers. Of the seven calixarene carriers chosen, the highest selectivity of Sr^{2+}/Na^{+} and of Cs^{+}/Na^{+} were obtained with compounds **19** and **23** shown in Figure 1.21.

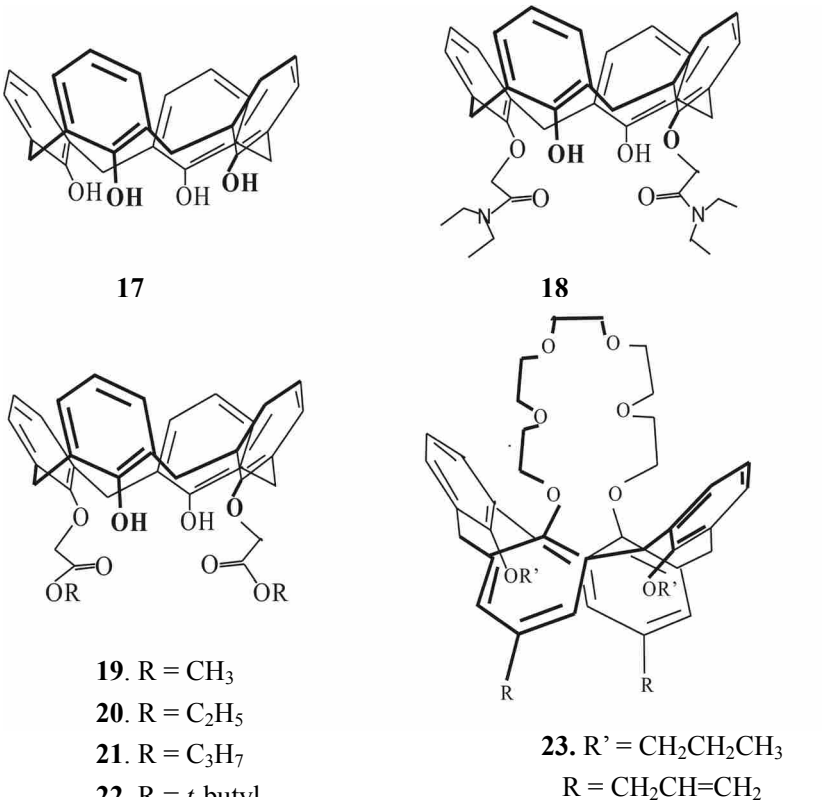

Figure 1.21 Structure of calixarene carriers used in PIM separation of Cs^+ and Sr^{2+}.[82]

Competitive Cs^+ ion transport in PIMs using calix[4]arene-mono- and bis-crown-6 carriers was also studied.[83] The calix-bis-crown **25** (Figure 1.22) exhibited slightly more efficient Cs^+ transport than with the mono-crown **24** (Figure 1.22) since the diffusion coefficient of the $Cs{\cdot}\mathbf{1}^+$ complex is only one fourth that of $Cs{\cdot}\mathbf{25}^+$. The selectivity values ($\alpha_{Cs/M}$) for Cs^+ over K^+, Na^+, UO_2^{2+}, Pb^{2+}, and Al^{3+} with carrier **24** were greater than that with carrier **25**, a result which was attributed to the higher association constant of Cs^+ with carrier **24** in the membrane solvent.

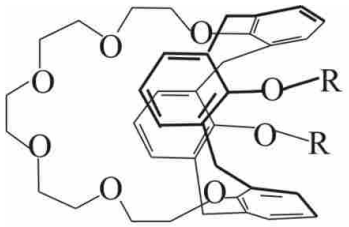

24. 1,3-Bis(dodecyloxy)calix[4]arene-crown-6

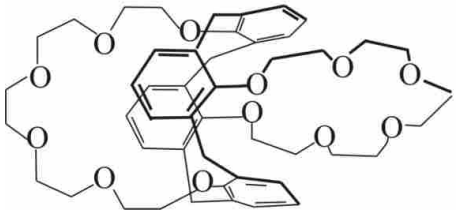

25. 1,3-Calix[4]arene-biscrown-6

Figure 1.22 Structure of the calix[4] arene-mono- and biscrown-6 carriers, R = -$C_{12}H_{25}$. [83]

Wlakowiak and Kozlowski[84] recently reviewed the application of macrocycle carriers including crown ethers, calixarenes, calixcrowns and cyclodextrins in liquid membrane processes. The role of macrocyclic ligands as ion carriers for cations such as alkali and alkaline metals, and heavy metals such as Zn^{2+}, Cd^{2+}, Hg^{2+}, Pb^{2+}, etc. was summarized. Mutihac[85] reviewed the calixarenes as membrane transporters for biological compounds such as amino acids, peptides, and acetylcholine.

When acidic macrocycles are used as membrane carriers of cations, the ionized macrocycle serves as the counterion in the transport process. For example, Bartsch's group has synthesized and studied cation separations using a series of acidic lariat ethers in liquid membranes.[86, 87] Lariat ethers are crown ether derivatives with one or more side functional groups. The ligand in Figure 1.23 was used as a carrier in BLMs to transport alkali metal cations. Several membrane solvents such as dichloromethane, chloroform, carbon tetrachloride, 1,2-dichloroethane, 1,1,1-trichloroehane, *o*-dichlorobenzene, toluene, and *p*-yxlene were chosen. In all the solvent systems, this crown ether carboxylic acid carrier showed the highest selectivity for

Na^+; however, the degree of selectivity was found to be solvent dependent. For example, the selectivity ratios of Na^+/K^+ and Na^+/Li^+ in chloroform were 160 and 180, respectively, while in carbon tetrachloride, they were 1.3 and 1.2, respectively. Figure 1.24 shows the selectivity and fluxes of cations in different solvents. They showed that membrane solvent affects the flux of ions through membranes in ways related to dielectric constant, polarity, and hydrogen bonding ability.

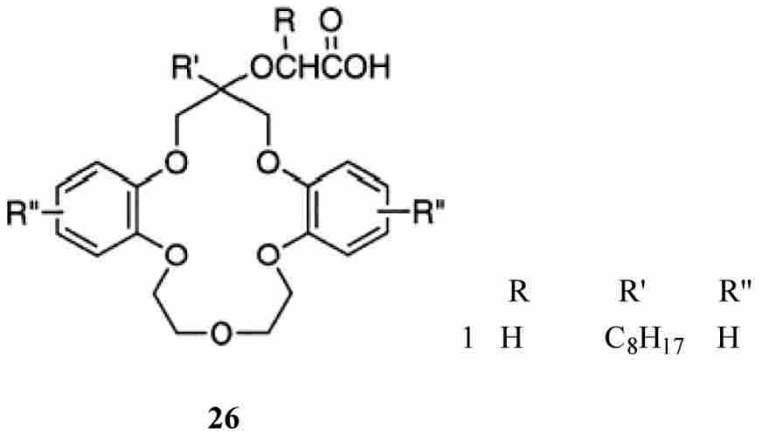

26

Figure 1.23 Structure of sym-(octyl)dibenzo-16-crown-5-oxyacetic acid.[86]

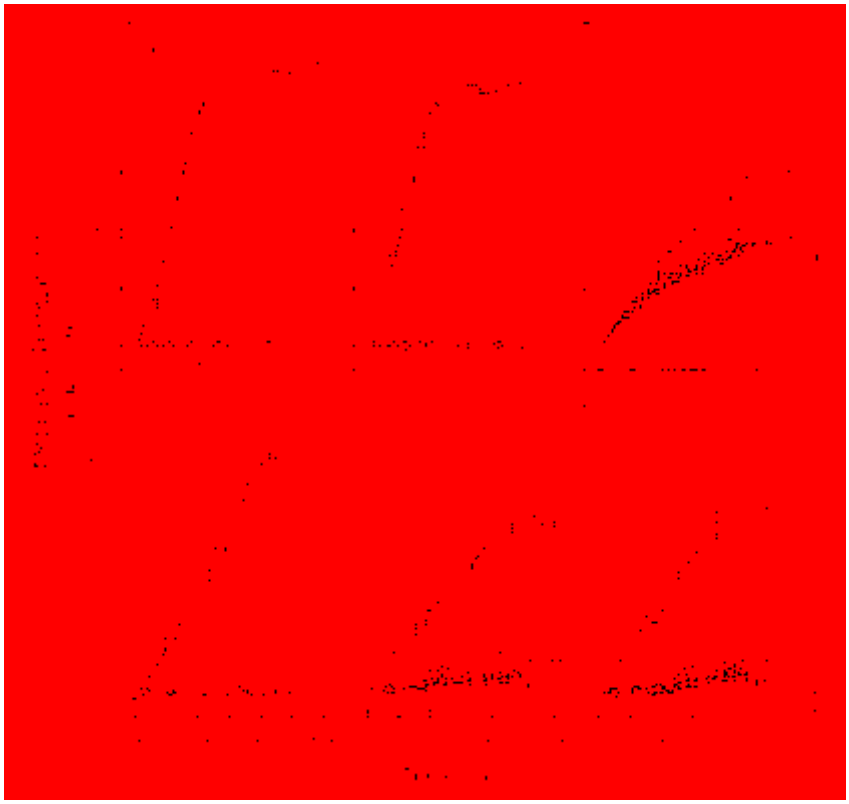

Figure 1.24 Amounts of metal cations (mol $\times 10^4$) transported into the receiving phase versus time (h) for competitive BLM transport of alkali metal cations (0.20 M in each) by 0.010 M 2 in (a) chloroform, (b) dichloromethane, (c) carbon tetrachloride, (d) 1,2-dichloroethane, (e) 1,1,1-trichloroethane, and (f) o-dichlorobenzene.[87]

A clever application of macrocycle selectivity in membrane separations was reported by Anzai et al., [88] who actually used complexation to prevent transport. Specifically, they described the separation of isomers of disubstituted benzenes (*o*-, *m*, and *p*-nitroaniline) by a poly(vinyl chloride) membrane based on cyclodextrin complexation. The source phase was the aqueous solution of guests and α-CD, the receiving phase was pure water, and the accumulation of guest in the receiving phase was quantified by HPLC. Without adding α-CD to the source phase, the concentration ratio of *o*-, *m*, and *p*-nitroaniline in the receiving phase was 1.4: 1.2: 1.0. After

adding 5×10^{-2} M α-CD to the source phase, the concentration ratio after 23 h was 44 : 14 : 1.0. No α-CD was detected in the receiving phase, implying that only the uncomplexed guests passed through the membrane. Consequently, they concluded that the order of the binding strength between α-CD and these isomers was *p*- > *m*- >*o*- nitroaniline.

While most liquid membrane separations involve hydrophobic membranes, it is possible to use an aqueous membrane to separate species between organic layers. For example, Armstrong *et al.*[89] reported the use of cyclodextrins as membrane carriers used to separate hydrophobic isomers. They found that cyclodextrin carriers can enhance, inhibit, or reverse the bulk membrane selectivity among different guests. For example, cyclodextrin carriers greatly enhance the transport of *p*-nitroaniline over the *o*- isomer. In the blank membranes containing no cyclodextrin carrier, *trans*-stilbene is favored over *cis*-; however, the transport of *cis*-isomer is greatly enhanced when cyclodextrin carriers were included in the membrane.

While much of the research using macrocycles in liquid membranes has focused on cation separations, anion separations are also an important field of study. Resorcinarenes provide a promising framework for constructing molecular anion carriers, given that the upper and lower rims can be modified with many functional groups. Lamb and coworkers have modified the upper rim of resorcinarene with aza-18-crown-6[90] or bis(pyridylmethyl)amine (BPA)[91] (Figure 1.25) and studied their anion separation capabilities in PIMs or BLMs. The focus was on the separation of ReO_4^-, a non-radioactive surrogate for pertechnetate, from other anions. Anion transport was studied using the Li^+, Na^+, K^+ and Pb^{2+} salts of anions in the source phase. The anions were co-transported through the membrane with the complexed cation in order to

maintain charge neutrality. The monomer undecyl-aza-18-crown-6 (ACU) was compared to the carrier performance of ACR to examine the effect of the preorganized anion-attractive cavity in the ACR molecule.[90] The selectivity of the carrier to anions depended on the type of counter cation. For example, K^+ or Na^+ or a mixture of these two cations facilitated greater transport of ClO_4^- and ReO_4^-, while Pb^{2+} promoted the transport of NO_3^-.

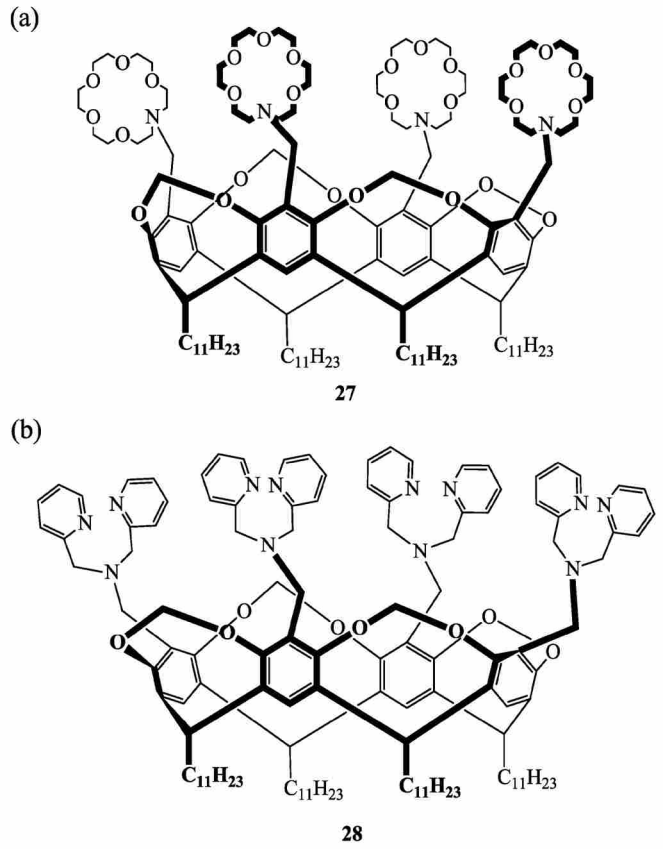

Figure 1.25 Structures of the resorcinarene derivatives. (a) aza-crown resorcinarene (ACR); (b) bis(pridylmethyl)amine resorcinarene (BPAR).[90, 91]

As described above, PIMs consist of a polymer network, a plasticizer liquid and a carrier. Typically, cellulose triacetate (CTA) is used as the polymer network and *o*-nitrophenyloctyl ether is used as plasticizer. However, depending on the solubility of the macrocyclic carrier, it may be

desirable to use an alternate plasticizer with different properties. Lamb's group studied the effect on separations of several alternate plasticizers such as ethyl benzoate (EB), 2-ethoxyethyl ester benzoic acid (EEB), dibutylphthalate (DBPT), ethyl phthalyl ethyl glycolate (EPEG), 2-nitrophenyl octyl ether (NPOE) and tris(2-butoxyethyl) phosphate (TBEP) using the resorcinarene-based carrier BPAR (shown in Figure 1.25). The nitrogen donors of BPA moiety make BPAR good coordination ligands for transition metals.[91] The transition metal (Cu^{2+}, Zn^{2+}, Fe^{3+}) complexes of BPAR were used as the carriers for anion transport through the membranes. The polarity and viscosity of the plasticizers play an important role in anion transport. More polar plasticizers stabilized anions in the solvents, thus promoting the partitioning of anions into the membrane, while higher viscosity inhibited the diffusion of anions and decreased transport. For example, halide transport decreased with decreasing polarity of the plasticizer, except in the case of the fairly polar EPEG, which has the highest viscosity.

Among cation separations using macrocyclic membrane carriers, an interesting potential application is the separation of Cs^+ from nuclear waste. ^{137}Cs is responsible for over 40% of the short-term radioactivity from many nuclear waste tank materials. In one novel study, self-assembly to form a macrocyclic structure was employed to effect selective transport of Cs^+ from a simulated nuclear waste mixture. Specifically, the Davis group showed that guanosine derivatives like the molecule 5'-(tert-butyldimethylsilyl)-2',3'-O-isopropylidene isoguanosine (isoG 1) (Figure 1.26a) can self-assemble to form a hydrogen bonded pentamer. (Figure 1.26b).[92]

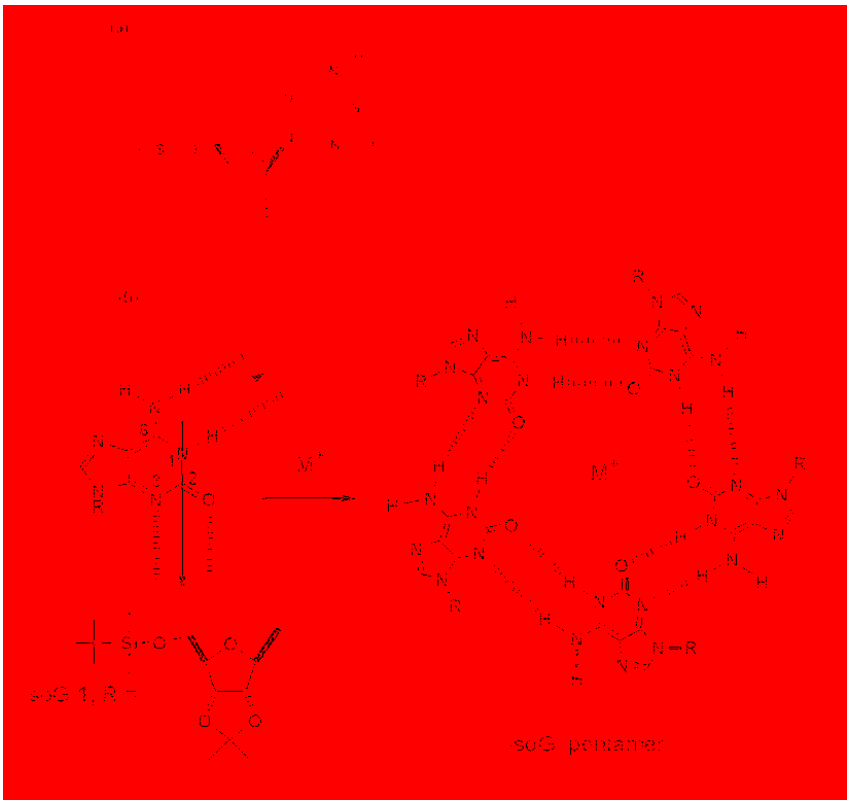

29

Figure 1.26 (a) Structure of isoG1. (b) Hydrogen bonding in the self-assembled pentamer.[93, 94]

Cai et al.[93] first reported the single crystal structure of the $(\text{isoG 1})_{10}Cs^{+}BPh_4^{-}$ complex (Figure 1. 27). In this complex, the Cs^{+} ion is sandwiched between two hydrogen bonded self-assembled isoG 1 pentamers. Lamb's group subsequently made PIMs and BLMs with isoG1 as carrier to examine its selectivity among alkali and alkaline metals. Excellent flux of Cs^{+} and selectivity over other alkali metal cations was observed.[94] In addition, an interesting carrier concentration effect was noticed. Specifically, if the self-assembled pentamer was pre-complexed with Cs^{+}, it performed as an effective Cs^{+} carrier at all concentrations; but if only isoG 1 monomer was added, with the expectation that it would spontaneously form the cyclic pentamer carrier, the expected flux of Cs^{+} was obtained only below a certain critical concentration. Above

that concentration, no flux was obtained, implying that cyclic pentamer was not forming but rather some other conglomerate which did not serve as a cation carrier. The selectivity of Cs^+ over Na^+ in the PIM reached nearly 10,000:1 with this carrier.

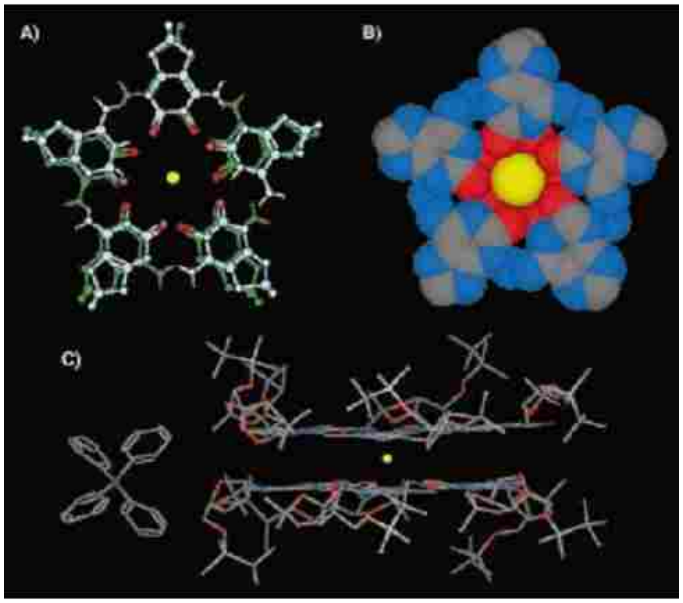

Figure 1.27 Crystal structures of $(isoG1)_{10}Cs^+BPh_4^-$ from top view, space-filling top view, and side view.[93]

Crown ethers have been modified with many substituent groups to provide specific separation functionalities in liquid membranes. In designing lipophilic carriers for membrane transport of saccharides, Smith's group bonded 3-(chloromethyl)benzo-15-crown-6 to a boronic acid group to design a crown boronic acid, which is the first example of an artificial heterotopic sodium saccharide co-transporter.[95] (Figure 1.28) Arylboronic acid was chosen for its strong Lewis acidity and lipophilicity. Transport of *p*-nitrophenyl β-D-glucopyranoside through the membrane was found to be pH dependent. At pH = 11.0, flux was about 3 times faster than at pH

= 6.3. Also, transport of the glucoside was about five times faster with the carrier than without. The glucoside was transported together with Na^+ to maintain electrical neutrality. Therefore, to increase the flux of glucoside, both the concentrations of glucoside and Na^+ can be increased.

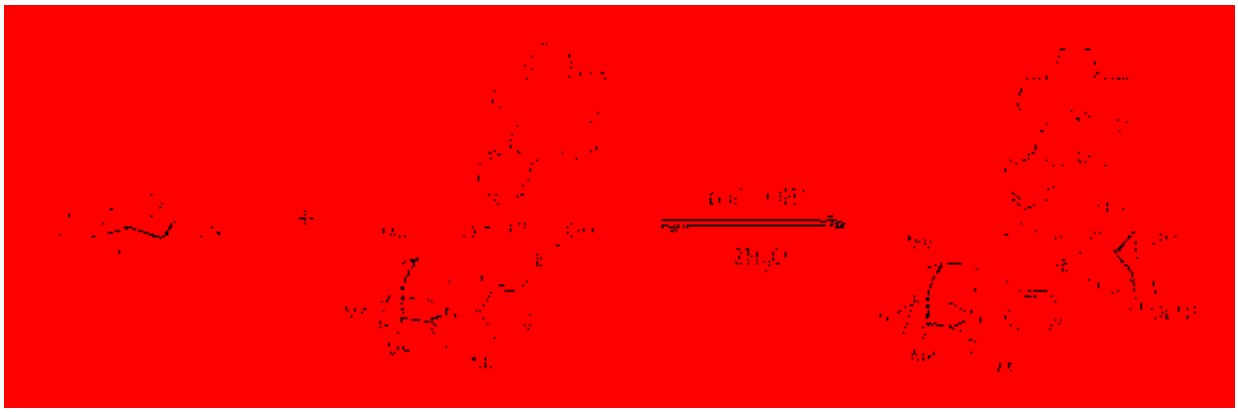

30

Figure 1.28 Cooperative transport of Na^+ and glucoside by a crown boronic acid carrier.[95]

Given that counterions must be extracted along with ions of interest into the membrane, efforts have been made to provide macrocyclic structures with the ability to associate directly with ions of both charges. Another example of a heterotopic receptor from Smith's group is shown in Figure 1.29.[96] This receptor contained an aza crown ring which was designed to include cations, while anions may be bound by hydrogen bonding to the amine group to maintain electrical neutrality. This receptor has similar selectivity to that of the monotopic receptor-dicyclohexano-

18-crown-6 among alkali metal ions ($K^+ > Na^+ > Li^+$); however, the flux obtained with this ditopic receptor was up to 10 times higher than with the monotopic receptor.

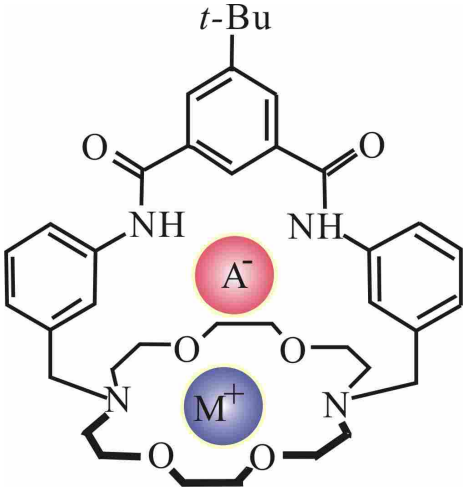

Figure 1.29 Cooperative inclusion of a cation and a anion in a heterotopic receptor.[96]

6. Conclusions

The host-guest selectivity of macrocyclic ligands as measured in homogeneous solution can translate effectively into multiphase separations systems such as ion chromatography and liquid membranes, even when macrocyclic structures must be modified to accommodate system demands. Separations scientists have applied this selectivity in novel ways to these two methodologies to effect separations which have potential or realized practical uses, both in analytical chemistry and preparative separations. To date, only a fraction of the macrocyclic structures which exhibit such potential have been studied, and to the degree that this line of research is pursued vigorously, many further innovations can be expected.

References:

1. James, L. K. Nobel Laureates in Chemistry 1901-1992, Merck & Co., Inc. U.S., 1993, 708-714.

2. Data from Scifinder Scholar, a database of chemical abstracts service (CAS) of American Chemical Society.

3. Lamb, J. D.; Gardner, J. S. Macrocyclic Chemistry: Current Trends and Future Perspectives, Gloe, K. (Ed) Springer, Netherlands, 2005, 349-363.

4. Major, J. L.; Boiteau, R. M.; Meade, T. J. Mechanisms of Zn^{II}-Activated Magnetic Resonance Imaging Agents. *Inorg. Chem.* **2008**, *47*, 10788-10795.

5. Lam, O. P.; Feng, P. L.; Heinemann, F. W.; O'Connor, J. M.; Meyer, K. Charge-Separation in Uranium Diazomethane Complexes Leading to C−H Activation and Chemical Transformation. *J. Am. Chem. Soc.* **2008**, *130*, 2806-2816.

6. Steed, J. W. First- and second-sphere coordination chemistry of alkali metal crown ether complexes. *Coord. Chem. Rev.* **2001**, *215*, 171-221.

7. Lamb, J. D.; Izatt, R. M.; Christensen, J. J.; Eatough, D. J. Coordination Chemistry of Macrocyclic Compounds, G. A. Melson (Ed), Plenum Press, New York and London, **1979**, 145-217.

8. Lamb, J. D.; Izatt, R. M.; Swain, C. S.; Christensen, J. J. A systematic study of the effect of macrocycle ring size and donor atom type on the logK .DELTA.H. and T.DELTA.S of reactions at 25.degree.C in methanol of mono- and divalent cations with crown ethers. *J. Am. Chem. Soc.* **1980**, *102*, 475-479.

9. Zhang, X. X.; Izatt, R. M.; Bradshaw, J. S.; Krakowiak, K. E. Approaches to improvement of metal ion selectivity by cryptands. *Coord. Chem. Rev.* **1998**, *174*, 179-189.

10. Lehn, J. M.; Sauvage, J. P. Cryptates. XVI. [2]-cryptates. Stability and selectivity of

alkali and alkaline-earth macrobicyclic complexes. *J. Am. Chem. Soc.* **1975**, *97*, 6700-6707.

11. Masci, B.; Thuéry, P. Versatility of {M(30-crown-10)}(M=K^+, Ba^{2+}) as a guest in UO_2^{2+} complexes of [3.1.3.1]- and [3.3.3]homooxacalixarenes. CrystEng. *Comm.* **2007**, *9*, 582-590.

12. Hope, H.; Olmstead, M. M.; Power, P. P.; Xu, X. J. X-ray crystal structures of the diphenylphosphide and arsenide anions: use of a crown ether to effect complete metal cation and organometalloid anion separation. *J. Am. Chem. Soc.* **1984**, *106*, 819-821.

13. Ungaro, R.; Casnati, A.; Ugozzoli, F.; Pochini, A.; Dozol, J.; Hill, C.; Rouquette, H. 1,3-Dialkoxycalix[4]arenecrowns-6 in 1,3-alternate conformation: cesium-selective ligands that exploit cation-arene interactions. *Angew. Chem. Int. Ed*. **1994**, *33*, 1506-1509.

14. Solov'ev, V. P.; Strakhova, N. N.; Kazachenko, V. P.; Solotnov, A. F.; Baulin, V. E.; Raevsky, O. A.; Rüdiger, V.; Eblinger, F.; Schneider, H. Steric and stereoelectronic effects in Aza crown ether complexes. *Eur. J. Org. Chem.* **1998**, *7*, 1379-1389.

15. Thaler, A.; Cox, B. G.; Schneider, H. Stability constants of aza-oxa-crown ether complexes with silver (I) in nonaqueous polar solvents. *Inorg. Chim. Acta* **2003**, *351*, 123-132.

16. Kodama, M.; Kimura, E.; Yamaguchi, S. *Dalton Trans.* **1980**, *12*, 2536-2538.

17. Monsef, Z.; Rounaghi, G.; Sarafraz, A. A polarographic study of Tl^+, Pb^{2+} and Cd^{2+} complexes with aza-18-crown-6 and dibenzopyridino-18-crown-6 in some binary mixed non-aqueous solvents. *J. Inclusion Phenom. Macrocyclic Chem.* **2001**, *39*, 321-325.

18. Shchori, E.; Jagur-Grodzinski, J. Conductomeric study of complexation of macrocyclic polyethers with sodium salts. *Isr. J. Chem.* **1973**, *11*, 243-253.

19. Chi, K. W.; Shim, K. T.; Huh, H.; Lee, U.; Park, Y. Diaza-18-crown-6 ethers containing partially-fluorinated benzyl side arms: effects of covalently bonded fluorine on the alkali metal complexation. J. *Bull. Korean Chem. Soc.* **2005**, *26*, 393-398.

20. Stark, P. C.; Huff, M.; Babaian, E. A.; Barden, L. M.; Hrncir, D. C.; Bott, S. G.; Atwood, J. L. Indium-based liquid clathrates. II. Inclusion compounds derived from salts of the tetrachloroindate anion, $InCl_4^-$, and the crystal structure of [Li.15-c-5][$In(CH_3)_3Cl$](15-c-5=15-crown-5). *J. Inclusion Phenom. Macrocyclic Chem.* **1987**, *5*, 683-688.

21. Watson, K. A.; Fortier, S.; Murchie, M. P.; Bovenkamp, J. W.; Rodrigue, A.; Buchanan, G. W.; Ratcliffe, C. I. Synthesis, NMR spectroscopy, and crystal structure of the 1:2 host : guest complex of 18-crown-6 with lithium phenoxide. *Can. J. Chem.* **1990**, *68*, 1201-1207.

22. Antsyshkina, A. S.; Sadikov, G. G.; Porai-Koshits, M. A.; Konoplev, V. N.; Silina, T. A.; Sizareva, A. S. Crystal and molecular structure of $2LiBH_4$**.**18-crown-6. *Russ. J. Coord. Chem*. **1994**, *20*, 274-278.

23. Izatt, R. M.; Terry, R. E.; Haymore, B. L., Hansen, L. D.; Dalley, N. K.; Avondet, A. G.; Christensen, J. J. Calorimetric titration study of the interaction of several uni- and bivalent cations with 15-crown-5, 18-crown-6, and two isomers of dicyclohexo-18-crown-6 in aqueous solution at 25.degree.C and .mu. = 0.1. *J. Am. Chem. Soc.* **1976**, *98*, 7620-7626.

24. Ohtsu, K.; Kawashima, T.; Ozutsumi, K. Thermodynamics of complexation of sodium, potassium, rubidium, cesium and ammonium ions with 18-crown-6 in acetonitrile and propylene carbonate. *J. Chem. Soc., Faraday Trans.* **1995**, *91*, 4375-4380.

25. Danil de Namor, A. F.; Zapata-Ormachea, M. L.; Jafou, O.; Rawi, N. A. Thermodynamics

of alkali-metal cations and macrocycles (18-crown-6, ethyl *p-tert*-butylcalix(6)arenehexanoate, cryptand 222) in solution and in the solid state. *J. Phys. Chem. B* **1997**, *101*, 6772-6779.

26. Katsuta, S.; Tachibana, H.; Takeda, Y. Stability in water of alkali metal ion complexes with dibenzo-24-crown-8 and dibenzo-18-crown-6 and their transfer activity coefficients from water to nonaqueous solvents. *J. Solution Chem.* **2002**, *31*, 499-510.

27. Arnett, E. M.; Moriarity, T. C. Heats of complexing of alkali metal ions with a crown ether in aprotic solvents. *J. Am. Chem. Soc.* **1971**, *93*, 4908-4910.

28. Haddad, P. R. Peer reviewed: ion chromatography restrospective. *Anal. Chem*. **2001**, *73*, 266A-273A.

29. Small, H.; Stevens, T. S.; Bauman, W. C. Novel ion exchange chromatographic method using conductimetric detection. *Anal. Chem*. **1975**, *47*, 1801-1809.

30. Atkins, P.; Paula, J. De. Atkins' Physical Chemistry, Oxford University Press, Seventh edition, 2002.

31. Small, H. Ion Chromatography, Plenum Press, New York and London, 1989.

32. Haddad, P. R.; Jandik, P. Ion Chromatography, ed, J. G. Tarter, Marcel Dekker, Inc., New York and Basel, 1987, 87-156.

33. Haddad, P. R.; Foley, R. C. Aromatic bases as eluent components fro conductivity and indirect ultraviolet absorption detection of inorganic cations in nonsuppressed ion chromatography. *Anal. Chem.* **1989**, *61*, 1435-1441.

34. Weiss, J.; Jensen, D. modern stationary phases for ion chromatography. *Anal. Bioanal.*

Chem. **2003**, *375*, 81-98.

35. Sarzanini, C. Recent developments in ion chromatography. *J. Chromatogr. A* **2002**, *956*, 3-13.

36. Haddad, P. R.; Nesterenko, P. N.; Buchberger, W. Recent developments and emerging directions in ion chromatography. *J. Chromatogr. A* **2008**, *1184,* 456-473.

37. Gjerde, D. T.; Fritz, J. S.; Schmuckler, G. Anion chromatography with low-conductivity eluents. *J. Chromatogr.* **1979**, *186*, 509-519.

38. Karim, K. J. B. A.; Jin, J. Y.; Takeuchi, T. Simultaneous separation of inorganic anions and cations by using anion-exchange and cation-exchange connected in tandem in ion chromatography. *J. Chromatogr. A* **2003**, *995*, 153-160.

39. Mullins, F. G. P. Determination of inorganic anions by non-suppressed ion chromatography with indirect ultraviolet absorption detection. *Analyst* **1987**, *112*, 665-671.

40. Hayakawa, K.; Sawada, T.; Shimbo, K.; Miyazaki, M. Effect of (ethylenediaminetetraacetato)copper(II) and bis(ethylenediamine)copper(II) eluents on nonsuppressed ion chromatography by indirect photometric detection. *Anal. Chem.* **1987**, *59*, 2241-2245.

41. Paull, B.; Nesterenko, P. N. Novel ion chromatographic stationary phases for the analysis of complex matrices. *Analyst* **2005**, *130*, 134-146.

42. Hatsis, P.; Lucy, C. A. Improved sensitivity and characterization of high-speed ion chromatography of inorganic anions. *Anal. Chem.* **2003**, *75*, 995-1001.

43. Zakaria, P.; Hutchinson, J. P.; Avdalovic, N.; Liu, Y.; Haddad, P. R. Latex-coated

polymeric monolithic ion-exchange stationary phases. 2. Micro-ion chromatography. *Anal. Chem.* **2005**, *77*, 417-423.

44. Chambers, S. D.; Glenn, K. M.; Lucy, C. A. Developments in ion chromatography using monolithic columns. *J. Sep. Sci.* **2007**, *30*, 1628-1645.

45. Nordborg, A.; Hilder, E. F. Recent advances in polymer monoliths for ion-exchange chromatography. *Anal. Bioanal. Chem.* **2009**, *394*, 71-84.

46. Haddad, P. R. Ion chromatography. *Anal. Bioanal. Chem.* **2004**, *379*, 341-343.

47. Dorsey, J. G.; Cooper, W. T.; Siles, B. A.; Foley, J. P.; Barth, H. G. Liquid chromatography: theory and methodology. *Anal. Chem.* **1998**, *70*, 591R-644R.

48. Hajos, P.; Revesz, G.; Horvath, O.; Peear, J.; Sarzanini, C. The simultaneous analysis of metal-EDTA complexes and inorganic anions by suppressed ion chromatography. *J. Chromatogr. Sci.* **1996**, *34*, 291-299.

49. Divjak, B.; Novič, M.; Goessler, W. Determination of bromide, bromate and other anions with ion chromatography and an inductively coupled plasma mass spectrometer as element-specific detector. *J. Chromatogr. A* **1999**, *862*, 39-47.

50. Dotsevi, G.; Sogah, Y.; Cram, D. J. Total chromatographic optical resolutions of .alpha.-amino acid and ester salts through chiral recognition by a host covalently bound to polystyrene resin. *J. Am. Chem. Soc.* **1976**, *98*, 3038-3041.

51. Kimura, K.; Harino, H.; Hayata, E.; Shono, T. Liquid chromatography of alkali and alkaline-earth metal ions using octadecylsilanized silica columns modified in situ with lipophilic crown ethers. *Anal. Chem.* 1**986**, *58*, 2233-2237.

52. Lamb, J. D.; Smith, R. G.; Jagodzinski, J. Anion chromatography with a crown ether-based stationary phase and an organic modifier in the eluent. *J. Chromatogr. A* **1993**, *640*, 33-40.

53. Edwards, B. R.; Giauque, A. P.; Lamb, J. D. Macrocyle-based column for the separation of inorganic cations by ion chromatography. *J. Chromatogr. A* **1995**, *706*, 69-79.

54. Xu, Q.; Mori, M.; Tanaka, K.; Hu, W. Z.; Haddad, P. R. Ion chromatographic separation of hydrogen ion and other common mono-and divalent cations. *J. Chromatogr. A* **2004**, *1023*, 239-245.

55. Rey, M. A.; Pohl, C. A.; Jagodzinski, J. J.; Kaiser, E. Q.; Riviello, J. M. A new approach to dealing with high-to-low concentration ratios of sodium and ammonium ions in ion chromatography. *J. Chromatogr. A* **1998**, *804*, 201-209.

56. Blasius, E.; Janzen, K. P. Preparation and application of polymers with cyclic polyether anchor groups. *Pure Appl. Chem.* **1982**, *54*, 2115-2128.

57. Nakajima, M.; Kimura, K.; Shono, T. Liquid chromatography of alkali and alkaline earth metal salts on poly(benzo-15-crown-5)- and bis(benzo-15-crown-5)-modified silicas. *Anal. Chem.* **1983**, *55*, 463-467.

58. Bruzzoniti, M. C.; De Carlo, R. M.; Fungi, M. Simultaneous determination of alkali, alkaline earths and ammonium in natural waters by ion chromatography. *J. Sep. Sci.* **2008**, *31*, 3182-3189.

59. Dumont, P. J.; Fritz, J. S. Ion chromatographic separation of alkali metals in organic solvents. *J. Chromatogr. A* **1995**, *706*, 149-158.

60. Richens, D. A.; Simpson, D.; Peterson, S.; McGinn, A.; Lamb, J. D. Use of mobile phase 18-crown-6 to improve peak resolution between mono-divalent metal and amine cations in ion chromatography. *J. Chromatogr. A* 2003, **1016**, 155-164.

61. Jane Y. S.; Shih, J. S. Application of crown ether coated piezoelectric crystal as a detector for ion chromatography. *Analyst* **1995**, *120*, 517-522.

62. Lamb, J. D.; Drake, P.A.; Woolley, K. E. Advances in Ion Chromatography, Vol. 2, Century International, P. Jandik, and R.M. Cassidy (Eds), Franklin, MA, 1990, pp. 215.

63. Woodruff, A.; Pohl, C. A.; Bordunov, A.; Avdalovic, N. Adjustable-capacity anion-exchange separator. *J. Chromatogr. A* **2002**, *956*, 35-41.

64. Bruzzoniti, M. C.; De Carlo, R. M.; Horvath, K.; Perrachon, D.; Prelle, A.; Tófalvi, R.; Sarzanini, C.; Hajós, P. High performance ion chromatography of haloacetic acids on macrocyclic cryptand anion exchanger. *J. Chromatogr. A* **2008**, *1187*, 188-196.

65. Limtiaco, J. F. K.; Jones C. J.; Larive, C. K. Characterization of heparin impurities with HPLC-NMR using weak anion exchange chromatography. *Anal. Chem.* **2009**, *81*, 10116-10123.

66. Abballe, F.; Lombardi, A.; Maccone, I.; Palazzo, G.; Severoni, A.; Travaini, S.; Venturini, A. New method for low molecular weight heparin quantification in tablets by suppressed conductivity detection and cryptand column. *J. Pharm. Biomed. Anal.* **2008**, *48*, 467-471.

67. Lamb, J. D.; Simpson, D.; Jensen, B. D.; Gardner, J. S.; Peterson, Q. P. Determination of perchlorate in drinking water by ion chromatography using macrocycle-based concentration and separation methods. *J. Chromatogr. A* **2006**, *1118*, 100-105.

68. Lin, R.; De Borba, B.; Srinivasan, K.; Woodruff, A.; Pohl, C. A. Matrix diversion methods for improved analysis of perchlorate by suppressed ion chromatography and conductivity detection. *Anal. Chim. Acta* **2006**, *567*, 135-142.

69. Wagner, H. P.; Pepich, B. V.; Pohl, C. A.; Later, D.; Joyce, R.; Srinivasan, K.; Thomas, D.; Woodruff, A.; De Borba, B.; Munch, D. J. US Environmental Protection Agency Method 314.1, an automated sample preconcentration/matrix elimination suppressed conductivity method for the analysis of trace levels (0.50 μg/L) of perchlorate in drinking water. *J. Chromatogr. A* **2006**, *1118*, 85-93.

70. Haddad, P. R.; Doble, P.; Macka, M. Developments in sample preparation and separation techniques for the determination of inorganic ions by ion chromatography and capillary electrophoresis. *J. Chromatogr. A* **1999**, *856*, 145-177.

71. Arena, G.; Contino, A.; Longo, E.; Sciotto, D.; Spoto, G.; Torrisi, A. Two Calix-Crown Based Stationary Phases. Synthesis, Chromatographic Performance and X-ray Photoelectron Spectroscopy Investigation. *J. Supramol. Chem.* **2002**, *2*, 521-531.

72. Wang, J.; Harrison, R. G.; Lamb, J. D. Anion separation and preconcentration with cyclen and cyclen-resorcinarene derivatives. *J. Chromatogr. Sci.* **2009**, *47*, 510-515.

73. Thuaud, N.; Sébille, B.; Deratani, A.; Pöpping, B.; Pellet, C. Enantiomer separations with chromatographic supports based on β-cyclodextrin polymers immobilized on porous silica. Role of the polymer structure in separating ability. *Chromatographia* **1993**, *36*, 373-380.

74. Wößner M.; Ballschmiter, K. New stationary phase based on β-cyclodextrin for normal-phase HPLC group separation of organic nitrates. *Fresenius J. Anal. Chem*. **2000**, *366*, 346-

351.

75. Pullen, R. H.; Brennan, J. J.; Patonay, G. Chiral separation retention mechanisms in high-performance liquid chromatography using bare silica stationary phase and β-cyclodextrin as a mobile phase additive. *J. Chromatogr. A* **1995**, *691*, 187-193.

76. Kitamaki, Y.; Takeuchi, T. Cyclodextrin-aided determination of lodate and bromated in drinking water by microcolumn ion chromatography with precolumn enrichment. *Anal. Sci.* **2004**, *20*, 1399-1402.

77. Kitamaki, Y.; Jin, J. Y.; Takeuchi, T. Determination of inorganic anions via postcolumn reaction with iodide in ion chromatography. *J. Pharm. Biomed. Anal.* **2003**, *30*, 1751-1757.

78. Strathmann, H. Membrane separation processes: current relevance and future opportunities. *AIChE j.* **2001**, *47*, 1077-1087.

79. San Román, M. F.; Bringas, E.; Ibañez, R.; Ortiz, I. Liquid membrane technology: fundamentals and review its application. *J. Chem. Technol. Biotechnol.* **2010**, *85*, 2-10.

80. Izatt, R. M.; Lindh, G. C.; Bruening, R. L.; Bradshaw, J. S.; Lamb, J. D.; Christensen, J. J. Design of cation selectivity into liquid membrane systems using macrocyclic carriers. *Pure Appl. Chem.*, **1986**, *58*, 1453-1460.

81. Christensen, J. J.; Lamb, J. D.; Izatt, S. R.; Starr, S. E.; Weed, G. C.; Astin, M. S.; Stitt, B. D.; Izatt, R. M. Effect of anion type on rate of facilitated transport of cations across liquid membranes via neutral macrocyclic carriers. *J. Am. Chem. Soc.*, **1978**, *100*, 3219-3220.

82. Arena, G.; Contino, A.; Magri, A.; Sciotto, D.; Lamb, J. D. Selective transport of cesium and strontium ions through polymer inclusion membranes containing calixarenes as carriers.

Supramol. Chem. **1998**, *10*, 5-15.

83. Levitskaia, T. G.; Lamb, J. D.; Fox, K. L.; Moyer, B. A. Selective carrier-mediated cesium transport through polymer inclusion membranes by calix[4]arene-crown-6 carriers from complex aqueous mixtures. *Radiochim. Acta* **2002**, *90*, 43-52.

84. Walkowiak, W.; Kozlowski, C. A. Macrocycle carriers for separation of metal ions in liquid membrane processes—a review. *Desalination* **2009**, *240*, 186-197.

85. Mutihac, L. Functionalized Calix[n]arenes as Membrane Transporters for Biological Compounds. A Mini review**.** *Curr. Drug Discovery Technol.* **2008**, *5*, 98-104(7).

86. Bartsch, R. A.; Jeon, E. G.; Walkowiak, W.; Apostoluk, W. Effect of solvent in competitive alkali metal cation transport across bulk liquid membranes by a lipophilic lariat ether carboxylic acid carrier. *J. Membr. Sci.* **1999**, *159*, 123-131.

87. Bartsch, R. A.; Dalley, N. K.; Talanov, V. S.; Purkiss, D. W.; Vogel, H. F. Structures of *sym*-(R)dibenzo-16-crown-5-oxyacetic acids and their alkali metal cation binding. *Tetrahedron* **2005**, *61*, 8351-8357.

88. Anzai, J.; Kobayashi, Y.; Ueno, A.; Osa, T. Selective transport of benzene derivatives through a poly(vinyl chloride) membrane based on cyclodextrin complexation. *J. Chem. Soc., Chem. Commun.* **1985**, *15*, 1023-1024.

89. Armstrong, D. W.; Jin, H. L. Enrichment of enantiomers and other isomers with aqueous liquid membranes containing cyclodextrin carriers. *Anal. Chem.*, **1987**, *59*, 2237-2241.

90. Lamb, J. D.; Morris, C. A.; West, J. N.; Morris, K. T.; Harrison, R. G. Cation effect on anion separations by aza-crown ligands in liquid membranes. *J. Membr. Sci.* **2008**, *321*, 15-

21.

91. Gardner, J. S.; Peterson, Q. P.; Walker, J. O.; Jensen, B. D.; Adhikary, B.; Harrison, R. G.; Lamb, J. D. Anion transport through polymer inclusion membranes facilitated by transition metal containing carriers. *J. Membr. Sci.* **2006**, *277*, 165-176.

92. Davis, J. T.; Tirumala, S.; Marlow, A. L. A self-assembled ionophore eith remarkable Cs^+ selectivity. *J. Am. Chem. Soc.* **1997**, *119*, 5271-5272.

93. Cai, M.; Marlow, A. L.; Fettinger, J. C.; Fabris, D.; Haverlock, T. J.; Moyer, B. A.; Davis, J. T. The localization of guests in water-soluble oligoethyleneoxy-modified poly(propylene imine) dendrimers. *Angew. Chem. Int. Ed.* **2000**, *39*, 1283-1285.

94. Lee, S. C.; Lamb, J. D.; Cai, M.; Davis, J. T. Cs^+ and Ba^{2+} Selective Transport by a Novel Self-Assembled Isoguanosine Ionophore Through Polymer Inclusion and Bulk Liquid Membranes. *J. Inclusion Phenom. Macrocyclic Chem.* **2001**, *40*, 51-57.

95. Bien, J. T.; Shang, M. Y.; Smith, B. D. Modification of a boronic acid cleft produces a sodium-saccharide cotransporter. *J. Org. Chem*. **1995**, *60*, 2147-2152.

96. Mahoney, J. M.; Nawaratna, G. U.; Beatty, A. M.; Duggan, P. J.; Smith, B. D. Transport of alkali halides through a liquid organic membrane containing a ditopic salt-binding receptor. *Inorg. Chem.* **2004**, *43*, 5902-5907.

Chapter 2 Application of Resorcinarene Derivatives in Chemical Separations

Abstract[2]

The applications of resorcinarene derivatives in modern separation techniques including high performance liquid chromatography (HPLC), gas chromatography (GC), capillary electrophoresis (CE), ion chromatrography (IC), and liquid membranes are reviewed in this paper. Resorcinarene are macrocyclic molecules which can be modified with various substituents on upper and lower rims to provide specific functionality and selectivity. The derivatives can be adsorbed or covalently bound to the stationary phase of HPLC, GC, and IC, or used as pseudo-stationary phase in CE to separate organic or inorganic species. In liquid membranes, they have been tested as carriers in bulk liquid membranes (BLMs), support liquid membranes (SLMs), and polymer inclusion membranes (PIMs) to selectively transfer species from source phase to receiving phase. These broad applications of resorcinarene-based macrocycles indicate that they are a promising class of compounds to synthesize and are worthwhile to be explored in both synthesis and separation applications.

1. Introduction

The products of resorcinol-aldehyde condensation reactions have found industrial application since the 1930's. For example, they have been used as adhesives or formulated to

[2] Li, N. Harrison, R. G.; Lamb, J. D. Review for *J. Inclusion Phenom. Macrocyclic Chem.* **2013**.

penetrate into textiles to improve resistance to crushing or wrinkling.[1] However, the structures of these compounds were difficult to establish since variable amounts of water were incorporated into the crystals and limited techniques were available at that time.[2] It was assumed that these products were low molecular weight compounds of acetal, diphenylalkane, or vinyl-resorcinols. In 1940, Joseph B. Niederl and Heinz J. Vogel first used elemental analysis to establish that the reaction product of resorcinol and acetaldehyde was a cyclic tetramer.[2] A. G. Sverker Högberg and coworkers later in the 1980s reinvestigated the condensation reaction of resorcinol with several aldehydes, including benzaldehyde, p-bromobenzaldehyde, and acetaldehyde in acidic solutions. They found that the acid-catalyzed condensation reaction produced two cyclic tetramers with different conformations.[3-5] The two isomers displayed identical infrared and mass spectra; however, the melting points, R_f values from TLC plates, and ^{1}H NMR spectra were different. In one isomer, the ^{1}H NMR spectrum in hexachlorobutadiene solution was well-resolved at 28^{o}C and showed no change when heated to 180 ^{o}C. The other isomer showed a similar NMR spectrum under low temperatures; however, the NMR signals collapsed into broad peaks at 28^{o}C which indicated rotational barriers in this isomer. The structure and molecular models of resorcinarene are shown in Figure 2.1.

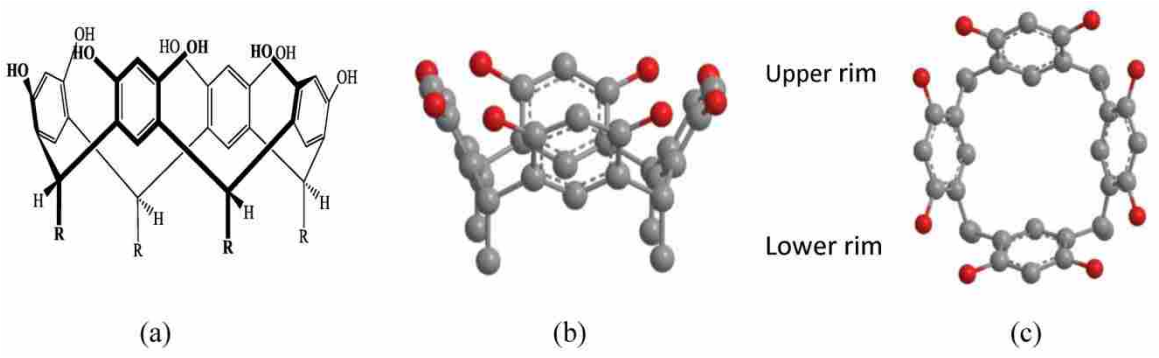

Figure 2.1 (a) Structure of resorcinarene; molecular models of resorcinarene (b) side view; (c) top view.

As a result of these early efforts, resorcinarene derivatives have interested chemists because of the wide range of ring sizes available and the variety of functional groups with which the molecules may be derivatized. The many possible structural variations lead to potential applications as nanoscale reaction containers, supramolecular recognition agents, chiral NMR solvating agents, catalysts, chromatographic separation exchange sites, and agents for drug encapsulation, protection, and delivery.[6-11] For example, typical structures of resorcinarene derivatives used as catalysts and chiral NMR solvating agents are shown in Figure 2.2.

In another application area, namely catalysis, resorcinarene derivatives have been applied to reactions such as the Heck reaction, Mannich-type reactions, aminolysis of a choline derivative, and C-H oxidation.[12-18] In one such case, Simizu et al. [13,15] synthesized a water soluble resorcinarene derivative to use as a catalyst for the Mannich-type reaction shown in Scheme 2.1. The yield without catalyst after reacting 8 hours was 5%, but this was increased to 89% after 3 hours when 10 mol% of catalyst was used. The catalyst was then recovered and

reused. After recovering the resorcinarene-based catalyst five times, a yield of 81% was achieved after reacting eight hours.

In supramolecular chemistry, resorcinarene derivatives have demonstrated particular promise. For example, Wenzel et al.[8,19] synthesized water-soluble resorcinarenes containing chiral amino acids on the upper rim and sulfonic groups on the lower rim. The sulfonic groups on the lower rim improve the solubility of resorcinarenes in water, which enhances the potential for small, hydrophobic chiral molecules to be sequested in the hydrophobic cavity of the host. One derivative with chiral hydroxyproline on the upper rim showed effective chiral discrimination for enantiomers of pyridyl, phenyl, and bicyclic aromatic compounds. The enantiomers exhibited two sets of distinct chemical shifts in the NMR spectra when the resorcinarene-based chiral solvating agents were present in the solution. Rebek et al.[20] introduced fluorenylmethyloxycarbonyl (Fmoc) protected chiral alanine chlorides on the upper rim of a deepened resorcinarene to create a hydrophobic pocket with a chiral opening. Two sets of upfield NMR signals corresponding to the diastereometic complexes of (+)- and (-)- pinanediol were observed clearly. These examples demonstrate the feasibility of creating asymmetric resorcinarene-based cavitands by introducing chiral substituent groups for chiral discrimination.[20]

Compared with the broad application of other macrocyclic ligands such as calixarenes[21] and crown ethers[22] to chemical separations, the use of resorcinarene derivatives is still in its infancy. However, preliminary studies imply that resorcinarenes and their derivatives offer significant promise in this area as well. In this paper, we review the present state of the art in

applying resorcinarenes to separation techniques including high performance liquid chromatography (HPLC), gas chromatography (GC), electrokinetic chromatography (EKC), capillary electrophoresis (CE), and liquid membranes for the separation of a variety of organic and inorganic species, including chiral species.

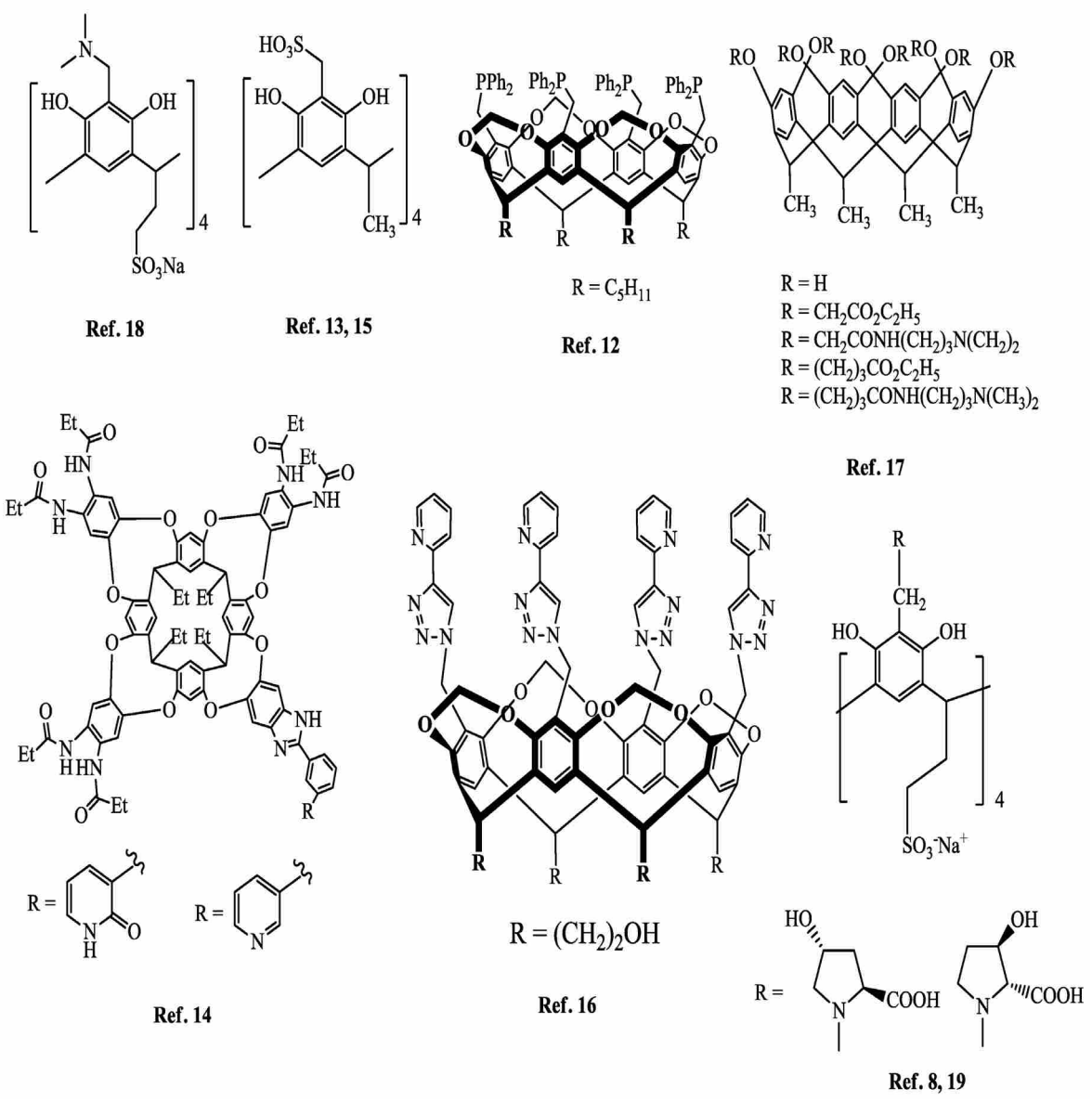

Figure 2.2 Structures of resorcinarenes applied as catalysts and chiral discrimination reagents.

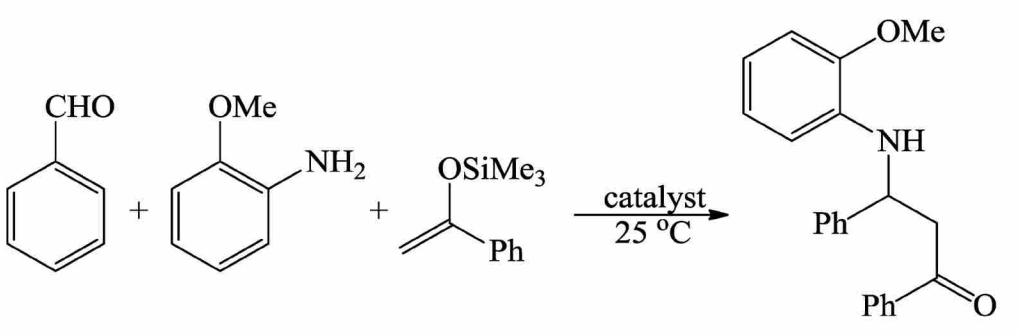

Scheme 2.1 Resorcinarene derivative used as catalyst in Mannich-type reactions.[13,15]

2. High Performance Liquid Chromatography (HPLC)

Resorcinarene derivatives have been applied as stationary[23-28] and mobile phases[29] in HPLC. Resorcinarenes used as stationary phases in HPLC can be divided into two types: (1) the lower rim of the resorcinarene covalently bonded to silica particles; (2) the lower rim modified with long alkyl chains for effective adsorption onto polystyrene resin beads. In either case, the upper rim of the resorcinarene may or may not be modified with various functional groups for specific separation purposes. Although adding resorcinarene derivatives to the mobile phase might be an option to provide specific selectivity for analytes, certain factors limit their application including solubility, UV absorptivity, cost, and toxicity.

In one example, Pietraszkiewicz et al.[23-26] modified the resorcinarene lower rim with four $–C_{11}H_{23}$ alkyl chains to increase the hydrophobicity of the ligand, while leaving the upper rim unchanged (Figure 2.3). The resulting C-tetra-*n*-undecylcalix[4]resorcinarene was dissolved in acetonitrile and passed through a reverse phase C18 (RP-18) column to coat the surface of the column, as shown in Figure 2.3. The column showed good stability during extensive use in five

months even when 40% methanol was added to the aqueous mobile phase. Figure 2.4 compares the separation of three pyrimidine bases on untreated and treated columns. Better resolution was obtained between the three analytes using the treated RP-18 column using phosphoric acid (Figure 2.4b) and or pure water (Figure 2.4c) as eluents. Protonation of the pyrimidine bases by the hydroxyl groups of the resorcinarene and hydrogen bonding between the resorcinarene and analytes were cited as two main contributors to the retention of these bases on the treated column. In Figure 2.4(c), the elution order changed from cytosine = uracil > thymine on the untreated column to uracil > thymine > cytosine on the treated column. This phenomenon was attributed to the higher basicity of cytosine compared to the other two bases in deprotonating the hydroxyl groups of resorcinarene, which in turn results in stronger electrostatic attraction between the two.

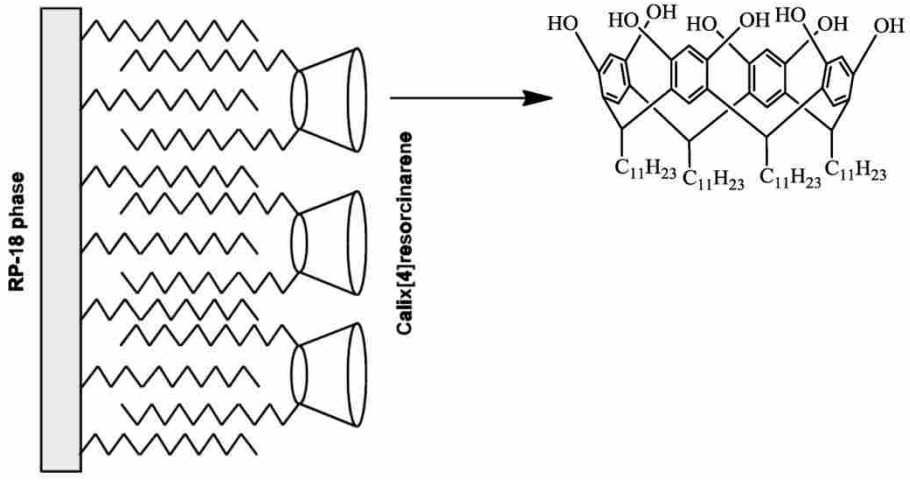

Figure 2.3 C-tetra-*n*-undecylcalix[4]resorcinarene coated RP-18 stationary phase.[23]

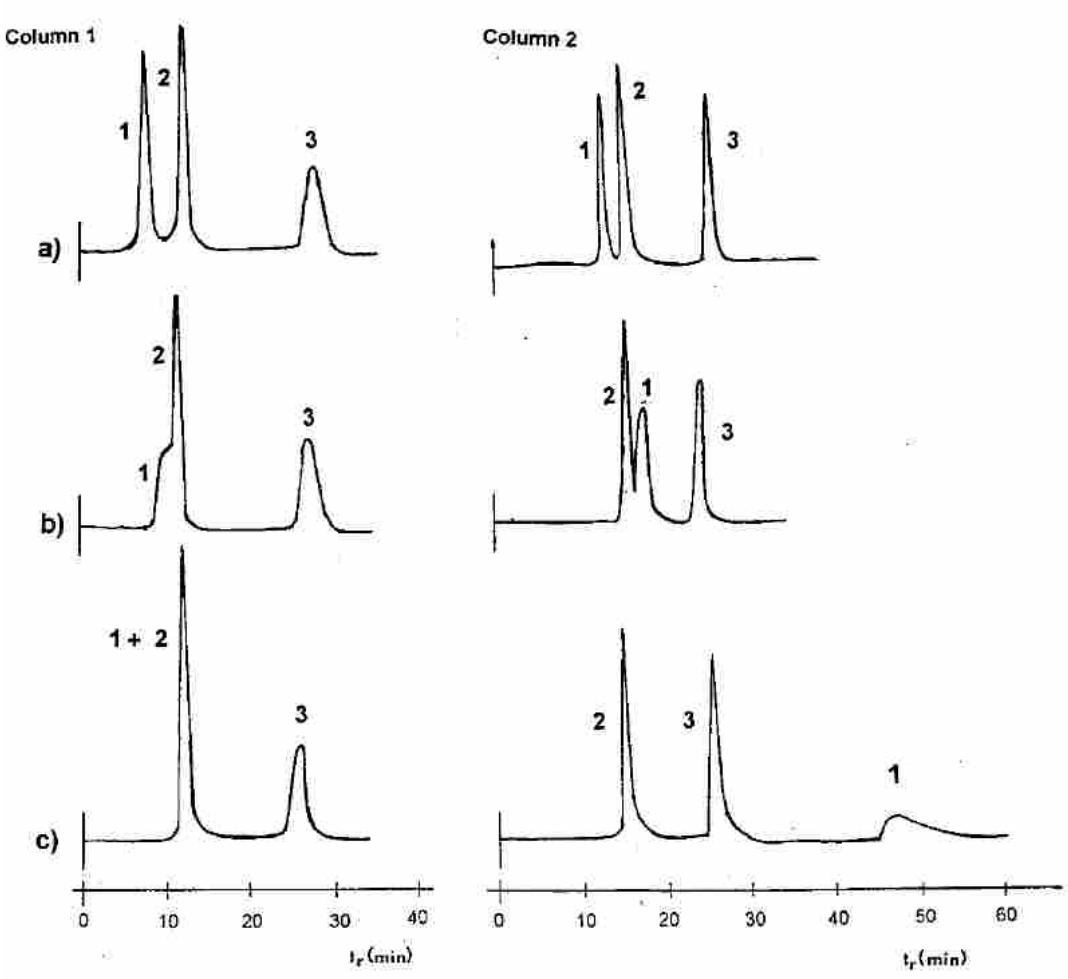

Figure 2.4 Separation of three pyrimidine bases (1 = cytosine; 2 = uracil; 3 = thymine) on untreated (column 1) and treated columns (column 2). (a) eluent: water adjusted to pH = 2 with phosphoric acid; (b) eluent: water adjusted to pH = 4 with phosphoric acid; (c) eluent: water. Column 1 = RP-18 column; Column 2 = RP-18 column coated with resorcinarene derivative.[23]

Ruderisch and coworkers[27] prepared a polar-headed stationary phase for HPLC by covalently bonding a resorcinarene derivative with polar carboxylic acid groups on the upper rim to a silica substrate. The polar groups with relative high polarity provide several advantages, such as enhanced hydrolytic stability of the stationary phase under highly aqueous conditions, high efficiency for polar analytes, and selectivity to low molecular weight acids.[27] The synthetic

route for the resorcinarene-based silica particles is shown in Figure 2.5.

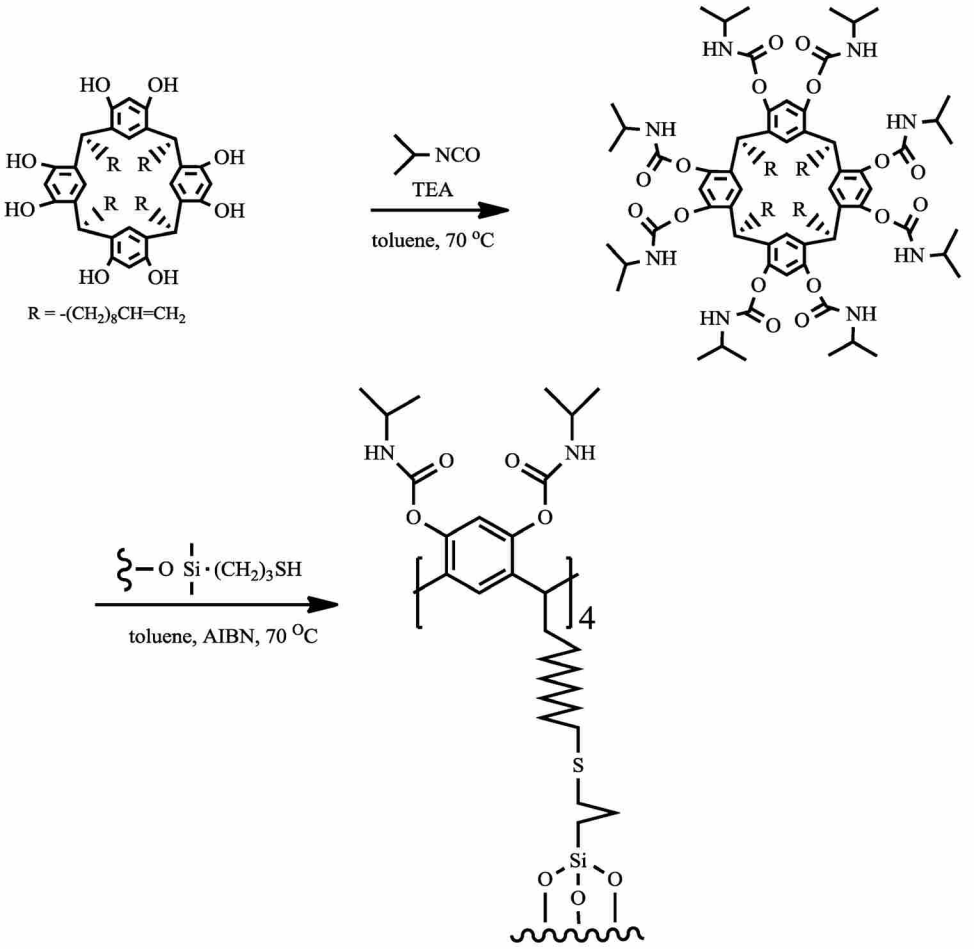

Figure 2.5 Synthetic pathway towards the silica-bonded and polar functionalized resorcinarene RP-type stationary phase.[27]

The separation of four compounds including uracil, phenol, naphthalene and anthracene was performed with this stationary phase and compared to that obtained with the commonly used n-octadecyl (C18), less common n-octyl (C8) and a C8 Nautilus stationary phase, which contains a polar group within the alkyl chain. The four compounds were separated under the same chromatographic conditions. Unlike the C18 column, the resorcinarene-based stationary phase retained the polar analyte phenol most strongly. One might have expected the hydrophobic

naphthalene and anthracene to be trapped in the hydrophobic resorcinarene pocket. However, the experimental results indicate that this interaction is at best weak. The overcrowding of the cavity by the polar head groups impedes the formation of host-guest complexes.

In another example, Tan et al.[28] made two resorcinarene-based silica columns for HPLC separations with (3-(*C*-methylcalix[4]resorcinarene)-2-hydroxypropoxy)-propylsilyl-appened silica particles (MCR-HPS) and bromoacetate-substituted MCR-HPS (BAMCR-HPS) (structures shown in Figure 2.6).

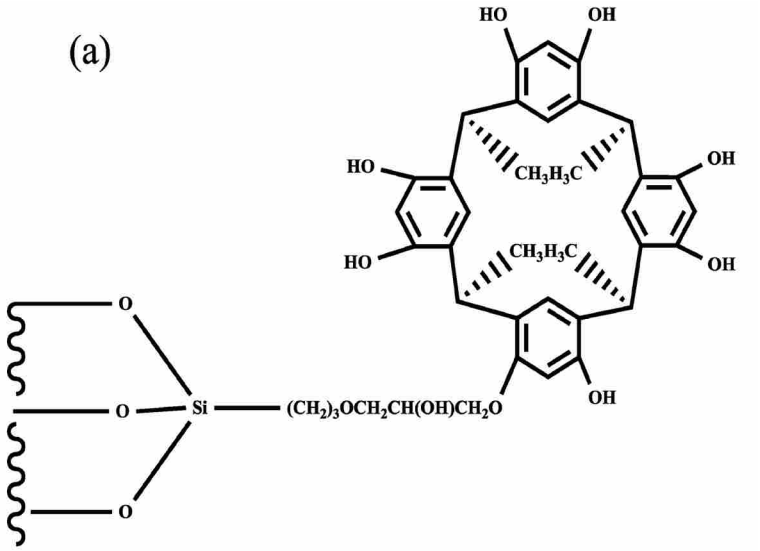

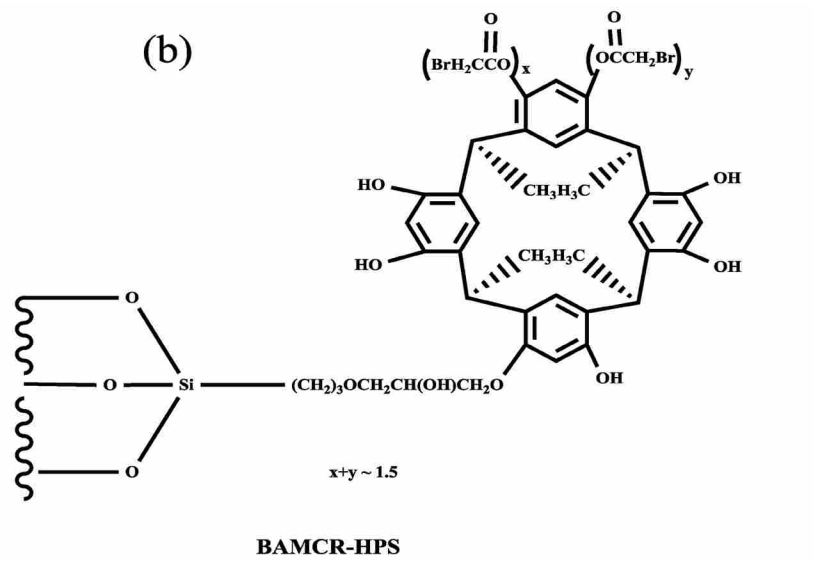

Figure 2.6 Structures of (3-(*C*-methylcalix [4] resorcinarene)-2-hydroxypropoxy)-propylsilyl- appended silica particles (a) MCR-HPS and bromoacetate-substituted MCR-HPS particles (b) BAMCR-HPS.[28]

These two columns were used to separate benzene derivatives. In addition, BAMCR-HPS was used to separate a series of chiral drug compounds. Specifically, water/methanol mixtures were used as mobile phases to separate three positional isomers of nitrophenol as shown in Figure 2.7.

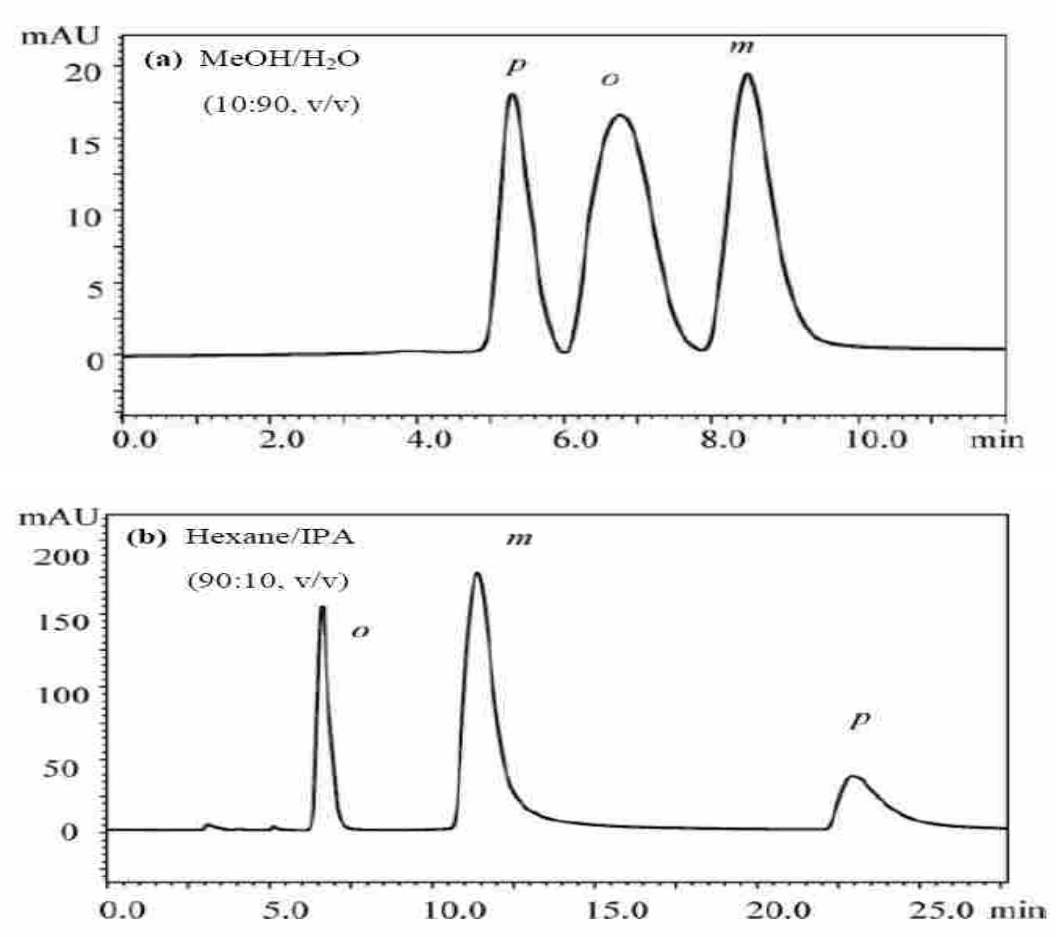

Figure 2.7 Separation of *o*-, *m*-, *p*-nitrophenol positional isomers on (a) the MCR-HPS column and (b) the BAMCR-HPS column.[28]

The retention factor of each isomer increased when the percentage of methanol in the mobile phase decreased, implying that retention is based on a hydrophobic interaction. The percentage of methanol in the mobile phase affected not only the retention time, but also the elution order. For example, the elution order of *o*-, *m*-, *p*-nitrophenol on the MCR-HPS column was *p*- < *m*- < *o*- when the methanol percentage ranged between 100% and 60%; yet between 40% and 20%, the elution order changed to *p*- < *m*- < *o*-. This phenomenon was not observed on the underivatized octadecylsilane-bonded (ODS) column. The difference was attributed to a

combination of the host-guest interaction, hydrogen bonding, and hydrophobic interactions between the resorcinarenes and analytes. When the MCR-HPS and BAMCR-HPS columns were applied to chiral drug compound separations, the BAMCR-HPS column exhibited much better chiral separation efficiency. The enantiomers of α-methylbenzylamine, indapamide, and proglumide were baseline separated on the BAMCR-HPS column (Figure 2.8).

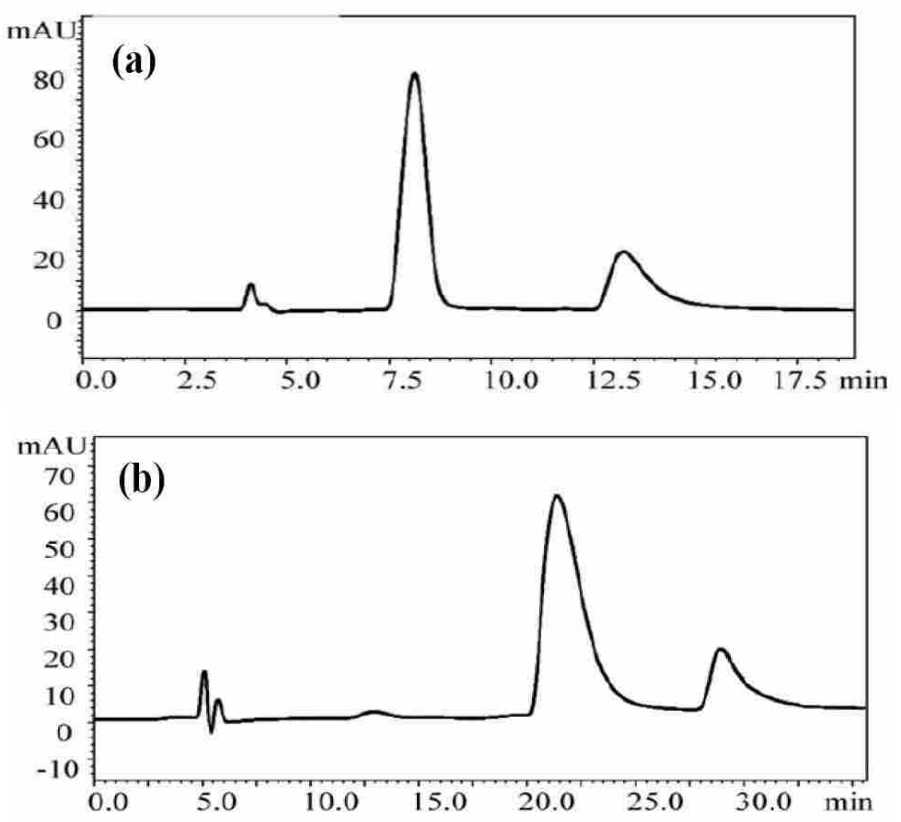

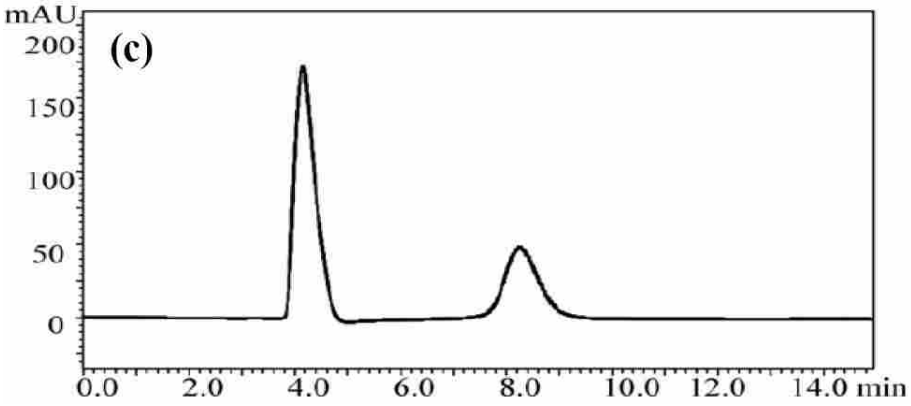

Figure 2.8 Enantioseparations of drugs on the BAMCR-HPS-packed column. (a) α-methylbenzylamine, mobile phase: ACN/TEAA, pH 4 (99:1, v:v); (b) indapamide, mobile phase: MeOH/H_2O, (10:90, v/v); (c) proglumide, mobile phase: ACN/TEAA, pH 7 (99:1, v/v); 254 nm UV detection. ACN = acetonitrile; TEAA =1% triethylamine-acetate buffer solution.[28]

In another example, Lipkowski et al.[29] added resorcinarenes to the mobile phases to separate a series of benzene derivatives including: benzene, ethylbenzene, *p*-xylene, *p*-cresol, and toluene on a LiChrosorb RP-18 packed reverse phase column (250 × 1 mm i.d.). Several resorcinarene derivatives (structures shown in Figure 2.9) were added to the acetonitrile-water (86:14, v/v) mobile phase to investigate the host-guest interactions of resorcinarenes with benzene derivatives and the effect of macrocyclic ligands on the separation efficiency. First, the retention time of each resorcinarene was determined using compounds 1-5, and the effect of steadily increasing the alkyl chain length on the lower rims of resorcinarenes on their retention time on the column was studied. Compound 5, with the longest chain length was retained to a much higher degree than compound 1; specifically, the retention time of compound 5 was >80.0 min while that of compound 1 was 3.67 min. The gradual increase in capacity factor is shown in Figure 2.10. As we can see in Figure 2.10, 1/*k*' increased with increasing resorcinarene

concentration. The higher the number of resorcinarene-based host molecules in the mobile phase, the more benzene derivative molecules can partition into the mobile phase to form host-guest complexes. As a result, when higher concentrations of resorcinarene derivatives were added to the mobile phase, shorter retention times of benzene derivatives were observed. Also, they found that when 3×10^{-3} M resorcinarene derivatives were added to the aceonitrile-water mixture, bezene-*p*-xylene resolution and ethylbenzene-toluene resolution were improved because of the difference in affinity of resorcinarene-based hosts to benzene derivatives as shown in Figure 2.10(a) and (b), respectively.

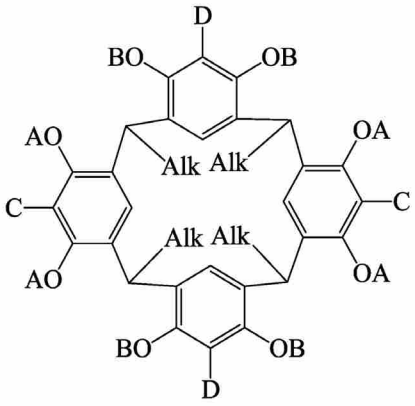

1. Alk = CH_3 A = B = C = D = H
2. Alk = C_3H_7 A = B = C = D = H
3. Alk = C_5H_7 A = B = C = D = H
4. Alk = C_7H_{15} A = B = C = D = H
5. Alk = $C_{15}H_{31}$ A = B = C = D = H
6. Alk = CH_3 A = Ts, B = C = D = H
7. Alk = CH_3 A = p-$ClC_6H_4SO_2$, B = C = D = H
8. Alk = CH_3 A = Ts, B = C = H, D = $CH_2N(C_2H_5)_2$
9. Alk = CH_3 A = B = H, C = D = $CH_2N(C_6H_{13})_2$
10. Alk = CH_3 A = B = Ts, C = D = H
11. Alk = CH_3 A = $P(O)(OC_3H_7)_2$, B = C = H, D = $CH_2N(C_2H_5)_2$
12. Alk = CH_3 A = $P(O)(OC_3H_7)_2$, B = C = D = H

Figure 2.9 Structures of resorcinarene derivatives.[29]

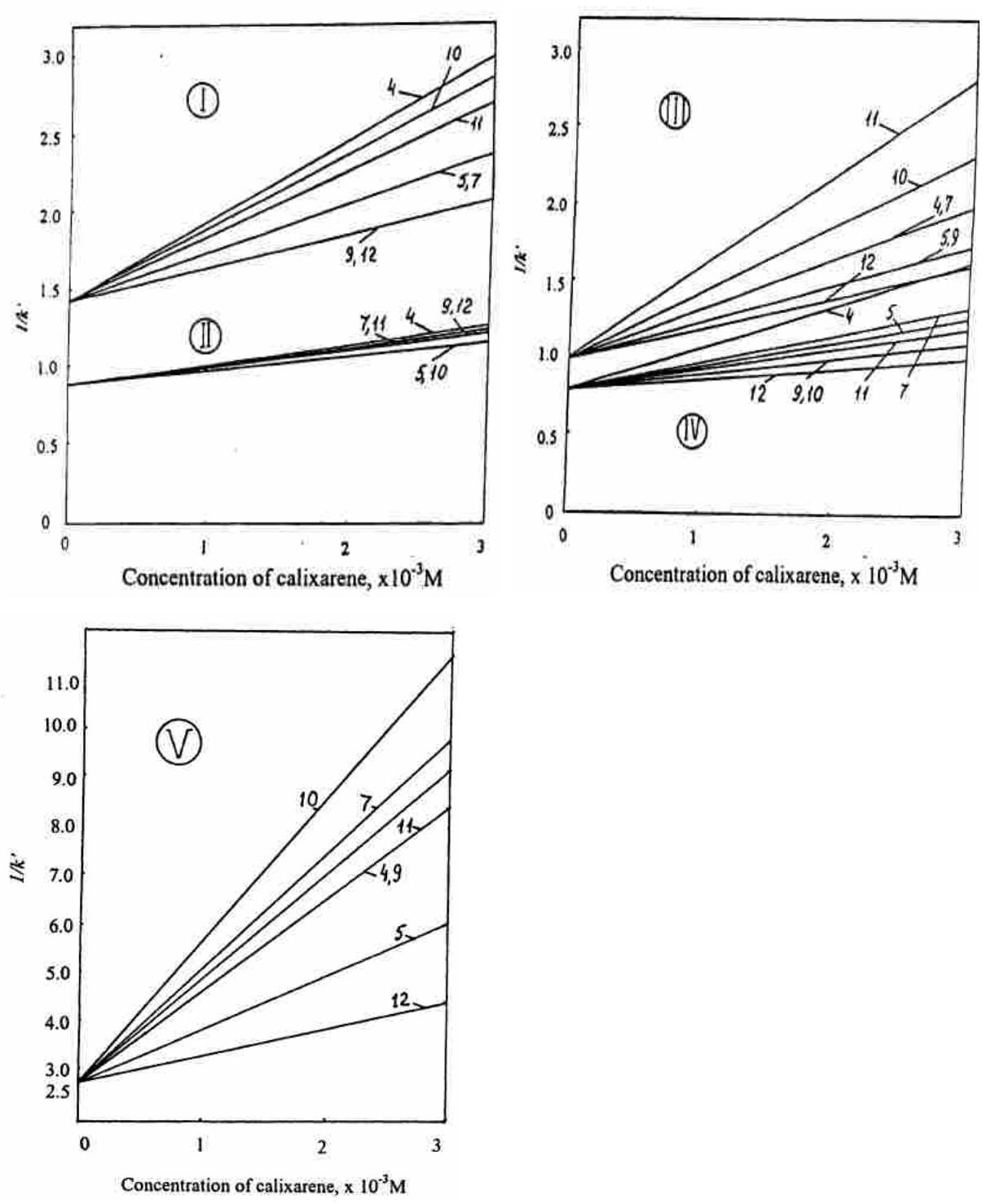

Figure 2.10 Plot of 1/*k*' for (I) benzene, (II) *p*-xylene, (III) ethylbenzene, (IV) toluene, (V) *p*-cresol against concentration of calix[4]resorcinarenes 4, 5, 7, and 9-12. Mobile phase: solution of calix[4]resorcinarene (1×10^{-3} - 3×10^{-3} M) in acetonitrile – water mixture. *k*': capacity factor.[29]

3. Gas Chromatography (GC)

Resorcinarene derivatives have been coated or covalently bonded to the inner wall of fused-silica capillary GC columns. In this application, the thermal stability of the resorcinarene derivatives is a factor which must be addressed. In one example of this approach, Zhang and coworkers[30] modified the lower and upper rims of resorcinarenes with phenyl and n-C_5H_{11} groups, respectively (structure shown in Figure 2.11). The resorcinarene was dissolved in dichloromethane (0.50%, w/v) and flowed through a fused-silica capillary GC column at 35^{o}C. The resulting film thickness on the inner wall was 0.31 μm. The column was used to separate alkanes, alkanols, phenols and aromatic hydrocarbons, especially chlorotoluene, cresol, and xylenol isomers. This column showed satisfactory thermal stability under 220 ^{o}C, but a dramatic baseline drift was observed when the column temperature was raised above 240 ^{o}C. In GC separations, the elution order of analytes is generally consistent with their boiling points; however, o-nitrochlorobenzene, with a boiling point of 235-236 ^{o}C, was eluted later than its p-isomer (boiling point 242 ^{o}C). This result indicates that the column is capable of structural selectivity. At 140 ^{o}C, the column showed good separation of the positional isomers 2,5-xylenol, 2,4-xylenol, 3,5-xylenol, and 2,3-xylenol that have close boiling points (as shown in Figure 2.12). Dimethylnaphthalene (DMN) isomers were also tested. These are hard to separate because of their similar physical properties. Among these isomers is 2,6-DMN, which has important industrial application as a starting material for a high performance engineering plastics such as polyethylene naphthalate. Using Zhang's resorcinarene derivatized column, 2,6-DMN was

baseline separated from six other DMN isomers as shown in Figure 2.13.

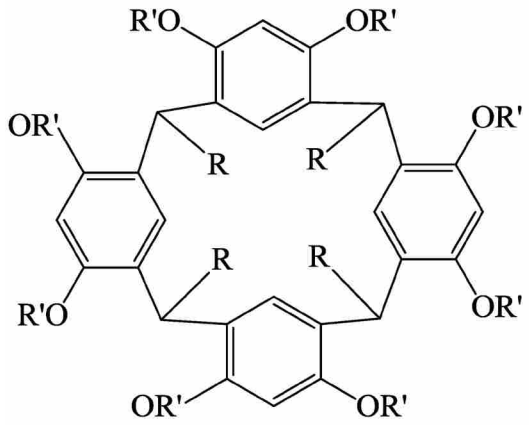

R = phenyl, R' = n-C_5H_{11}

Figure 2.11 Structure of the phenyl-pentyloxy-resorcinarene.[30]

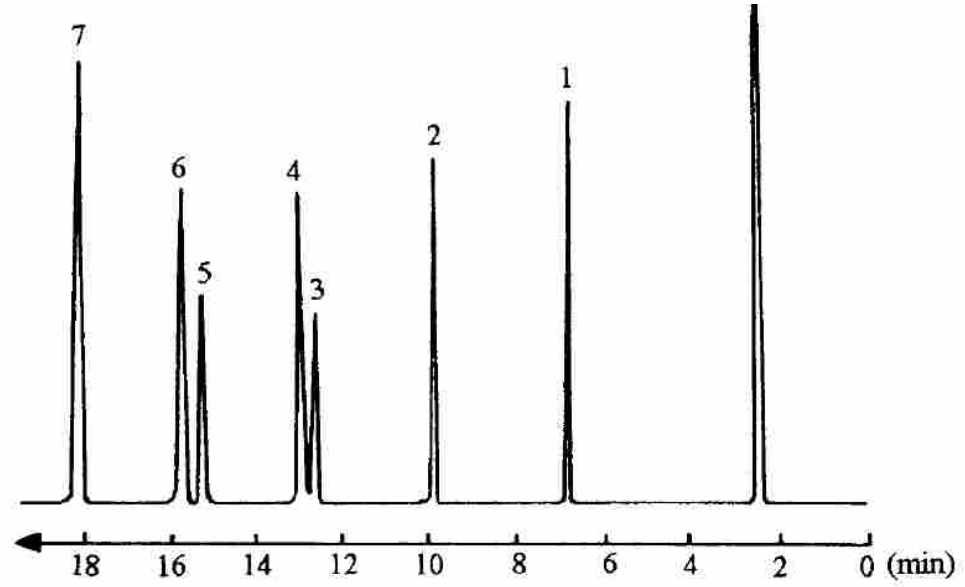

Figure 2.12 Separation of isomers on GC column coated with phenyl-pentyloxy-resorcinarene at 140 ^{o}C. N_2 linear velocity: 14.3 cm/s. Peak: 1 = phenol; 2 = 2,6-xylenol; 3 = 2,5-xylenol; 4 = 2,4-xylenol; 5 = 3,5-xylenol; 6 = 2,3-xylenol; 7 = 3,4-xylenol.[30]

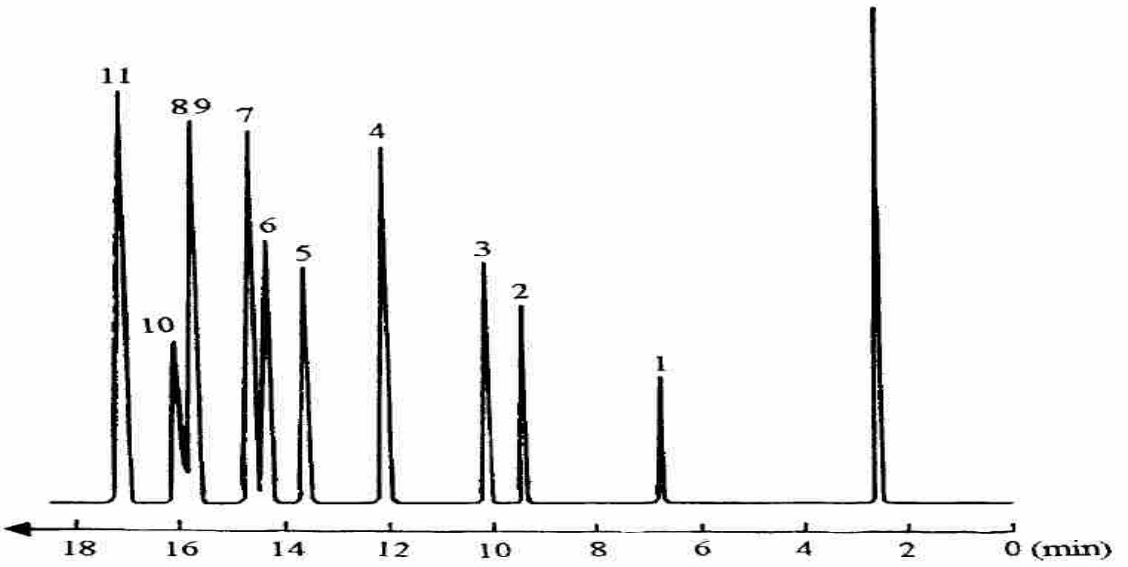

Figure 2.13 Separation of naphthalene and its analogs on GC column coated with the phenyl-pentyloxy-resorcinarene at 180 ^{o}C. N_2 carrier linear velocity: 14.3 cm/s. Peak: 1 = naphthalene; 2 = 2-methylnaphthalene; 3 = 1-methylnaphthalene; 4 = biphenyl; 5 = 2,6-dimethylnaphthalene (DMN); 6 = 1,7-DMN; 7 = 1,6-DMN; 8 and 9 = 1,4- and 2,3- DMN; 10 = 1,5-DMN; 11 = 1,2-DMN.[30]

In another example, Schurig's group adsorbed a resorcinarene derivative (Chirasil-Calix, structure shown in Figure 2.14a) with L-valine on the upper rim to a polysiloxane substrate. The synthetic procedures[31] and the application of the resulting stationary phase in GC were studied.[32-34] *N*-bromoacetyl-L-valine-*tert*-butyl-amide was attached to the resorcinarene upper rim via alkylation under basic conditions. The resulting ligand was covalently bonded to a poly(hydro)dimethylsiloxane (structure shown in Figure 2.14a) by hydrosilation using a platinum catalyst. A fused-silica capillary GC column was coated with the ligand by flowing Chirasil-Calix in diethyl ether through the column, yielding a film thickness of 0.25 μm. Fifteen proteinogenic amino acids were derivatized with *N*(*O,S*)-trifluoroacetylmethyl esters and

separated into their enantiomers on the coated GC column. The investigators expected that amino acids containing aromatic rings would be retained longer on the column because of the inclusion in the hydrophobic cavity of the ligand. However, when tyrosine (Tyr) and ornithine (Orn) were injected onto the column separately, Tyr with its aromatic ring was retained much longer (26.72 min) than Orn (11.62 min), yet when these were injected with other amino acid isomers, Tyr had a shorter retention time than Orn. The coated column exhibited excellent separation efficiency and thermal stability under 200 ^{o}C.

Later, Schurig's group used a one-pot reaction to covalently bond two kinds of macrocyclic ligands: β-cyclodextrin and Chirasil-Calix to poly(hydromethyl)-dimethylsiloxane by a Pt-catalyzed alkene hydrosilylation reaction.[34] Among these two ligands, permethylated β-cyclodextrin was used as an inclusion-type selector; the resorcinarene ligand was used as a hydrogen bonding selector. The resulting compound, Chirasil-Calixval-Dex (structure shown in Figure 2.14b), was coated onto the surface of a fused-silica capillary column (0.25 μm thickness) by a static method for chiral separation by GC of amino acids and hydrocarbons. Chirasil-Calixval-Dex was compared with another chiral selector, Chirasil-Dex, which contains only the cyclodextrin ligand. Enantiomers of polar amino acid derivatives and apolar unfunctionalized hydrocarbons were separated on the Chirasil-Calixval-Dex column. By contrast, the Chirasil-Dex column yielded insufficient chiral separation efficiency for proteinogenic amino acid derivatives. Only isomers of alanine, serine, cysteine, phenylalanine and proline were separated with acceptable resolution on the Chirasil-Dex column. But the *N*(*O,S*)-trifluoroacetylmethyl esters of sixteen amino acid enantiomers were separated with good resolution on the Chirasil-Calixval-

Dex column (shown in Figure 2.15). This behavior resembles the separation of amino acids on the previous Chirasil-Calix column which doesn't contain cyclodextrin groups implying that the enatioselectivity of the Chirasil-Calixval-Dex column is generated by the resorcinarene-based ligand only. In addition, the hydrocarbon derivatives that could not be separated on the Chirasil-Calix column were separated on the Chirasil-Calixval-Dex column which implies that the separations of these apolor moleculers were resulted from the cyclodextrin ligands of the Chirasil-Calix-Dex column. The separation performance showed by the Chirasil-Calixval-Dex column is the additive effects of cyclodextrin and resorcinarene-based ligands. The thermal stability of this mixed stationary phase is higher than Chirasil-Calix but lower than Chirasil-Dex.[32-34]

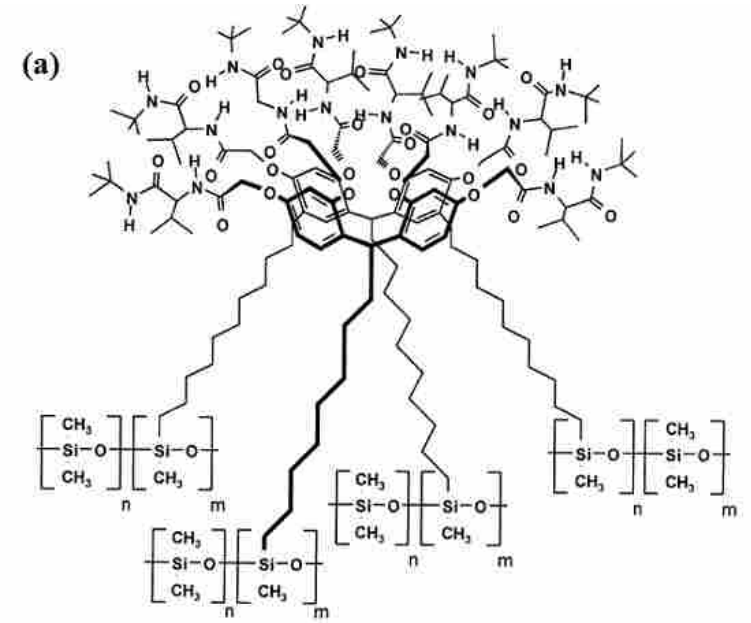

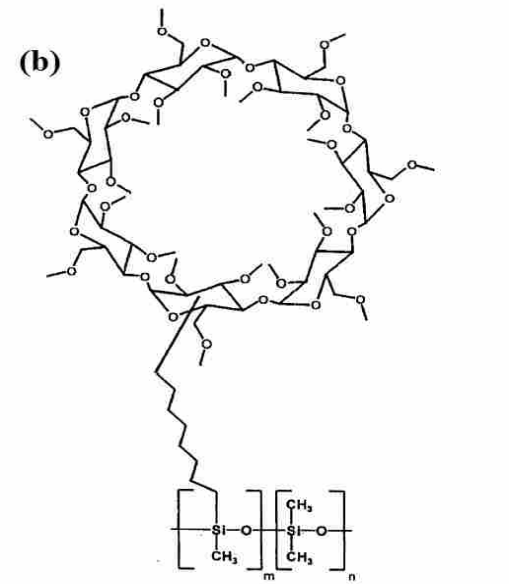

Figure 2.14 Structure of (a) Chiralsil-Calix; (b) the β-cyclodextrin in Chirasil-Calixval-Dex.[31-34]

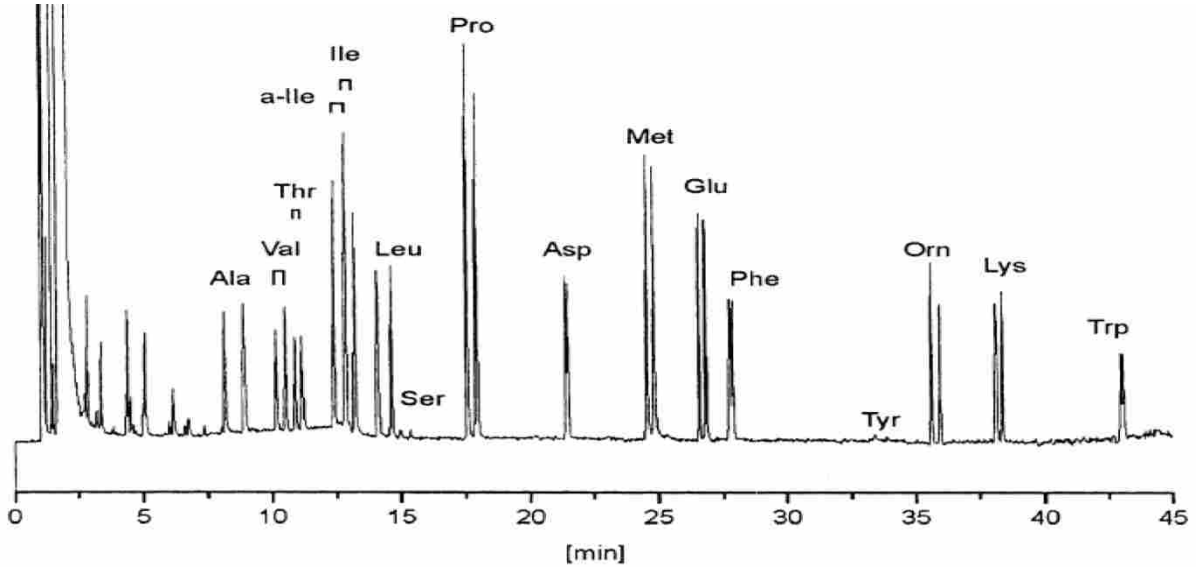

Figure 2.15 Gas chromatographic separation of enantiomers of 16 *N*(*O*)-trifluoroacetyl-DL-amino acid ethyl esters on a 20 m × 0.25 mm fused-silica column coated with Chirasil-Calixval-Dex (film thickness 0.25 μm). Temperature program: 70 ^{o}C (3 min); 3 ^{o}C/min; 170 ^{o}C; carrier gas: 0.5 bar hydrogen; split: 1:100.[33]

4. Electrokinetic Chromatography (EKC) and Capillary Electrophoresis (CE)

Capillary electrophoresis separates ionic species by their distinct electrophoretic mobility. In a fused-silica capillary, the silanol (Si-OH) groups on the capillary wall are ionized when the pH of the buffer solution is higher than 3. Positively charged ions in the buffer solution are attracted to the negatively charged capillary wall and directed toward the cathode by Coulomb forces. The buffer liquid moves through the capillary via electroosmotic flow (EOF). As a result, positively charged ions, negatively charged ions, and neutral species, reach the detector at different rates. Typically, CE doesn't separate neutral species since they move to the detector at the same rate as the EOF. Adding resorcinarene derivatives is an option for separating neutral species in CE. These ligands serve as pseudo-stationary phases in which neutral species are separated by their distinct affinity with these stationary phases; after that, they move to the detector at the same rate as the EOF. When using resorcinarene derivatives as pseudo-stationary phases, two main factors should be considered: (1) the solubility of the resorcinarene derivatives in the aqueous buffer solution. In most cases, organic solvents such as CH_3OH, CH_3CN, or DMSO are added to improve the solubility of the resorcinarene derivatives. (2) Resorcinarene derivatives may interfere with the detection of analytes especially when their UV absorptions are quite close to that of the analytes. Several published papers have discussed these problems, as described below.

Bächmann et al.[35, 36, 38]applied a series of resorcinarene-based derivatives as the peudostationary phases in EKC for the separation of uncharged species. In one study,

resorcinarene was modified on the lower rim (structures shown in Figure 2.16) with different alkyl chains.[35] The separation of 12 polycyclic aromatic hydrocarbons (PAHs) including: naphthalene, phenanthrene, anthracene, fluoranthene, pyrene, triphenylene, chrysene, benzo[*k*]fluoranthene, benzo[*a*]-pyrene, indeno[l,2,3-*cd*]pyrene, anthanthrene, and benzo[*ghl*]perylene with those resorcinarene based pseudostationary phases were performed as shown in Figure 2.17. Compared with micellar electrokenetic chromatography (MEKC), these resorcinarene based pseudostationary phases showed several advantages, such as better tolerance to high content of organic modifiers (i.e. >80% acetonitrile), high electrophoretic mobility due to negative charges delocalized and stabilized over hydrogen bonds on the upper rim, and potential high hydrophobic interaction with the hydrophobic PAHs. The host-guest interaction between resorcinarenes and PAHs was not observed in the experiments. Resorcinarenes are considered as a 'platform' with adjustable hydrophobicity and as a carrier of negative charges. However, the length of alkyl chains on the lower rim of resorcinarenes had a significant effect on the separation efficiency and selectivity among the PAHs. Of the four resorcinarenes studied, compound 16(C) with the longest alkyl chain showed appropriate selectivity for separation of all 12 PAHs. Compounds 16(b) and 16(d) showed much better separation efficiency than 16(a) but were inferior to 16(c). The PAHs were well-detected with a UV detector at 260 nm. Resorcinarenes themselves have UV absorption due to the aromatic ring on the scaffold; however, the authors didn't mention interference of resorcinarenes to the detection of PAHs.

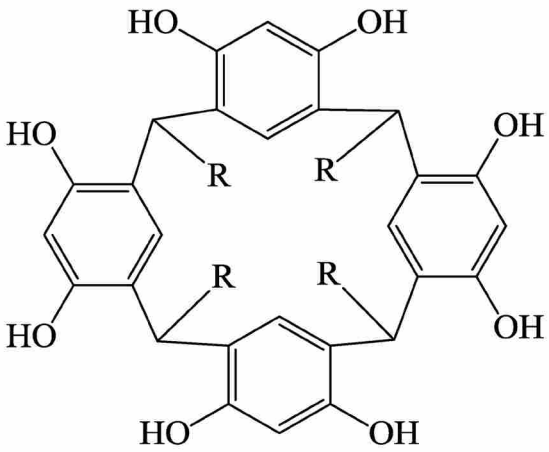

(a) R = -CH_3; (b) R = -C_5H_{11}; (c) R = -$C_{11}H_{23}$; (d) R = p-chlorophenyl

Figure 2.16 Structures of four resorcinarene derivatives.[35]

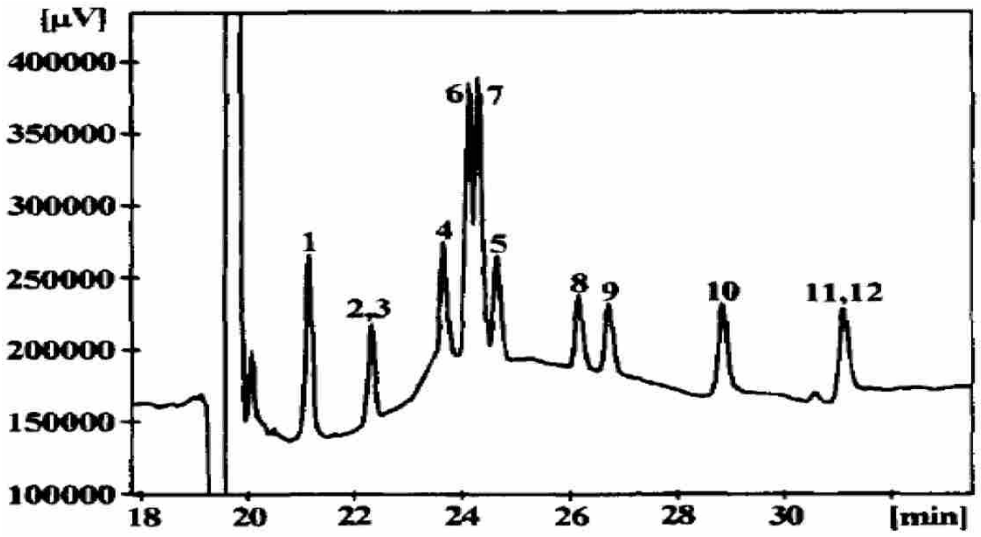

Figure 2.17 Separation of 12 PAHs with resorcinarene 15(d). Conditions: electrolyte, 6.4 mM 15D; current 5 μA. Peaks: (1) naphthalene, (2) phenanthrene, (3) anthracene, (4) fluoranthene, (5) pyrene, (6) triphenylene, (7) chrysene, (8) benzo[q]fluoranthene, (9) benzo[*a*]-pyrene, (10) indeno[l,2,3-*cd*]pyrene, (11) anthanthrene, and (12) benzo[*ghl*]perylene.[35]

In the other study,[36] the upper rim of resorcinarene was modified with eight carboxylic

acid groups and the lower rim was modified with alkyl chains of different lengths. The formed resorcinarene – octacarboxylic acids (structure shown in Figure 2.18) have good solubility and electrophoretic mobility in electrolytes and were used as pesudostationary phases in EKC for the separation of thirteen homologous or isomeric amines. In order to avoid UV interference by resorcinarenes in the detection of amines, a KF-2 Laser Induced Fluorescence (LIF) detector with HeCd laser was used (excitation 325 nm, emission > 389 nm using a cut off filter). The thirteen amine analytes were pre-derivatized with *o*-phthaldialdehyde and 2-mercaptoethanol to generate fluorescence and were separated in a fused-silica capillary column with a 75 μm I.D. and a 75 cm length (effective length = 50 cm). Similar to the previous study,[35] the length of alkyl chains on the lower rim affected the selectivity of the separation rather than the macrocyclic scaffold. The resorcinarene with longest alkyl chain, $-C_{11}H_{23}$ showed the highest selectivity among amines, while the one with the shortest alkyl chain, $–CH_3$ yielded no separation.

The separation of thirteen amine derivatives using compound 18(c) as the pseudostationary phase is shown in Figure 2.19. Separation efficiency up to three million plates per meter was obtained for pentylamine. Several factors including in-column band broadening(σ_{col}) and extra-column band broadening from the injection and detection systems (σ_{inj} and σ_{det}) resulted in the extreme high efficiency, as discussed in Terabe's paper.[37] σ_{det} did not contribute to band broadening when a low detection volume LIF detector was used with improved sample focusing of the laser beam. Furthermore, because the sample injection zone was about 1% of the effective capillary length, σ_{inj} was not a significant contributor to band broadening. In addition, when resorcinarene derivatives are used as the pseudostationary phase in

EKC, the preorganized bowl-shaped structure and charge density distribution avoid the microheterogeneity in the capillary column which results from the different affinities of molecules to pseudostationary phases and the differences in electrophoretic mobility of the analytes. The microheterogeneity, an important factor to in-column band broadening, was reduced. The improvements made in the detection and injection systems and the use of preorganized resorcinarene structures improved the plate height of the capillary so that plate numbers as high as three million plates per meter were obtained. Equation 1 shows the factors contributing to the band broadening in the capillary.

$$\sigma_{tol}{}^2 = \sigma_{col}{}^2 + \sigma_{inj}{}^2 + \sigma_{\mathrm{det}}{}^2 \qquad (2.1)$$

(σ_{tol} is the total peak variance, σ_{col} is the in-column variance, σ_{inj} and σ_{det} are extra-column variances from the injection and the detection systems, respectively.)

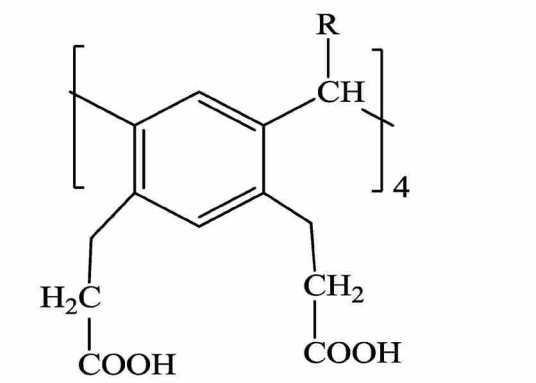

R = (a) -CH_3, (b) -C_5H_{11}, (c) -$C_{11}H_{23}$

Figure 2.18 Structures of resorcinarene derivatives used in the EKC system.[36]

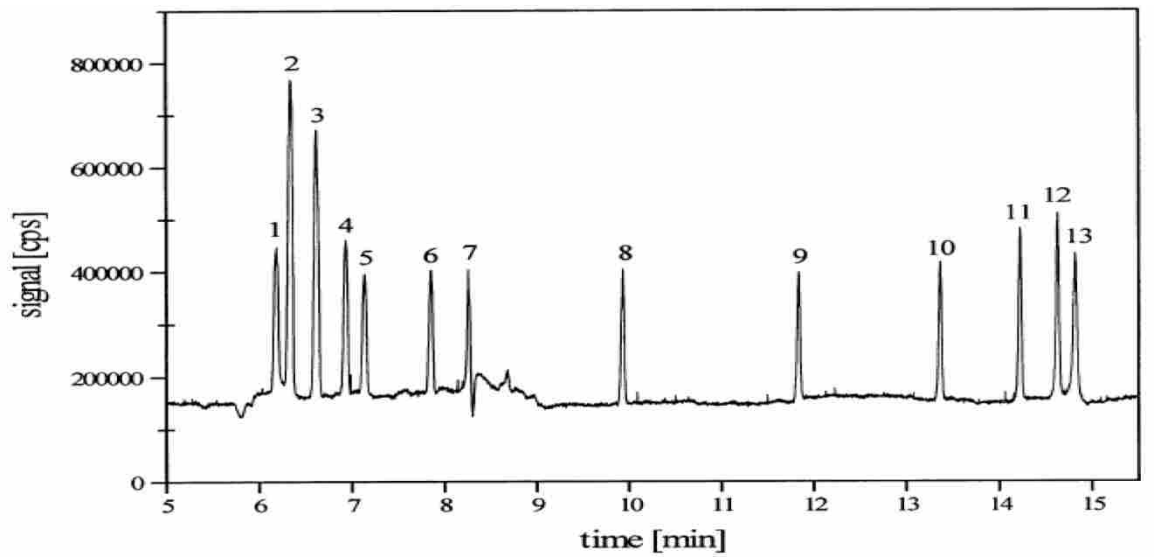

Figure 2.19 Separation of 13 amines using resorcinarene 18(C) as pseudostationary phase in EKC; Electrolyte: 0.75 mM resorcinarene 18(C), 5 mM sodium phosphate, 10 mM sodium tetraborate, 10% acetonitrile (v/v), (pH 9.5). Voltage: 20 kV, current 46 mA. Peaks: 1- amino-2-propanol, 2 = methylamine, 3 = ethylamine, 4 = isopropylamine, 5 = propylamine, 6 = isobutylamine, 7 = butylamine, 8 = pentylamine, 9 = hexylamine, 10 = heptylamine, 11 = octylamine, 12 = nonylamine, 13 = decylamine. Sample concentration: 10 μM, derivatized with OPA–2-mercaptoethanol.[36]

The same group explored the application of phosphate substituted resorcinarenes (structure shown in Figure 2.20) as pseudostationary phases in EKC.[38] To avoid interference by the resorcinarene derivatives in the detection of uncharged homologous 4-hydroxybenzoic esters (parabens) in EKC, the authors developed a discontinuous mode of analysis. In CE, the EOF is generally larger than the electrophoretic velocity of the ions and is sufficient to drive positive, neutral, and even negatively charged species toward the cathode, thus all three species can be detected at the cathode. In this work, the capillary was first filled with an electrolyte containing the resorcinarene. The electrolyte pH was below approximately 5.5, at which the mobility of the

resorcinarene derivatives exceeds the EOF. After the analytes were injected at the anode, a sodium dihydrogen phosphate electrolyte containing no resorcinarene derivatives was passed through the capillary. 0.5 % v/v acetonitrile was added into the electrolyte in order to increase the solubility of resorcinarene derivatives. After a high voltage was applied to the capillary, negatively charged resorcinarene derivatives moved towards the anode with velocity higher than the EOF until completely moved out of the detection window. Simultaneously, the parabens were separated on the resorcinarene-based stationary phase and pumped to the cathode by the EOF. Parabens were only transported to the detector by the EOF and no further separation took place after they left the resorcinarene-based zone. Figure 2.21 shows the discontinuous separation of parabens with this resorcinarene system 20(b). After three minutes, resorcinarene 20(b) was completly removed from the detector after about 3 minutes and the background UV absorption decreased dramatically. Four neutral paraben species were baseline separated. However, maximum retention and selectivity in this study were achieved with the resorcinarene substituted with the medium chain length -C_8H_{17}. This result differs from the previous studies in which the highest selectivity was achieved with the longest chain length -$C_{11}H_{23}$. The authors assumed that optimum chain length in terms of selectivity is associated with the sizes of the analytes.

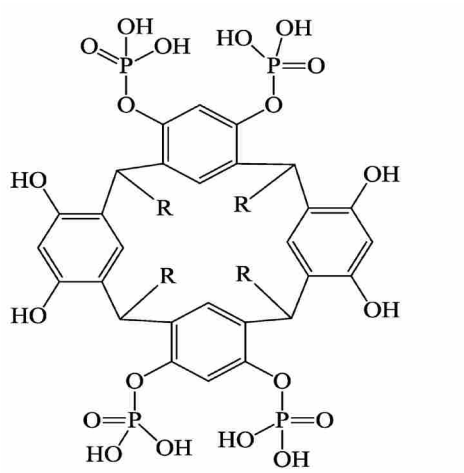

Figure 2.20 Structures of resorcinarene derivatives used in the EKC system.[38]

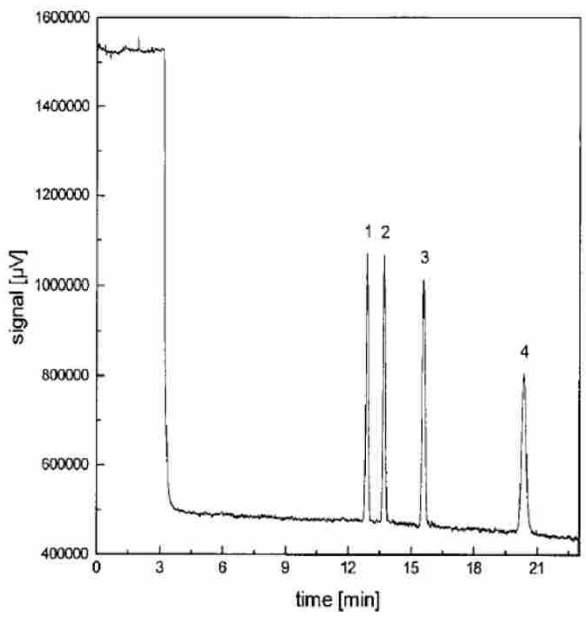

Figure 2.21 Separation of parabens using resorcarene 4b as pseudostationary phase. Capillary: 68cm in length, 75 mm ID, 53 cm effective to detector; Voltage: 25 kV; Detection wavelength: 250 nm. Electrolyte 1: 1 mM resorcarene 19(b), 20 mM sodium dihydrogenphosphate, 5% v/v acetonitrile, pH 4.6. Electrolyte 2: 20 mM sodium. dihydrogenphosphate, 5 % v/v acetonitrile, pH 4.6. Peaks: 1, methyl-; 2, ethyl-; 3, propyl-; 4, butylparaben.[38]

Chen et al.[39] explored the application of a tetraethylsulfonate derivative of 2-methylresorcinarene (TESMR, structure shown in Figure 2.22) in capillary electrophoresis (CE). They compared the separations of six para-substituted phenols with TESMR and another macrocycle sulfobutyl ether-β-cyclodextrin (SBE-*β*-CD). Several characteristics of resorcinarene detivatives make them good potential addictives in CE including diversity of cavity size, affinity, and functionalities resulting from the substituent groups on both upper and lower rims; high solubility in aqueous solution, e.g. TESMR and thus less aggregates and micelles formed by hydrophilic resorcinarene derivatives; economic starting reagents for synthesis; and high charge density concentrated on the preorganized bowl-shaped molecules.

Figure 2.23 shows the separation of three neutral positional isomers of nitrophenol with and without TESMR. Adding TESMR to the capillary provided much improved resolution for the three positional isomers; however, severe peak asymmetry was observed (shown in Figure 2.23). Electokinetic dispersion and surface adsorption are two factors that contribute to the peak asymmetry. Conductivity or pH differences between sample and buffer zones result in the perturbation of the electric field distributed along the capillary resulting in electrokinetic dispersion. This can be minimized by reducing the additive or analyte concentration. In this study, electrokinetic dispersion was not considered as a cause of peak asymmetry, since only a low concentration of TESMR was applied. The peak asymmetry caused by surface adsorption resulted from the absorption of analytes or macrocyclic ligands on the capillary wall by hydrophobic or electrostatic effects. In this case, when TESMR or nitrophenols were added to the capillary separately, symmetric peaks were observed; however, when TESMR and

nitrophenols were both present in the capillary, obvious skewed peaks were observed, which indicates that the hydrophobic interactions between capillary wall and nitrophenols were enhanced in the presence of TESMR. The effect of ionic strength, buffer pH and organic modifier on the separation and peak symmetry were discussed by the authors. Higher ionic strength yielded no improvement in peak symmetry. When the buffer pH > 7.6, the peak shape was significantly improved. Since the deprotonation of silanol groups was enhanced, this in turn reduced the hydrophobic interaction between capillary wall and nitrophenols.

Organic modifiers were added to the capillary for this purpose as well. However, a polar protic solvent, i.e. methanol showed minimal effect on peak shape, but the polar aprotic solvent, DMSO provided the largest improvement in peak shape compared to other polar protic solvent DMF, ACN, and methanol. The separation of nitrophenol isomers with TESMR and SBE-*β*-CD additives was compared as shown in Figure 2.25. When SBE-*β*-CD was used as eluent, a large percentage of DMSO (30%) was used in order to minimize the peak asymmetry. The possible explanation for this phenomenon is that the high charge density in the vicinity of the macrocyclic molecules restrains the mass transfer of the lipophilic analytes. In Figure 2.25, TESMR showed reverse selectivity to nitrophenol isomers compared to SBE-*β*-CD. Size, shape, and hydophobicity of the macrocyclic ligands are the factors that determine the affinity of the nitrophenol isomers to TESMR and SBE-*β*-CD macrocyclic molecules.

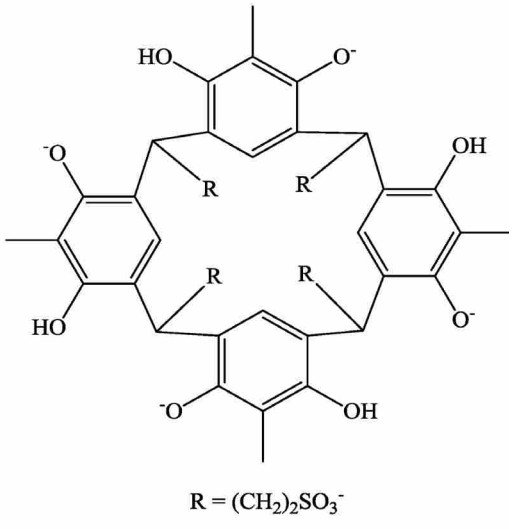

Figure 2.22 Structure of the tetraethylsulfonate derivative of 2-methylresorcinarene (TESMR).[38]

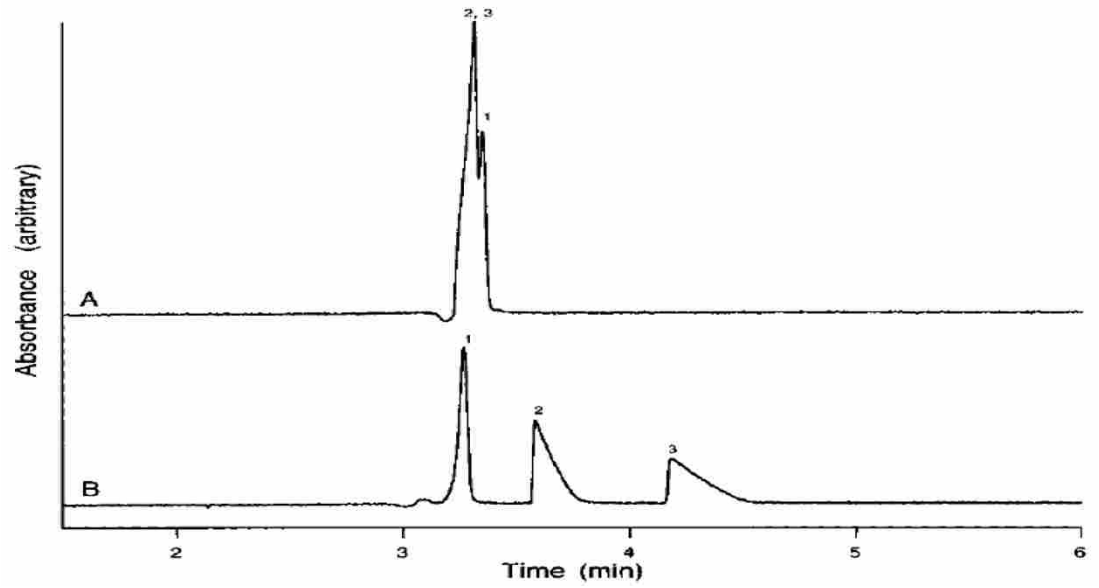

Figure 2.23 Separation of three neutral positional isomers with and without TESMR: (A) 0 and (B) 1.0 mM TESMR. Peaks: (1) *p*-nitrophenol; (2) *m*-nitrophenol; (3) *o*-nitrophenol. Capillary length: 37 cm; voltage: 28 kV; absorption 305 nm.[39]

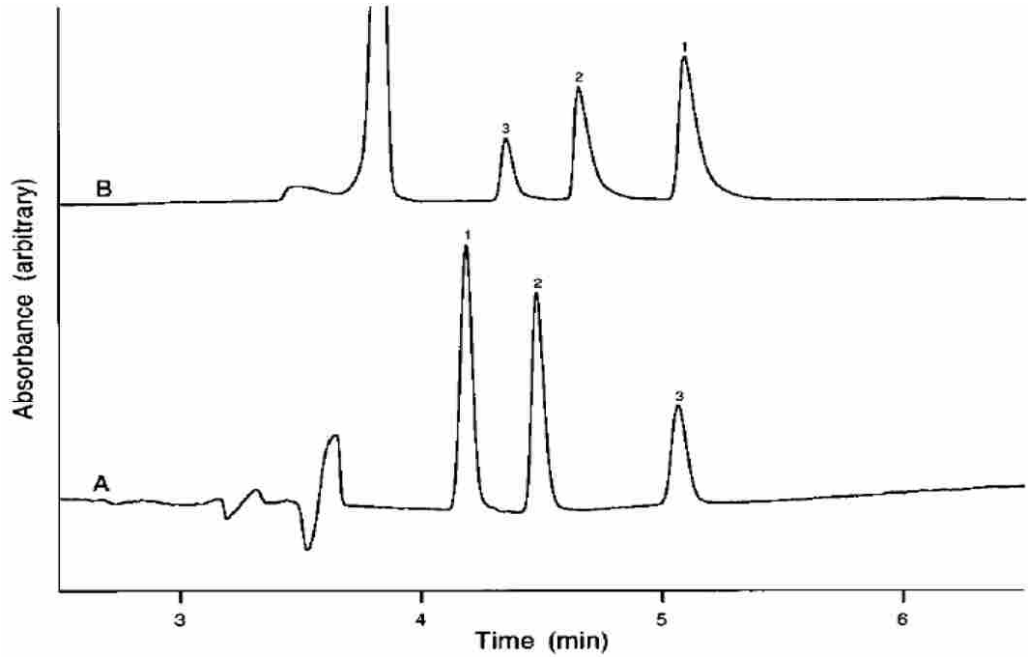

Figure 2.24 Comparison of the separation of nitrophenol isomer with two different additives: (a) 6 mM TESMR (2.5% DMSO) and (b) 2 mM SBE-*β*-CD (30% DMSO). Peaks: (1) *p*-nitrophenol; (2) *m*-nitrophenol; (3) *o*-nitrophenol. Voltage: (a) 20 kV, (b) 25 kV.[39]

Sokoließ and coworkers[40, 41] applied calixarenes and resorcinarenes (structures shown in Figure 2.25) for the separation of (*Z*)- and (*E*)-isomers of thioxanthene and dibenz[*b,e*]oxepin derivatives (structures shown in Figure 2.26) by nonaqueous capillary electrophoresis. The flow direction of calixarenes and resorcinarenes was adjusted to be opposite the EOF by adding sodium dodecyl sulfate (SDS) and thus avoiding UV interference from the calixarenes and resorcinarenes. In this way, the macrocyclic ligands were moved out of the detection widow, while the four pairs of E/Z isomers were detected at 214 nm. Figure 2.27shows the apparent electrophoretic mobility of calixarenes and resorcinarenes as a function of the concentration of SDS. Calix[6]- and calix[8]arenes had poor solubility in methanol-containing electrolytes, so they were not discussed and applied to the CE system. The resorcinarene showed the same

cathodic electrophoretic mobility as the EOF until 70 mM SDS was added, while anodic electrophoretic mobility was observed for all calixarenes, even when no SDS was present in the solution. It is assumed that the complex formed between resorcinarene and SDS, because a hydrophobic interaction would change the direction of the resorcinarene electrophoretic mobility. Calixarenes a1, b1, and allyl-a1provided close and much smaller eletrophoretic mobility than ss-a1 and cm-a1. Although a1, b1, and allyl-a1 contain alkyl chains of different length at the para-position, the alkyl chain length had no clear effect on electrophoretic mobility, as shown in Figure 2.27. However, when the hydroxyl groups of the calixarene were retained and the para-positions were modified with sulphonic groups (HSO_3^-, ss-a1) or carboxylic acid groups (-COOH, cm-a1), the anode electrophoretic mobilities of ss-a1 and cm-a1 were enhanced.

The fact that adding SDS has a marginal effect on the electrophoretic mobility of the calixarenes indicates that calixarenes have no obvious tendency to form strong complexes with SDS-monomers, unlike the resorcinarene. The application of a1, b1, and allyl-a1 to CE was carried out in an NH_4Ac - methanol buffer solution (pH $\geq$ 7) in which SDS was also added in order to maintain calixarene solubility. Compared to other calixarenes and the resorcinarene, compound ss-a1 had the highest anode electrophoretic mobility and the best selectivity among the isomers. The effect of the electrolyte pH, ionic strength, voltage, organic solvents, and ss-a1 concentration ss-a1on the separation of Z/E isomers was discussed. Increasing the ionic strength, voltage, and the ss-a1 concentration did not result in a better separation. The best resolution among the four analytes was observed when 5 mM ss-a1along with the lowest ionic strength (40 mM NH_4Ac) and the lowest voltage (12 kV) were applied. The simultaneous separation of four

pairs of Z/E isomer was successfully achieved under the conditions shown in Figure 2.28.

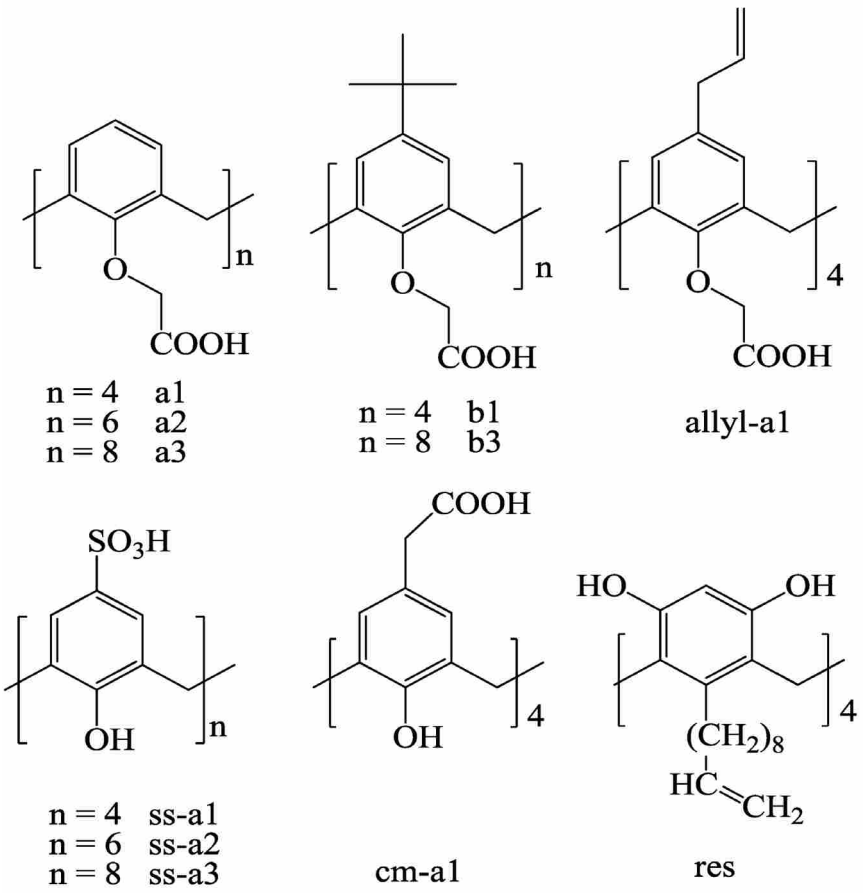

Figure 2.25 Structures of calixarenes and resorcinarenes as selectors.[40]

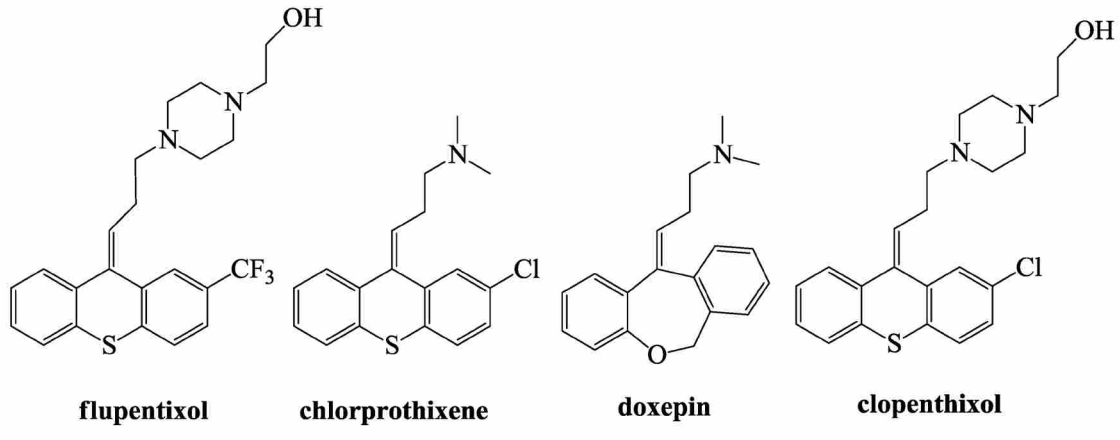

Figure 2.26 Structure of the flupentixol, chlorprothixene, doxepin, and clopenthixol.[40]

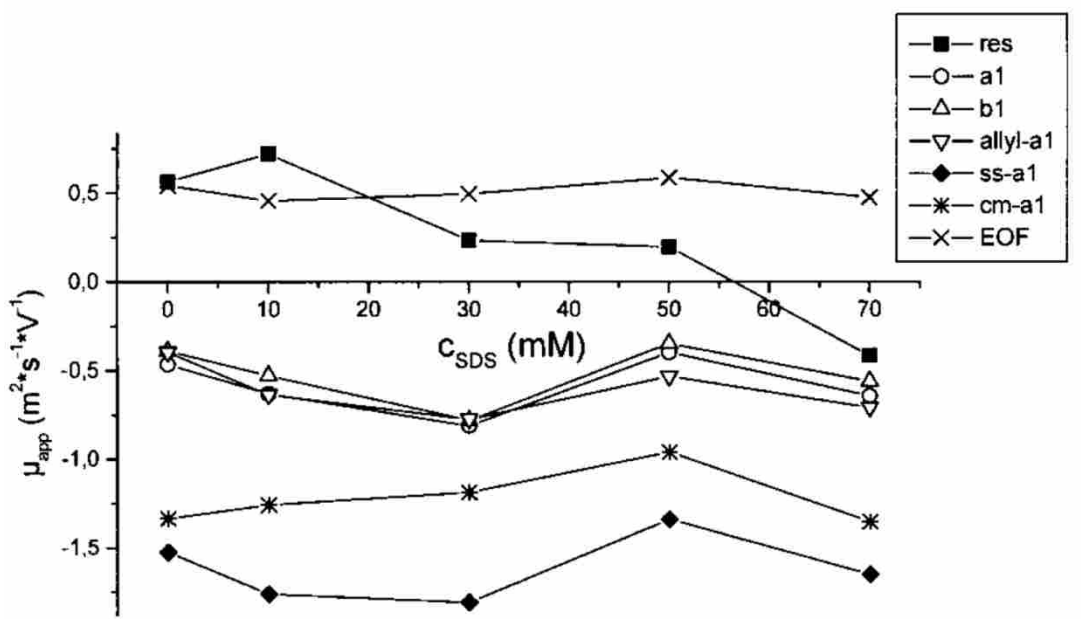

Figure 2.27 Apparent electrophoretic mobility of calixarenes and resorcinarenes as dependant on the SDS concentration. Conditions: 40 mM NH_4Ac in MeOH, pH = 8.0, 12.5 kV, 214 nm, 25°C.[40]

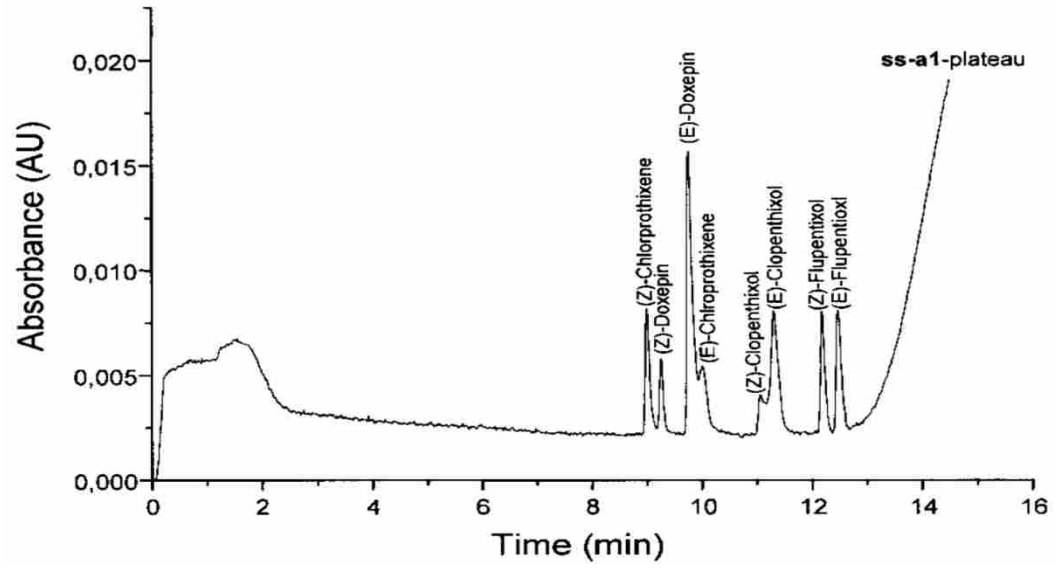

Figure 2.28 Separation of Z/E isomers of flupentixol, chlorprothixene, doxepin, and clopenthixo. Conditions: 40 mM NH_4Ac in MeOH; pH = 5.0; voltage = 18 kV; 5 mM ss-a1; wavelength = 214 nm; T = 25°C; t_{fill} =1.4 min with a plug length of 24 cm.[40]

5. Membrane separations

A liquid membrane contains a liquid medium that permits species to selectively transfer from the source phase (or feed phase) to the receiving phase. The selectivity of a liquid membrane is given by the relative flux of chemical species, flux being the rate at which chemical species pass through the membrane. A carrier is often dissolved in the membrane to shuffle species across. Macrocylic ligands such as calixarenes and crown ethers have been incorporated as carriers into four types of liquid membrane: bulk liquid membranes (BLMs), emulsion liquid membranes (ELMs), support liquid membranes (SLMs), and polymer inclusion membranes (PIMs). The selectivity of these ligands serving as carriers is transferred to the membrane so that the carrier selectively transports analytes from the source phase to the receiving phase. The application of resorcinarene in liquid membranes is still in the early stages. However, several research groups have explored the application of resorcinarenes as carriers in BLMs, SLMs, and PIMs.

For example, Fedorenko's group[42] studied the appilication of resorcinarene derivatives in BLMs. A chloroform solution of resorcinarene (30 mL) separated the aqueous source and receiving phases (5 mL each) in a U-tube. The transport of Cu^{2+} and Co^{3+} complexes with diamines and amino acid carriers was tested. Figure 2.30 shows the structures of the resorcinarene derivatives that have been evaluated as carriers in the BLMs. Ligand 2.29(a) serves as an anionic ionophore to transport complex cations (in equation 2.2 and 2.3) across the membrane. This result was confirmed by the fact that extraction of complexes in the receiving

phase was significantly enhanced when the acidity of receiving phase was increased. However, the other five resorcinarene derivatives transport the complexes by forming ternary or quaternary complexes with the metal complexes as shown in equation 2.4 and 2.5. The transport efficiency did not increase with the increasing acidity of the source or receiving phase.

$$H_8L + [Cu(Phen)(PhAl)(H_2O)]^+ \rightleftharpoons H_7L[Cu(Phen)(PhAl)(H_2O)] + H^+ \quad (2.2)$$

$$H_8L + [Cu(Phen)_2(H_2O)]^{2+} \rightleftharpoons H_6L[Cu(Phen)_2(H_2O)] + 2H^+ \quad (2.3)$$

$$H_8L + [Cu(Phen)(PhAl)(H_2O)]ClO_4 \rightleftharpoons H_7L[Cu(Phen)(PhAl)(H_2O)]ClO_4 \quad (2.4)$$

$$H_8L + [Cu(Phen)_2(H_2O)]Cl_2 \rightleftharpoons H_8L[Cu(Phen)_2(H_2O)]Cl_2 \quad (2.5)$$

Phen is 1,10-phenanthroline, $PhAl^-$ is phenylalanine.

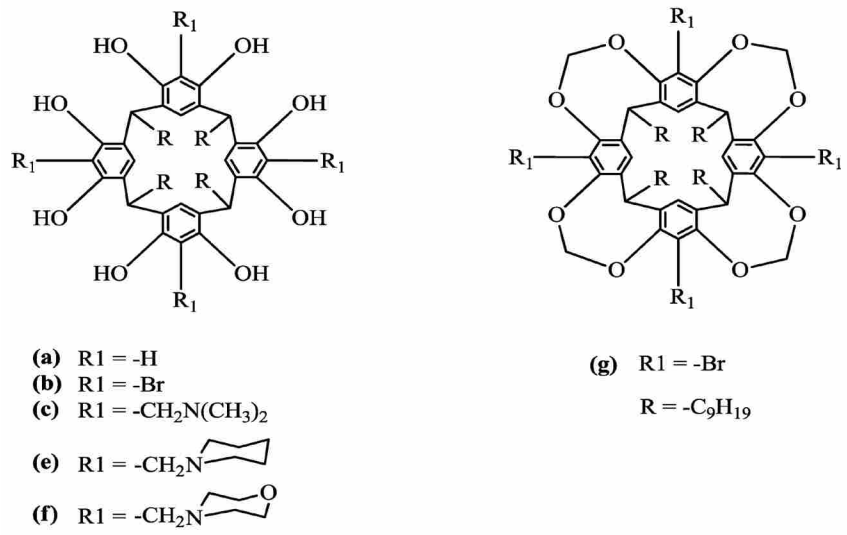

Figure 2.29 Structures of the resorcinarene derivatives incorporated in the BLMs.[42]

Polymer inclusion membranes (PIM) generally contain three components: a polymer support, e.g. cellulose triacetate (CTA), a plasticizer (solvent), and carrier molecules. Resorcinarene derivatives were included in PIMs as carriers by our group[43] as potential anion

carriers. The results have been reviewed in Chapter 1.

Boutemeur's group[44] tested the application of two resorcinarenes containing $–C_4H_9$ or $–C_8H_{17}$ chains on the lower rim as carriers in PIMs. The transport of metal ions including Zn^{2+}, Pb^{2+}, and Cd^{2+} was investigated from aqueous nitrate source phase (pH = 5.5). The polymer support in PIMs was cellulose triacetate (CTA). Two plasticizers, 2-nitrophenyl octyl ether (NPOE) and 2-nitrophenyl octanoate (NPOT, Figure 2.30) were used to form the membranes. The effect of alkyl chain length of the resorcinarene, the concentration of carrier in the membrane, the plasticizers, and the pH values of the receiving phase on the metal ion flux was determined. Figure 2.31 shows the effect of the alkyl chain length of the resorcinarene on the transport of Pb^{2+}. Apparently, the resorcinarene with $–C_8H_{17}$ chains yields twice the flux of Pb^{2+} than the one with the shorter $–C_4H_9$ chains. The flux of Pb^{2+} increased linearly with the carrier ($–C_8H_{17}$ chains) concentration which ranged from 0.01 to 0.07 mg/cm^{-2} (weight transported/membrane surface area). Compared to the commonly used plasticizer NPOE, the Pb^{2+} flux was about two times lower when the other plasticizer, NPOT, was used and the $–C_8H_{17}$ resorcinarene was used as carrier. The difference in dielectric constant between NPOT (5.8) and NPOE (24.2) resulted in the different fluxes. NPOE, with its higher dielectric constant, reduced the resistance to metal ion mass transfer from the aqueous phase to the membrane. In addition, the dielectric constant can affect the association and dissociation of metal ions at the membrane interface. Ion pairs can dissociate more readily in the media with the higher dielectric constant. In the receiving phase pH values used ($1 < pH < 5.5$), the maximum flux of Pb^{2+} was obtained at pH = 1. When the pH value of the receiving phase increased gradually, a decrease of lead flux

was observed. Furthermore, the stability of the PIMs was tested. Membranes with both NPOE and NPOT plasticizers were stable for three days. Thereafter, the membranes deteriorated slightly and the Pb^{2+} flux decreased by about 20% after 5 days. This may result from the harsh acidic conditions applied in both the source and receiving phases.

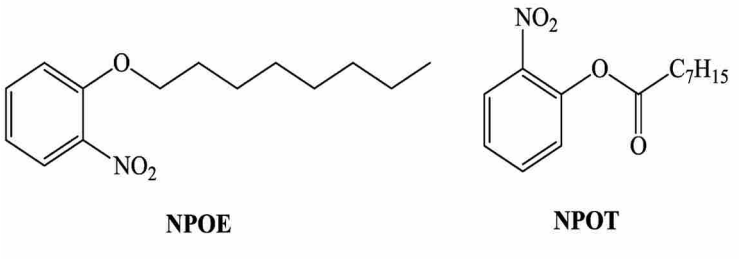

Figure 2.30 Structure of the plasticizer NPOE and NPOT.[44]

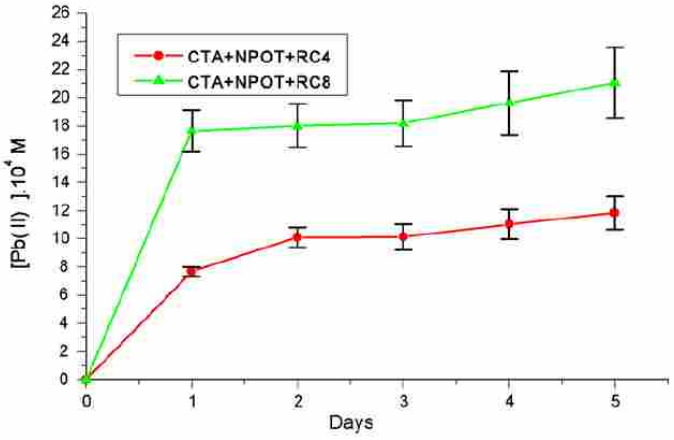

Figure 2.31 The effect of the alkyl chain length of the resorcinarene on the transport of Pb^{2+} Effect of alkyl chain length of carriers on the Pb^{2+} ions transport. Source phase: $Pb(NO_3)_2$ concentration = 10^{-2} M, $NaNO_3$ = 0.1 M, pH = 5.5. Receiving phase: HNO_3, pH = 1. PIM = 0.01 g of carriers + 0.25 mL of NPOT.[44]

Verchère and coworkers[45-47] used a resorcinarene with four $–C_{11}H_{23}$ alkyl chains on the lower rim as a carrier in supported liquid membranes (SLMs) for selectively transporting

monosaccharides and alditols. The upper rim was not modified. The membrane support was a microporous polytetrafluoethylene (PTFE) film which was impregnated with a CCl_4 solution containing resorcinarene carrier. Two PTFE membrane supports with different porosity and pore size were used for sugar transport. Porosity and pore size values of the two membranes were 78% and 0.2 μm and 84% and 0.45 μm, respectively. The permeability of sorbose through the second SLM was about 30 times higher than through the first.

One of the problems with SLMs is that the carrier and organic solvent can dissolve to some degree in the aqueous phases, which reduces the stability of membranes. In this work, the second SLM was stable during the experimental period because of the high hydrophobicity of the resorcinarene carriers. The feed phases were sugars and alditols. The receiving phases were pure water without any buffer. The mechanism for the transport of sugar was considered to involve five steps. First, the analytes diffused from the bulk feed phase to the membrane interface. Second, the resorcinarene carriers form complexes with the analytes at the interface. The complexation between sugars and resorcinarene has been reported by Aoyama's group.[48] Third, the formed complex diffuses through the SLM towards the SLM-receiving phase interface. Fourth, the resorcinarene-analyte complexes dissociate at the SLM-receiving phase interface. Fifth, the analytes diffuse into the bulk receiving phase. Among these steps, the third was considered as rate-determining. However, the third step was found not to be controlled purely by diffusion, but also involved a term caused by the convection of the organic phase within the PTFE pores. The selectivity of membranes on sugars and alditols depends among their sizes and configurations. Miloudi et al.[49, 50] also applied the same SLM for transport of methyl

aldopyranosides and alditols. The flux of each methyl aldopyranoside depends on initial concentration of resorcinarene carrier and methyl aldopyranoside. The permeability of each analyte was calculated and the mechanism of transport was described.

6. Ion chromatography (IC)

In our group, we are developing resorcinarene derivatives as selective ion-exchangers in IC. In Chapter 1, the applications of these ligands to IC were reviewed.[11] My project is to design and synthesize new resorcinarene-based ligands and to use them for IC separations. This project has three parts. First, the resorcinarene-based macrocyclic ligands containing amino acid groups on the upper rim were synthesized and characterized by NMR, MS, and dynamic light scattering techniques. Next, molecular recognition between the macrocyclic ligands and a series of amine guests was investigated. Finally, IC columns were prepared with the synthesized ligands and used for transition metal ion separations.

References

1. Petrov, G. S.; Grigor'ev, A. P. Resorcinol-aldehyde resins. *Zhurnal Khimicheskoi Promyshlennosti* **1941**, *18*, 23-24.

2. Niederl, J. B.; Vogel, H. J. Aldehyde-resorcinol condensations. *J. Am. Chem. Soc.* **1940**, *62*, 2512-2514.

3. Högberg, A. G. S. Stereoselective synthesis and DNMR study of two 1,8,15,22-tetraphenyl[1_4]metacyclophan-3,5,10,12,17,19,24,26-octols. *J. Am. Chem. Soc.* **1980**, *102*, 6046-6050.

4. Högberg, A. G. S. Two stereoisomeric macrocyclic resorcinol-acetaldehyde condensation products. *J. Org. Chem.* **1980**, *45*, 4498-4500.

5. Erdtman, H.; Högberg, S.; Abrahamsson, S.; Nilsson, B. Cyclooligomeric phenol-aldehyde condensation products I. *Tetrahedron Lett.* **1968**, *9*, 1679-1682.

6. Rudkevich, D. M.; Rebek, J. Jr. Deepening cavitands. *Eur. J. Org. Chem.* **1999**, *9*, 1991-2005.

7. Salorinne, K.; Weimann, D. P.; Schalley, C. A.; Nissinen, M. Resorcinarene podand with amine-fuctionalized side arms-synthesis, structure, and binding properties of a neutral anion receptor. *Eur. J. Org. Chem.* **2009**, *35*, 6151-6159.

8. O'Farrell, C. M.; Hagan, K. A.; Wenzel, T. J. Water-soluble calIx[4]resorcinarenes as chiral NMR solvating agents for bicyclic aromatic coumpounds. *Chirality.* **2009**, *21*, 911-921.

9. Chio, H. J.; Park, Y. S.; Youn, S. J.; Kim, H. S.; Kim, S. H.; Koh, K.; Paek, K. Structure properties of benzimidazole cavitand and its selective recognition toward 4-methylbenzamide over 4-methylanilide. *J. Org. Chem.* **2005**, *70*, 5974-5981.

10. Ghaedi, M.; Karami, B.; Ehsani, Sh.; Marahel, F.; Soylak, M. Preconcentration-separation of Co, Ni, Cu and Cd in real samples by solid phase extraction of a

calix[4]resorcinarene modified amberlite XAD-16 resin. *J Hazard. Mater.* **2009**, *172*, 802-809.

11. Wang, J.; Harrison, R. G.; Lamb, J. D. Anion separation and preconcentration with cyclen and cyclen-resorcinarene derivatives. *J. Chromatogr. Sci.* **2009**, 47, 510-515.

12. Moll, H. E.; Sémeril, D.; Matt, D.; Youinou, M. T.; Toupet, L. Synthesis of a resorcinarene-based tetraphosphine-cavitand and its use in Heck reaction. *Org. Biomol. Chem.* **2009**, *7*, 495-501.

13. Shimizu, S.; Shimada, N.; Sasaki, Y. Mannich-tyoe reactions in water using anionic water-soluble calixarenes as recoverable and reusable catalysts. *Green Chem*. **2006**, *8*, 608-614.

14. Gissot, A.; Rebek, J. Jr. A functionalized, deep cavitand catalyzes the aminolysis of a choline derivative. *J. Am. Chem. Soc.* **2004**, *126*, 7424-7425.

15. Shirakawa, S.; Shimizu, S. Dehydrative amination of alcohols in water using a water-soluble calix[4]resorcinarene sulfonic acid. *Synlett* **2008**, *10*, 1539-1542.

16. Djernes, K. E.; Moshe, O.; Mettry, M.; Richards, D. D.; Hooley, R. J. Metal-coordinated water-soluble cavitands act as C-H oxidation catalysts. *Org. Lett.* **2012**, *14*, 788-791.

17. Cevasco, G.; Thea, S.; Vigo, D.; Williams, A.; Zaman, F. Catalysis and inhibition of ester hydrolysis in the presence of resorcinarene hosts functionalized with dimethylamino groups. *J. Phys. Org. Chem*. **2006**, *19*, 630-636.

18. Kashapov, R. P.; Pashirova, T. N.; Zhiltsova, E. P.; Lukashenko, S. S.; Ziganshina, A. Y.; Zakharova, L. Y. Supramolecular systems based on aminomethylated calixa[4]resorcinarene

and a cationic surfactant catalysts of the hydrolysis of esters of phosphorus acids. *Russ. J. Phys. Chem. A* **2012**, *86*, 200-204.

19. O'Farrell. C. M.; Chudomel, J. M.; Collins, J. M.; Dignam, C. F.; Wenzel, T. J. Water-soluble calyx[4]resorcinarenes with hydroxyproline groups as chiral NMR solvating agents. *J. Org. Chem.* **2008**, *73*, 2843-2851.

20. Mann, E.; Rebek, J. Jr. Deepened chiral cavitands. *Tetrahedron* **2008**, *64*, 8484-8487.

21. Gebauer, S.; Friebe, S.; Scherer, G.; Gübitz, G.; Krauss, G. High performance liquid chromatography on calixarene-bonded silica gels. III. Separations of cis/trans isomers of proline-containing peptides. *J. Chromatogr. Sci.* **1998**, *36*, 388-394.

22. Hyun, M. H. Characterization of liquid chromatographic chiral separation on chiral crown ether stationary phase. *J. Chromatogr. Sci.* **2003**, *26*, 242-250.

23. Pietraszkiewicz, O.; Pietraszkiewicz, M. Separation of Pyrimidine Bases on a HPLC stationary RP-18 Phase Coated with Calix[4]resorcinarene. *J. Inclusion Phenom. Macrocyclic Chem.* **1999**, *35*, 261-270.

24. Sokoließ, T.; Menyes, U.; Roth, U.; Jira, T. Separation of *cis*- and *trans*-isomers of thioxanthene and dibenz[*b*,*e*]oxepin derivatives on calixarene- and resorcinarenebonded high-performance liquid chromatography stationary phases. *J. Chromatogr. A* **2002**, *948*, 309-319.

25. Pietraszkiewicz, O.; Pietraszkiewicz, M. Separation of pyrimidine bases on HPLC stationary RP-18 phase coated with calix[4]resorcinarene. *Pol. J. Chem.* **1998**, *72*, 2418-2422.

26. Pietraszkiewicz, M.; Pietraszkiewicz, O.; Kozbial M. Calix[4]resorcinarene as dynamic coating for modified stationary RP-18 phase for HPLC. *Pol. J. Chem.* **1998**, *72*, 1963-1970.

27. Ruderisch, A.; Iwanek, W.; Pfeiffer, J.; Fischer, G.; Albert, K.; Schurig, V. Synthesis and characterization of a novel resorcinarene-based stationary phase bearing polar headgroups for use in reversed-phase high-performance liquid chromatography. *J. Chromatogr. A* **2005**, *1095*, 40-49.

28. Tan H. M.; Soh, S. F.; Zhao, J.; Yong, E. L.; Gong, Y. H. Preparation and Application of Methylcalix[4]resorcinarene-bonded Silica Particles as Chiral Stationary Phase in High-performance Liquid Chromatography. *Chirality* **2011**, *23*, E91-97.

29. Lipkowski, J.; Kalchenko, O. I.; Slowikowska, J.; Kalchenko, V. I.; Lukin, O. V.; Markovsky, L. N.; Nowakowski, R. Host-guest interactions of calix[4]resorcinarenes with benzene derivatives in conditions of reversed-phase highperformance liquid chromatography. Determination of stability constants. *J. Phys. Org. Chem.* **1998**, *11*, 426-435.

30. Zhang, H. B.; Dai, R. J.; Ling, Y.; Wen, Y. X.; Zhang, S.; Fu, R. N.; Gu, J. L. Resorcarene derivative used as a new stationary phase for capillary gas chromatography. *J. Chromatogr. A* **1997**, *787*, 161-169.

31. Ruderisch, A.; Pfeiffer, J.; Schurig, V. Synthesis of an enatiomerically pure resorcinarene with pendant L-valine residues and attachment to a polysiloxane (Chirasil-Calix). *Tetrahedron: asymmetry* **2001**, *12*, 2025-2030.

32. Pfeiffer, J.; Schurig, V. Enantiomer separation of amino acid derivatives on a new polymeric chiral resorc[4]arne stationary phase by capillary gas chromatography. *J. Chromatogr. A* **1999**, *840*, 145-150.

33. Ruderisch, A.; Pfeiffer, J.; Schurig, V. Mixed chiral stationary phase containing modified resorcinarene and β-cyclodextrin selectors bonded to a polysiloxane for enantioselective gas chromatography. *J. Chromatogr. A* **2003**, *994*, 127-135.

34. Levkin, P. A.; Ruderisch, A.; Schurig, V. Combining the enantioselectivity of a cyclodextrin and a diamide selector in a mixed binary gas-chromatographic chiral stationary phase. *Chirality,* **2006**, *18*, 49-63.

35. Bächmann, K.; Bazzanella, A.; Haag, I.; Han, K. Y.; Arnecke, R.; Böhmer, V.; Vogt, W. Resorcinarenes pseudostationary phases with selectivity for electrokinetic chromatography. *Anal. Chem.* **1995**, *67*, 1722-1726.

36. Bazzanella, A.; Mörbel, H.; Bächmanna, K.; Milbradt, R.; Böhmer, V.; Vogt, W. Highly efficient separation of amines by electrokinetic chromatography using resorcarene-octacarboxylic acids as pseudostationary phases. *J. Chromatogr. A* **1997**, *792*, 143–149.

37. Terabe, S.; Otsuka, K.; Ando, T. Band Broadening in Electrokinetic Chromatography with Micellar Solutions and Open-Tubular Capillaries. *Anal. Chem.* **1989**, *61*, 251-260.

38. Bazzanella, A.; Bächmann, K.; Milbradt, R.; Böhmer, V.; Vogt, W. Discontinuous electrokinetic chromatography of parabens using different substituted resonances as pseudostationary phases. *Electrophoresis*, **1999**, *20*, 92-99.

39. Britz-Mckibbin, P.; Chen, D. D. Y. A water-soluble tetraethylsulfonate derivative of 2-methylresorcinarene as an addictive for capillary electrophoresis. *Anal. Chem.* **1998**, *70*, 907-912.

40. Sokoließ, T.; Gronau, M.; Menyes, U.; Roth, U.; Jira, T. Separation of (*Z*)- and (*E*)-isomers of thioxanthene and dibenz[*b,e*]oxepin derivatives with calixarenes and resorcinarenes as additives in nonaqueous capillary electrophoresis. *Electrophoresis* **2003**, *24*, 1648-1657.

41. Sokoließ, T.; Opolka, A; Menyes U; Menyes, U.; Roth U.; Jira, T. Separation of racemic drugs on chiral resorcinarene-bonded HPLC-columns. *Pharmazie* **2002**, *57*, 589-590.

42. Fedorenko, S. V.; Mustafina, A. R.; Ziganshina, A. U.; Kazakova, E. K.; Konovalov, A. I. Calix[4]resorcinarene and alkylaminomethylated calix[4]resorcinarene-mediated transport of some metal complexes through chloroform bulky liquid membrane. *Mater. Sci. Eng. C* **2001**, *18*, 271-274.

43. Gardner, J. S.; Peterson, Q. P.; Walker, J. O.; Jensen, B. D.; Adhikary, B.; Harrison, R. G.; Lamb, J. D. Anion transport through polymer inclusion membranes facilitated by transition metal containing carriers. *J. Membr. Sci.* **2006**, *277*, 165-176.

44. Benosmane, N.; Hamdi, S. M.; Hamdi, M.; Boutemeur, B. Selective transport of metal ions across polymer inclusion membrane (PIMs) containing calix[4]resorcinarenes. *Sep. Purif. Technol*. **2009**, *65*, 211-219.

45. Rhlalou, T.; Ferhat, M.; Frouji, M. A.; Langevin, D.; Métayer, M.; Verchère, J. F. Facilitated transport of sugars by a resorcinarene through a support liquid membrane. *J. Membr. Sci.* **2000**, *168*, 63-73.

46. Verchère, J. F. Facilitated transport of saccharides through a support liquid membrane containing a neutral lipophilic resorcinarene carrier. *Macromol. Symp.* **2002**, *188*, 205-116.

47. Tbeur, N.; Rhlalou, T.; Hlaïbi, M.; Langevin, D.; Métayer, M.; Verchère, J. F. Molecular recognition of carbohydrates by a resorcinarene, selective transport of alditols through a supported liquid membrane. *Carbohydr. Res.* **2000**, *329*, 409-422.

48. Aoyama, Y.; Tanaka, Y.; Sugahara, S. Molecular recognition 5. Molecular recognition of sugars via hydrogen-bonding interaction with a synthetic polyhydroxy macrocycle. *J. Am. Chem. Soc.* **1989**, *111*, 5397-5404.

49. Touaj, K.; Tbeur, N.; Hor, M.; Verchère, J. F.; Hlaïbi, M. A support liquid membrane (SLM) with resorcinarene for facilitated transport of methyl glycopyranosides: parameters and mechanism relating to the transport. *J. Membr. Sci.* **2009**, 337, 28-38.

50. Hlaïbi, M.; Tbeur, N.; Benjjar, A.; Kamal, O.; Lebrun, L. Carbohydrate-resorcinarene complexes involved in the facilitated transport of alditols across a support liquid membrane. *J. Membr. Sci.* **2011**, *377*, 231-240.

Chapter 3 Resorcinarene-based Cavitands with Chiral Amino Acid Substituents for Chiral Amine Recognition

Abstract[3]

Resorcinarene-based deep cavitands alanine methyl resorcinarene acid (**AMA**), alanine undecyl resorcinarene acid (**AUA**) and glycine undecyl resorcinarene acid (**GUA**), which contain chiral amino acids, have been synthesized. The upper rim of the resorcinarene host is elongated with four identical substituents topped with alanine and glycine groups. The structures of the new resorcinarenes were elucidated by nuclear magnetic resonance (NMR), mass spectrometry (MS) and the sustained *off*-resonance irradiation collision induced dissociation (SORI-CID) technique in FTICR-MS. These studies revealed that eight water molecules associate to the cavitand, two per each alanine group. The alanine substituent groups are proposed to form a kite-like structure around the resorcinarene scaffold. The binding of **AMA**, **AUA**, and **GUA** with chiral *R*- and *S*-methyl benzyl amines was studied by ^{1}H NMR titration, and compared to that of a binary *L*-tartaric acid and the monoacid phthalyl alanine (**PA**). The results show that these compounds interact with amine guests; however, with four carboxylic acid groups, they bind several amine molecules strongly while the binary *L*-tartaric acid only binds one amine guest strongly. The simple compound, **PA**, which contains one carboxylic group, shows weak binding

[3] Part of this research has been published.
Li, N.; Yang, F.; Stock, H. A.; Dearden, D. V.; Lamb, J. D.; Harrison, R. G. *Org. Biomol. Chem.* **2012**, *10,* 7382-7401.

to the amines. The ^{1}H NMR titration of **AUA** with primary, secondary, and tertiary chiral amines showed that it can discriminate between these three types of amines and between enantiomers of secondary amines.

1. Introduction

Resorcinarenes are cyclic tetramers that are synthesized from the condensation of resorcinol and various aldehydes, as originated by Hogberg[1] and further developed by Cram and coworkers. [2] These host molecules are relatively easy to synthesize in a wide range of sizes and functional groups.[3] They have applications in supramolecular recognition,[4] nanoscale reaction containment,[5] catalysis,[6] chiral NMR shift agents,[7] chromatographic separations,[8] and drug encapsulation, protection, and delivery.[9]

Chiral resorcinarene-based cavitands are rare, but have been prepared in several ways.[7b,10] One particularly effective approach is to introduce chiral substituent groups on the upper rim of the resorcinarene. It is hoped that the cavitand will bind guests having complementary functional groups by non-covalent interactions. In this way, the cavitand might selectively bind guests of proper size, shape, chirality, hydrophobicity, and surface charge characteristics. Usually, the binding of a guest is indicated by an upfield shift in the NMR signal of the guest due to shielding by the resorcinol rings.

Selective binding of enantiomers by macrocyclic ligands has significant potential application in separation of pharmaceuticals and enantioselective catalysis. Asymmetrically functionalized resorcinarenes were used as catalysts for the addition reaction of diethylzinc to

benzaldehyde.[11] A bridged dimethoxy ketal diamine ligand containing asymmetric units was bonded to the upper rim of the resorcinarene and demonstrated enantioselectivity for (*R*)-1-phenyl propyl alcohol (ee. 51%). Also, water-soluble resorcinarenes used as chiral NMR solvating agents for green chemistry applications and pharmaceutical delivery have been prepared.[7] Chiral NMR solvating agents associate with enantiomers selectively by non-covalent interaction and the resulting diastereomeric complexes may exhibit different chemical shifts in the NMR spectrum. As a result, chiral NMR solvating agents can be used to estimate the purity of enantiomers. The cavitands containing hydroxyproline groups demonstrated chiral discrimination for pyridyl, phenyl, and bicyclic aromatic substrates.

The synthesis of chiral resorcinarenes based on stereo centers atop elongated side panels to provide a deep pocket for substrate sequestration has been reported.[12] These hosts were shown to discriminate between enantiomeric guests. The upper rim of a deepened resorcinarene was modified with Fmoc-protected chiral alanine chlorides to create a hydrophobic pocket with a chiral opening. Two sets of upfield NMR signals corresponding to the diastereomeric complexes formed by (+)- and (-)-pinanediol were observed. This work confirmed the feasibility of creating asymmetric deep resorcinarene-based cavitands by introducing chiral substituent groups on the upper rim. Amino acids have been used previously to modify such hosts, but in a very different configuration from that used in the work described herein.

We report in this paper designed and characterized deep chiral cavitands using amino acid substituents on the upper rim of resorcinarenes. The elongated cavitand design has potential advantages. Specifically, different amino acids can be bonded to the resorcinarene and as a result,

the acidity of the host and design of the chiral center can be modified. The chiral alanine groups provide stereo centers, while the carboxylic acid groups concentrated on the upper rim can enhance the non-covalent interactions with guests via hydrogen bonding and electrostatic forces. Furthermore, the lower rim of the resorcinarenes can be modified with long alkyl chains making it possible to adsorb the compounds to a hydrophobic resin for separations applications.[8,13] We present a detailed structural study of the alanine containing resorcinarene and its binding to chiral primary, secondary and tertiary amines.

2. Experimental

2.1 General methods

Deuterated NMR solvents were obtained from Cambridge Isotope Laboratories, Inc. All other chemical reagents were used as supplied from Aldrich Chemical Inc., unless otherwise noted. The resorcinarenes were synthesized using the method of Hogberg,[1] employing acetaldehyde to yield the methyl-substituted version and undecyl aldehyde for the undecyl-substituted version. Compounds **1**,[14] **2**,[15] **3**,[16] and 4,[16] as well as phthalyl alanine **(PA)**[17] were synthesized according to published methods. For clarity in this paper, we refer to individual resorcinarene compounds using acronyms constructed as follows: **A** or **G** = alanine or glycine substitution on the resorcinarene upper rim; **M** or **U** = methyl or undecyl substitution on the resorcinarene lower rim; **E**, **A**, or **Na** = ester, acid, or sodium salt of the amino acid.

^{1}H and ^{13}C NMR spectra were recorded using a VXR 500-MHz multinuclear FT-NMR spectrometer. Proton chemical shifts (^{1}H) were reported in parts per million (δ) with respect to

tetramethylsilane (TMS, δ = 0 ppm) or solvent peaks. Most of the mass spectrometric experiments were performed on a Bruker model APEX 47e Fourier transform ion cyclotron resonance (FT-ICR) mass spectrometer with a MIDAS system.[18] The micro-electrospray ionization (ESI) source with a heated metal capillary drying tube was modified based on the design of Eyler.[19] The typical operating flow rate of the ESI source was 10 $\mu L \cdot h^{-1}$. Compounds **5**, **6** and **AME** were acquired in positive mode on an Agilent 1100 LC/MS series with ESI source. The Zetasizer nano ZS dynamic light scattering instrument (Malvern instrument, Malvern, Worcestershire, UK) was used to analyze the particle size distribution of the compounds. Melting points were determined using a SRS DigiMelt MPA 160 apparatus from Stanford Research Systems, Inc. Optical rotations were measured using a Perkin-Elmer 241 polarimeter (sodium D-line, 529 nm) and D values are given in 10^{-1} deg cm^2 g^{-1}, concentration (c) in g per 100 mL. Elemental analyses were performed by M-H-W Laboratories, Phoenix, AZ.

2.2 Synthesis

Methyl 2-(2,3-dichloro-5,7-dioxo-5*H*-pyrrolo[3,4-*b*] pyrazin-6 (7*H*)-yl) propanoate (5). 5,6-Dichloropyrazine-2,3-dicarboxylic acid anhydride (**4**, 0.4380 g, 2 mmol) and L-alanine methyl ester hydrochloride (0.5030 g, 3.6 mmol) were put in a closed container. Two mL of acetic anhydride were added to the mixture and it was stirred at 120 °C for 2 h and then was poured into 20 mL of distilled water. The yellow precipitate that formed was filtered and dried under vacuum for 2 h (0.400 g, 65.8 % yield). Mp: 119-120 °C. ^{1}H NMR (500 MHz, d_6-acetone): δ (ppm) = 1.658 (d, J = 28, 3H), 3.726 (s, 3H), 5.146 (q, J = 28, 1H). ^{13}C NMR (500 MHz, d_6-

acetone) δ (ppm): 170.2, 162.8, 153.5, 145.3, 53.3, 48.9, 15.3. $[\alpha]_D^{23}$ = -32.0 (c 1.00, acetone). MS (MH^+, ESI) m/z 305.16 (Calculated: 305.09).

Ethyl 2-(2,3-dichloro-5,7-dioxo-5H-pyrrolo[3,4-b] pyrazin-6(7H)-yl) acetate (6). 5,6-Dichloropyrazine-2, 3-dicarboxylic acid anhydride (**4**, 0.4380 g, 2 mmol) and glycine ethyl ester hydrochloride (0.5025 g, 3.6 mmol) were put in a closed container. Two mL of acetic anhydride were added to the mixture and it was stirred at 120 °C for 2 h and then was added to 20 mL of distilled water. The yellow precipitate was filtered and dried under vacuum for 2 h (0.450 g, 74.0 % yield). Mp: 133-134 °C. ^{1}H NMR (500 MHz, d_6-acetone) δ (ppm): 1.265 (t, J = 30, 3H), 4.208 (q, J = 28, 2H), 4.561 (s, 2H). ^{13}C NMR (500 MHz, d_6-acetone) δ (ppm): 167.6, 162.8, 153.7, 145.3, 62.6, 40.1, 14.4. MS (MH^+, ESI) m/z 305.18 (Calculated: 305.09).

Alanine methyl resorcinarene ester (AME). Compound **5** (0.1000 g, 0.329 mmol) and methyl-resorcinarene (0.0404 g, 0.075 mmol) with methyl groups on the lower rim were put in a 10 mL two-necked flask connected to a condenser and nitrogen gas inlet. 2.5 mL of dry dimethyl formamide (DMF) was added to the flask. Triethylamine (TEA) (0.0756 g, 0.75 mmol) was mixed with 0.50 mL of dry DMF and injected into the flask drop-wise. The mixture was stirred at room temperature for 12 h and the white precipitate that formed was filtered under vacuum. The filtrate was evaporated by rotary evaporator and the white solid was purified by column chromatography with eluent ethyl acetate and hexane (v:v 3:1) to yield 0.0583 g (53.1 %). ^{1}H NMR (500 MHz, $CDCl_3$) δ (ppm): 1.705 (d, J = 18, 12H), 1.714 (d, J = 12, 12H), 3.726 (s, 12H), 4.069(q, J = 28, 4H) 5.012 (q, J = 28, 4H), 6.915(s, 4H), 7.345 (s, 4H). ^{1}H NMR (500 MHz, d_6-acetone) δ (ppm): 1.505 (d, J = 30, 12H), 1.585 (d, J = 28, 12H), 3.566 (s, 12H), 4.077 (q, J = 28,

4H), 4.932 (q, J = 30, 4H), 7.156 (s, 8H). ^{13}C NMR (500 MHz, d_6-acetone) δ (ppm): 170.4, 163.4, 152.5, 141.6, 135.2, 53.1, 48.4, 32.8, 17.8, 15.5. $[\alpha]_D^{23}$ = -16.2 ± 0.0 (c 1.00, acetone). MS [$(M+8H_2O+H)^+$, ESI] m/z 1614.46 (Calculated: 1614.37).

Alanine methyl resorcinarene sodium salt (AMNa). Compound **AME** (0.1000 g) was dissolved in 3 mL of tetrahydofuran (THF) and 0.100 g of NaOH in 10 mL of H_2O was added. The mixture was refluxed for 12 h until the water layer became clear. The solvent was evaporated and the solid was washed with CH_2Cl_2 and extracted with H_2O. The H_2O layer was collected and evaporated. A red solid was obtained and the yield was 0.0780 g (76.3%). ^{1}H NMR (500 MHz, D_2O,) δ (ppm): 1.240 (br, 12 H), 1.407 (d, J = 30, 12H), 4.121 (br, 4H), 4.288 (q, J = 28, 4H). ^{13}C NMR (500 MHz, D_2O) δ (ppm): 180.2, 173.4, 171.0, 161.3, 51.2, 50.9, 50.6, 48.8, 17.5, 17.4. $[\alpha]_D^{23}$ = 34.6 ± 0.8 (c 1.00, H_2O). FTICR-MS [$(M+8H_2O-4Na+2H)^{2-}$, ESI)] m/z 777.24 (Calculated: 777.17). The Li and K salts were synthesized in a similar manner except LiOH and KOH were used instead of NaOH.

Alanine methyl resorcinarene acid (AMA). Compound **AMNa**, 0.1000 g, was dissolved in H_2O and acidified with diluted HCl (2 M). The yellow precipitate that formed was filtered, dissolved in methanol and filtered. The filtrate was evaporated by rotary evaporator to yield 0.0842 g (89.4 %). ^{1}H NMR (500 MHz, d_6-DMSO) δ (ppm): 1.260 (br, 12 H), 1.409 (br, 12H), 3.925 (br, 4H), 4.291 (br, 4H). ^{13}C NMR (500 MHz, D_2O) δ (ppm): 173.4, 155.7, 148.5, 48.6, 42.0, 17.5. $[\alpha]_D^{23}$ = +11.2 ± 0.4 (c 1.00, methanol). FTICR-MS [$(M+8H_2O-H)^-$, ESI)] m/z 1556.50 (Calculated: 1556.28).

Glycine undecyl resorcinarene ethyl ester (GUE). Compound **6** (0.1000 g, 0.329

mmol) and undecyl-resorcinarene (0.0825 g, 0.075 mmol) were put in a 10 mL two-necked flask connected to a condenser and nitrogen gas inlet. 2.5 mL of dry DMF was added to the flask. TEA (0.0756 g, 0.75 mmol) was mixed with 0.5 mL of dry DMF and injected into the flask drop-wise. The mixture was stirred at room temperature for 12 h. The large amount of white precipitate that formed was removed by filtration. The filtrate was evaporated to dryness by rotary evaporator and the white solid purified by column chromatograph with eluent ethyl acetate and hexane (v:v 3:1) yielded 0.1207 g (79.6 %). ^{1}H NMR (500 MHz, $CDCl_3$,) δ (ppm): 0.88 (t, *J* = 28, 12H), 1.25 (b, 72H), 1.39 (t, *J* = 32, 12H), 4.14 (s, 4H), 4.19 (q, *J* = 30, 8H), 4.48 (s, 8H), 6.93 (s, 4H), 7.45 (s, 4H). ^{1}H NMR (500 MHz, d_6-acetone) δ (ppm): 0.75 (t, *J* = 30, 12H), 1.12 (b, 84H), 2.10 (s, 12H), 3.92 (t, *J* = 30, 4H), 4.07 (q, *J* = 28, 8H), 4.36 (s, 8H), 7.10 (s, 4H), 7.20 (s, 4H). ^{13}C NMR (500 MHz, d_6-acetone) δ (ppm): 168.0, 163.7, 153.1, 142.1, 134.5, 126.2, 62.5, 39.8, 38.4, 32.8, 23.5, 32.0, 28.0, 14.5. Anal. calcd. for $C_{112}H_{132}N_{12}O_{24}$□$8H_2O$: C 61.86, H 6.86, N 7.73%; found: C 61.98, H 7.03, N 7.99%. MS [$(M+8H_2O+H)^+$, ESI] m/z 2174.97 (Calculated: 2174.04).

Glycine undecyl resorcinarene sodium salt (GUNa). GUE (0.1000 g) was dissolved in 3 mL of THF and 0.100 g of NaOH in 10 mL of H_2O was added. The mixture was refluxed for 12 h until the water layer became clear. The solvent was evaporated and the solid was washed with CH_2Cl_2 and extracted with H_2O. The H_2O layer was collected, evaporated and yielded 0.0878 g (88.0 %) of a red solid. ^{1}H NMR (500 MHz, D_2O) δ (ppm): 0.84 (br, 12 H), 1.24 (br, 72H), 1.82 (br, 8H), 3.56 (br, 4H), 3.91 (br, 8H). ^{13}C NMR of GUNa (500 MHz, D_2O) δ (ppm): 177.1, 165.7, 119.1, 43.6, 43.2, 31.9, 29.7, 22.6, 13.9. FTICR-MS GUNa [$(M+8H_2O -4Na)^{4-}$,

ESI)] m/z 514.27 (Calculated: 514.22).

Glycine undecyl resorcinarene acid (GUA). Compound **GUNa**, 0.1000 g, was dissolved in H_2O and acidified with diluted HCl (2 M). The yellow precipitate that formed, was filtered, dissolved in methanol and filtered. The filtrate was evaporated to dryness by rotary evaporator and yielded 0.0880 g (92.0 %). ^{1}H NMR (500 MHz, d_6-DMSO) δ (ppm): 0.82 (t, J = 24, 12 H), 1.21 (br, 72H), 1.78 (br, 8H), 3.76 (br, 8H), 3.92 (br, 4H). ^{13}C NMR (500 MHz, d_6-acetone) δ (ppm): 42.5, 33.0, 23.6, 14.7. Anal. calcd. for $C_{104}H_{116}N_{12}O_{24}$□$8H_2O$: C 60.57, H 6.45, N 8.15%; found: C 60.73, H 6.64, N 7.98%. FTICR-MS [$(M+8H_2O-2H)^{2-}$, ESI)] m/z 1030.10 (Calculated: 1030.11).

Alanine undecyl resorcinarene methyl ester (AUE). Compound **5** (0.1000 g, 0.329 mmol) and undecyl-resorcinarene (0.0825 g, 0.075 mmol) were put in a 10 mL two-necked flask connected to a condenser and nitrogen gas inlet. 2.5 mL of dry dimethyl formamide (DMF) were added to the flask. Triethylamine (TEA) (0.0756 g, 0.75 mmol) was mixed with 0.5 mL of dry DMF and injected into the flask drop-wise. The mixture was stirred at room temperature for 12 h and the white precipitate that formed was removed. The filtrate was evaporated by rotary evaporator and the white solid was purified by column chromatography with eluent ethyl acetate and hexane (v:v 3:1) to yield 0.1359 g (89.7%). ^{1}H NMR (500 MHz, $CDCl_3$) δ (ppm): 0.879 (t, J = 28, 12H), 1.25 (s, 72H), 1.69 (d, J = 28, 12H), 2.100 (d, J = 24, 8H), 3.713 (s, 12H), 4.196 (t, J = 28, 4H) 5.011 (q, J = 30, 4H), 6.929 (s, 4H), 7.457 (s, 4H). ^{1}H NMR (500 MHz, d_6-acetone) δ (ppm): 0.88 (t, J = 28, 12H), 1.27 (m, 72H), 1.64 (d, J = 30, 12H), 2.21 (d, J = 20, 8H), 3.68 (s, 12H), 4.04 (t, J = 32, 4H), 5.06 (q, J = 30, 4H), 7.22 (s, 4H), 7.32 (s, 4H). ^{13}C NMR (500 MHz,

d_6-acetone) δ (ppm): 170.5, 163.5, 153.0, 141.8, 134.5, 126.1, 53.1, 48.4, 32.4, 23.4, 15.5, 14.5. $[\alpha]_D^{23}$ = -2.57 ± 0.0 (c 1.00, $CHCl_3$). Anal. calcd. for $C_{112}H_{132}N_{12}O_{24}\square H_2O$: C 65.67, H 6.59, N 8.21%; found: C 65.72, H 6.64, N 8.03%. MS [$(M+8H_2O+H)^+$, ESI] m/z 2174.94 (Calculated: 2175.04).

Alanine methyl resorcinarene sodium salt (AUNa). **AUE** (0.1000 g) was dissolved in 3 mL of tetrahydofuran (THF) and 0.100 g of NaOH in 10 mL of H_2O was added. The mixture was refluxed for 12 h until the water layer became clear. The solvent was evaporated and the solid was washed with CH_2Cl_2 and extracted with H_2O. The H_2O layer was collected and evaporated to dryness to yield 0.0780 g (76.3 %) of a red solid. ^{1}H NMR (500 MHz, D_2O,) δ (ppm): 0.78 (br, 12 H), 1.17 (br, 84 H), 1.85 (d, 8H), 3.99 (br, 4H), 4.23 (br, 4H). ^{13}C NMR (500 MHz, D_2O) δ (ppm): 180.2, 173.4, 171.0, 161.3, 51.2, 50.9, 50.6, 48.8, 17.5, 17.4. FTICR-MS [$(M+8H_2O-2Na-H)^{3-}$, ESI)] m/z 719.67(Calculated: 719.77).

Alanine undecyl resorcinarene acid (AUA). Compound **AUNa**, 0.1000 g, was dissolved in H_2O and acidified with diluted HCl (2 M). The yellow precipitate that formed was filtered, dissolved in methanol and filtered. The filtrate was evaporated by rotary evaporator to yield 0.0862 g (90.0%). ^{1}H NMR (500 MHz, d_6-DMSO) δ (ppm): 1.26 (br, 12 H), 1.41 (br, 12H), 3.92 (br, 4H), 4.29 (br, 4H). ^{13}C NMR (500 MHz, d_6-acetone) δ (ppm): 42.5, 33.0, 23.6, 14.7. $[\alpha]_D^{23}$ = 4.48 ± 0.4 (c 1.00, methanol). Anal. calcd. for $C_{108}H_{124}N_{12}O_{24}\square 8H_2O$: C 61.23, H 6.66, N 7.93%; found: C 61.31, H 6.75, N 7.78%. FTICR-MS **AUA** [$(M+8H_2O-3H)^{3-}$, ESI)] m/z 744.99 (Calculated: 705.11).

2.3 NMR and 1H NMR titrations

All of the ^{1}H NMR titration experiments were performed in d_6-DMSO or d_4-methanol. The samples (5 mM, 500 μL) **AMA**, **GUA**, *L*-tartaric acid, and **PA** were placed in individual NMR tubes. Microliter aliquots of amine guests (100 mM) were added drop-wise to the solutions. The chemical shift changes of amine guests were monitored after each addition. The titration curves were obtained by plotting the Δδ of the methyl group of the amine against the concentration ratio of the sample to the amine.

2.4 Mass spectrometry

The FTICR-MS sustained off-resonance irradiation collision-induced dissociation (SORI-CID)[18] method was used to elucidate the structure of the resorcinarene and its complexes. In these experiments, the target peak of interest was isolated using stored waveform inverse Fourier transform (SWIFT) techniques, and the off-resonance excitation was applied for 5 s at 1 kHz below the resonance frequency of the ion of interest. The collision gas, high purity nitrogen, was pulsed into the ICR cell by a Freiser-type pulsed leak valve[20] and a 10 s delay was used to allow the background pressure in the trapping cell to drop from 10^{-5} mbar to the baseline pressure (about 10^{-8} mbar) prior to detection.

2.5 Dynamic Light Scattering

The instrument was operated at 25 °C with a detection angle of 90°. The esters (**AME** 1.1 mM, **AUE** 0.68 mM, and **GUE** 0.65 mM) were dissolved in chloroform and filtered through filter paper (2.7 μm pore size, Whatman, USA). The sodium salts (**AMNa** 0.81 mM, **AUNa** 0.63 mM, and **GUNa** 0.64 mM) and the acids (**AMA** 0.92 mM, **AUA** 0.64 mM, and **GUA** 0.75 mM)

were dissolved in distilled water and methanol, respectively, and filtered with a 25 mm syringe filter with a 0.45 μm polyethersulfone membrane (VWR international, USA).

3. Results and Discussion

The synthesis and characterization of these new amino acid containing cavitands provides host molecules with two major components, the resorcinarene scaffold and the quinoxoline panels. The resorcinarene scaffolds are formed in a one step process by combining alkyl aldehyde with resorcinol. Synthesis of the panels is a more complex process, and indeed it is through these that the amino acid functionality is introduced. To begin, 1,2-phenylenediamine is converted to the dichloropyrazine anhydride following published procedures (Scheme 1). The anhydride can be converted into the glycine or alanine-containing panel by addition of the amino acid ester. After this moiety is added to resorcinarene, the new cavitand is formed (**AME**, **AUE**, or **GUE**, Scheme 2). The undecyl chains are incorporated into some of the molecules to increase solubility in nonpolar solvents. The cavitands have four pyrazine panels on the same face of the molecule, each with an amino acid group on its upper rim. To form the salts of the amino acids, sodium hydroxide is used to hydrolyze the ester. The salts can then be converted to the acids by addition of hydrochloric acid. The target molecule has four amino acid groups held in proximity to each other, bonded to heteroatoms containing five- and six- membered rings. These will potentially be able to bind molecules through hydrogen bonding and dipole-dipole interactions.

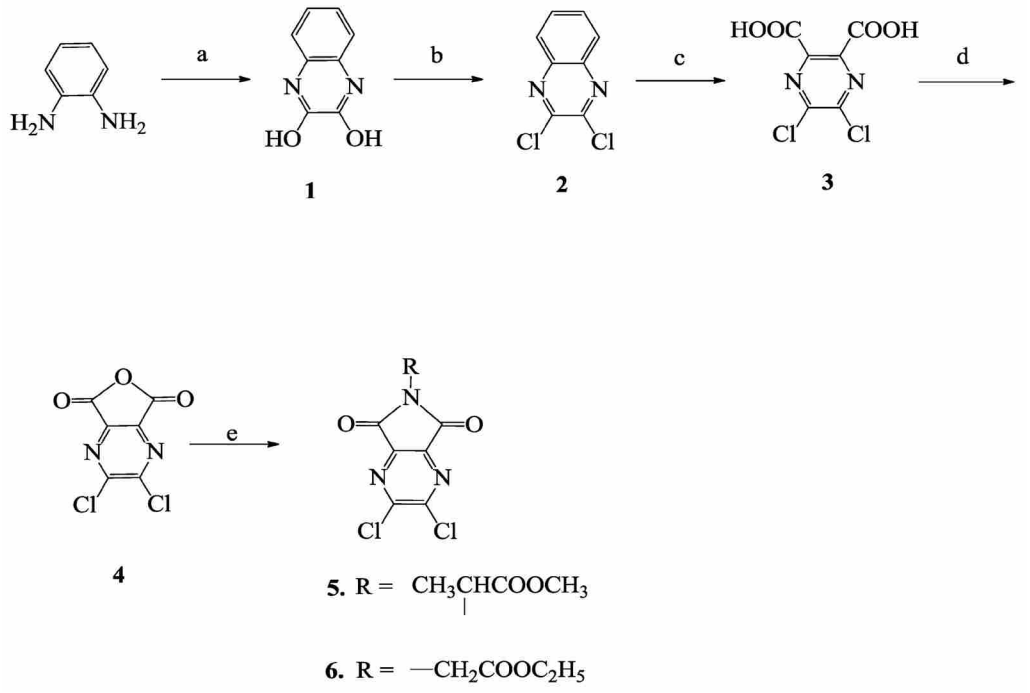

Scheme 3.1 Synthetic scheme for the amino acid containing pyrazine. Conditions: (a) oxalic acid, 2 M HCl, 2 h; (b) N,N-diethylanaline, phosphoryl chloride ($POCl_3$), 120 °C 4 h; (c) $KMnO_4$, reflux 1.5 h, HCl; (d) oxalyl chloride $(COCl)_2$, pyridine, dry THF, 0 °C 2 h, 50 °C 1 h; (e) L-alanine methyl ester hydrochloride or glycine ethyl ester hydrocholride in acetic anhydrire, 120 °C 2 h.

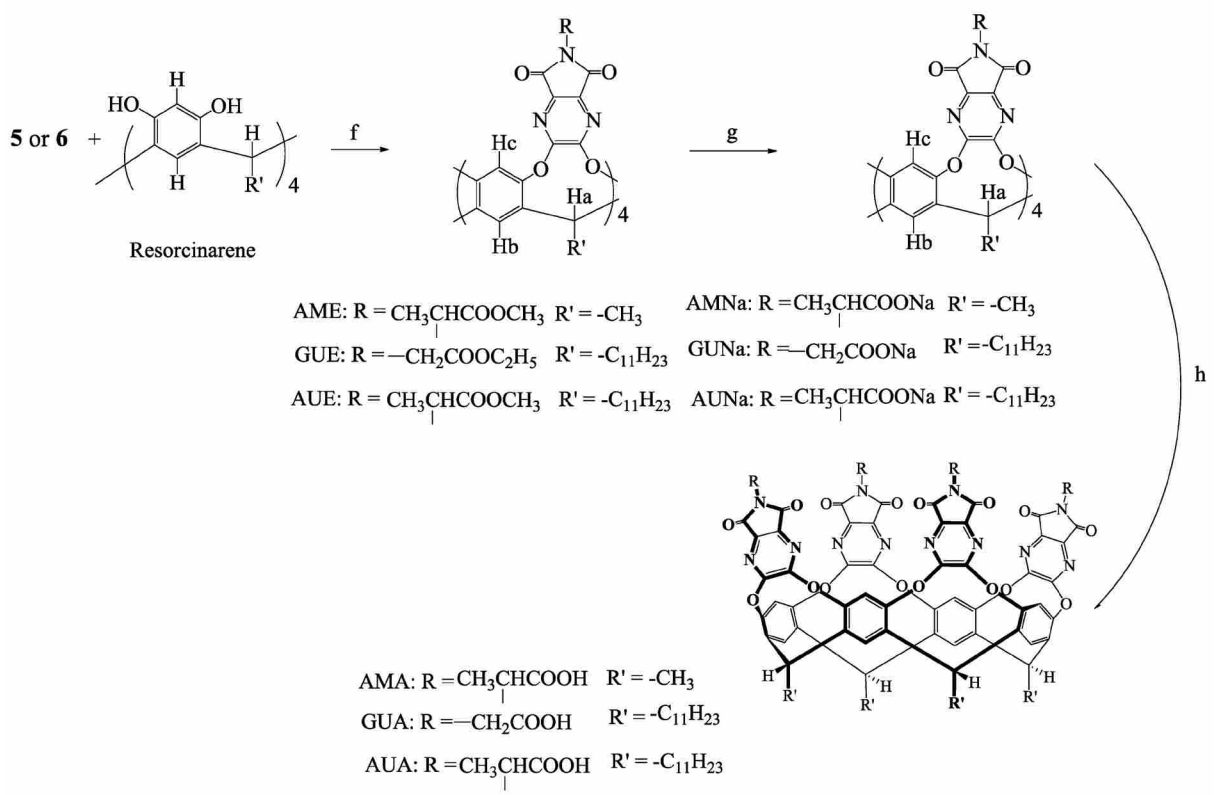

Scheme 3.2 Synthetic steps to form the amino acid containing resorcinarene cavitands. Conditions: (f) dry DMF, rt 12 h; (g) THF, NaOH, 12 h; (h) HCl, H_2O.

3.1 NMR Characterization

One of the well-known characteristics of resorcinarene-based cavitands is the conformational variation from C_{4v} to C_{2v}, namely, from the vase structure to the kite structure. In the vase structure, the four substituent groups on the upper rim of the resorcinarene are positioned vertically, forming a large vase-shape cavity; in the kite conformation, they are oriented outward, forming a flatter structure. The conformation is influenced by temperature and variations in pH. At low temperature, solvation energies stabilize the kite structure with its solvent-exposed surface; at high temperature, the entropic term predominates, and the vase

structure is favored.[21] When the nitrogen atoms of the substituent groups on the resorcinarene are protonated under acidic conditions, the repulsion between protonated nitrogen atoms promotes the kite conformation.[22] The NMR chemical shift of the methine proton on the lower rim of resorcinarene (H_a) is usually found further downfield in the vase structure than that in the kite structure, and this difference is symptomatic of compound conformation.

As mentioned above, the chemical shift of the methine proton H_a is usually considered an indicator of vase versus kite conformation. Specifically, in less polar solvents like chloroform, benzene, and THF, the methine proton of other compounds appears at $\delta \approx 5.5$ ppm or further downfield in the vase conformation and at $\delta \approx 3.7$ ppm in the kite conformation.[23] For our alanine-containing cavitand, **AME**, the chemical shifts of H_a in $CDCl_3$ and d_6-acetone are 4.069 and 4.077 ppm, respectively. These values are intermediate in chemical shift between cases of vase and kite structures reported,[23] but closer to kite conformation. Similar results were obtained for the glycine-containing analog **GUE**. Specifically, the chemical shifts of H_a in **GUE** in $CDCl_3$ and d_6-acetone are 4.145 and 3.925 ppm, respectively. These results imply that **AME** and **GUE** have relatively open kite-like structures in $CDCl_3$ and d_6-acetone.

^{1}H NMR experiments of **AME** in d_6-acetone and $CDCl_3$ at variable temperatures (VT-NMR) were performed to determine the conformation of the compound as shown in Figure 3.1. The proton H_a on the methine group of the resorcinarene became broad, lost splitting and moved upfield (about 0.1 ppm), as temperature was lowered from 40 to -20 °C. The signal of the two protons on the phenyl ring of the resorcinarene broadened and underwent coalescence as temperature was lowered. Others have reported that the phenyl protons of the resorcinarene

divided into two singlets as the temperature is lowered, indicating conformation exchange between two kite structures.[22-23] However, we didn't find that the protons split into two singlets at lower temperature, implying that **AME** maintains a stable kite-like structure. Also, VT-NMR experiments were performed on **AMNa** and **AMA** to study their conformations in solution as shown in Figure 3.2 and 3.3. The chemical shift of the methine proton H_a in **AMNa** (about 3.9 ppm) didn't change in D_2O from 9 to 60 °C as shown in Figure 2. This implies that, like the ester analog, **AMNa** maintains a kite structure. Likewise, the chemical shifts of the acid analog **AMA** in d_6-DMSO didn't show any obvious movement from 23 to 80 °C as shown in Figure 3, implying that **AMA** maintains a kite structure in DMSO.

Figure 3.1 ^{1}H NMR spectra of **AME** (500 MHz, d_6-acetone) at different temperatures.

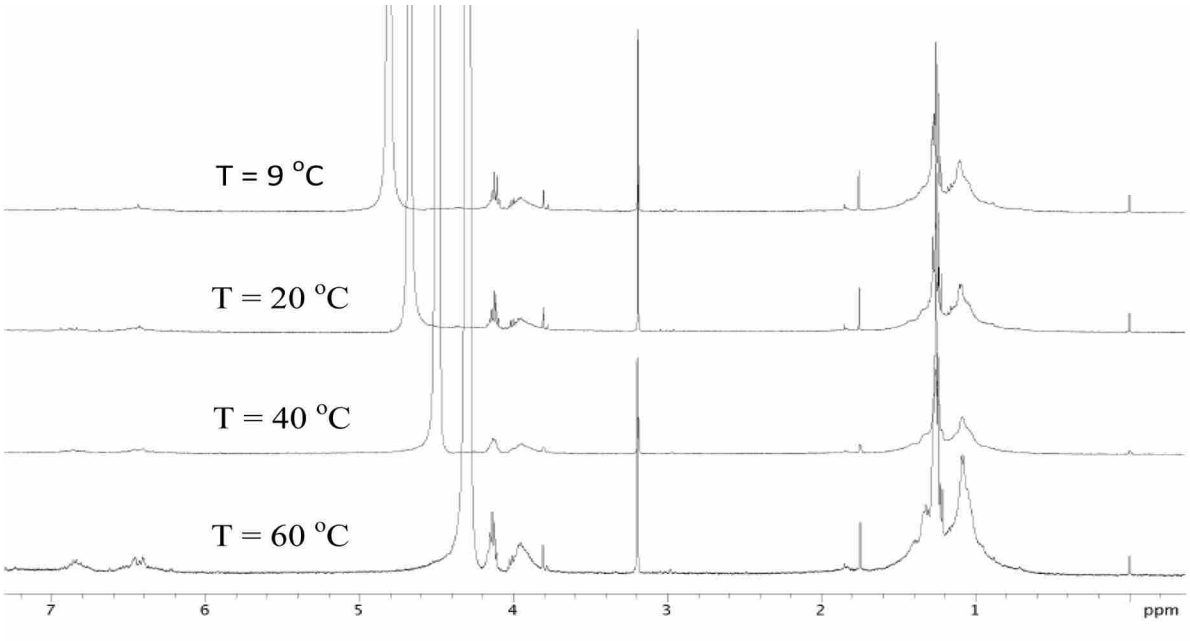

Figure 3.2 ^{1}H NMR spectra of **AMNa** (500 MHz, D_2O) at different temperatures.

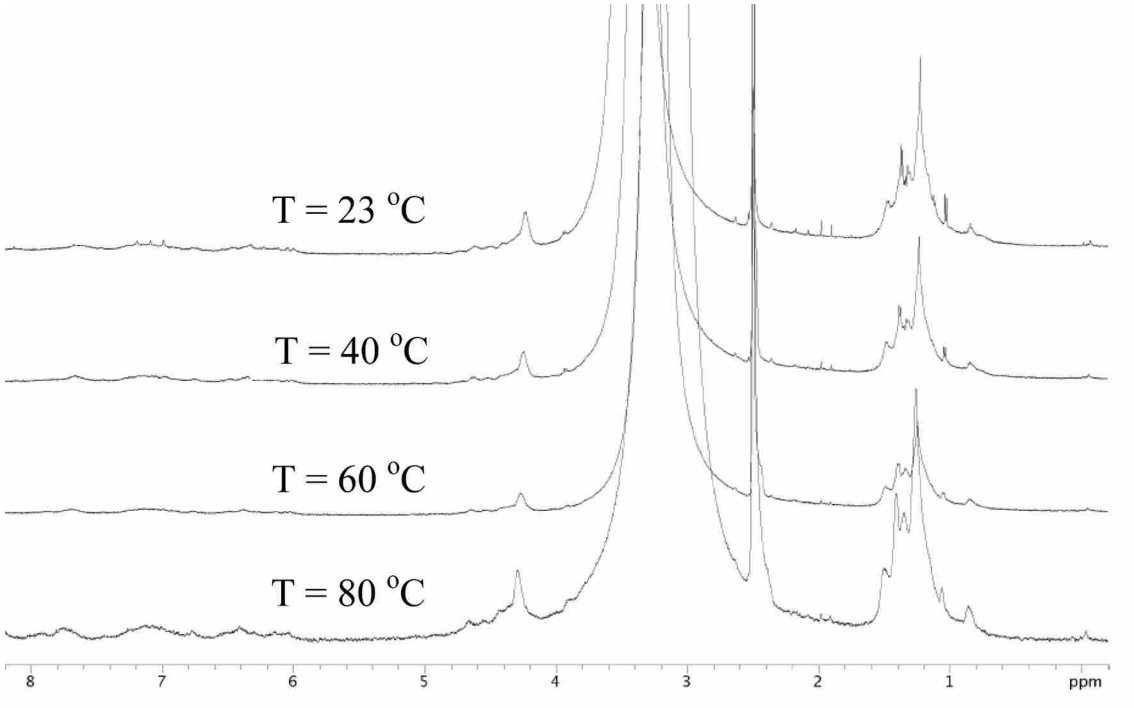

Figure 3.3 ^{1}H NMR spectra of **AMA** (500 MHz, d_6-DMSO) at different temperatures.

3.2 Particle Size Analysis

The broad NMR signals for the acid and salt molecules led us conclude that because they have polar and nonpolar ends, they might be aggregating. In polar solvents the amino acid groups will be solvated while the alkyl chains might congregate to form micelle structures. Aggregate formation would result in protons not being able to freely rotate and thus chemically equivalent protons would be in different environments, making for broad NMR signals.

Dynamic light scattering is a technique that measures Brownian motion of small particles in solution and relates it to the size distribution of small particles. The Stokes-Einstein equation shown below is used to calculate the hydrodynamic diameter of particles from their Brownian motion.[24]

$$D_H = \frac{kT}{f} = \frac{kT}{3\pi\eta D} \qquad (3.1)$$

D_H : hydrodynamic diameter; k : Boltzmann constant; f : particle frictional coefficient; η : solvent viscosity; T : absolute temperature; D : diffusion coefficent.

When a light source shines on a small particle, the light is scattered in all directions by the particles. The scattered light may interfere constructively or destructively and form bright and dark areas on a screen. In solution, particles are moving randomly and constantly due to Brownian motion such that large particles move slowly while small particles move quickly. The intensity of the dark and bright specks fluctuates due to the movement of the particles. The Zetasizer Nano instrument measures the fluctuation rate of the intensity and then uses this to calculate the size of the particles.

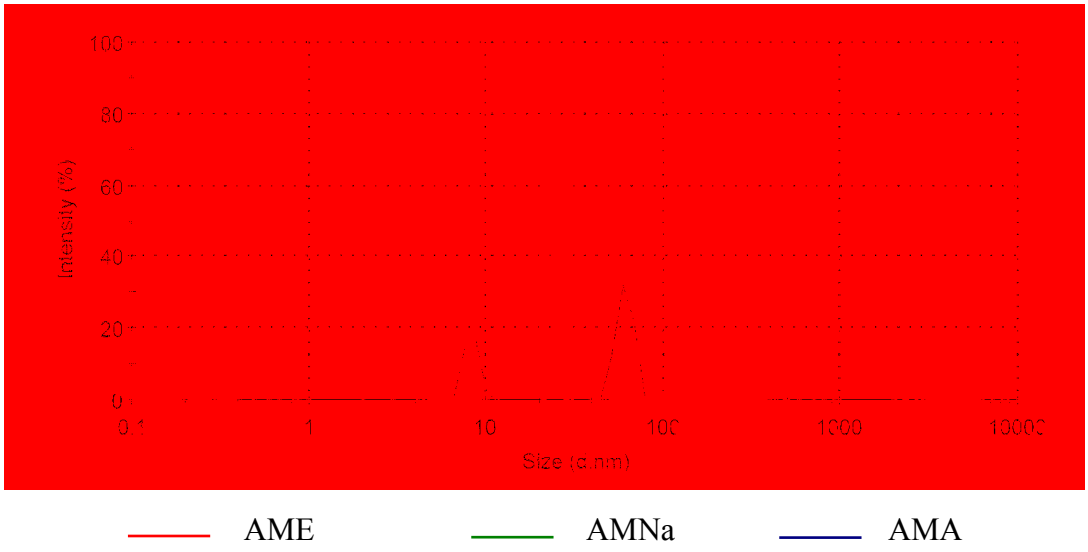

Figure 3.4 Particle size comparisons between **AME**, **AMNa**, and **AMA**.

Analysis using dynamic light scattering of the sodium salts (**AUNa**, **GUNa**, and **AMNa**) in water showed two major particle distributions, one at a small diameter particle size and another at a larger diameter. The acids (**AUA**, **GUA**, and **AMA**) dissolved in methanol also showed two broad peaks for small and large diameter sized particles. This was different from what was seen for the esters (**AUE**, **GUE**, and **AME**), where only one small diameter particle peak was observed. Even when low concentrations of the salts and acids were analyzed, large diameter particles were observed. We conclude that the salts and acids aggregate, which could explain their broad NMR signals. Size distributions of the macrocyclic ligands are shown in Figure 3.4, 3.5, and 3.6.

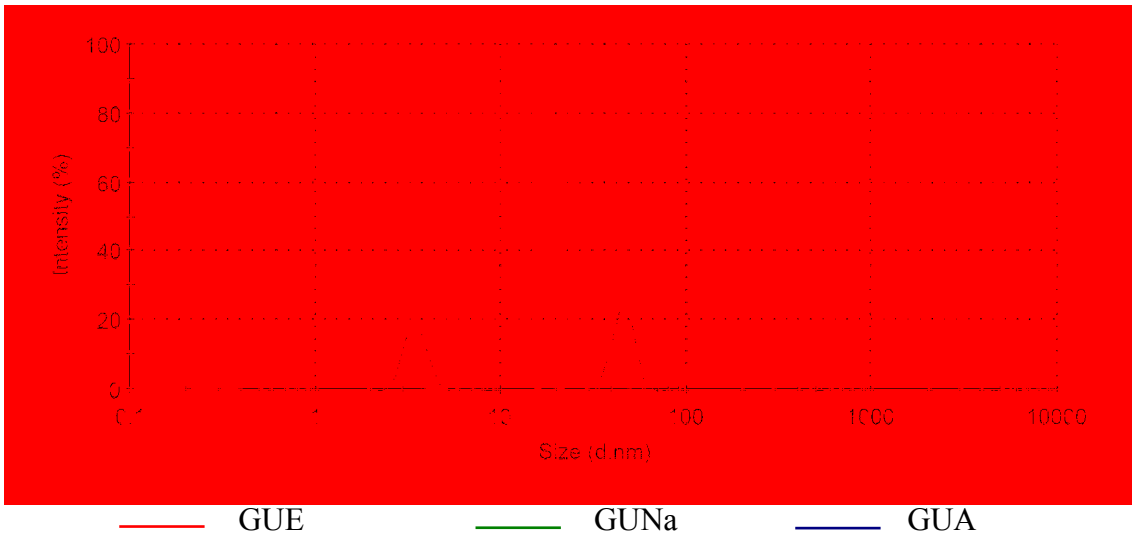

Figure 3.5 Particle size comparisons between **GUE**, **GUNa**, and **GUA**.

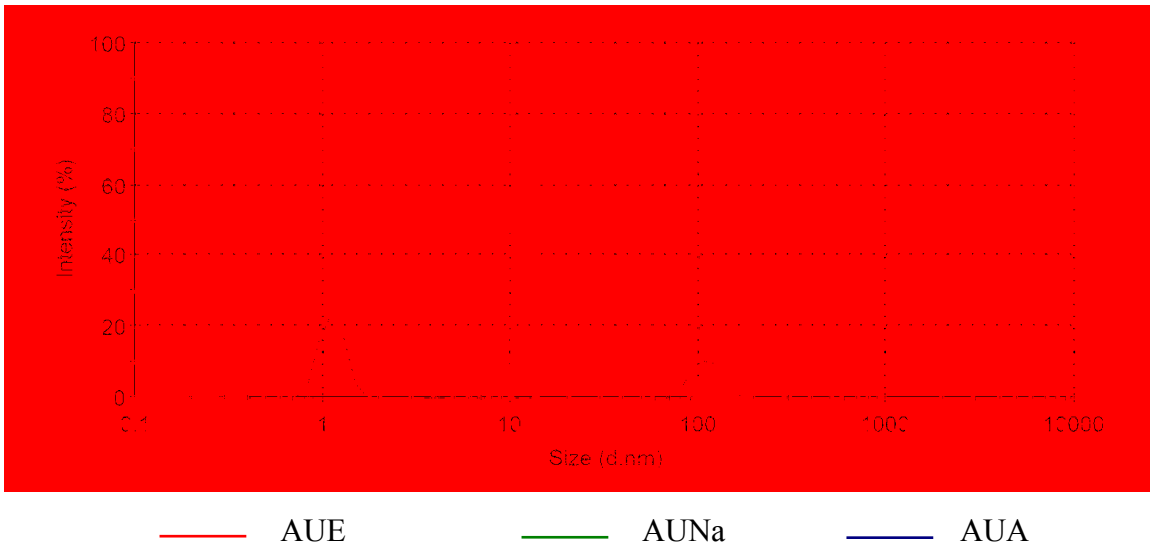

Figure 3.6 Particle size comparisons between **AUE**, **AUNa**, and **AUA**.

3.3 Mass Spectrometry Characterization

To further characterize the new amino acid containing resorcinarenes, we used mass spectrometry. The mass spectrum of **AME** was obtained by dissolving it in mixed solvents of methanol and chloroform and operating in positive mode. We obtained a +1 molecular ion peak

at m/z 1614.46. The mass difference between the calculated value and this experimental value (1469.25 amu) is 145.21 amu. A clue to the source of the difference was provided in the ^{1}H NMR spectrum of **AME**, which was sharp and clean and showed a water peak. We propose that this mass difference in the MS results from eight water molecules that are associated with **AME**. Thus, the calculated molecular peak for (**AME** + $8H_2O$) in positive mode is 1614.41 amu, which is consistent with the experimental value 1614.46 amu.

Along with characterizing the ester **AME** by mass spectrometry, we also used mass spectrometry to characterize the sodium salt and acid. First, the mass spectrum of **AMNa** in negative mode from methanol/water solvent was obtained (Figure 3.7a). The largest peak observed was a minus two ion at 777.24 m/z. In order to better understand the spectrum of **AMNa**, we also prepared the analogous potassium and lithium salts, **AMK** and **AMLi**, and obtained their mass spectra for comparison (Figure 3.7b, 3.7c). All compounds displayed a -2 peak around 777 m/z and several other higher mass peaks. For **AMNa**, the mass difference between the peak at 777 m/z and the next large peak at 788 m/z is 22 (when multiplied by 2 for charge considerations). Comparable differences were found for **AMK** and **AMLi**. Specifically, these mass differences were about 38 and 6, respectively, which correspond to the addition of an alkali metal and loss of a proton. Based on these result, we conclude that in the negative MS mode, metal ions such as Li^+, Na^+, and K^+, can be dissociated from the cavitand molecule, leaving a stable -2 charged molecular ion (mass ≈ 777). This mass at 777 amu corresponds to a parent molecular ion of 1554 amu, which is 144 amu larger than the mass of **AMA**. This mass difference is the same mass as eight water molecules, implying that once again the cavitand

associates with water in the MS. Although two THF molecules (144.12 amu), which was used as solvent during the synthesis of **AMNa**, has a similar mass to eight water molecules, it was not detected in the NMR and was not in the MS solvent. As with the ester, a water peak was observed in the NMR spectrum of **AMA**, however, it's integration was less than eight waters per **AMA**. By elimination, we conclude that **AMNa** is associated with eight water molecules, just as was true for **AME**.

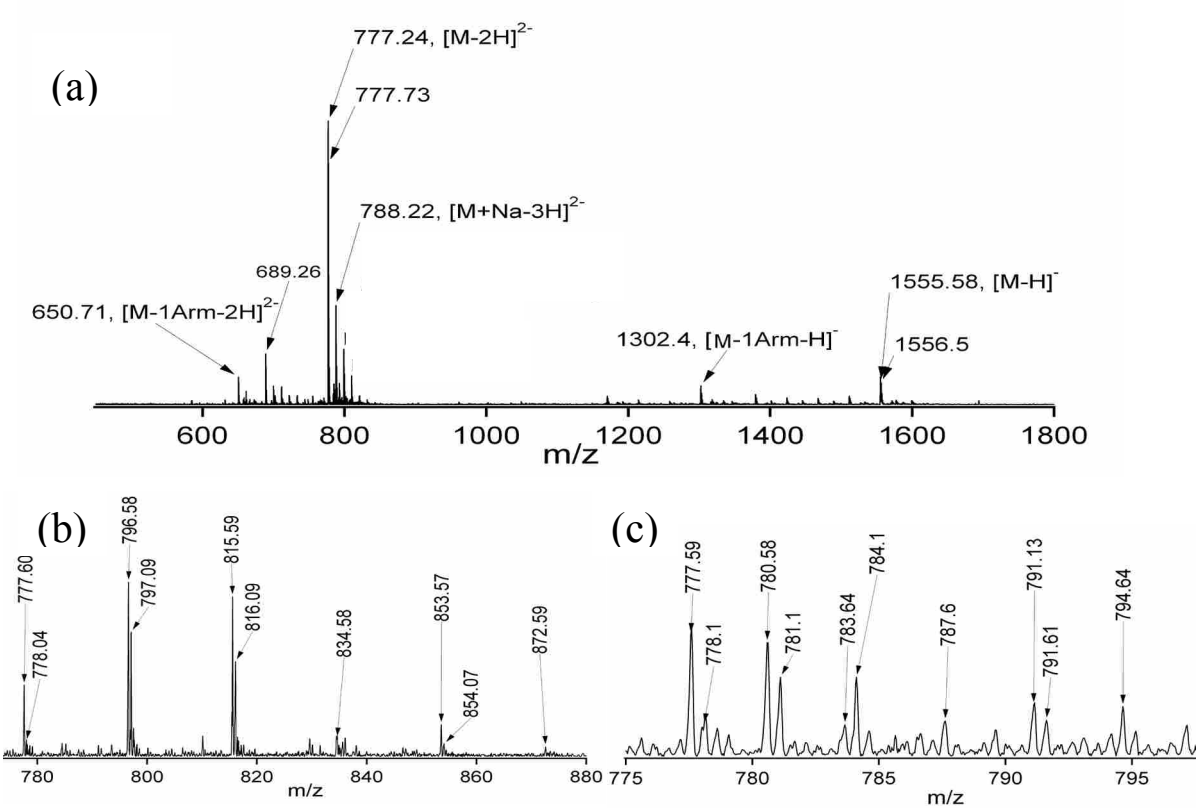

Figure 3.7 The ESI mass spectra of (a) **AMNa**, (b) **AMK**, and (c) **AMLi** in negative ion mode.

In order to shine further light on the structure of **AMNa** and its eight water molecules, SORI-CID FTICR MS was used to study it. SORI-CID MS is one of the more robust methods to study large ions and can provide complementary structural data to NMR. In SORI-CID, an *RF* pulse is applied slightly above or below the resonance frequency of the preselected ion, which

causes the kinetic energy of the ion to increase, and allows the ion to collide repeatedly with background neutral gas molecules, such as N_2, Ar, or CO_2. As a result, the internal energy of the preselected ion increases, which causes fragmentation of the ion. Fragments of a chemical species, especially those that are not covalently bonded to the species, can be observed directly.

The ion with the highest intensity at 777.24 m/z was chosen and isolated from other fragments. An *rf* pulse was applied at slightly above the resonance frequency of this ion; nitrogen gas molecules were introduced to collide with this preselected ion, and as a result, the kinetic energy of the ion was converted to the internal energy necessary to fragment the ion. The resulting mass spectrum was recorded as shown in Figure 3.8(a). The -2 peaks at 755.2, 733.22, 711.22, and 689.23 m/z have a mass difference of 22, and this corresponds to the stepwise loss of CO_2 (mass 44), one from each carboxylic acid. The rate of the reduction of the 777 m/z peak corresponds to the increase in the other mass peaks (shown in Figure 3.8b). The loss of CO_2 is commonly found in SORI-CID for compounds containing carboxylic acid groups.[25] In addition, the mass difference between -2 peak 768.2 and 777.21 m/z is 9.1, which corresponds to the mass of a water molecule. Also, two water molecules were lost from peak 755.2 m/z, with corresponding peaks at 746.2 and 737.19 m/z, respectively. The same situation was found after losing the second CO_2. The loss of the second CO_2 (peak at 733.22 m/z) was followed by the loss of two water molecules. The corresponding peaks appear at 724.21 and 715.21 m/z. These results indicate that two water molecules are associated with each carboxylic acid group. Once again, the results are consistent with the association between **AMNa** and eight water molecules. Thus, the -2 peak in the **AMNa** spectrum at 777.24 m/z corresponds to the addition of eight water

molecules, loss of all sodiums and addition of two protons (calculated value: 777.17 m/z).

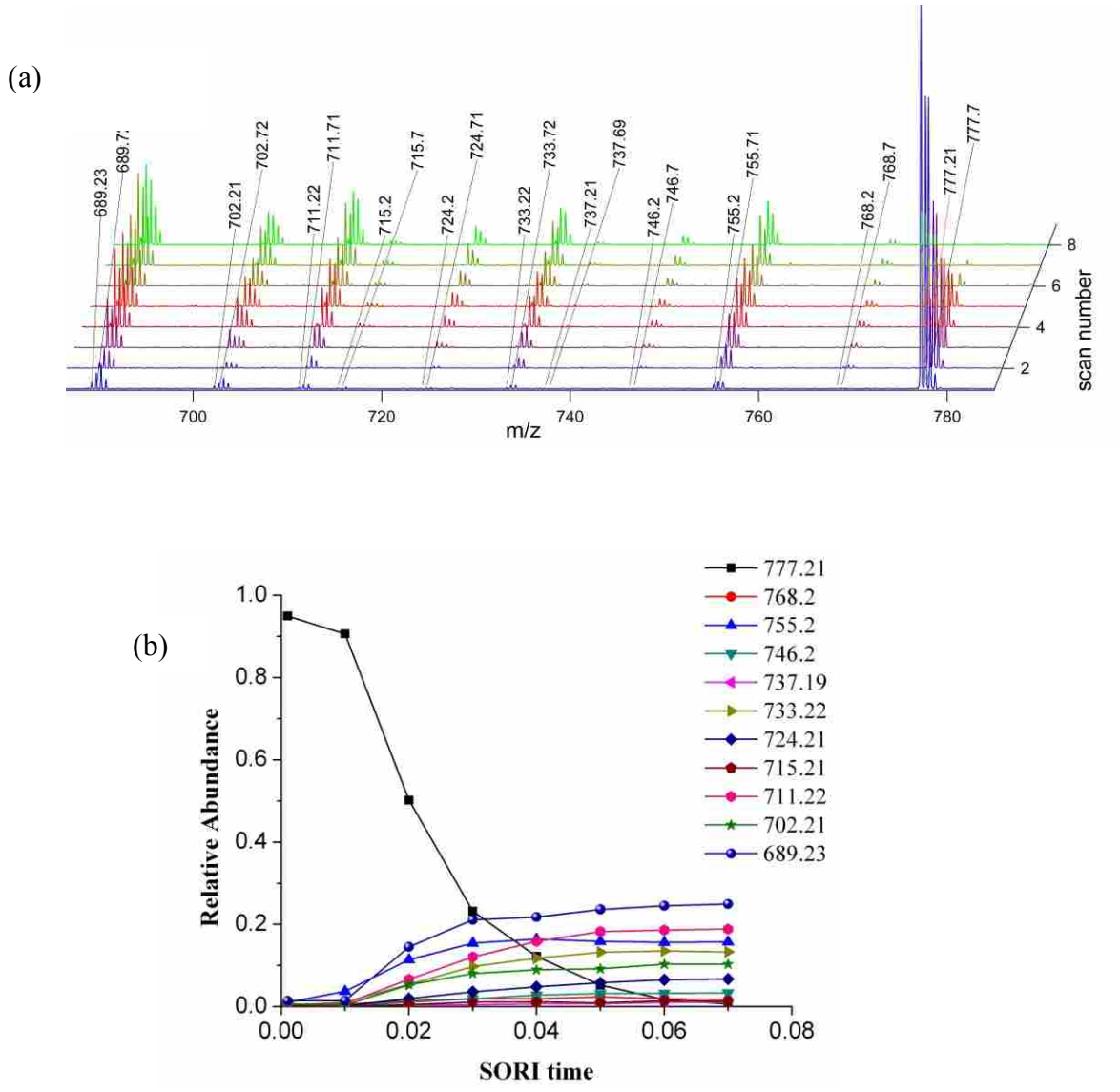

Figure 3.8 Mass spectra analysis of **AMNa** by SORI-CID. (a) MS/MS spectrum of **AMNa** showing parent peak at 777 m/z and the fragments from it as they grow in over time. (b) Relative abundance of fragment ions (p = peak) showing as the quantity of the parent ion decreases, the quantity of the fragments increase.

Mass spectrometry was also used to help characterize the acid **AMA**. The FTICR-MS spectrum of **AMA** in negative mode shows -1 and -2 molecular ion peaks at 1556.5 and 777.44

m/z, respectively (Figure 3.9). The calculated molecular weight for **AMA** is 1413.14 amu and thus the mass difference between the experimental and calculated -1 molecular ion is 144 amu. Once again, we considered different possible guest molecules that might account for the mass difference. Specifically, we had added HCl to **AMNa** to prepare **AMA**. The molecules potentially associated with the cavitand would be HCl (mass of four HCl molecules = 143.92) or H_2O (mass of eight H_2O molecules = 144.08). We calculated the isotope distribution of **AMA** + 4HCl and **AMA** + 8 H_2O and found the calculated isotope distribution of **AMA** + 4HCl is quite different from the experimental result in the size and distribution of peaks. The isotope distribution of **AMA** + 8 H_2O is similar to what was found experimentally. Thus, we conclude that **AMA** is associated with eight water molecules.

We found an interesting regularity in the -1 MS spectrum of **AMA**. The mass difference between peaks 1556.5 and 1303.03 m/z is 253.47, which is almost exactly the mass of one amino acid substituent group and two OH groups. Furthermore, we found another peak at 1049.81 m/z, which corresponds to the loss of a second such group. We should note here that the two OH groups and the two protons left on the parent molecule are most likely from water molecules. Based on these experimental results, we propose that each amino acid group is associated with two water molecules, which is consistent with the various MS experiments described above for **AMA** and **AMNa**.

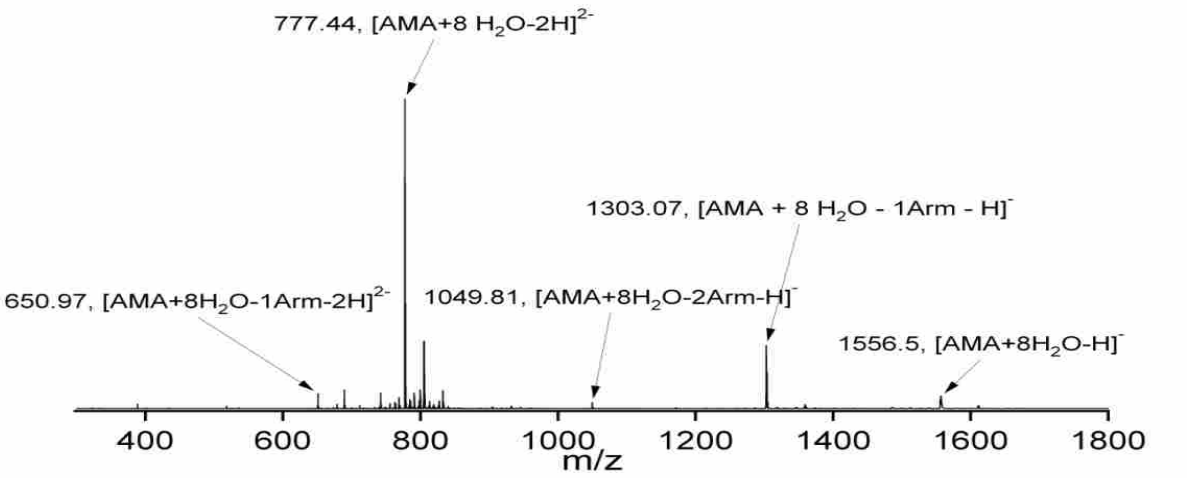

Figure 3.9 Mass spectrum of **AMA** in negative mode (FTICR MS with ESI source).

MS studies of the glycine-containing **GUNa**, **GUA**, **AUNa**, and **AUA** yielded results similar to those with the alanine-containing cavitands described above. Specifically, molecular ion peaks belonging to **GUNa**·8H_2O, **GUA**·8H_2O, **AUNa**·8H_2O and **AUA**·8H_2O were obtained, which indicates that the designed substituent groups attached on the resorcinarene scaffold are quite hydrophilic and have great affinity to polar water molecules.

3.4 Interaction with amines

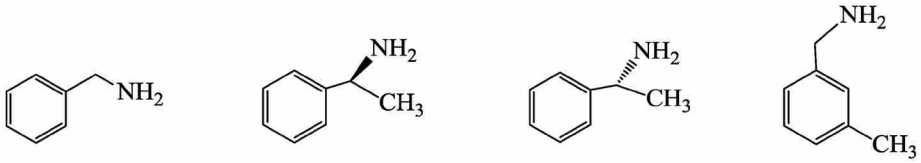

1. benzylamine **2.** (S)-(-)-α-methylbenzylamine **3.** (R)-(+)-α-methylbenzylamine **4.** 3-methylbenzylamine

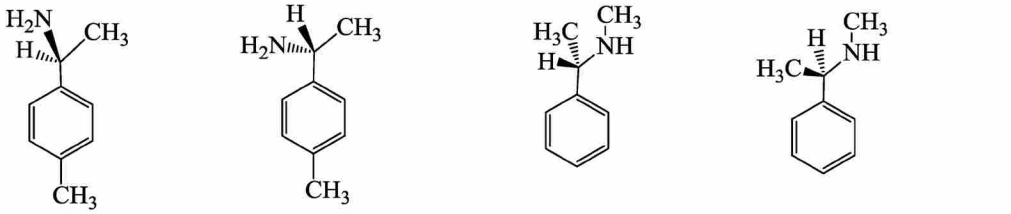

5. (S)-(-)-α,4-dimethyl benzylamine **6.** (R)-(+)-α,4-dimethyl benzylamine **7.** (S)-(-)-N, α-dimethylbenzylamine **8.** (R)-(+)-N, α-dimethylbenzylamine

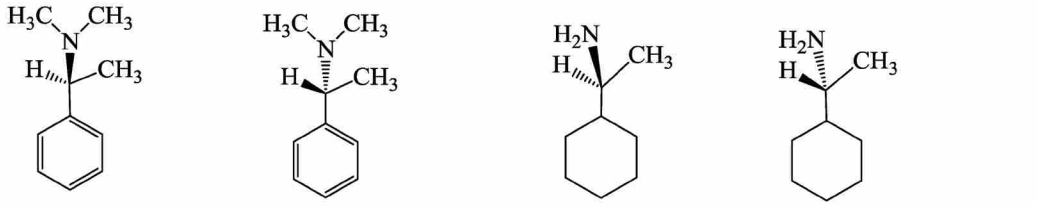

9. (S)-(-)-N, N-dimethyl-1-phenethylamine **10.** (R)-(+)-N, N-dimethyl-1-phenethylamine **11.** (S)-(+)-1-cyclohexylethylamine **12.** (R)-(-)-1-cyclohexylethylamine

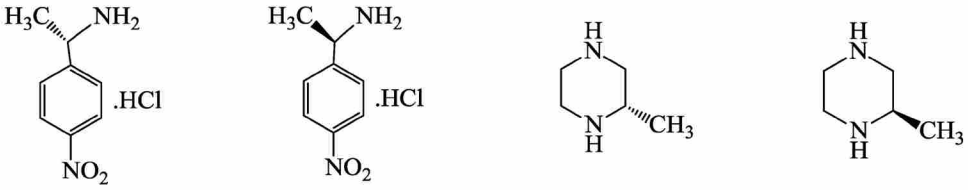

13. (S)-(-)-(α)-methyl-4-nitrobenzylamine hydrochloride **14.** (R)-(+)-(α)-methyl-4-nitrobenzylamine hydrochloride **15.** (S)-(+)-2-methylpiperazine **16.** (R)-(-)-2-methylpiperazine

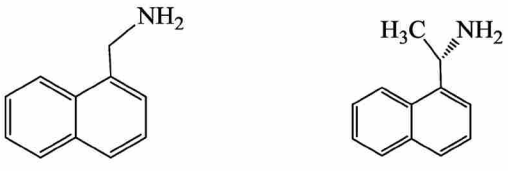

17. 1-naphthyl methylamine **18.** (S)-(-)-(1-naphthyl)ethylamine

Figure 3.10 Structures of amine guests.

A series of amine guests with benzyl rings were chosen and their interactions with **AUA** host were studied by ^{1}H NMR titration. We expected that amine groups would interact with the carboxylic groups of **AUA** by hydrogen bonding while the benzyl ring of the guest could be sequestered in the hydrophobic cavity of **AUA**. In most published work, guest molecules were added to the host and the chemical shift of the host was monitored; or, alternatively, host molecules were added to guest and the chemical shifts of the guest molecules were monitored.[26] In our case, the ^{1}H NMR signals of the host **AUA** are very broad, which makes it impossible to monitor the chemical shift of the host. Thus, we added guest to host and monitored the chemical shift of the guest. To illustrate the point, we compared the NMR titration by two methods: adding host to guest and adding guest to host as shown in Figure 3.11.

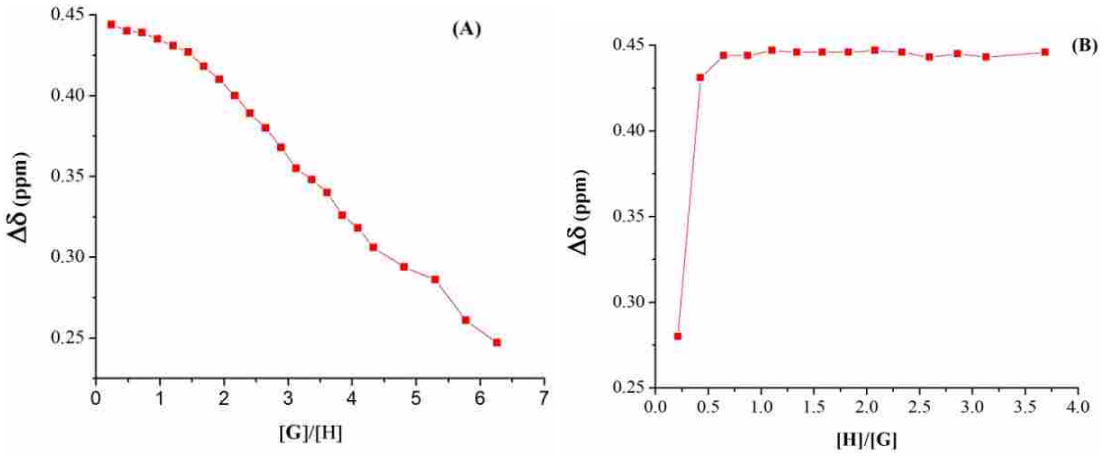

Figure 3.11 (a) Adding guest **2** to host and monitoring the chemical shift change of guest; (b) Adding host to guest **2** and monitoring the chemical shift change of guest **2** in d_6-DMSO. The chemical shift change (Δδ) of the proton on the α-C of the amine is plotted versus the ratio of amine to AUA([G]/[H]). Structures of guests are shown in Figure 3.10.

The observed chemical shift of the amine guest (δ_{Gobs}) can be expressed by equation 3.2.

$$\delta_{Gobs} = X_G\delta_G + X_{HG}\delta_{HG} \qquad (3.2)$$

X_G is the fraction of free guest ($X_G = \frac{[G]}{[G]+[HG]}$), δ_G is the chemical shift of free guest, X_{HG} is the fraction of host-guest complex ($X_{HG} = \frac{[HG]}{[G]+[HG]}$), and δ_{HG} is the chemical shift of bound guest.

When amine was added to **AUA**, the $-NH_2$ group of the amine was protonated to the $-NH_3^+$ form by **AUA** as shown in Equation 3.3 below:

$$R\text{-}NH_2 + R'\text{-}COOH \rightarrow R\text{-}NH_3^+ + R'\text{-}COO^- \qquad (3.3)$$

This neutralization reaction between the amine with the carboxylic acid groups of **AUA** resulted in the downfield movement of the chemical shift of amine protons.

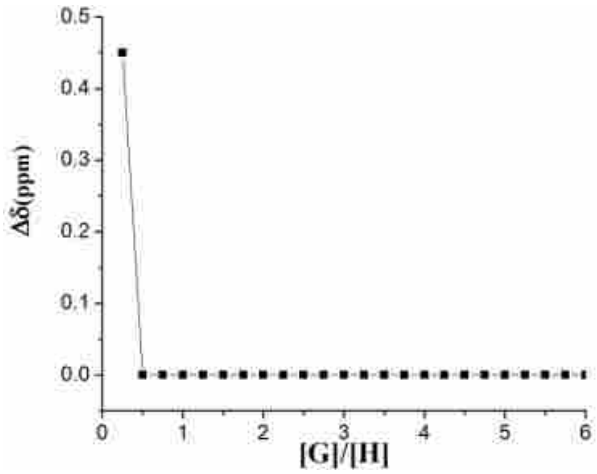

Figure 3.12 A typical titration curve model shows no interaction between host and guest. The chemical shift change (Δδ) of the proton on the amine is plotted versus the ratio of amine to host ([G]/[H]).

If no host-guest complex formed between the protonated guest and **AUA**, X_{HG} in the equation 3.2 will be 0. Ideally, when more amine is added to **AUA** after the amine is protonated, the observed chemical shift δ_{Gobs} equals the chemical shift of the guest, which means the

chemical shift of the amine moves upfield quickly and Δδ (Δδ = δ_{Gobs} - δ_G) will be 0 as shown in Figure 3.12 . However, the Δδ in the titration curve (Figure 3.11A) remained close to the same value before about 2 equivalents of guest were added to **AUA**. As the fraction of free guest X_G increased, the observed chemical shift of the amine guest (δ_{Gobs}) moved upfield gradually. The nearly flat region of the titration curve reflects the binding capability of **AUA** to amine molecules. The decay rate of Δδ reflects the strength of $-NH_3^+ \ldots COO^-$ bonding between amine and **AUA**. The slower the Δδ moves back to 0, the higher the binding. Figure 3.11(A) clearly shows that as least 2 equivalents of guest can bind to **AUA** rather strongly.

In contrast, when the host is added to the guest, the guest molecules are protonated gradually, so the chemical shift change (Δδ) of the amine increases gradually until enough host molecules are added to protonate all the amine molecules. After that, all amines are protonated to $-NH_3^+$ and remain in this form in solution. The Δδ remains unchanged after the right amount of host is added. Figure 3.11(B) reflects the change of Δδ. From the curve, we observed after about 0.5 equivalents of host was added to guest, the Δδ remained unchanged, which indicates that the binding ratio of **AUA** to amine is about 1:2 as well. From these experiments, we found that the two methods, adding host to guest and adding guest to host, are complementary. But adding host to guest is not effective, so we added guest to host and monitored the chemical shift change of the guest through the remainder of the work.

The binding constants of **AUA** and amines were obtained by nonlinear least-squares fitting of the ^1H NMR titration curves using the Solver tool in Excel. The equilibrium equations can be written for amines binding to **AUA** (H = the host **AUA**; G = amine guest):

$$H + G \rightleftharpoons HG \qquad K_1 = \frac{[HG]}{[H][G]} \qquad (3.4)$$

$$K_2 = \frac{[HG_2]}{[HG][G]} \qquad (3.5)$$

A similar method published by our group was used to calculate the association constants.[26]

Briefly, we assume that the binding sites on **AUA** are independent of each other and that $K_1 = K_2 = K_3 = K_4$. Thus, we can use a 1:1 binding isotherm of amines binding to **AUA**.

$$H + G \rightleftharpoons HG \quad K_1 = \frac{[HG]}{[H][G]} \qquad (3.6)$$

The observed chemical shift of amine guest can be expressed as:

$$\delta_{obs} = f_{10}\delta_G + f_{11}\delta_{HG} \qquad (3.7)$$

where $f_{10} = \frac{[G]}{[G]+[HG]}$ is the fraction of free guest, δ_G is the chemical shift of free guest, $f_{11} = \frac{[HG]}{[G]+[HG]}$ is the fraction of host-guest complex, and δ_{HG} is the chemical shift of host-guest complex. Since $f_{10} + f_{11} = 1$, equation 3.7 can be written

$$\delta_{obs} = (1- f_{11})\delta_G + f_{11}\delta_{HG} \qquad (3.8)$$

Defining the chemical shift difference $\Delta = \delta_{obs} - \delta_G$, $\Delta_{11} = \delta_{HG} - \delta_G$, and combining equation 3.8 with equation 3.6,

$$f_{11} = \frac{\Delta}{\Delta_{11}} = \frac{K[H]}{1 + K[H]} \qquad (3.9)$$

Equation 3.9 can be rewritten as:

$$\frac{\Delta}{[H]} = -K\Delta + \Delta_{11}K \qquad (3.10)$$

To put [H] in terms of total host concentration, we can use the mass balance equation:

$$[H_t] = [HG] + [H] = [H] + \frac{\Delta}{\Delta_{11}}[G_t] \qquad (3.11)$$

where $[H_t]$ is the total concentration of the guest.

Equation 3.10 can then be written as:

$$\Delta = \frac{\Delta_{11}K([H_t] - \frac{\Delta}{\Delta_{11}}[G_t])}{1 + K([H_t] - \frac{\Delta}{\Delta_{11}}[G_t])} \qquad (3.12)$$

If we set $\frac{\Delta}{\Delta_{11}} = a$, (3.13)

Equation 3.12 can be arranged to $Ka^2[G_t] - a(K[G_t] + K[H_t] + 1) + K[H_t] = 0$ (3.14)

Therefore,

$$\Delta = \Delta_{11} \times a = \Delta_{11} \times \left[\frac{(K[Gt] + K[Ht] + 1) \pm \sqrt{(K[Gt] + K[Ht] + 1)^2 - 4 \times K[Gt] \times K[Ht]}}{2 \times K[Gt]}\right] \qquad (3.15)$$

So the calculated $\delta_{obs} = \Delta + \delta_G$ (3.16)

We used the Solver feature in Excel with a sum squared error method to perform a nonlinear fit to minimize the difference between the calculated δ_{obs} and the δ_{obs} from the titration. From this minimization, the unknown K and Δ_{11} fit to each amine titration was determined from equation 3.15. The binding constants of **AUA** and amines are listed in Table 3.1.

Table 3.1 Binding constants of **AUA** and amines in d_6-DMSO.

Guest[a]	*K*	Guest	*K*	Guest	*K*
1	0.042	**7**	6.9	**13**	2.2×10^{-4}
2	9.3	**8**	22.9	**14**	6.4×10^{-1}
3	8.8	**9**	2.3	**15**	1.6
4	6.9	**10**	2.1	**16**	2.5
5	18.2	**11**	12.4	**17**	20.4
6	16.4	**12**	9.2	**18**	21.9

[a] 2 and 3, 5 and 6, 7 and 8, 9 and 10, 11 and 12, 13 and 14, 15 and 16 are enantiomers.

In Chapter 1, we described several factors that may affect the selectivity of host to guest molecules including: the size, the type, number, and position of substituent groups, solvent etc. These factors were considered when we chose the amine guests. Their effects on molecular recognition between **AUA** and amines are discussed in the following paragraphs.

3.4.1 The effect of solvent

The compound **AUA** slightly dissolves in acetone and dissolves well in methanol and DMSO. **AUA** was titrated with guest **2** in deuterated methanol and DMSO. The titration results are shown in Figure 3.13(A). A monoacid (acetic acid) and a binary acid (*L*-tartaric acid) were also titrated with guest **2** as shown in Figure 3.13(C) and (B) for comparison. Table 3.2 shows the binding constants of **AUA**, L-tartaric acid, and acetic acid with guest **2** in methanol and DMSO. Methanol is a polar mildly protic solvent; predictably, methanol would hydrogen bond to guest or host, which may interfere with the molecular recognition between the host and guest.

But the polar aprotic solvent DMSO can't hydrogen bond to **AUA**. With its four carboxylic acid groups, **AUA** shows a higher binding capability than the binary acid *L*-tartaric acid and the monoacid acetic acid whether in DMSO or methanol. Correspondingly, *L*-tartaric acid showed a higher binding constant with guest **2** than acetic acid. All of the three acids showed higher binding constants in methanol than in DMSO. The titration curves of *L*-tartaric acid and acetic acid indicate that these two acids showed higher binding ratio to amine guest in methanol than in DMSO. As shown in Figure 3.13(B), the binding ratio of *L*-tartaric acid to guest **2** in methanol is 1:2, while it is 1:1 in DMSO. The binding ratio of acetic acid to guest **2** is 1:1 in methanol, while no clear binding ratio was observed in DMSO. However, **AUA** showed a binding ratio of about 1:2 to the amine guest, while no clear binding ratio was observed in methanol. We used DMSO as the titration solvent throughout the paper to avoid the interference of methanol.

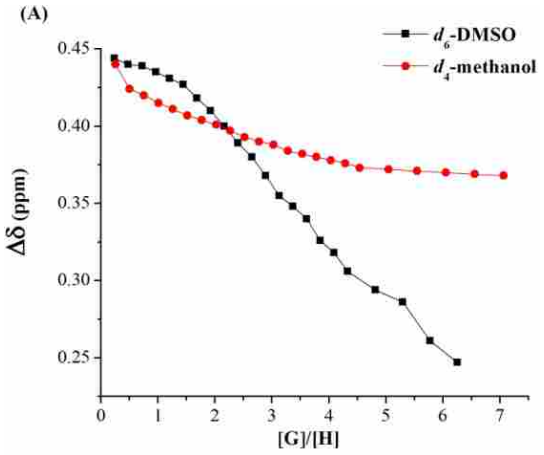

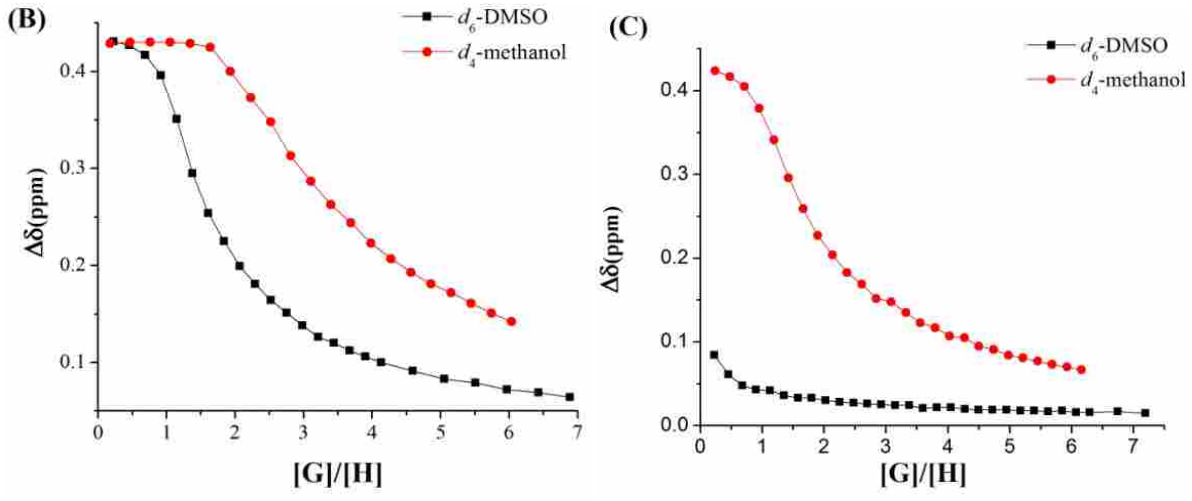

Figure 3.13 ^{1}H NMR titration curves of (a) **AUA**; (b) *L*-tartaric acid; (c) acetic acid with guest **2** in d_6-DMSO and d_4-methanol. The chemical shift change (Δδ) of the proton on the α-C of the amine is plotted versus the ratio of amine to acids ([G]/[H]). Structures of guests are shown in Figure 3.10.

Table 3.2 Binding constants (*K*) of guest **2** with acids in methanol and DMSO.

Host	*K* (in d_6-DMSO)	*K* (in d_4-methanol)
AUA	9.3	77.8
L-tartaric acid	1.7	2.2
Acetic acid	9.1×10^{-2}	3.3×10^{-1}

3.4.2 The effect of guest size

Size-fit selectivity has been observed with many macrocyclic ligands, such as crown ethers, cryptands, and cyclodextrin. We selected guests of different size to study their interaction with **AUA**. Guest **17** has one more phenyl ring than guest **1**, and the binding constant of guest **17** is much higher than guest **1**. A similar situation was observed with guests **2**, **3** and **18**. Guest **18**

showed a higher binding constant with **AUA** than guests **2** and **3**. The NMR characterizations of **AUA** indicate that it has a kite rather than a bowl configuration. Potentially, amine guests would not be trapped in the cavity of **AUA**, but associate with **AUA** through the carboxylic acid groups, or via other interactions. The stronger interaction between **AUA** with guests containing more phenyl rings would be caused by the π-π stacking between these guests and the phenyl rings of **AUA**.

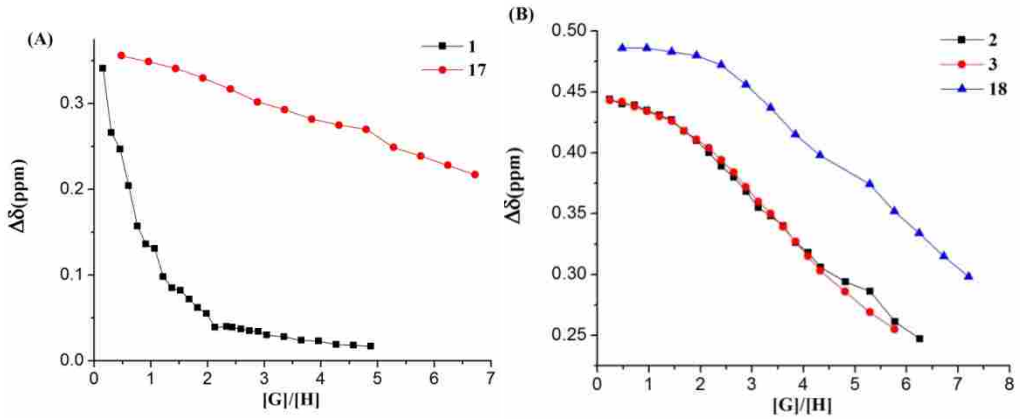

Figure 3.14 The effect of guest sizes on the ^{1}H NMR titration curves of **AUA** and amine guests. The chemical shift change (Δδ) of the proton on the α-C of the amine is plotted versus the ratio of amine to **AUA** ([G]/[H]). Structures of guests are shown in Figure 3.10.

3.4.3 The effect of substituent group type, position, and number

3.4.3.1 The type of substituent group

The titration curve of guest **1** with **AUA** (shown in Figure 3.15A) is similar to the model curve in Figure 3.12. The titration curves of guest **1**, **2**, and **3** with **AUA** are shown in Figure

3.15(A). The titration curves of guest **17** and **18** with **AUA** are shown in Figure 3.15(B). Compared to guest **1**, guests **2** and **3** have an electron donating $–CH_3$ group on the α-carbon which increases the electron donating ability of the neighboring $-NH_3^+$ group by an inductive effect, thereby enhancing the binding between amine and **AUA**. The calculated binding constant of guest **1** with **AUA** is small and much lower than that of **2** or **3**, which also indicates weak binding between **AUA** and **1**. A similar situation was found with guests **17** and **18**. Guest **18** has a $–CH_3$ group on the α-carbon and shows a higher binding constant than guest **17,** as shown in Table 3.1. Guests **11** and **12** contain the same substituent groups ($-NH_3$ and $–CH_3$) as compounds **2** and **3**, but the latter ones have conjugated phenyl rings. The binding constants of **2**, **3**, **11**, and **12** are quite close, as shown in Table 3.1, which indicates that the weakly electron donating groups $–C_6H_5$ and $–C_6H_{11}$ have nearly identical influence on binding strength between **AUA** and amines. Guest **4** contains one more $–CH_3$ on the benzyl ring than guest **1**. The binding strength between **AUA** and guest **4** was significantly enhanced by this electron donating $–CH_3$ group. As shown in Figure 3.15(D), guest **4** has a binding ratio of 2:1 to **AUA** approximately and a binding constant of 6.9, which is about two orders of magnitude higher than that of guest **1**. Compared to guests **2** and **3**, guests **5** and **6** contain one more $–CH_3$ group on the phenyl ring. As it is observed in Figure 3.15(E), this methyl group enhances the binding strength of guests **5** and **6**. Specifically, the binding constants of **5** and **6** to **AUA** are 18.2 and 16.4, respectively, which is slightly higher than that of guests **2** and **3**. The binding constants of **2** and **3** to **AUA** are 9.3 and 8.8, respectively. These experimental results clearly indicate that the electron donating $–CH_3$ group on the phenyl ring or the α-carbon have effect on the binding capability of the guest.

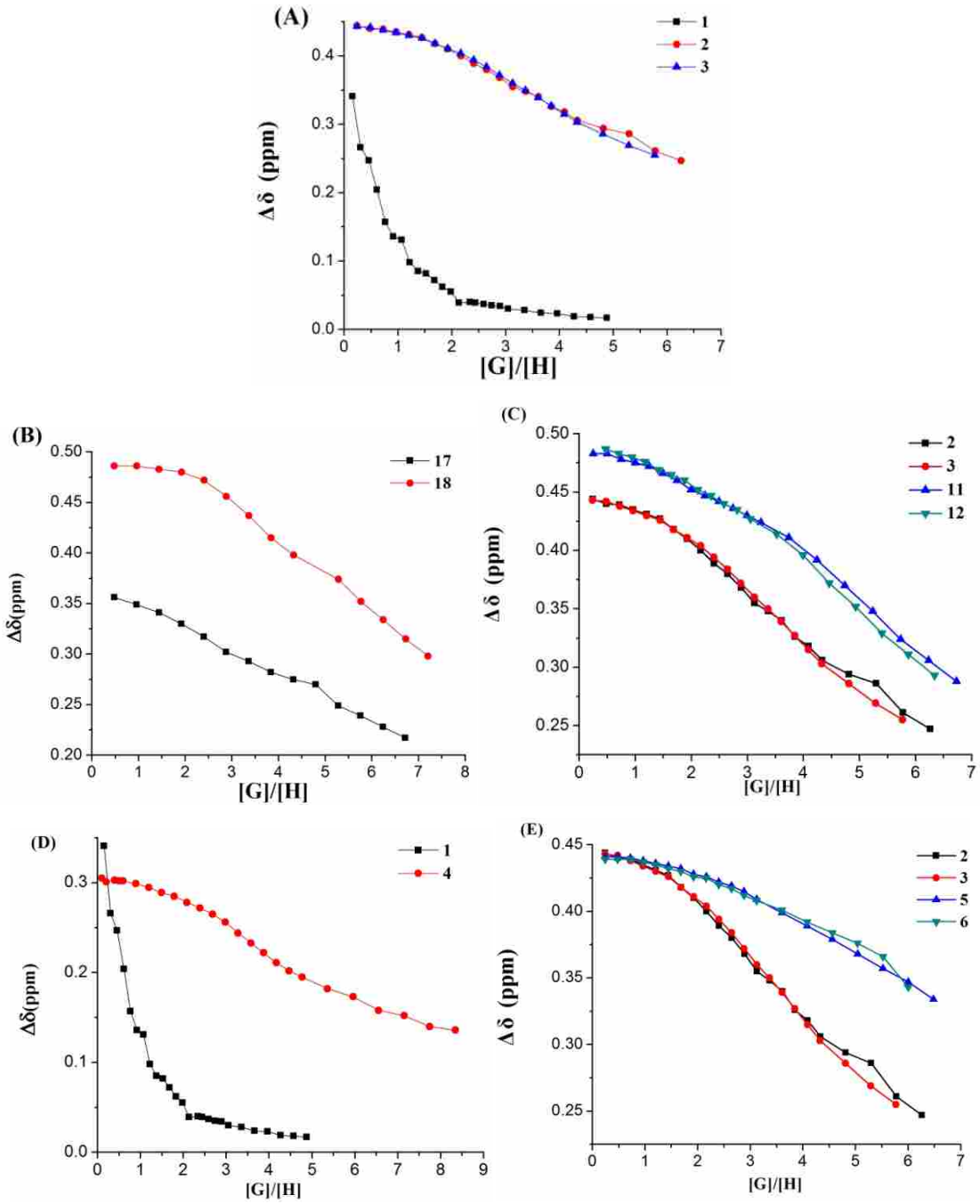

Figure 3.15 The effect of substituent groups on the ^{1}H NMR titration curves of **AUA** and amine guests. The chemical shift change (Δδ) of the proton on the α-C of the amine is plotted versus the ratio of amine to **AUA** ([G]/[H]). Structures of guests are shown in Figure 3.10.

3.4.3.2 The position of substituent groups

Guest **4** is a structural isomer of guests **2** and **3**. Chiral guests **5** and **6** are structural isomers of chiral guests **7** and **8**. The titration curves of these structural isomers with host **AUA** are compared in Figure 3.16. The binding constants of **2** (K = 9.3) and **3** (K = 8.8) are slightly higher than that of guest **4** (K = 6.9). This phenomenon is understandable since the $-CH_3$ group is on the α-carbon of guests **2** and **3** while it is on the phenyl ring of guest **4**. The longer distance between $-CH_3$ and $-NH_2$ in guest **4** results in a weaker inductive effect introduced by the $-CH_3$ group. A similar situation was observed for guests **5**, **6**, and **8**. Guest **8** (K = 22.9) with a $-CH_3$ on the α-carbon showed a higher binding constant with **AUA** than guests **5** (K = 18.2) and **6** (K = 16.4) in which the $-CH_3$ is on the phenyl ring. Guest **7** is different from the other three guests, as discussed in the following paragraphs.

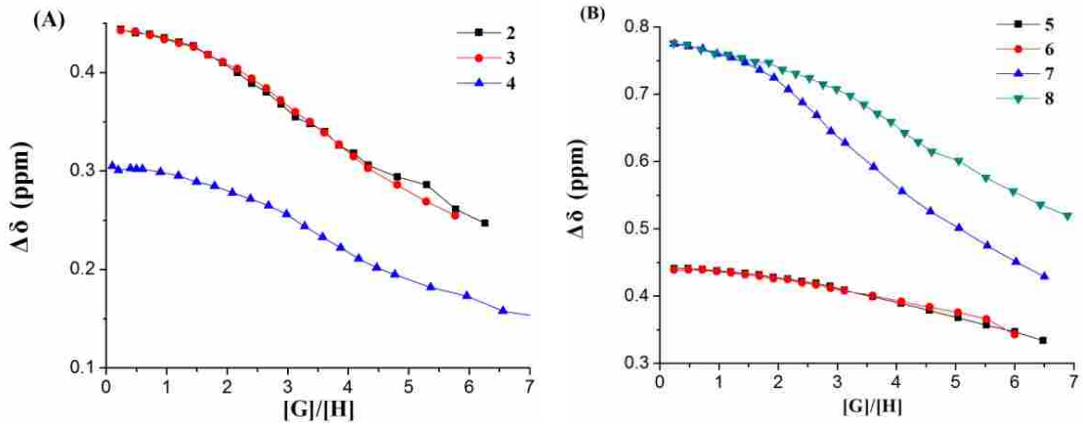

Figure 3.16 The effect of substituent group positions on the ^{1}H NMR titration curves of **AUA** and amine guests. The chemical shift change (Δδ) of the proton on the α-C of the amine is plotted versus the ratio of amine to **AUA** ([G]/[H]). Structures of guests are shown in Figure 3.10.

3.4.3.3 The number of substituent groups

The effect of the number of $-CH_3$ groups on AUA on the interaction of the ligand with a series of amine guests was studied. Among these amines, **2** and **3** are primary amines; **7** and **8** are secondary amines, and **9** and **10** are tertiary amines. The titration curves of these amines with **AUA** are summarized in Figure 3.17 and the binding constants are listed in Table 3.1. Primary and secondary amines showed higher binding constants than tertiary amines. With the later, steric hindrance around the NR_3H^+ group of tertiary amines would impede the binding between $-(CH_3)_2NH^+$ to the $-COO^-$ groups of **AUA**. Guest **8** showed a higher binding constant to **AUA** than guests **2** and **3**. Two electron donating $-CH_3$ groups on the α-carbon should increase the electron donating ability of the $-(CH_3)NH_2^+$ group of the secondary amines and thereby enhance the interaction with **AUA**. However, guest **7** showed lower binding constants than guests **2**, **3**, and **8**. The chiral effect is discussed below.

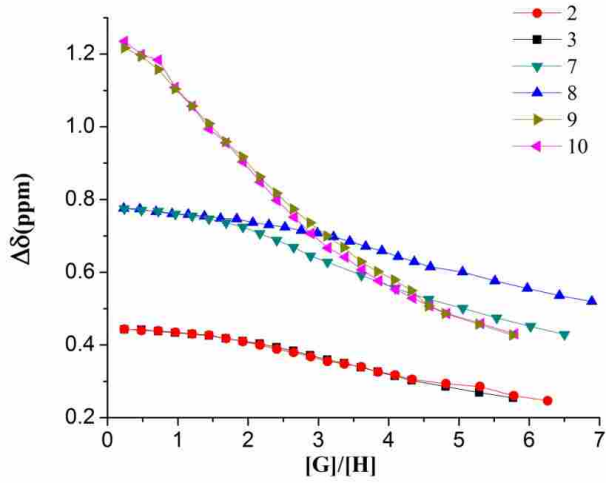

Figure 3.17 ^{1}H NMR titrations of **AUA** with chiral primary (**2** and **3**), secondary (**7** and **8**), and tertiary amines (**9** and **10**). The chemical shift change (Δδ) of the proton on the α-C of the amine is plotted versus

the ratio of amine to **AUA** ([G]/[H]).

3.4.4 Chirality

Since the alanine-containing cavitands **AUA** and **AMA** carry chiral groups on the upper rim, experiments were conducted to examine the ability of these hosts to discriminate between enantiomeric guest molecules. Discrimination by **AMA** and **AUA** between chiral amines (Structures shown in Figure 3.10) was studied by ^{1}H NMR titration with the expectation that enantiomers may exhibit different chemical shifts upon complexation. The optical activity of **AMA** and **AUA** was studied by polarimetry, confirming that these molecules are chiral. Baseline NMR titration studies were performed using various compounds for comparison of results with **AMA**. These included ^{1}H NMR titration experiments associating enantiomeric guest **2** and **3** with *L*-tartaric acid, phthalyl alanine (**PA**) (an analog of a cavitand side panel, Figure 3.18), and **GUA**, a non-chiral analog of **AMA**. Also, NMR titration experiments of **AUA** with chiral secondary and tertiary amines (Figure 3.19) were performed to further understand the interaction between **AUA** and amines.

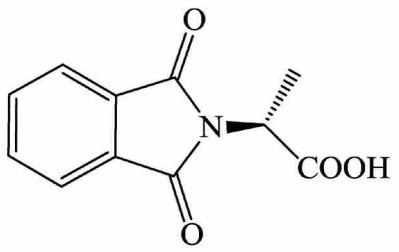

PA

Figure 3.18 Structure of **PA**, an analog of a cavitand side panel.

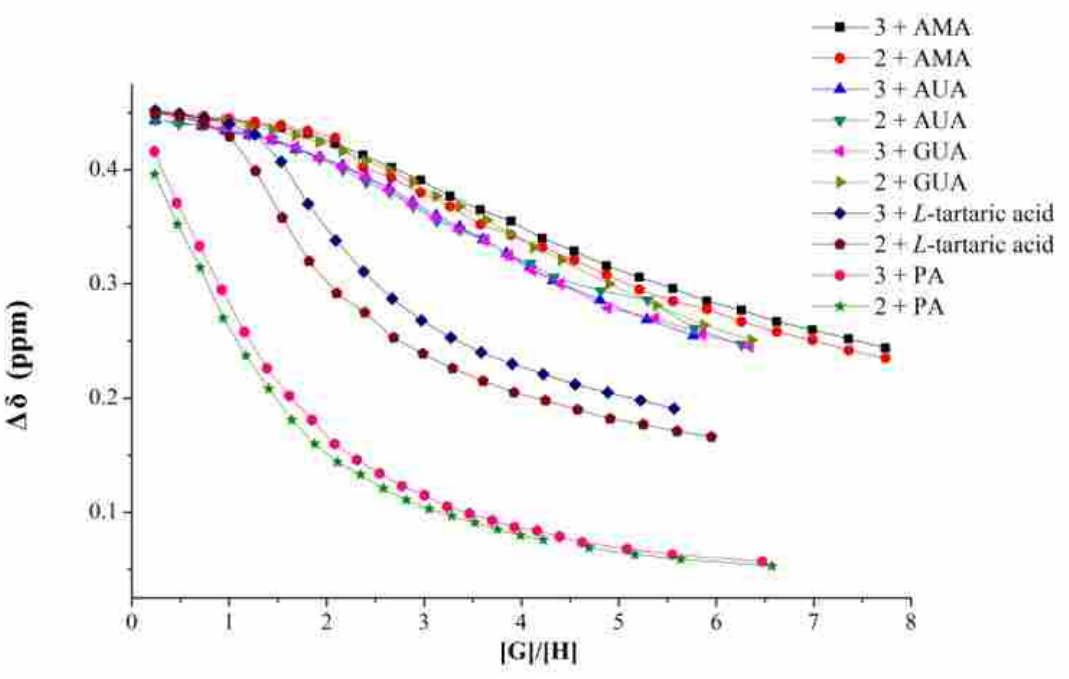

Figure 3.19 ^{1}H NMR titrations of **AMA**, **AUA, GUA**, **PA**, and *L*-tartaric acid with *R*- and *S*-methyl benzyl amine (**2** and **3**). The chemical shift change (Δδ) of the proton on the α-C of the amine is plotted versus the ratio of amine to host molecule ([G]/[H]).

Table 3.3 Binding constant (*K*) of **AUA**, **GUA**, **AMA**, *L*-tartaric acid and PA with guests **2** and **3**

	K (with Guest **2**)	*K* (with Guest **3**)
AUA	9.3	8.8
GUA	10.3	8.4
AMA	12.1	14.6
L-tartaric acid	1.7	2.3
PA	0.31	0.34

When the chiral amines were titrated with **AMA**, **GUA**, *L*-tartaric acid, and PA in DMSO, the chemical shift of the α-carbon proton moved downfield. After more guest molecules were

added, the chemical shift of guest moved upfield just as we observed previously. The titration curves show that **AMA** and **GUA** bind guests **2** and **3**, but they do not show chiral discrimination. This result is consistent with the fact that the binding constants of **AUA**, **AMA**, and **GUA** with guests **2** and **3** are quite close, as shown in Table 3.3. It is well known that if a guest is encapsulated in a cavitand, the ^{1}H NMR chemical shifts of the guest will appear more upfield due to the shielding of guest by the cavity.[21-23] However, we didn't observe any such upfield shifts of guest protons.

Chiral secondary (**7** and **8,** S and R-N, α-dimethyl benzyl amine) and tertiary (**9** and **10**, S and R-N, N-dimethyl-1-phenethylamine) amines were also titrated with **AUA** and the chemical shift change of the proton on the α-C of the amine was monitored. **AUA** showed distinct discrimination among primary, secondary, and tertiary amines (Figure 3.20). The chemical shift changed most for the most basic amines – i.e., tertiary amines moved further downfield (about 1.2 ppm) than less basic secondary and primary amines (0.8 and 0.45 ppm, respectively). As more amine was added, the chemical shift of the primary and secondary amines stayed fairly constant for up to two equivalents of amine and then began to go back upfield. This indicates that for primary and secondary amines, the first amine equivalents interact strongly with **AUA**. However, the chemical shift of the tertiary amine moved back upfield when more amine was added, which indicates that the equilibrium between the protonated and nonprotonated tertiary amines shifts to the nonprotonated form more easily than it does for the other amines. The titration curves of the enantiomeric primary amines are almost overlapped, as are those of the chiral tertiary amines, which indicates that there is not chiral discrimination of **AUA** for primary

and tertiary amines. However, chiral discrimination of **AUA** for chiral secondary amines was observed after about 2 equivalents of amine were added (Figure 3.17). These titration experiments were repeated and the results were consistent. The chiral discrimination occurs at the region of weaker guest binding.

Phthalyl alanine (**PA**), an analog of a cavitand side panel, was also titrated with primary, secondary, and tertiary amine for comparison to cavitand behavior. The titration curve is shown in Figure 3.20. Compared to **AUA**, **AMA**, and **GUA** which contain four carboxylic acid groups on the upper rim, the monoacid PA showed much weaker interactions with amines. The chemical shifts of amines moved downfield first because of the protonation of $-NH_2$ groups, and then move back upfield quickly. The binding constants of **PA** with primary, secondary, and tertiary amines in Table 3.4 are much lower than that of **AUA** which also confirmed the very weak interaction between PA and amines. Clearly from the titration curve and binding constants, **PA** showed no chiral discrimination for chiral guests.

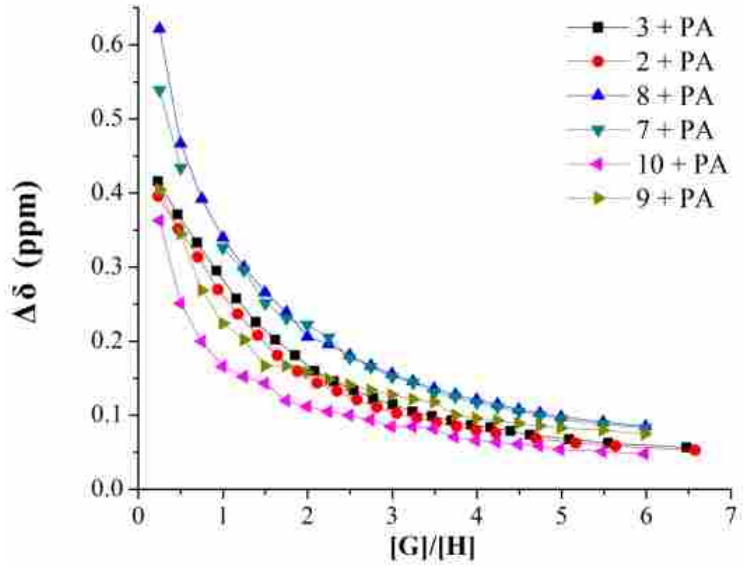

Figure 3.20 ^{1}H NMR titrations of **PA** with primary, secondary, and tertiary amines. The chemical shift change (Δδ) of the proton on the α-C of the amine is plotted versus the ratio of amine to host molecule ([G]/[H]).

Table 3.4 Binding constant (*K*) of **PA** with primary, secondary, and tertiary amines

PA	2	3	7	8	9	10
K	0.31	0.34	0.39	0.30	0.54	0.30

4. Conclusions

The structure characterizations of chiral cavitands **AMA**, **AUA**, **GUA** indicate they have four amino acid groups on their upper rim. The electrospray mass spectroscopic characterization showed eight water molecules associated to the cavitands. The effects of guest size, type, number, and position of substituent groups, and solvent on the recognition between the synthesized

cavitands and a series of amine guests were studied. The comparison of NMR titration cures of **AMA**, **GUA**, *L*-tartaric acid, and **PA** with *R*- and *S*-methyl benzyl amines show that **AMA** and **GUA** bind more amine guests strongly than monoacid **PA** and binary acid *L*-tartaric acid. The ^{1}H NMR titration experiments with chiral primary, secondary, and tertiary amines show that **AUA** causes different chemical shift changes for these three types of amines. Also, **AUA** shows chiral discrimination between secondary amines at equivalents greater than two.

References

1. Högberg, A.G. S. Two stereoisomeric macrocyclic resorcinol-acetaldehyde condensation products. *J. Org. Chem.* **1980**, *45*, 4498-4500.
2. Moran, J.R.; Karbach, S.; Cram, D. J. Cavitands: synthetic molecular vessels. *J. Am. Chem. Soc.* **1982**, *104,* 5826-5828.
3. (a) Wieser, C.; Dieleman, C. B.; Matt, D. Calixarene and resorcinarene ligands in transition metal chemistry. *Coord. Chem. Rev.* **1997**, *165*, 93-161. (b) Purse, B.; Rebek, J. Jr. Fuctional cavitands: Chemical reactivity in structured environments. *Proc. Natl. Acad. Sci. U. S. A.* **2005**, *102*, 10777-10782.
4. Szumna, A. Water co-encapsulation in an inverted molecular capsule. *Chem. Commun.* **2009**, *28*, 4191-4193.
5. Restorp, P.; Rebek, J. Jr. Reaction of isonitriles with carboxylic acids in a cavitand: observation of elusive isoomide intermediates. *J. Am. Chem. Soc.* **2008**, *130*, 11850-11851.
6. Hooley, R. J.; Rebek, J. Jr. A deep cavitand catalyzes the Diels-Alder reaction of bounf

maleimides. *Org. Biomol. Chem.* **2007**, *5*, 3631-3636.

7. (a) Yanagihara, R.; Tominaga, M.; Aoyama, Y. Chiral host-guest interaction. A water-soluble calix[4]resorcinarene having L-proline moieties as a non-lanthanide chiral NMR shift reagent for chiral aromatic guests in water. *J. Org. Chem.* **1994**, *59*, 6865-6867. (b) Pham, N. H.; Wenzel, T. J. A water-soluble calix[4]resorcinarene with α-methyl-L-prolinylmethyl groups as a chiral NMR solvating agent. *J. Org. Chem.* **2011**, *76*, 786-789. (c) O'Farrell. C. M.; Chudomel, J. M.; Collins, J. M.; Dignam, C. F.; Wenzel, T. J. Water-soluble calyx[4]resorcinarenes with hydroxyproline groups as chiral NMR solvating agents. *J. Org. Chem.* **2008**, *73*, 2843-2851. (d) O'Farrell. C. M.; Hagan, K. A.; Wenzel, T. J. Water-soluble calIx[4]resorcinarenes as chiral NMR solvating agents for bicyclic aromatic compounds. *Chirality* **2009**, *21*, 911-921.

8. Wang, J.; Harrison, R. G.; Lamb, J. D. Anion separation and preconcentration with cyclen and cyclen-resorcinarene derivatives. *J. Chromatogr. Sci.* **2009**, *47*, 510-515.

9. Śliwa, W.; Kozlowski, C. Calixarenes and resorcinarenes: synthesis, properties and applications. Wiley-VCH, Verlag GmbH & Co. KGaA, Weinheim, 2009, 288.

10. (a) Botta, B.; Caporuscio, F.; Subissati, D.; Tafi, A.; Botta, M.; Filippi, A.; Speranza, M. Flattened cone 2,8,14,20-tetrakis(L-valinamido)-[4]resorcinarene: an enantioselective allosteric receptor in the gas phase. *Angew. Chem. Int. Ed.* **2006**, *45*, 2717-2720. (b) Kuberski, B.; Pecul, M.; Szumna, A. A chiral "Frozen" hydrogen bonding in C_4-symmetric inherently chiral resorcin[4]anenes: NMR, X-ray, circular dichrosim, and theoretical study. *Eur. J. Org. Chem.* **2008**, 3069-3078. (c) McIldowie, M. J.; Mocerino, M.; Ogden, M. I. A brief review of

C_n-symmeric calixarenes and resorcinarenes. *Supramol. Chem.* **2010**, *22*, 13-39. (d) Iwanek, W.; Wzorek, A. Introduction to the chirality of resorcinarenes. *Mini-Rev. Org. Chem.* **2009**, *6*, 398-411. (e) Szumna, A. Chiral encapsulation by directional interactions. *Chem. Eur. J.* **2009**, *15*, 12381-12388.

11. Arnott, G.; Heaney, H.; Hunter, R.; Page, P. C. B. Synthesis of the First Chiral, Functionalised-Bridged Resorcinarenes in Asymmetric Catalysis: Evidence for Intracavity Asymmetric Catalysis. *Eur. J. Org. Chem.* **2004**, *24*, 5126-5134.

12. (a) Saito, S.; Nuckolls, C.; Rebek, J. Jr. New molecular vessels: synthesis and chiroselective recognition. *J. Am. Chem. Soc.* **2000**, *122*, 9628-9630. (b) Mann, E.; Rebek, J. Jr. Deepened chiral cavitands. *Tetrahedron* **2008**, *64*, 8484-8487.

13. Edwards, B. R.; Giauque, A. P., Lamb, J. D. Macrocyle-based column for the separation of inorganic cations by ion chromatography. *J. Chromatogr. A*, **1995**, *706*, 69-79.

14. Romer, D. R. Synthesis of 2,3-dichloroquinoxalines via vilsmeier reagent chlorination. *J. Heterocycl. Chem.* **2009**, *46*, 317.

15. Sastry, C. V. Reddy; Jogibhukta, M.; Krishnan, V. S. H.; Rao, P. Shanthan; Vemana, K.; Shridhar, D. R.; Tripathi, R. M.; Verma, R. K.; Kaushal, Renu. Synthesis and biological activities of some 1,5-dihydro[1,2,4]Ditriazolo[4,3-a:3',4'-c] quinoxaline-1,6-diones. *Indian J. Chem., sect. B* **1988**, *27*, 1110-1112.

16. Azov, V. A.; Skinner, P. J.; Yamakoshi, Y.; Seiler P.; Gramlich, V.; Diederich, F. Functionalized and partially or differentially bridged resorcin[4]arene cavitands: synthesis and solid-state structures. *Helv. ChiM. Acta* **2003**, *86*, 3648-3670.

17. Billman, J. H.; Harting, W. F.; Amino aicd. V. phthalyl derivatives. *J. Am. Chem. Soc.* **1948**, *70*, 1473-1474.

18. Zhang, H. Z.; Paulsen, E. S.; Walker, K. A.; Krakowiak, K. E.; Dearden, D. V. Cucurbit[6]uril Pseudorotaxanes: Distinctive Gas-Phase Dissociation and Reactivity. *J. Am. Chem. Soc.* **2003**, *125*, 9284-9285.

19. Laskin, J.; Futrell, J. H. Activation of large ions in FT-ICR mass spectrometry. *Mass Spectrometry Reviews*. **2005**, *24*, 135-167.

20. Jiao, C. Q.; Ranatunga, D. R. A.; Vaughn, W. E.; Freiser, B. S. A pulsed-leak valve for use with ion trapping mass spectrometers. *J. Am. Soc. Mass Spectrom.* **1996**, *7*, 118-122.

21. Moran, J. R.; Ericson, J. L.; Dalcanale, E.; Bryant, J. A.; Knobler, C. B.; Cram, D. J. Cases and kites as cavitands. *J. Am. Chem. Soc.* **1991**, *113*, 5707-5714.

22. Shirtcliff, L. D.; Xu, H.; Diederich, F. Complexation and dynamic switching properties of fluorophore-appended resorcin[4]arene cavitands. *Eur. J. Org. Chem*. **2010**, *5*, 846-855.

23. (a) Azov, V, A.; Beeby, A.; Cacciarini, M.; Gheetham, A. G.; Diederich, F.; Frei, M.; Gimzewski, J. K.; Gramlich, V.; Hecht, B.; Jaun, B.; Latychevskaia, T.; Lieb, A.; Lill, Y.; Marotti, F.; Schlegel, A.; Schlittler, R. R.; Skinner, P. J.; Seiler, P.; Yamakoshi, Y. Resorcin[4]arene cavitand-based molecular switches. *Adv. Funct. Mater.* **2006**, *16*, 147-156. (b) Cram, D. J.; Choi, H. J.; Bryant, J. A.; Knobler, C. B. Host-guest complexation. 62. solvophobic and entropic driving forces for forming velcralexes, which are 4-fold, lock-key dimmers in organic media. *J. Am. Chem. Soc.* **1992**, *114*, 7748-7765.

24. Zetasizer Nano Series user manual. Malvern Instruments Ltd. 2003, UK.

25. (a) Kanawati, B.; Schmitt-Kopplin, P. Exploring rearrangements along the fragmentation of glutamic acid negative ion: a combined experimental and theoretical study. *Rapid. Commun. Mass Spectrom*. **2010**, *24*, 1198-1206. (b) Cui, L. J.; Isbell, M. A.; Chawengsub, Y.; Falck, J. R.; Campbell, W. B.; Nithipatikon, K. Srucural characterization of monohydroxyleicosatetraenoic aicds and dihydroxy- and trihydroxyeicosatrienoic acids by ESI-FTICR. *J. Am. Soc. Spectrom.* **2008**, *19*, 569-585.

26. Gardner, J. S.; Sheridan, M. C.; Smith, D. N.; Harrison, R. G.; Lamb, J. D. Anion binding by a tertadipicolyamine-substituted resorcinarene cavitand. *Inorg. Chem.* **2005**, *44*, 4293-4300.

Chapter 4 Cation Separation and Preconcentration Using Columns Containing Cyclen and Cyclen-Resorcinarene Derivatives

Abstract[4]

The selectivity and separation of transition metal ions on two columns packed with cyclen-based macrocycles adsorbed onto 55% cross-linked styrene-divinylbenzene resin are presented. The N-cyclen and cyclen-resorcinarene stationary phases were made by adsorbing hydrophobically-substituted N-cyclen or a cyclen-resorcinarene derivative (cyclenbowl) on the resin, respectively. The stability constants of cyclen with transition metal ions demonstrate that cyclen has selectivity for Cu^{2+} over other transition metal ions. Mn^{2+}, Co^{2+}, Ni^{2+}, Cd^{2+}, and Zn^{2+} ions were separated from Cu^{2+} using HNO_3 eluent with the cyclenbowl column. The preconcentration of Cu^{2+} in parts per billion level from a high concentration matrix of Mn^{2+}, Co^{2+}, Ni^{2+}, Cd^{2+}, and Zn^{2+} ions was achieved in the cyclenbowl column using a nitric acid eluent gradient. Recovery of Cu^{2+} at > 98% was obtained based on direct interaction of metal ion and cyclen. Although Mn^{2+}, Co^{2+}, Ni^{2+}, Cd^{2+}, and Zn^{2+} were not separated by HNO_3 eluent, addition of oxalic acid yielded a very good separation. A retention mechanism is proposed for the latter system in which the protonated cyclen units attract negatively charged $HC_2O_4^-$ ions that cooperate with cyclen sites in retaining transition metal ions.

[4]This research has been published.

Li, N.; English, C.; Eaton, A.; Gillespie, A.; Ence, T. C.; Christensen, T. J.; Sego, A.; Harrison, R. G.; Lamb, J. D. *J. Chromatogr. A* **2012**, *1245*, 83-89.

1. Introduction

The development of new stationary phases with selective ion exchangers continues to be one of the most challenging research objectives in ion chromatography.[1,2] There are several ways to modify the selectivity in ion chromatographic systems. A common approach is the development of novel ion exchange sites in separator columns. The synthesis of new ion exchangers containing special functional groups is central to this approach. Another approach is to use columns of different selectivity in series to obtain the desired separation. For example, Saari-Nordhaus et al.[3] linked two packed columns together that contain carboxylic acid and crown ether functional groups, respectively, for separation of alkali, alkaline earth, and ammonium ions. These two columns used in series showed significantly increased resolution between sodium and ammonium ions and between potassium and ammonium ions.[3] In a third approach, eluent modification can affect column selectivity. For example, improved resolution between ammonium and sodium ions was obtained by our group[4] and Bruzzoniti's group[5], respectively, when 18-crown-6 was added to the mobile phase.

In the work we report here, we have adopted the first approach, preparing separator columns with novel exchange sites based on the cyclen ligand unit. The development of novel ion chromatographic stationary phases often involves the use of ligating agents for chelation ion chromatography. In recent years, iminodiacetic acid (IDA)-functionalized stationary phases have been among the most intensively studied.[6-9] These columns have selectivity for transition metals over alkali and alkaline earth metals. For example, preconcentration and separation of transition

metals in samples containing alkali and alkaline metals can be achieved with a single column using IDA functionalized silica.[6]

Macrocyclic ligands were incorporated into chromatographic separation systems early on[10] and continue to be good candidates as synthetic ion exchangers. Crown ethers and cryptands were incorporated into ion chromatographic separator columns by our group for the separation of both cations and anions.[11] The commercially available IonPac CS15 column from Dionex was developed containing 18-crown-6, carboxylic acid, and phosphonate groups covalently bonded to the resin. The column showed better resolution between ammonium and sodium ions than the IonPac CS12 column containing carboxylic acid and phosphonate groups only.[12] In other work, Hsu et al.[13] grafted the macrocyclic ligand [24]ane-N_6 to silica and used the resulting stationary phase for separation of transition metal ions with eluents containing organic acids such as oxalic acid, malonic acid, or succinic acid. Transition metal ions formed complexes with the organic acids and were retained on the protonated [24]ane-N_6 sites.

In our group, we continue to explore the application of selective macrocyclic ligands in ion chromatography. One type of macrocycle, the resorcinarenes, are cyclic tetramers synthesized from the condensation of resorcinol and various aldehydes. The upper rim and lower rim of resorcinarenes can be modified with various functional groups to provide specific selectivity for anions, cations, and small organic molecules.[14,15] For example, the resorcinarene can serve as an organic scaffold to position a set of four cyclen ligands in proximity when these are bonded to the upper rim. Specifically, we demonstrated that this so-called cyclenbowl ligand (Figure 4.1) can be used for anion separation and has selectivity for perchlorate and perrhenate ion, respectively.[16] The cyclenbowl column has improved performance over a comparable column containing the cyclen monomer. N-cyclen and cyclenbowl contain cyclen units and hydrophobic alkyl chains

that make it possible to adsorb the molecule onto a hydrophobic resin for use as stationary phases for IC separations. The protonation constant of cyclen is 10.9; consequently, it can be protonated under lightly basic conditions and used as anion exchanger. In addition, cyclen is an effective Lewis base that can form stable coordination complexes with many transition metal ions. Among these ions, the stability constant of cyclen with Cu^{2+} is much higher than that with other transition metals (shown in Table 4.1)[17] resulting in a natural selectivity of cyclen for Cu^{2+}. Potentially, the two cyclen-based ligands can be used to prepare columns either for preconcentration of trace amounts of Cu^{2+} in the presence of a large matrix background of other transition metals or for the separation of transition metal ions from one another.

Preconcentration[18] and separation of trace metals on a single column is a convenient way to analyze trace metal ions,[6, 16] avoiding the need for separate concentrator and separator columns. In such a case, special valving and a separate sample loading pump are not needed, thus simplifying the separation system.[6,19] Also avoided is the need for the sample loading direction and sample injection directions to be reversed in the concentrator column, as is usually required to wash the concentrator column with deionized water to avoid potential interference from residual ions.[20]

In this paper, we report the separation of transition metal ions with the N-cyclen and cyclenbowl columns and the preconcentration of Cu^{2+} with the cyclenbowl column. The effect of the chelating ligands oxalic acid and IDA in the eluent is discussed. The retention mechanism of the separation of transition metals is also considered.

2. Materials and methods

2.1 Reagents

All reagents used, including nitrate salts of transition metal cations, were analytical grade unless specified. Trace metal grade nitric acid and ammonium hydroxide were obtained from Fisher (Pittsburgh, PA). Other common trace metal grade cations were obtained from Sigma-Aldrich (Milwaukee, WI). All eluents and standards were prepared using Milli-Q water of 18 Megaohm/cm resistivity. Post column reagents for vis detection used in the studies were 0.5 mM 4-(2-pyridylazo) resorcinol (PAR), 1.0 M 2-dimethylaminoethanol, 0.50 M ammonium hydroxide, and 0.30 M sodium bicarbonate.[19]

2.2 Column preparation

The column was prepared by the method reported previously.[16] Briefly, 95.2 mg of N-undecylcyclen or 138 mg of cyclenbowl ligands were dissolved in methanol and mixed with 1.3 g of resin, respectively, to be adsorbed on the resin by the hydrophobic effect. The slurry of the coated resin was used to pack a 4×200 mm black PEEK column. The column was packed at 60 ^{o}C and 5000 psi for 15 minutes. The 55% cross-linked styrene-divinylbenzene polymeric macroporous resin was provided by Dionex Corporation (Sunnyvale, CA). The particle size of the resin was 5 μm resin. The average pore size and the surface area of the resin were 100-150 Å and 350 m^2/g, respectively. A column containing unsubstituted polystyrene-divinylbenzene resin was also packed (1.3 g resin, 4×200 mm PEEK column) under the same conditions to do a comparison study.

2.3 Instrumentation

A Dionex ICS-3000 system with an AS40 autosampler and a PDA-100 photodiode array detector was used throughout this study. Data were collected and analyzed using the Dionex Chromeleon workstation (version 6.8). The eluted peaks were recorded by dual wavelength[21] at 520 nm and 620 nm and simple arithmetic manipulation (520 - 620 nm) was applied using Chromeleon software from Dionex to minimize the baseline noise. A PC10 postcolumn pneumatic delivery system was used to pump post column reagent PAR. The flow rate of PAR was 0.2 mL/min. The Perkin Elmer optima 2000 DV ICP-OES instrument was used to analyze the effluent from the column.

3. Results and discussion

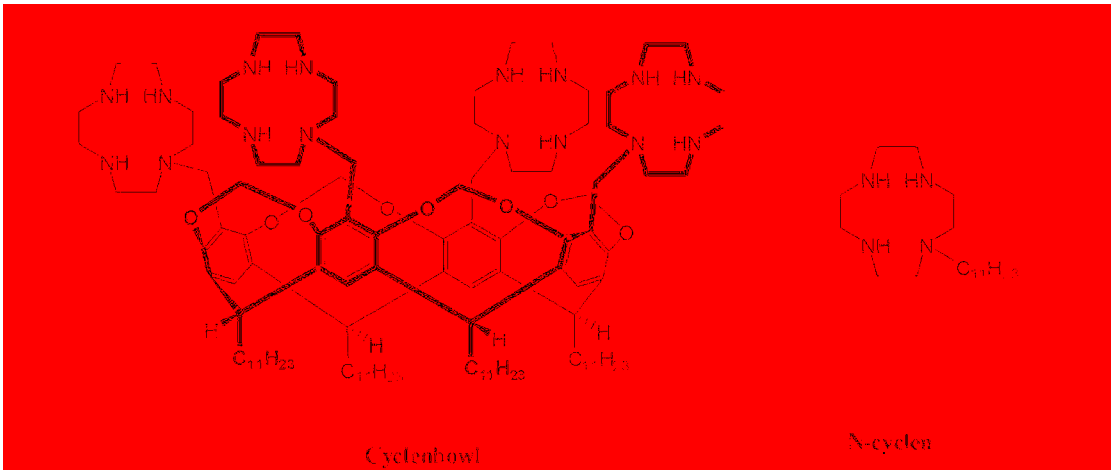

Figure 4.1 Structures of cyclenbowl and N-cyclen ligands.

The stability constants of several transition metal ions with cyclen are shown in Table 4.1. As indicated, the first protonation constant of cyclen is 10.97. Our previous study[16] showed that

the capacity of the cyclen-based columns could be regulated by controlling the protonation of the cyclen unit. When 10 mM $NaHCO_3$ (pH = 7.6~8.0) was used as the eluent, cyclen units of the cyclenbowl column were protonated and could act as anion exchangers. Seven anions including F^-, Cl^-, NO_2^-, NO_3^-, SO_4^{2-}, and ReO_4^- were retained and separated on this column. The preconcentration of the most strongly retained anion, ReO_4^-, was achieved by using a capacity gradient. Specifically, the other anions were eluted by 10 mM $NaHCO_3$, while ReO_4^- was retained and enriched on the column. Switching the eluent to 10 mM NaOH (pH = 12) caused the capacity of the column to be reduced, so that ReO_4^- was eluted.

Table 4.1 Protonation constants (log *K*) of cyclen, iminodiacetic acid (IDA), oxalic acid, and 4-(2-pyridylazo) resorcinol (PAR) and their stability constants (log *K*) with metal cations[17, 22]

	Cyclen (T= 25 °C)	IDA (T = 20 °C)[e]	Oxalic acid (T = 20 °C)[f]	PAR
H^+	10.97[a]	K_1= 9.33, K_2 =2.58	K_1= 3.81, K_2 = 1.37	12.5
Mn^{2+}			3.75 ± 0.05 [f]	9.7
Co^{2+}		K_1 = 6.91, β_2 = 12.31	6.79 ± 0.07 [f]	10.5
Ni^{2+}	16.4[b]	K_1 = 8.19, β_2 = 14.3	7.88 ± 0.04 [f]	13.2
Cd^{2+}	14.3[d]	K_1 = 5.13, β_2 = 10.19	3.71 ± 0.03 [f]	10.5
Zn^{2+}	16.2[d]	K_1 = 7.27, β_2 = 12.60	7.59 ± 0.05 [f]	11.6
Cu^{2+}	23.29[b], 24.8[c]	K_1 = 10.63, β_2 = 16.68	10.46 ± 0.04 [f]	11.7

[a] I = 0.5 mol/L KNO_3; [b] I = 0.1 mol/L $NaNO_3$; [c] I = 0.2 mol/L; [d] I = 0.2 mol/L $NaClO_4$, [e] I = 0.1 mol/L KNO_3; [f] I = 0.1 mol/L $KClO_4$; [g] I = 0.1 mol/L $NaClO_4$.

In addition to acting as an anion exchanger, the cyclenbowl ligand also has the potential to act as a chelating cation exchanger. The four nitrogen atoms of each cyclen unit form stable coordination complexes with transition metal ions, especially Cu^{2+}, which forms the most stable complex (Table 4.1). Furthermore, cyclen has little or no affinity for alkali or alkaline earth cations. The selectivity of cyclen for Cu^{2+} raises the prospect to use the cyclenbowl column to separate and preconcentrate Cu^{2+} in the presence of high concentrations of matrix cations. HNO_3 or chelating ligands such as iminodiacetic acid (IDA) or oxalic acid make good eluent candidates for this system.

3.1 Effect of HNO_3 concentration

We first used HNO_3 as the eluent with the cyclenbowl column. Under acidic conditions, cyclen units can be protonated, and the competition between protons and transition metal ions for the cyclen units provides the basis for the separation. The cyclenbowl column was used for separation of six cations including Mn^{2+}, Co^{2+}, Ni^{2+}, Cd^{2+}, Zn^{2+} and Cu^{2+}. With 5 mM HNO_3 as eluent, a single peak was obtained at 8.2 min with a flow rate of 0.35 mL/min. Spiking experiments identified this peak as a mixture of five cations, namely, Mn^{2+}, Co^{2+}, Ni^{2+}, Cd^{2+}, and Zn^{2+}. This result is similar to that shown in Figure 4.2 under slightly different flow rate conditions. Cu^{2+} was not observed to elute before 30 min. When 10 mM HNO_3 was used at 0.35 mL/min, two peaks appeared. The peak at 8.1 min was again the mixture of 5 cations, while Cu^{2+} appeared as a broad peak at 16.7 min. In contrast, when using 50 mM HNO_3 as eluent, Cu^{2+} appeared as a sharp symmetrical peak at 11.1 min, while the retention time of the 5 other cations

was 7.9 min. Peak resolution was 2.55. This result is consistent with the relative stability constants of cyclen among these metal cations.

3.2 Preconcentration of Cu^{2+} with cyclenbowl column

The above results demonstrate that preconcentration of Cu^{2+} is possible using this column in the following manner. Low concentrations of HNO_3 (5 mM) were used to elute the mixture of Mn^{2+}, Co^{2+}, Ni^{2+}, Cd^{2+}, and Zn^{2+} while Cu^{2+} in the sample was retained on the column. As several 2-mL injections of sample were made, Cu^{2+} accumulated and was enriched on the column. An acid eluent step change using a higher concentration of HNO_3 was then applied to elute Cu^{2+}. This preconcentration of Cu^{2+} is particularly applicable to a complex matrix that contains a large concentration of matrix cations and trace amounts of Cu^{2+}. In this case, Cu^{2+} was enriched on the column by making several injections as described and then eluted for quantification. In this way, trace amounts of Cu^{2+} were detected. Figure 4.2 shows the preconcentration of Cu^{2+} using a sequence of injections followed by an acid eluent step change. 15 μg L^{-1} of Cu^{2+} in a matrix containing 1 mg L^{-1} each Mn^{2+}, Co^{2+}, Ni^{2+}, Cd^{2+}, and Zn^{2+} was well separated using this approach. When using a 5 mM to 50 mM HNO_3 eluent step change, Cu^{2+} was eluted with a peak area of 6.03 ± 0.11 mAU·min. When two injections were applied, a sharper and larger peak was obtained with a peak area twice as large as that from the single injection. An even sharper and larger peak was obtained with four injections and the recovery of Cu^{2+} was higher than 98%. With this preconcentration method, this very low concentration of Cu^{2+} could be determined with high accuracy (see Table 4.2).

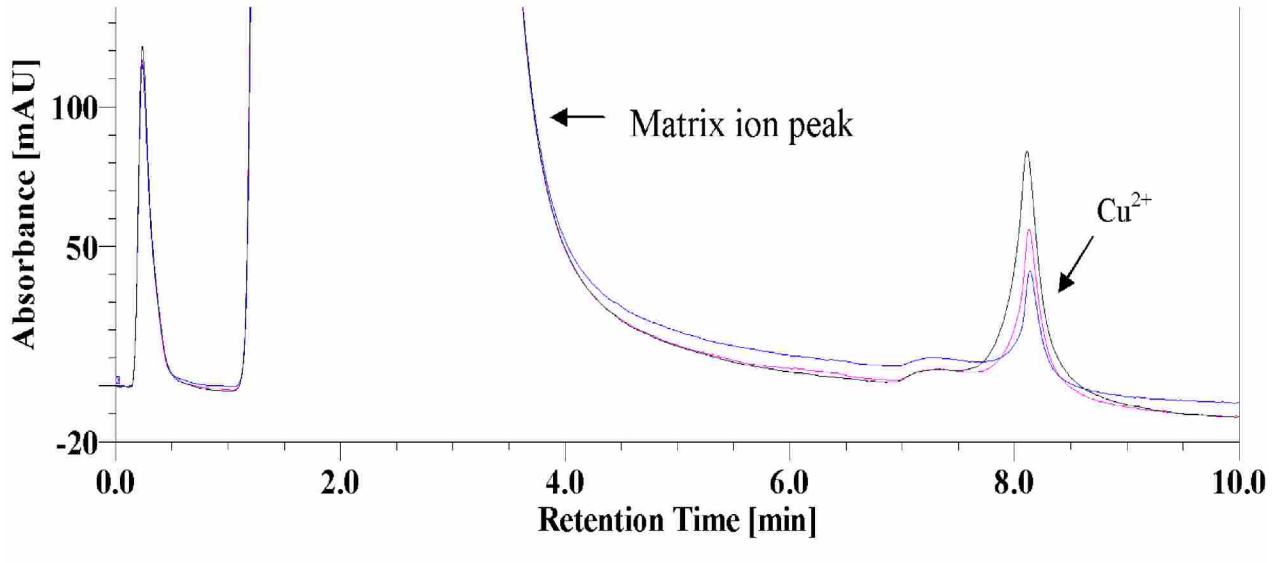

Figure 4.2 Preconcentration of Cu^{2+} using HNO_3 as eluent (Blue: 2 mL injection, 5 mM HNO_3 for 5 min step to 50 mM HNO_3; Red: one injection; isocratic eluent 5 mM HNO_3 for 5 minutes; followed by second injection, 5 mM HNO_3 for 5 minutes followed by step to 50 mM HNO_3, chromatogram shown in red was recorded after the second injection; Black: three injections, isocratic 5 mM HNO_3 for 5 minutes, respectively; then the fourth injection, 5 mM HNO_3 for 5 minutes followed by step to 50 mM HNO_3, chromatogram shown in black was recorded after the fourth injection. Mixture of analytes: Mn^{2+}, Co^{2+}, Ni^{2+}, Cd^{2+}, Zn^{2+} (1 mg L^{-1} each), and 15 µg L^{-1} Cu^{2+}. Eluent flow rate: 1.0 mL/min.

Table 4.2 Preconcentration and recovery of Cu^{2+} using cyclenbowl column

	1 injection	2 injections	4 injections
Peak area of Cu^{2+} (mAU·min)	6.0± 0.1	11.9 ± 0.0	24.0 ± 0.0
Recovery (%)		98.7 ± 1.7	99.3 ± 1.8

3.3 Transition metal cation separations: Effect of chelating ligand oxalic acid in the eluent

Beyond preconcentrating Cu^{2+}, we investigated the use of the cyclen-based column to make separations among transition metal cations. Previous studies have found that the addition of chelating ligands to the eluent can enhance transition metal cation separation and considerably reduce separation times. These ligands form complexes with transition metals that increase the degree of partition of transition metal ions to the mobile phase, reducing retention time. Ligands such as pyridine-2,6-dicarboxylic acid (PDCA), tartaric acid, iminodiacetic acid (IDA), picolinic acid, dipicolinic acid, maleic acid, malonic acid, citric acid and oxalic acid have been used. For example, Jones et al.[23] found that the addition of picolinic acid to the eluent can speed the separation of Cu^{2+} and Ni^{2+} when using a column packed with IDA-bonded silica particles. Nesterenko et al.[6] found that 0.1 M oxalic acid can achieve the fastest separation of transition metals on a IDA-bonded silica column when compared to other organic acid eluents such as maleic acid, malonic acid, citric acid, and tartaric acid.

To begin our studies using chelating ligands in the mobile phase with the cyclenbowl column, oxalic acid or IDA was used without any other component present. Among the six analyte transition metal ions, no peaks appeared up to 60 min after injection using concentrations of oxalic acid ranging from 1 mM to 80 mM in isocratic mode. Furthermore, from the work described above (Figure 4.2), 5 mM HNO_3 alone did not yield a separation of the five transition metal cations aside from Cu^{2+}. It was expected therefore that a combination of oxalic acid and nitric acid would be effective, given the stability constant differences between complexes of

oxalic acid with different transition metal ions. Oxalic acid was mixed at different concentrations (0.5 mM, 1 mM, 2 mM, and 3 mM) with 5 mM HNO_3. This isocratic eluent combination yielded separate peaks within 20 minutes for Co^{2+}, Zn^{2+}, and Ni^{2+}, with coelution of Mn^{2+} and Cd^{2+}, at oxalic acid concentrations of 2 mM and higher (see Figure 4.3). Under these conditions, Cu^{2+} did not appear. In an attempt to separate Cu^{2+}， after 15 minutes an eluent step change to 100 mM of HNO_3 was applied. Cu^{2+} was eluted but not detected, as described below.

We found that the retention time of transition metal ions increased with increasing oxalic acid concentrations. These results imply that oxalic acid may interact with the stationary phase cyclen units and in this way have an important effect on retention. To test this hypothesis, before analyte injection, we flowed oxalic acid solution of different concentrations (0.5 mM, 1 mM, 2 mM, 3 mM, and 4 mM) through the column for 10 minutes to load the column with oxalic acid. We then injected a 2-mL sample of the transition metal ions, followed by 50 mM HNO_3 (without oxalic acid) as eluent. These results are shown in Figure 4.4. Resolution among Cd^{2+}, Co^{2+}, Zn^{2+}, and Ni^{2+} increased steadily with increased preliminary loading of oxalic acid.

The calculated pH values of the oxalic acid solutions used were between 2.4~3.3. In this pH range, cyclen units are protonated, while most of the oxalic acid exists in the form of $HC_2O_4^-$ ions. The latter anions can be attracted to the positively charged protonated cyclen units on the column and assist in retaining transition metal cations. In support of this hypothesis, the observed elution order of transition metal ions is similar to the pattern of oxalic acid complexation constants (see Table 4.1). Furthermore, higher concentrations of oxalic acid should yield more

free $HC_2O_4^-$ ions for cation retention; this would result in increased column capacity and increased retention times, consistent with the data in Figure 4.4. It is clear that with oxalic acid present, a different retention mechanism is at work involving cooperation between cyclen and oxalic acid, in contrast to the direct cyclen-metal ion complexation at work in the Cu^{2+} preconcentration study in which oxalic acid is absent.

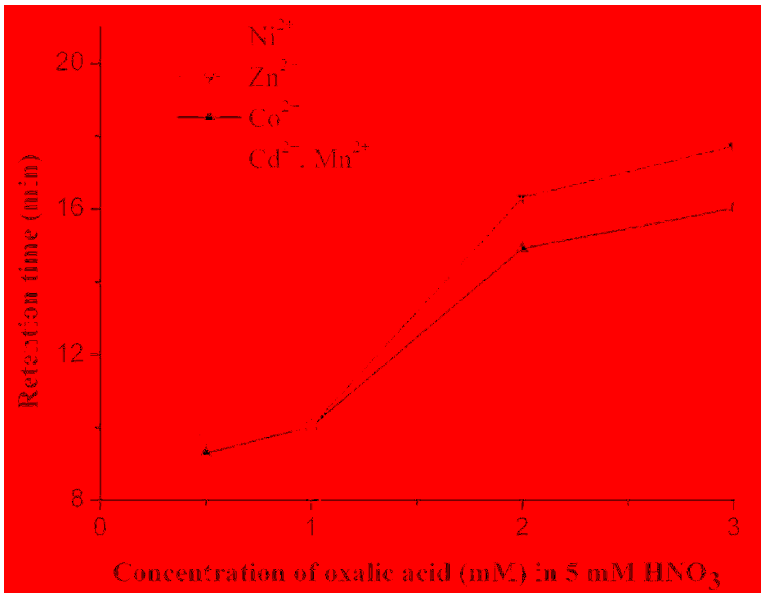

Figure 4.3 Effect of the concentration of oxalic acid on the retention time of transition metal ions on the cyclenbowl column. Eluent: 5 mM HNO_3 + oxalic acid at different concentrations (0.5 mM, 1 mM, 2 mM, and 3 mM, respectively) for 15 min, then stepped to pure 100 mM of HNO_3. Flow rate: 0.35 mL/min.

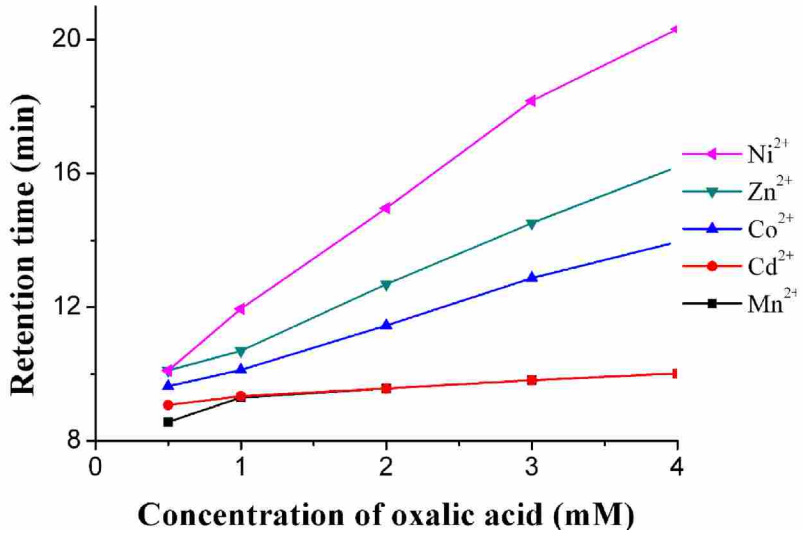

Figure 4.4 Change in retention time of transition metal ions on the cyclenbowl column with concentration of oxalic acid. Conditions: oxalic acid loaded at 0.5 mM, 1 mM, 2 mM, 3 mM, and 4 mM for 10 min, followed by injection of transition metal ions, followed by elution with 50 mM HNO_3. Above 1 mM oxalic acid, Cd^{2+} and Mn^{2+} coelute. Flow rate: 0.35 mL/min.

A very good separation of the transition metal ions was achieved using the approach of pre-loading the column with oxalic acid and eluting with nitric acid. Figure 4.5 shows the separation of transition metal ions using the cyclenbowl column in this way. Spiking experiments confirmed the identity of peaks 1-4, but experiments showed that peak 5 is not Cu^{2+}. Cu^{2+} did not elute with the other peaks. This issue is discussed further below.

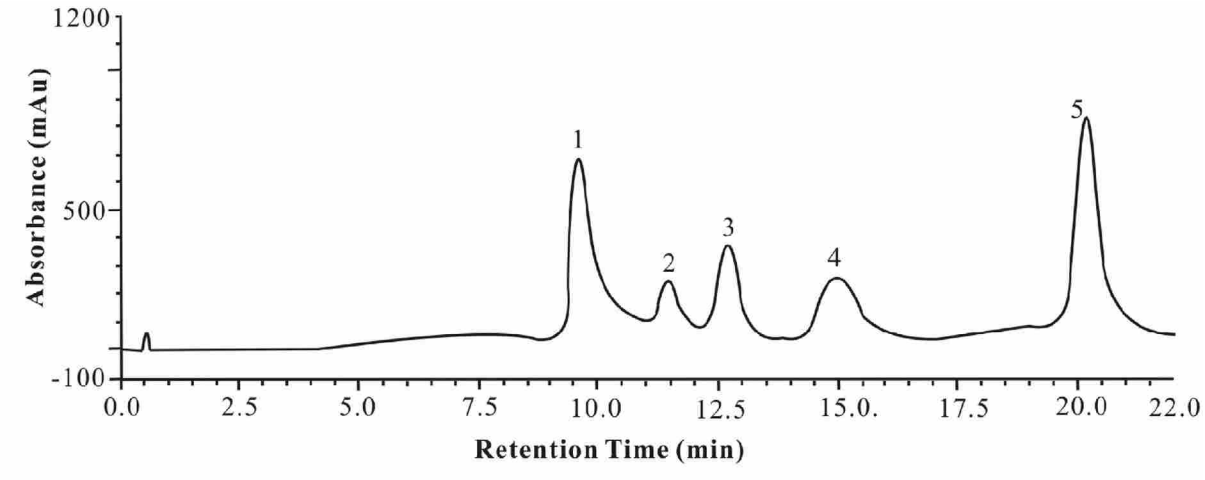

Figure 4.5 Separation of transition metals with the cyclenbowl column. Conditions: 2 mM oxalic acid for 10 minutes before injection followed by 50 mM HNO_3. Peaks: 1 = Mn^{2+} (0.6 mg L^{-1}), Cd^{2+} (0.8 mg L^{-1}); 2 = Co^{2+} (0.2 mg L^{-1}); 3 = Zn^{2+} (0.2 mg L^{-1}); 4 = Ni^{2+} (0.6 mg L^{-1}); 5 = system peak. Flow rate: 0.35 mL/min.

3.4 Oxalic acid gradient separation of transition metal ions

In the above work, Mn^{2+} and Cd^{2+} coeluted. Thus, an eluent gradient was sought to effect separation of these two ions. The first gradient period was designed to be a combination of oxalic acid loading and nitric acid elution; specifically, 1 mM oxalic acid + 10 mM HNO_3 for 10 min. The second period was elution with 50 mM HNO_3. Figure 4.6 shows that this eluent gradient separates all five metal ions, Mn^{2+}, Co^{2+}, Ni^{2+}, Cd^{2+}, and Zn^{2+} with baseline resolution. However again, a Cu^{2+} peak did not appear. To investigate this issue, the effluent of the separation up to 32 min was collected, and in a separate experiment, the effluent from peak 6 was collected and ICP analysis performed. The ICP analysis of peak 6 showed that the last peak is not Cu^{2+}. The analysis of the total effluent showed that Cu^{2+} was indeed eluted from the column since the

moles of Cu^{2+} determined by ICP matched the moles in the sample, but which were not detected by the detector.

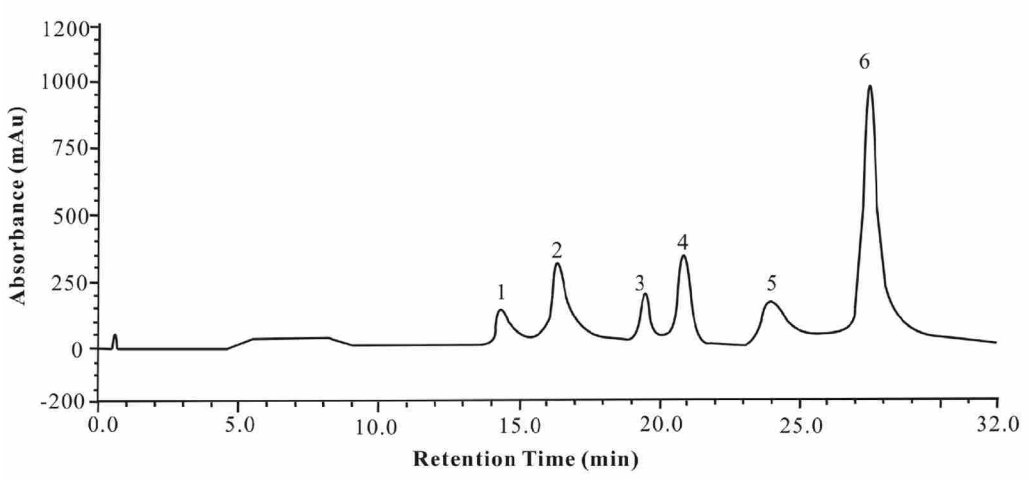

Figure 4.6 Separation of transition metal ions with gradient elution on the cyclenbowl column. Eluent: 2 mM oxalic acid for 10 minutes before injection; after injection, eluent step change: 0 - 10 min, 1 mM oxalic acid + 10 mM HNO_3; 10 – 32 min, 50 mM HNO_3. Peaks: 1 = Mn^{2+} (0.6 mg L^{-1}); 2 = Cd^{2+} (0.8 mg L^{-1}); 3 = Co^{2+} (0.2 mg L^{-1}); 4 = Zn^{2+} (0.2 mg L^{-1}); 5 = Ni^{2+} (0.6 mg L^{-1}); 6 = system peak. Flow rate: 0.35 mL/min.

3.5 Separation of transition metal ions on N-cyclen column

The resorcinarene structure was adopted as a scaffold at the base of the cyclenbowl ligand which serves to preorganize the four identical cyclen ion exchange sites for maximize exposure to analytes. To test our design, the N-cyclen ligand containing one cyclen ion exchange site was used for comparison and incorporated into a column for the separation of transition metal ions. As with the cyclenbowl column, we loaded the N-cyclen column with different concentrations of oxalic acid (0.5 mM, 1 mM, 2 mM, 3 mM, 4 mM and 6 mM) for 10 minutes;

after injecting the analytes, 50 mM HNO_3 was used as eluent. While the separations were very much poorer than with the cyclenbowl column, similarities in performance were observed. First, in both cases, the retention time of transition metal ions increases with increasing concentration of loaded oxalic acid (as shown in Figure 4.7). Second, the obtained elution order is the same with both columns. The separation of transition metal ions on the N-cyclen column is shown in Figure 4.8. We also performed the separation with the N-cyclen column using the gradient procedure, as shown in Figure 4.9. These separations are very much poorer than with the cyclenbowl column. In particular, the retention time of transition metal ions on the N-cyclen column is much shorter than on the cyclenbowl column. For instance, when 4 mM oxalic acid was loaded, Zn^{2+} and Ni^{2+} had the same retention time (11.9 min) on the N-cyclen column, whereas these were eluted at 16.2 and 20.3 min, respectively, on the cyclenbowl column. Furthermore, the cyclenbowl column showed much better resolution for transition metal ions under the same experimental conditions. For example, Figure 4.5 and Figure 4.8 are the chromatograms obtained from the cyclenbowl and N-cyclen columns, respectively, under the same experimental conditions. Co^{2+}, Zn^{2+}, and Ni^{2+} showed baseline resolution on the cyclenbowl column, but were coeluted on the N-cyclen column. These results indicate that the capacity and the separation efficiency are significantly enhanced by using the resorcinarene-based scaffold to host the cyclen ion-exchange sites, consistent with our design strategy. Similar improvement in column capacity of the cyclenbowl column over the N-cyclen column was observed in our previous study involving anion separations.[16]

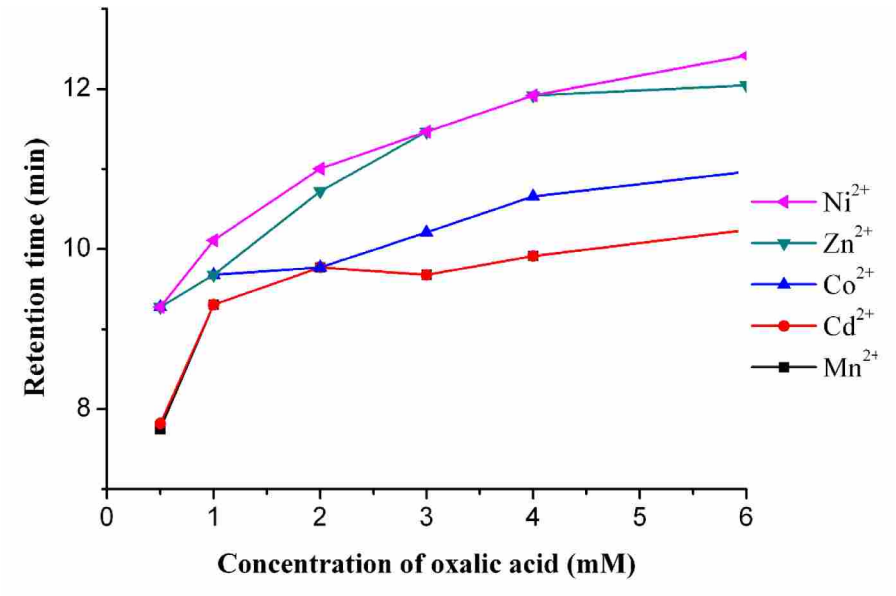

Figure 4.7 Change in retention time of transition metal ions on the N-cyclen column with concentration of eluent oxalic acid. Conditions: oxalic acid loaded at 0.5 mM, 1 mM, 2 mM, 3 mM, 4 mM, and 6 mM for 10 min, followed by injection of transition metal ions, followed by elution with 50 mM of HNO_3. Above 1 mM oxalic acid, Cd^{2+} and Mn^{2+} coelute. Flow rate: 0.35 mL/min.

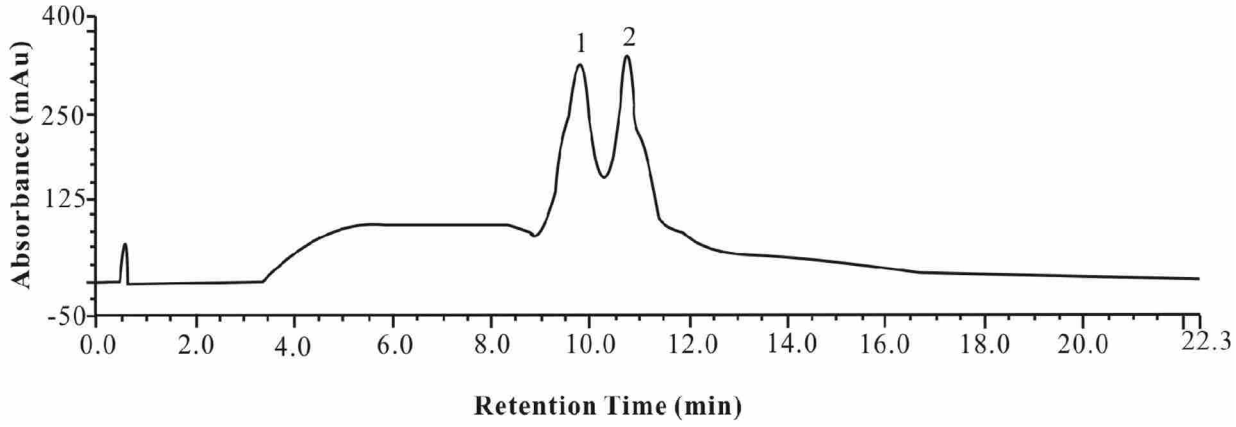

Figure 4.8 Separation of transition metal ions with the N-cyclen column. Conditions: 2 mM oxalic acid for 10 minutes before injection followed by 50 mM HNO_3. Peaks: 1 = Mn^{2+} (0.6 mg L^{-1}), Cd^{2+} (0.8 mg L^{-1}); 2 = Co^{2+} (0.2 mg L^{-1}); Zn^{2+} (0.2 mg L^{-1}) and Ni^{2+} (0.6 mg L^{-1}). Flow rate 0.35 mL/min.

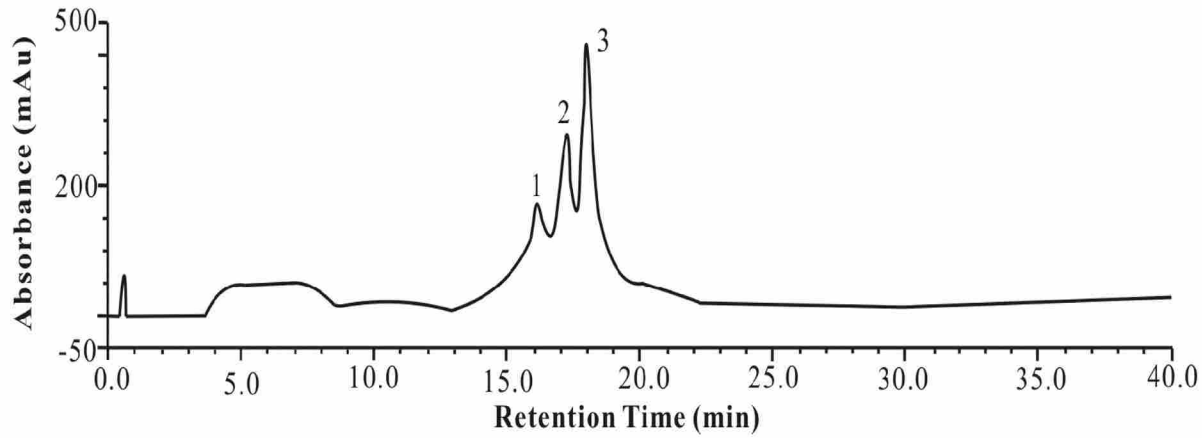

Figure 4.9 Separation of transition metal ions with gradient elution on the N-cyclen column. Conditions: 2 mM oxalic acid for 10 minutes before injection, followed by an eluent step change: 0 - 10 min, 1 mM oxalic acid + 10 mM HNO_3; 10 – 32 min, 50 mM HNO_3. Peaks: 1 = Mn^{2+} (0.6 mg L^{-1}); 2 = Cd^{2+} (0.8 mg L^{-1}) and Co^{2+} (0.2 mg L^{-1}); 3 = Zn^{2+} (0.2 mg L^{-1}) and Ni^{2+} (0.6 mg L^{-1}). Flow rate: 0.35 mL/min.

3.6 Unsubstituted resin column

Jones's group found that adding heterocyclic carboxylic acids in the eluent such as picolinic acid, dipicolinic acid, quinaldic acid, and 4-chlorodipicolinic acid can dynamically coat the neutral polystyrene-divinylbenzene resin to form a chelating stationary phase.[24-27] For example, an unsubstituted resin column can be used with 4-chlorodipicolinic acid in the mobile phase to separate seven metal ions (Mn^{2+}, Co^{2+}, Ni^{2+}, Zn^{2+}, Cu^{2+}, Pb^{2+}, and Cd^{2+}) with good resolution.[24] Merly et al.[28] packed a column with porous graphitic carbon (PGC) and found that oxalic acid in the mobile phase can be retained and modify the PGC surface to act as a chelating ion-exchange site. Baseline separation of Ni^{2+}, Cd^{2+}, Cu^{2+}, and Pb^{2+} ions was accomplished with oxalic acid in the mobile phase. We tested if the separation observed in the cyclenbowl column

was due to the macrocyclic ligand or simply to the presence of oxalic acid in the eluent. In order to answer this question, we packed a column with unsubstituted polystyrene resin and applied the same program used with the cyclenbowl column. Specifically, 2 mM oxalic acid flowed for 10 minutes before injecting analytes, and subsequently 50 mM HNO_3 was used as eluent. Mn^{2+} was separated from the other metal ions with retention time 8.5 min and Co^{2+}, Ni^{2+}, Zn^{2+}, Cu^{2+} and Cd^{2+} eluted together at 10.0 min with a resolution of 1.03. This result demonstrates that the cyclenbowl ligand is an important contributor to the separation process in these systems.

3.7 Effect of chelating ligand iminodiacetic acid (IDA) in the eluent

The chelating ligand IDA was also tested as an eluent component on the cyclenbowl column. No peaks appeared before 40 min when using IDA concentrations ranging from 0-80 mM with IDA as the sole eluent component. The addition of different concentrations of IDA (4 mM, 6 mM, 8 mM) in 50 mM HNO_3 yielded the same retention characteristics as obtained with nitric acid alone. This result is similar to that observed by Jones's group [21]. In addition, in fashion similar to the experiments with oxalic acid, different concentrations of IDA were pumped for 10 minutes before injection, followed by 50 mM HNO_3 after sample injection. Once again, only Mn^{2+} was separated from the other coeluted metal ions (Co^{2+}, Ni^{2+}, Zn^{2+}, Cu^{2+} and Cd^{2+}). Clearly IDA is not as effective as oxalic acid in this system.

Table 4.3 Comparison between two post-column reagent solutions.

	Sensitivity ($mAu \cdot min \cdot L \cdot mg^{-1}$)		Detection limit ($\mu g\ L^{-1}$)		Correlation coefficient	
	PAR 1	PAR 2	PAR 1	PAR 2	PAR 1	PAR 2
Mn^{2+}	233.0	95.4	46.5	139.0	0.9956	0.9964
Cd^{2+}	186.0	55.8	92.2	647.1	0.9900	0.9913
Co^{2+}	157.2	357.9	22.1	72.8	0.9909	0.9960
Zn^{2+}	627.0	125.4	6.7	33.6	0.9991	0.9991
Ni^{2+}	266.1	79.8	18.3	61.0	0.9993	0.9993

3.8 Effect of post column reagent composition

Different buffer solutions can be used to prepare the post column reagent solution (PAR). Typically, one of two buffer solutions is used. The first is prepared with ammonium hydroxide, sodium bicarbonate, and 2-dimethylaminoethanol; the second is prepared with an ammonia:ammonium acetate buffer. In our work, the first post column solution (PAR 1) contained 0.5 mM PAR, 1.0 M dimethylaminoethanol, 0.50 M ammonium hydroxide, and 0.30 M sodium bicarbonate.[19] The second post column solution (PAR 2) contained 0.3 mM PAR, 1.2 M acetic acid and 8.6 M ammonium hydroxide (pH=10.2).[29] Table 4.3 compares the results using these two post column solutions. Generally, PAR 1 showed better sensitivity and lower detection limits for most transition metal ions; however, PAR 2 showed better sensitivity for Co^{2+}. PAR 1 is especially effective for detecting Cd^{2+}. The detection limit of Cd^{2+} was significantly improved from 647.1 $\mu g\ L^{-1}$ to 92.2 $\mu g\ L^{-1}$ when using PAR 1.

4. Conclusions

The synthesized ligands cyclenbowl and N-cyclen were applied as cation exchange sites in chelation ion chromatography for the separation of transition metal ions. The column coated with cyclenbowl ligands containing preorganized macrocyclic structures yielded high capacity and separation efficiency. This result is consistent with our previous studies of anion separations with such columns. The cyclenbowl column exhibits maximum selectivity for Cu^{2+} ion, consistent with the thermodynamic selectivity of cyclen and making possible the preconcentration of trace amounts of Cu^{2+} in the presence of high concentrations of matrix ions. With oxalic acid in the eluent, good separation of five transition metal cations can be achieved, and a different mechanism of retention based on oxalic acid/resorcinarene coupling is at work. The resorcinarene class of macrocyclic ligands offers a promising scaffold to host various functional groups for liquid chromatographic separations.

References

1. Haddad, P. R.; Nesterenko, P. N.; Buchberger, W. Recent developments and emerging directions in ion chromatography. *J. Chromatogr. A* **2008**, *1184,* 456-473.
2. Nesterenko, P. N.; Jones, P. Recent developments in the high-performance chelation ion chromatography of trace metals. *J. Sep. Sci.* **2007**, *30*, 1773-1793.
3. Saari-Nordhaus, R.; Anderson, J. M. Jr. Alternative approach to enhancing cation selectivity in ion chromatography. *J. Chromatogr. A* **2004**, *1039*, 123-127.

4. Richens, D. A.; Simpson, D.; Peterson, S.; McGinn, A.; Lamb, J. D. Use of mobile phase 18-crown-6 to improve peak resolution between mono- and divalent metal and amine cations in ion chromatography. *J. Chromatogr. A* **2003**, *1016*, 155-164.

5. Bruzzoniti, M. C.; Carlo, R. M. D.; Fungi, M. Simutaneous determination of alkali, alkaline earth and ammonium in natrual waters by ion chromatography. *J. Sep. Sci.* **2008**, *31*, 3182-3189.

6. Nesterenko, P. N.; Jones, P. Single-column method of chelation ion chromatography for the analysis if trace metals in complex samples. *J. Chromatogr. A* **1997**, *770*, 129-135.

7. Bashir, W.; Paull, B. Ion stength, pH and temperatures effects upon selectivity for transition and heavy metal ions when using chelation ion chromatography with an iminodiacetic acid bonded silica gel column and simple inorganic eluents. *J. Chromatogr. A* **2002**, *942*, 73-82.

8. Barron, L.; O'Toole, M.; Diamond, D.; Nesterenko, P. N.; Paull, B. Separation of transition metals on a poly-iminodiacetic acid grafted polymeric resin column with post-column reaction detection utilising a paired emitter-detector diode system. *J. Chromatogr. A* **2008**, *1213*, 31-36.

9. Dias, J. C.; Kubota, L. T.; Nesterenko, P. N.; Dicinoski, G. W.; Haddad, P. R. A new high-performance chelation ion chromatographic system for the direct determination of trace metal transition metals in fuel ethanol. *Analyst* **2010**, *2*, 1565-1570.

10. Sogah, G. D. Y.; Cram. D. J. Total chromatographic optical resolution of α-amino acid and ester salts through chiral recognition by a host covalently bound to polystyrene resin. *J.*

Am. Chem. Soc. **1976**, *98*, 3038-3041.

11. Lamb, J. D.; Drake, P. A. Chemically suppressed anion chromatography based on macrocycle-cation complexation. *J. Chromatogr.* **1989**, *482*, 367-380.

12. Ray, M. A.; Pohl, C. A.; Jagodzinski, J. J.; Kaiser, E. Q.; Riviello, J. M. A new approach to dealing with high-to-low concentration satios of sodium and ammonium ions in ion chromatography. *J. Chromatogr. A* **1998**, *804*, 201-209.

13. Hsu, J. C.; Chang, C. H.; Liu, C. Y. Preparation and evaluation of a functionalized polymer-coated silica based sorbent for metal ion separation. *Fresenius J. Anal. Chem.* **1998**, *362*, 514-521.

14. Restorp, P.; Rebek, J. Jr. Reaction of isonitriles with carboxylic acids in a cavitand: observation of elusive isoomide intermediates. *J. Am. Chem. Soc.* **2008**, *130*, 11850-11851.

15. Lamb, J. D.; Morris, C. A.; West, J. N.; Morris, K. T.; Harrison, R. G. Cation effect on anion separations by aza-crown ligands in liquid membranes. *J. Membr. Sci.* **2008**, *321*, 15-21.

16. Wang, J.; Harrison, R. G.; Lamb, J. D. Anion separation and preconcentration with cyclen and cyclen-resorcinarene derivatives. *J. Chromatogr. Sci.* **2009**, *47*, 510-515.

17. Antunes, P.; Campello, P. M.; Delgado, R.; Drew, M. G. B.; Félix, V.; Santos, I. Metal complexes of a tertraazacyclophane: solution and molecular modelling studies. *Dalton Trans.* **2003**, *9*, 1852-1860.

18. Toofan, M., Pohl, C. A.; Stillian, J. R.; Jackson, P. E. , Factors affecting the ion chromatographic preconcentration behavior of inorganic and organic acids. *J. Chromatogr. A*

1997, *775*, 109-115.

19. Dionex technical note 10, Determination of Transition Metals by Ion Chromatography. Doc. #4691-tn10, Dionex, Sunnyvale, CA, USA.

20. Toofan, M.; Stillian, J. R.; Pohl, C. A.; Jackson, P. E. Preconcentration determination of inorganic anions and organic acids in power plant waters separation optimization through control of column capacity and selectivity. *J. Chromatogr. A* **1997**, *761*, 163-168.

21. Jones. P. Major sensitivity improvements in ion chromatography determinations involving post-column spectrophotometric reaction detectors through elimination of pump noise using a dual wavelength monitoring procedure. *Analyst* **2000**, *125*, 803-806.

22. Sillén, L. G.; Martell, A. E.; Stability Constants of Metal-ion Complexes, Special Publication No 25, Burlington House, London, 1971.

23. Jones, P.; Nesterenko, P. N. *J.* Use of complexing reagetns as additives to the eluent for optimization of separation selectivity in high-performance chelation ion chromatography. *Chromatogr. A* **2008**, *1213*, 45-49.

24. Shaw, M. J.; Hill, S. H.; Jones, P.; Nesterenko, P.N. High-performance chelation ion chrmatography of transition and heavy metal ions on polystyrene-divinlbenzene resin dynamically modified with 4- chlorodipicolinic acid. *Anal. Commun.* **1999**, *36*, 399-401.

25. Shaw, M. J.; Hill, S. J.; Jones, P.; Nesterenko, P. N. Determination of uranium in environmetal matrices by chelation ion chromatography using a high performace sustrate dynamically modified with 2,6-pyridinedicarboxylic acid. *Chromatographia* **2000**, *51*, 695-700.

26. Cowan, J.; Shaw, M. J.; Achterberg, E. P.; Jones, P.; Nesterenko, P. N. The ion chromatographic separation of high valence metal cations using neutral polystyrene resin dynamically modified with dipicolinic acid. *Analyst* **2000**, *125*, 2157-2159.

27. Shaw, M. J.; Hill, S. J.; Jones, P. Chelation ion chromatography of metal ions using high performace substrates dynamically modified with heterocyclic carboxylic acids. *Anal. Chim. Acta* **1999**, *401*, 65-71.

28. Merly, C.; Lynch, B.; Ross, P.; Clennon, J. D. Selective ion chromatography of metals on porous graphitic carbon. *J. Chromatogr. A* **1998**, *804*, 187-192.

29. Abas, M. R. B.; Takruni, I. A.; Abdullah, Z.; Tahir, N. M. On-line preconcentration and determination of trace metals using a flow injection system coupled to ion chromatography. *Talanta* **2002**, *58*, 883-890.

Chapter 5 Transition Metal Cation Separations with a Resorcinarene-based Amino Acid Stationary Phase

Abstract[5]

A resorcinarene-based macrocyclic ligand functionalized with alanine and undecyl groups (AUA) was synthesized and applied to ion chromatographic separations. The selectivity and separation of transition metal ions on a column packed with AUA adsorbed onto 55% cross-linked styrene-divinylbenzene resin are presented. The upper and lower rims of the resorcinarene were modified with amino acids and $–C_{11}H_{23}$ alkyl chains, respectively. The four carboxylic acid groups on the upper rim act as cation-exchangers while the four $–C_{11}H_{23}$ alkyl chains serve to anchor the ligand to the resin surface by the hydrophobic effect. A systematic study of the effect of different eluent components including non-metal-chelating (HNO_3) and chelating acids (oxalic acid, succinic acid, dipicolinic acid, and citric acid) on the retention of transition metal ions was investigated. Six metal ions (Mn^{2+}, Co^{2+}, Ni^{2+}, Cd^{2+}, Cu^{2+}, and Zn^{2+}) were separated on the AUA column within a reasonable time with a single eluent gradient using oxalic acid. The separation is compared to that obtained using a commercial column containing carboxylic acid functional groups. The AUA column containing four preorganized carboxylic acid groups showed selectivity for Cu^{2+} when no chelating eluent was present, a selectivity which was not observed with the comparison column.

[5]This research has been published.

Li, N.; Allen, L. J.; Harrison, R. G.; Lamb, J. D. *Analyst* **2013**, *138*, 1467-1474.

1. Introduction

The separation efficiency and selectivity of an ion chromatography (IC) column are determined by three main factors: the nature of the ion-exchanger, the stationary phase matrix, and the nature of the mobile phase. Specific factors contributing to the separation effectiveness of an IC packed column include the chemical nature of the stationary phase substrate (polymer-based or silica-based), the particle size, the mechanical stability of the stationary phase particles, the tolerance of the stationary phase to extreme pH values, and the length and width of the column.[1,2] Along with the mobile phase, the properties of ion-exchangers play a fundamental and essential role in determining the selectivity of an IC system.

Several aspects should be considered when designing selective ion-exchangers. Interactions between the analyte and ion-exchangers provide the basis for the separation and include factors such as electrostatic attraction, metal coordination, and hydrophobic interaction. These interactions should be of intermediate strength; otherwise the analyte is not eluted except under harsh chemical conditions. In other words, the temporary association of analyte to ion-exchanger should be thermodynamically stable but kinetically labile to allow analyte elution and rapid separation. Designing selective anion-exchangers is more difficult than for cations due largely to the complexity of polyatomic anion geometry and the smaller charge to radius ratio of anions in general and polyatomic anions in particular.[3,4] Sarzanini et al.[5] proposed that selective weak cation-exchangers with carboxylic acid or phosphonic groups are preferable to sulfonic cation-exchangers to avoid both long analysis time and the use of concentrated acidic eluents that

are usually associated with sulfonic cation-exchangers. In addition, when designing ion-exchangers for transition metal ion separations, the ideal ion-exchanger should complex transition metal ions with distinct stability constants so that complete resolution can be obtained.[6]

Zwitterions[7-11] form a promising class of ion-exchangers that can provide multiple retention mechanisms. Recent developments of zwitterions as ion-exchangers in ion chromatography have been reviewed.[7] Five main groups of stationary phases based on zwitterions were summarized and several unique properties of these stationary phases were presented, including simultaneous separation of cationic and anionic species, unusual selectivity, increasing separation efficiency, and lower background conductance. One of the five main classes of stationary phases based on zwitterions consists of amphoteric amino acids covalently bonded to a substrate such as silica. In one study, a series of amino acids including Asp, Glu, Val, Tyr, Pro, Hypro, Arg and Lys were immobilized on a silica surface and were used to separate cations. The ion exchange properties of amino acid-bonded silicas are controlled by the pH of the eluent and the specific structure of the amino acid.[8] More recently, lysine was covalently attached to a 0.46×10.0 cm silica monolithic column.[9] The flow rate applied on the monolithic column can reach 5 mL/min so that fast separation of six anions was achieved in 2 minutes, including nitrite, bromate, bromide, nitrate, iodide, and thiocyanate.

Although various methods are available for transition metal ion analysis including titrimetry, gravimetric analysis, and amperometric titration, these methods have limited sensitivity and are time-consuming. Spectroscopic methods, including atomic absorption spectroscopy (AAS), inductively coupled plasma – atomic emission spectrometry (ICP-AES) are

more commonly used. However, these methods also suffer from spectral and chemical interferences, especially when the analysis of trace amount of transition metal ions in the presence of large amount of matrix ions is required. Ion chromatography offers a proven alternative for metal ion analysis.

Macrocyclic ligands such as 18-crown-6,[12-13] cryptand,[14]and cyclodextrin[15] have been incorporated into stationary phases for chromatographic separations since the early days. We continue to design and explore the application of selective macrocyclic ligands for transition metal ion analysis in ion chromatography. Our current ligand design strategy is based on one class of macrocyclic ligand, the resorcinarenes.[16-17] Resorcinarenes are cyclic tetramers synthesized from the condensation of resorcinol and various aldehydes. The lower rim of the resorcinarene can be modified with four $–C_{11}H_{23}$ alkyl chains used to anchor the molecule on the surface of a polystyrene-divinylbenzene resin by the hydrophobic effect; concurrently, the upper rim can be modified with different functional groups to provide specific selectivity for anions, cations, and small organic molecules.[18,19]

In this work, we have modified the upper rim of the resorcinarene with four chiral alanine derivatives. The resulting AUA ligand (abbreviated from alanine undecyl acid resorcinarene) thus has four carboxylic acid groups on its upper rim (shown in Figure 5.1). Carboxylic acid groups are commonly used cation-exchangers, but in our design structure, four carboxylic acid groups are in proximity to each other and may potentially enhance the interactions between cations and AUA. In addition, the cyclic structure of this molecule may generate stereoselectivity towards substrate molecules, as we will pursue in future work.

We have focused on metal cation separations and specifically report the separation of six transition metal ions: Mn^{2+}, Co^{2+}, Ni^{2+}, Cd^{2+}, Zn^{2+}, and Cu^{2+} with the AUA column. The effects of four chelating eluents: oxalic acid, succinic acid, citric acid, and dipicolinic acid (PDCA) on the retention of transition metal ions are discussed. For comparison, separation of the same transition metal ions was performed on the commercial Ionpac CS12 column from Thermo Scientific – Dionex.[20,21] The Ionpac CS12 column contains only carboxylic acid ion-exchangers and was originally designed for alkali and alkaline earth metal ion separations. We have learned, however, that it can be effective for the separation of transition metal ions. The elution orders of transition metal ions are compared and discussed with the non-chelating eluent (HNO_3) and with the chelating eluents.

2. Experimental

2.1 Reagents

All reagents used, including nitrate salts of transition metal cations, were trace metal grade unless specified. Trace metal grade nitric acid and ammonium hydroxide were obtained from Fisher (Pittsburgh, PA). Other trace metal grade cations and dipicolinic acid solution (20 mM, 1 mL) were obtained from Sigma-Aldrich (Milwaukee, WI). All eluents and standards were prepared using Milli-Q water of 18 megaohm/cm resistivity. MetPac oxalic acid eluent concentrate was obtained from Thermo Scientific - Dionex Corporation. Post column reagents for vis detection used in the studies were 0.5 mM 4-(2-pyridylazo)resorcinol (PAR), 1.0 M 2-dimethylaminoethanol, 0.50 M ammonium hydroxide, and 0.30 M sodium bicarbonate.[22] A PC10

post-column pneumatic delivery system was used to pump post-column reagent PAR at a flow rate of 0.2 mL/min.

2.2 The pKa value of the AUA ligand

The p*K*a value of AUA was determined by pH titration with a combination glass membrance/SCE electrode pair that were pH calibrated with buffer solutions before each titration. Equivalence points were determined by finding the maximum slope in the pH titration curves. A mixed solution of methanol and water (v:v 1:1, 10 mL each) was used to dissolve AUA (16.1 mg) because of the poor solubility of AUA in water. A NaOH solution (3.60 ± 0.02 mM) which was calibrated three times with a standard potassium hydrogen phthalate (KHP) solution was used to titrate the AUA solution. The titration of AUA yielded equivalence points of 1.233, 1.226, and 1.226 mL of the NaOH solution. This yielded a concentration of acid 4.50 ± 0.04 mM at the 95% confidence level. The pH values of the half equivalence points were found to be 5.15, 5.22, and 5.20 which resulted in the pK_a of AUA 5.19 ± 0.08 at the 95% confidence level. Only one equivalence point was observed from the titration curve.

2.3 Synthesis and column preparation

The ligand AUA was synthesized according to the methods published by our group.[23] The column was prepared by the standard method reported previously.[16] Briefly, 115 mg of AUA was dissolved in methanol and mixed with 1.5 g of resin. The slurry of the coated resin was used to pack a 4×150 mm black PEEK column. The column was packed at 60 ^{o}C and 5000 psi for 15 minutes. The 55% cross-linked styrene-divinylbenzene polymeric macroporous resin was

provided by Thermo Scientific - Dionex Corporation (Sunnyvale, CA). The particle size of the resin was 5 μm. The average pore size and the surface area of the resin were 100-150 Å and 350 m^2/g, respectively. A commercially available Ionpac CS12 (4×250 mm) column was obtained from Thermo Scientific - Dionex Corporation.

2.4 Instrumentation

A Dionex ICS-3000 system with an AS40 autosampler and a PDA-100 photodiode array detector was used throughout this study. A Dionex Chromeleon 6.8 workstation was used for data collection and analysis. The eluted peaks were recorded by dual wavelength[24] at 520 nm and 620 nm and simple arithmetic manipulation (520 - 620 nm) was applied using Chromeleon software to minimize baseline noise.

3. Results and discussion

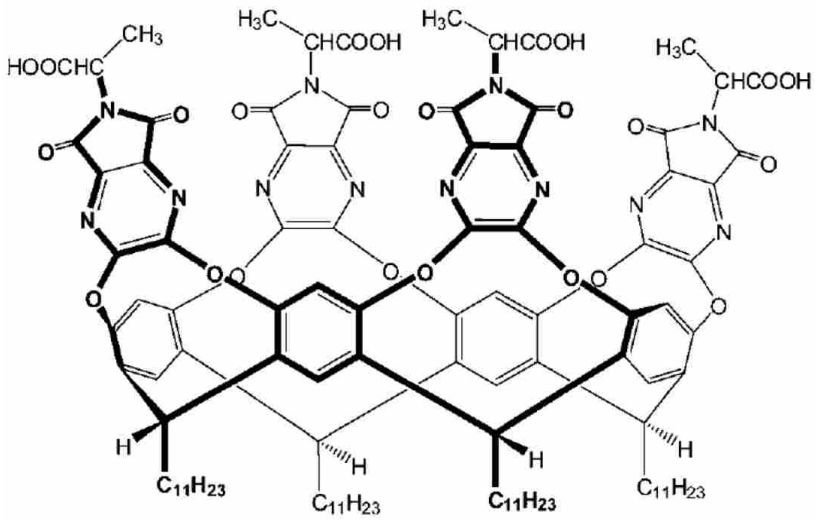

Figure 5.1 Structure of AUA.

3.1 Separation of transition metal ions with the AUA column

Table 5.1 Protonation constants (log *K*) of acids and stability constants (log *K'*) of oxalic acid, PDCA, succinic acid and citric acid complexes with metal cations.[25,26]

	Oxalic acid	PDCA	Succinic acid	Citric acid
H^{+} [a]	$\log K_1$=3.82±0.04[b]	$\log K_1$=4.68[d]	$\log K_1$=5.24±0.04 [b]	$\log K_1$=5.69±0.05[b]
	$\log K_2$=1.04±0.10[b]	$\log K_2$=2.10[d]	$\log K_2$=4.00±0.02 [b]	$\log K_2$=4.35±0.05[b]
				$\log K_3$=2.87±0.08[b]
Mn^{2+}	3.95[c]	5.01[d]	1.48[e]	4.15[g]
Co^{2+}	4.72[c]	6.65[d]	1.70[d]	5.00[d]
Ni^{2+}	5.16[c]	6.95[d]	1.6[b]	5.40[d]
Cd^{2+}	3.89[c]	6.75[d]	1.67[f]	3.75[d]
Zn^{2+}	4.87[c]	6.35[d]	1.76[d]	4.98[d]
Cu^{2+}	6.23[c]	9.14[d]	2.26[e]	5.9[d]

[a] for binary acids: $K_1 = [HA^-]/[A^{2-}][H^+]$, $K_2 = [H_2A]/[HA^-][H^+]$;

for citric acid: $K_1 = [HA^{2-}]/[A^{3-}][H^+]$, $K_2 = [H_2A^-]/[HA^{2-}][H^+]$, $K_3 = [H_3A]/[H_2A^-][H^+]$;

$K' = [ML]/[M]\cdot[L]$ (M: metal ion, L: ligand).

[b] T = 25.0 °C, I = 0.1; [c] T = 25.0 °C, I = 0; [d] T = 20.0 °C, I = 0.1; [e] T = 25.0 °C, I = 0.2;

[f] T = 20.0 °C, I = 1.0; [g] T = 25.0 °C, $(CH_3)_4N^+$ was used as background electrolyte.

3.1.1 Effect of HNO_3 concentration

In separating the six transition metal cations on the AUA column, HNO_3 was first used as eluent. Competition for binding to the carboxylic acid groups of AUA between eluent hydronium

ions and transition metal ions provides the basis for the chromatographic separation. The six transition metal ions included Mn^{2+}, Co^{2+}, Ni^{2+}, Cd^{2+}, Zn^{2+} and Cu^{2+}, while 1, 2, 5, 10, 15, 20, 30 and 50 mM HNO_3 were used as eluents in separate isocratic runs. No peak appeared within 30 min when using 1 and 2 mM HNO3, while a single peak appeared at 12.1 min when 5 mM HNO3 was used as eluent. Spiking experiments showed that this represented a coelution peak of Mn^{2+}, Co^{2+}, Ni^{2+}, Cd^{2+}, and Zn^{2+}, while Cu^{2+} was still retained on the column. When the HNO_3 concentration was increased to 10 mM, the retention time of the first five cations was reduced to 9.9 min, and Cu^{2+} was eluted as a broad peak at 27.8 min. When 30 mM HNO_3 was used, Cu^{2+} was well separated from the other five ions (coeluted at 9.3 min) with a retention time of 11.3 min. The resolution between the two peaks was 1.56. These results indicate that the AUA column shows selectivity for Cu^{2+} over the other five cations when HNO_3 is used as eluent. Figure 5.2(a) shows the change of retention factor with the HNO_3 concentration.

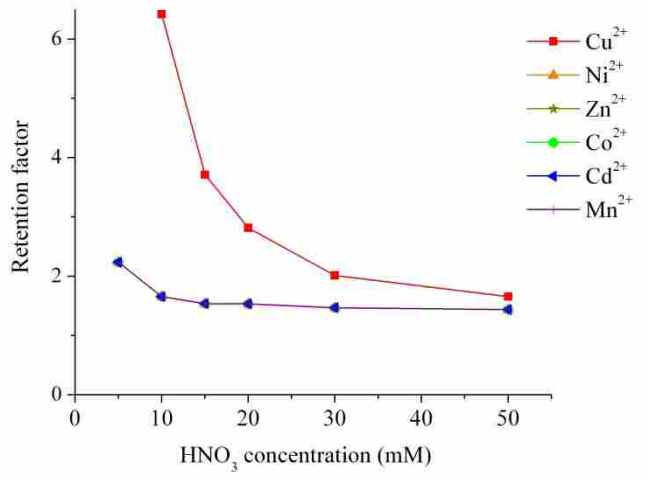
Retention factor
HNO3 concentration (mM)
Cu2+
Ni2+
Zn2+
Co2+
Cd2+
Mn2+

(b) **(c)**

(a)

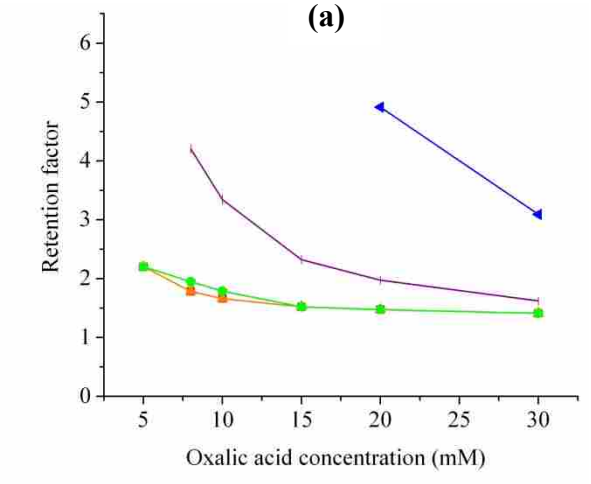
Retention factor
Oxalic acid concentration (mM)

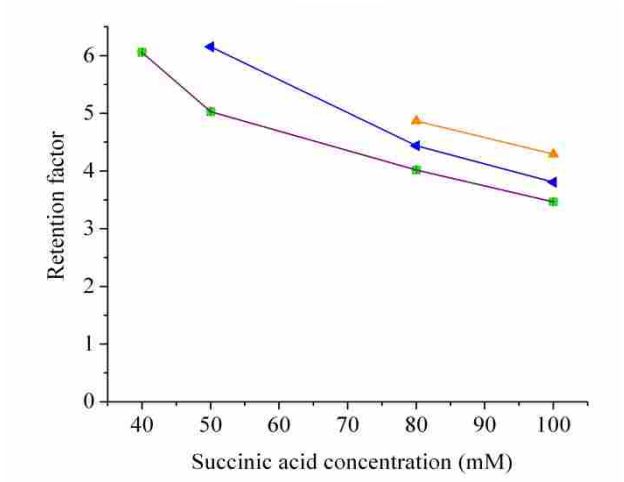
Retention factor
Succinic acid concentration (mM)

(d) **(e)**

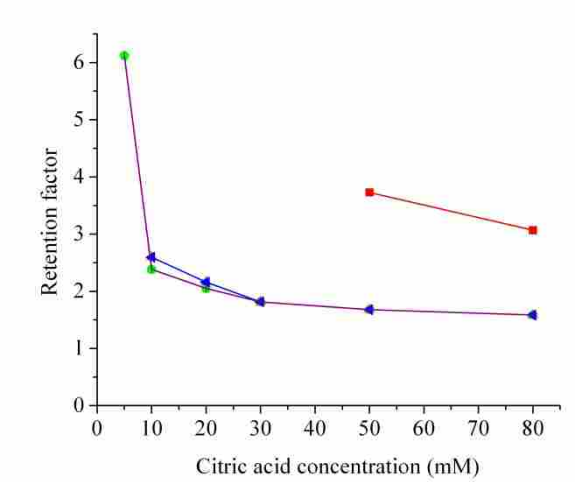
Retention factor
Citric acid concentration (mM)

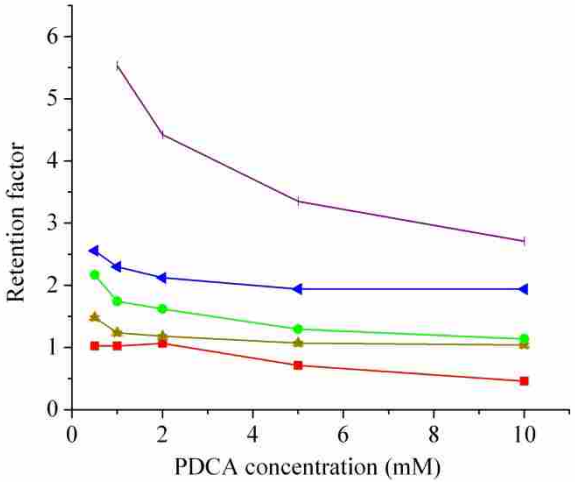
Retention factor
PDCA concentration (mM)

Figure 5.2 The retention factor change of each metal ion with eluent concentrations on the AUA column. (a) Eluent: HNO_3; Ni^{2+}, Zn^{2+}, Co^{2+}, Mn^{2+}, and Cd^{2+} coeluted (bottom curve); (b) Eluent: oxalic acid; Cu^{2+} and Ni^{2+} coeluted, Zn^{2+} and Co^{2+} coeluted; (c) Eluent: succinic acid; Cu^{2+}, Zn^{2+}, Co^{2+}, Mn^{2+} coeluted after 15 mM oxalic acid was used as eluent; (d) Eluent: citric acid; Zn^{2+}, Co^{2+}, Ni^{2+}, Cd^{2+}, and Mn^{2+} coeluted when more than 30 mM citric acid was used as eluent. When 5, 10 and 20 mM citric acid was used as eluents, the retention factors are slightly different. (e) Eluent: PDCA; Ni^{2+} and Zn^{2+} coeluted.

3.1.2 Effect of chelating ligand – oxalic acid in the eluent

The above results indicate that while good separation of Cu^{2+} from the other ions can be achieved, use of HNO_3 alone cannot separate Mn^{2+}, Co^{2+}, Ni^{2+}, Cd^{2+}, and Zn^{2+}. Adding chelating ligands to the mobile phase is a commonly used approach to achieve good separation of transition metal ions.[17] The chelating ligand in the mobile phase coordinates with analyte ions, increasing the partitioning of metal ions into the mobile phase. As a result, retention time is reduced. Meanwhile, differences between the thermodynamic stabilities of the resulting complexes result in more distinct separation of the ions.

We first chose to use oxalic acid as a chelating eluent. Isocratic elution of six metal ions with 1, 2, 5, 8, 10, 15, 20, and 30 mM oxalic acid only (pH = 2.96 ~ 1.62) was performed. No peaks appeared when 1 and 2 mM oxalic acid were used as eluents. When 5 mM oxalic acid was used, a broad peak appeared around 12 min. Spiking experiments confirmed that this peak was a mixture of Cu^{2+}, Ni^{2+}, Co^{2+}, and Zn^{2+}, while Mn^{2+} and Cd^{2+} were not eluted. Mn^{2+} was eluted when the oxalic acid concentration was increased to 8 mM, while Cd^{2+} eluted at 20 mM. At this latter eluent concentration, Cu^{2+}, Ni^{2+}, Co^{2+}, and Zn^{2+} coeluted at 9.3 min, while Mn^{2+} and Cd^{2+}

eluted at 11.2 and 22.2 min, respectively. The retention factor change with oxalic acid concentration of each metal cation is shown in Figure 5.2(b).

We found that flushing the chromatographic column with eluent before the injection of analytes greatly affects the separation results. As noted above, no peaks appeared when using 1, 1.5 and 2 mM oxalic acid eluents. However, when we equilibrated the AUA column with 10 mM HNO_3 for 10 minutes and then injected the analytes using 1.5 mM oxalic acid as eluent, the four metal cations including Cu^{2+}, Co^{2+}, Ni^{2+}, and Zn^{2+} were eluted within 30 minutes. Mn^{2+} and Cd^{2+} were eluted when 15 mM oxalic acid was applied (Figure 5.3). Before injecting analyte, the AUA column was washed with 10 mM HNO_3 for 10 minutes; next, 1.5 mM oxalic acid was used for 24 min to separate Cu^{2+}, Ni^{2+}, Co^{2+}, and Zn^{2+}; finally, a step eluent change to 15 mM oxalic acid eluted Mn^{2+} and Cd^{2+}. Baseline separations were obtained for most of the metal ions, except for Ni^{2+} and Zn^{2+} where the resolution was 1.47. The elution order of transition metal ions in this case is $Cu^{2+} > Ni^{2+} > Co^{2+} > Zn^{2+} > Mn^{2+} > Cd^{2+}$, which is consistent with the stability constants of the formed complexes of metal ions with oxalic acid (see Table 5.1).[23] The most strongly bound Cu^{2+} ion was eluted first, while the weakest, Cd^{2+}, was eluted last. The detection limit and the sensitivity in this system are calculated from the calibration curve and shown in Table 5.2. Sensitivity is the slope of the calibration curve. Detection limit is three times the standard deviation of the response divided by the slope of the calibration curve. The system shows the highest detection sensitivity for Mn^{2+}. The detection sensitivity of Cu^{2+}, Cd^{2+}, and Zn^{2+} are similar, while the detection sensitivities of Ni^{2+} and Co^{2+} are lower.

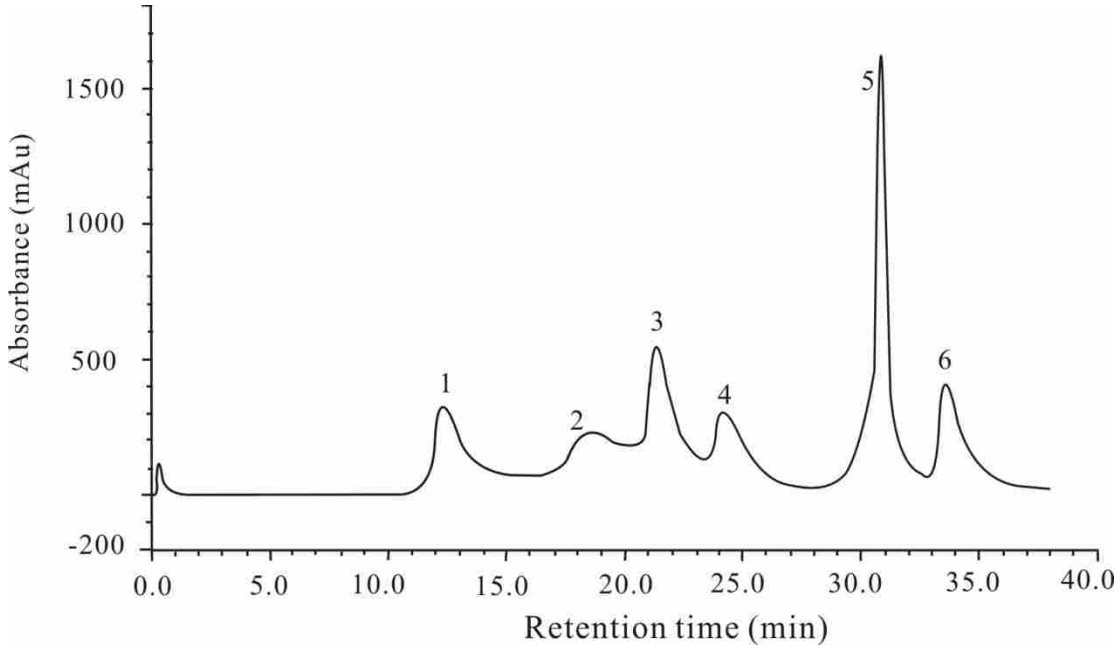

Figure 5.3 Separation of six transition metal ions with oxalic acid gradient on AUA column. Conditions: 10 mM HNO_3 for 10 minutes before injecting analyte, after injection, 0-24 min, 1.5 mM oxalic acid; 24-40 min, 15 mM oxalic acid. Peaks: 1 = Cu^{2+} (1.28 ppm); 2 = Ni^{2+} (1.28 ppm); 3 = Zn^{2+} (1.28 ppm); 4 = Co^{2+} (1.28 ppm); 5 = Mn^{2+} (0.32 ppm); 6 = Cd^{2+} (1.28 ppm).

Table 5.2 Detection limit and sensitivity of metal ions using the oxalic acid gradient

	Sensitivity ($mAu \cdot min \cdot ppm^{-1}$)	Detection limit (ppm)	Correlation coefficient (5 replicates)
Mn^{2+}	3020	0.0299	0.9958
Cd^{2+}	331	0.128	0.9952
Co^{2+}	197	0.0694	0.9986
Zn^{2+}	322	0.151	0.9933
Ni^{2+}	121	0.0845	0.9979
Cu^{2+}	356	0.0493	0.9993

3.1.3 Effect of chelating ligand – succinic acid in the eluent

To better understand the effect of chelating ligands on the retention of transition metal ions on the AUA column, another chelating ligand, succinic acid, was used in the eluent. Succinic acid contains two carboxylic acid groups, similar to oxalic acid, but separated by a longer alkyl chain and having weaker acidity (See Table 5.1). 5, 10, 20, 30, 40, 50, 80, and 100 mM succinic acid (pH = 3.18 ~ 2.50) were used as eluents. No peak appeared within 30 min when 30 mM or less succinic acid (pH = 2.77 or greater) was present. At this pH, both H_2A and HA^- ($A = C_4H_4O_4^{2-}$) ions exist in solution; however, the concentration fraction of H_2A (94.4%) is much higher than that of HA^- (5.6%). As the concentration of succinic acid increased, the fraction of HA^- decreased in the solution. When 40 mM succinic acid was used as eluent, a broad peak appeared at 26.5 min. When concentrated succinic acid (100 mM) was used, three peaks appeared with low resolution. The resolutions between adjacent peaks were 0.89 and 1.46, respectively. The retention factor change of each metal cation with succinic acid concentration is shown in Figure 5.2(c). Spiking experiments using 100 mM succinic acid as eluent showed the elution order was Cu^{2+}, Zn^{2+}, and Co^{2+} > Mn^{2+} and Cd^{2+} > Ni^{2+}.

Succinic acid is a weaker acid than oxalic acid. In the succinic acid pH range we used (3.18~2.50), both H_2A and HA^- ($A = C_4H_4O_4^{2-}$) ions exist in the solution, but most of the acid remained in the H_2A form (fraction of H_2A > 87%) while the fraction of HA^- was < 13%. By comparison, for the oxalic acid (from 1 to 30 mM, pH = 2.96 ~ 1.62), the fraction of HA^- is much higher (higher than 79%) than the fraction of H_2A (lower than 21%). The more HA^- ions that are present in the mobile phase, the stronger the interaction of eluent with transition metal

ions; and consequently, the shorter the retention time. Compared with oxalic acid, most succinic acid molecules exist in the H_2A form in the respective eluent pH ranges that we used, while oxalic acid exists primarily in the deprotonated form in its eluent pH range. Thus higher succinic acid concentrations are needed (higher than 40 mM) to elute the cations, compared to lower concentration of oxalic acid (higher than 15 mM).

3.1.4 Effect of chelating ligand – citric acid in the eluent

We also tested citric acid, a ternary acid, as the mobile phase component. 5, 10, 20, 30, 50, and 80 mM citric acid solutions were used as eluent for 30 min in separate isocratic runs. The changes in retention factor for each metal cation with citric acid concentration are shown in Figure 5.2(d). A broad peak appeared at 26.8 min when 5 mM of citric acid was used. Two peaks appeared at 16.8 and 19.0 min when 10 mM citric acid was applied. Spiking experiments showed that the first peak was the coelution of Mn^{2+}, Co^{2+}, and Zn^{2+} and the second peak at 19.0 min was the coelution of Cd^{2+} and Ni^{2+}. When the citric acid concentration was increased to 30 mM, these two peaks merged. Cu^{2+} was not eluted until the concentration of citric acid was increased to 50 mM. A citric acid eluent gradient of 10 mM citric acid for 24 minutes followed by 80 mM citric acid for 20 minutes was applied to elute all six transition metal ions. The elution order of six transition metal ions in this case is: Mn^{2+}, Co^{2+}, and Zn^{2+} > Cd^{2+} and Ni^{2+} > Cu^{2+}.

3.1.5 Effect of chelating ligand – dipicolinic acid (PDCA) in the eluent

PDCA is a commonly used mobile phase component in ion chromatography for transition metal ion separations.[22] The differences in thermodynamic stability of the coordination complexes formed between transition metal ions and PDCA provide the basis for the separation.

0.5, 1, 2, 5, and 10 mM PDCA solutions were used as eluent with the column. Using 0.5 mM PDCA as eluent, five cations, Co^{2+}, Zn^{2+}, Cd^{2+}, Ni^{2+}, and Cu^{2+}, were eluted in 30 minutes and Mn^{2+} was retained on the column. Mn^{2+} wasn't eluted until the PDCA concentration was higher than 1 mM. The retention factor change of each metal cation with PDCA concentration is shown in Figure 5.2(e). When 1 mM PDCA was used as eluent, the elution order was: $Cu^{2+} > Zn^{2+}$, $Ni^{2+} > Co^{2+} > Cd^{2+} > Mn^{2+}$. This is in the reverse order to the stability constants of transition metal ions with PDCA. The most strongly bonded ion, Cu^{2+}, was eluted first while the weakest bonded ion Mn^{2+} was eluted last.

The selectivity of the AUA column can be explained by pH and metal ion binding for the ligands. A p*K*a comparison between AUA and the acid eluent components helps explain the pH effect. The pKa value of AUA was determined as 5.19 ± 0.08 by pH titration. In the separation process, the transition metal ions become associated with AUA ligands by exchanging with the carboxylic acid protons. Acidic eluents provide protons that exchange with the transition metal ions on the column sites. The greater the concentration of protons provided in the mobile phase, the more the chemical equilibrium shifts to favor the elution of transition metal ions. In order of acidity, the five eluent acids used are: HNO_3 > oxalic acid > PDCA > citric acid > succinic acid. Thus higher concentrations of succinic acid were needed (up to 40 mM) for the cation elution,while 5 mM of the other four acids was sufficient to elute most of the transition metal ions. The elution order of transition metal ions on the AUA column was closely related to the thermodynamic stabilities of the complexes formed between these ions and the chelating ligands in the mobile phase. When oxalic acid and PDCA were used as eluents, the elution orders of

transition metal ions were reversed relative to the stability constants with the acids. The longer alkyl chains between the two carboxylic acid groups of succinic acid and citric acid render them inferior chelating ligands to oxalic acid and PDCA. Besides the weaker chelating ability of citric acid and succinic acid, they have similar acidity to that of the AUA ligand, causing the irregular elution order of transition metal ions when these two acids were used.

3.2 Separation of transition metal ions with the IonPac CS12 column

AUA was designed to preorganize four carboxylic groups on the upper rim of the resorcinarene scaffold in order to improve selectivity and enhance recognition between this macrocyclic ligand and cations. To understand the effect of this structural feature on cation selectivity, a commercially available cation-exchange column, IonPac CS12, was tested for comparison. The CS12 column employs carboxylic acid exchange sites. HNO_3, oxalic acid, and PDCA were used as eluents with this column.

3.2.1 Effect of HNO_3 concentration with Ionpac CS12 column

HNO_3 solutions at 10, 20, 30, 40 and 50 mM were used as eluents with the CS12 column to separate the six transition metal cations. When 10 mM HNO_3 was used, no peak appeared in 30 minutes. Three peaks appeared at 30.1, 32.0, and 38.9 minutes when 20 mM HNO_3 was used (see Figure 5.4a). The retention times of these three peaks decreased when higher HNO_3 concentrations (30 and 40 mM) were applied. The effect of HNO_3 concentration on the retention factor of each metal ion is shown in Figure 5.4(a). The elution order of transition metal ions using 30 mM HNO_3 as eluent was $Mn^{2+} > Cu^{2+}$, Ni^{2+}, Co^{2+}, $Zn^{2+} > Cd^{2+}$.

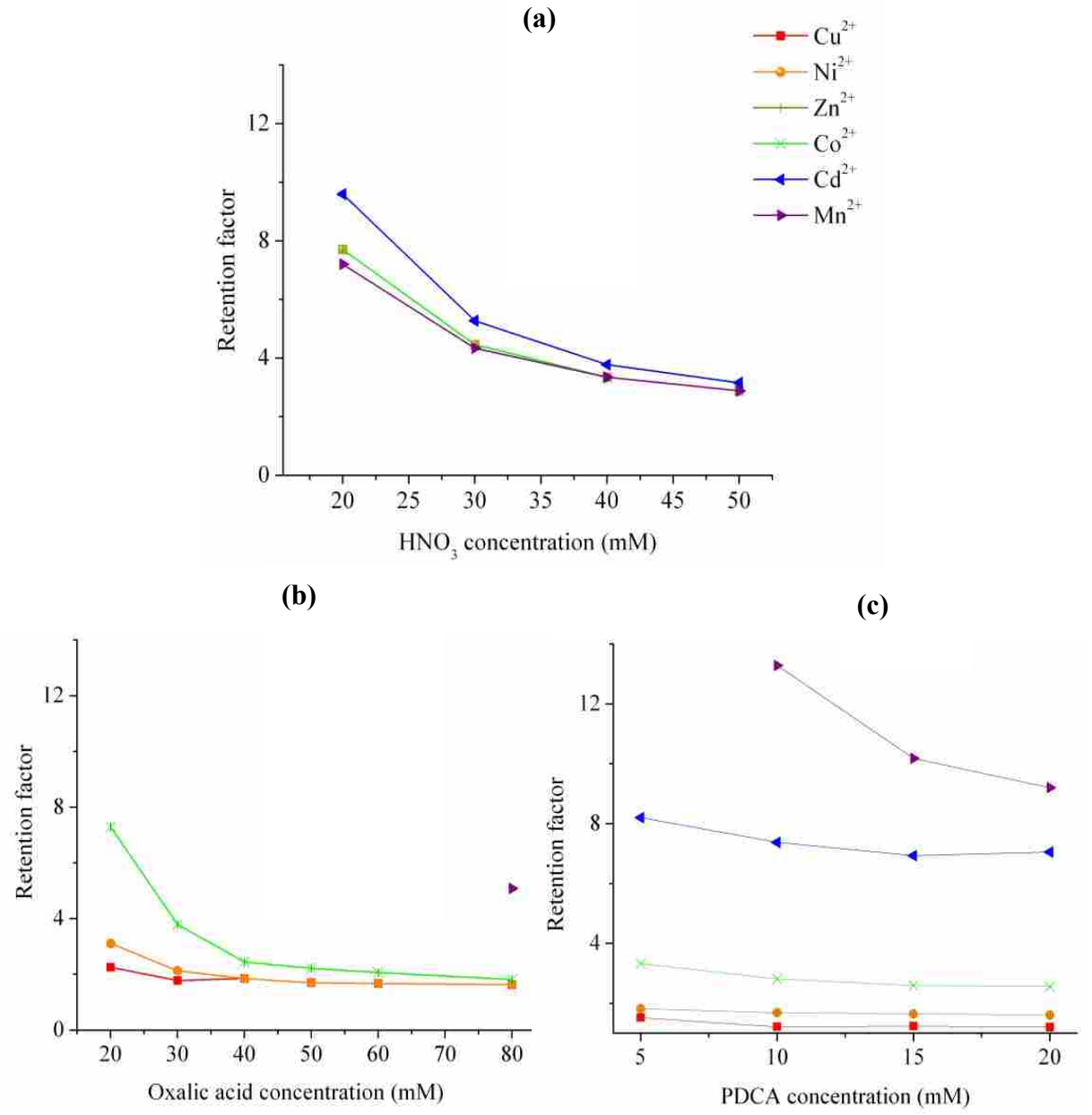

Figure 5.4 Retention factor change of each metal ion with eluent concentrations on the Ionpac CS12 column. (a) Eluent: HNO_3; Ni^{2+}, Zn^{2+}, Cu^{2+}, and Co^{2+} coeluted after higher than 30 mM HNO_3 was used. (b) Eluent: oxalic acid; Zn^{2+} and Co^{2+} coeluted; Ni^{2+} and Cu^{2+} coeluted after 40 mM oxalic acid was applied, Mn^{2+} was eluted when 80 mM oxalic acid was applied. Cd^{2+} was not eluted in the eluent

concentration range used. (c) Eluent: PDCA; Ni^{2+} and Zn^{2+} coeluted.

3.2.2 Effect of chelating ligand – oxalic acid in the eluent

Oxalic acid solutions at 10, 20, 30, 40, 50, 60, and 80 mM were used as eluent with the Ionpac CS12 column. 10 mM oxalic acid did not elute any of the six transition metal ions. Mn^{2+} did not elute until 80 mM oxalic acid was applied. Under this condition, Cd^{2+} was still retained on the column. The other four transition metal ions including Cu^{2+}, Co^{2+}, Ni^{2+}, and Zn^{2+} were well eluted when 20 mM oxalic acid was used. The oxalic acid concentration effect on the retention factor of each metal ion is shown in Figure 5.4(b). A step gradient elution using 20 mM oxalic acid for 25 min and then step eluent change to 10 mM PDCA were applied to separate the transition metal ions. The elution order was: $Cu^{2+} > Ni^{2+} > Zn^{2+}$, $Co^{2+} > Mn^{2+} > Cd^{2+}$.

3.2.3 Effect of chelating ligand – dipicolinic acid (PDCA) in the eluent

Dipicolinic acid solutions at 5, 10, 15, and 20 mM were used as eluent. The effect of PDCA concentration on the retention factor of each transition metal ions is shown in Figure 5.4(c). When 5 mM PDCA was used, Cu^{2+}, Ni^{2+}, Zn^{2+}, Co^{2+}, and Cd^{2+} were eluted within 60 minutes, but Mn^{2+} remained on the column. 10 mM PDCA eluted all six transition metal ions in 60 minutes. The elution order was the reverse of the stability constant, namely $Cu^{2+} > Ni^{2+}$, $Zn^{2+} > Co^{2+} > Cd^{2+} > Mn^{2+}$.

As we observed with the AUA column, we found that equilibrating the Ionpac CS12 column after each run with eluents before injecting analyte greatly affected the separation results. In Figure 5.5(a), we see the result of flowing 10 mM PDCA for 10 minutes before analyte injection using 10 mM PDCA as eluent. The elution order is $Cu^{2+} > Ni^{2+}$, $Zn^{2+} > Co^{2+} > Cd^{2+} >$

Mn^{2+}. Figure 5.5(b) shows the result when 20 mM oxalic acid flows through the column for 10 minutes before injection. After injection, 10 mM PDCA was used as eluent. The elution order of the six metal cations was the same as that in Figure 5.5(a). However, the retention time of Cd^{2+} was greatly reduced from 52 to 22 minutes as shown in Figure 5.5(b). When the column was pre-equilibrated with different concentrations of oxalic acid, higher oxalic concentration led to shorter retention times of Mn^{2+} and Cd^{2+}.

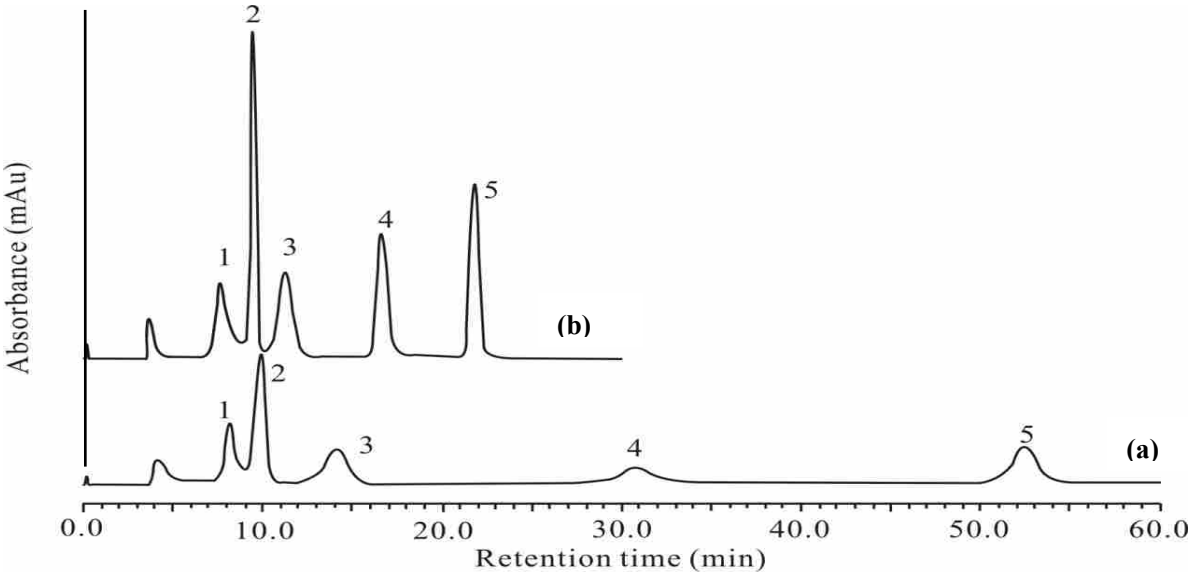

Figure 5.5 Separation of six transition metal ions on the Ionpac CS12 column under different conditions. Eluent conditions: (a) 10 mM PDCA for 10 minutes before injection of transition metal ions followed by 10 mM PDCA; (b) 20 mM oxalic acid for 10 minutes before sample injection followed by 10 mM PDCA. Peaks: 1 = Cu^{2+} (1.0 ppm); 2 = Ni^{2+} (1.0 ppm) and Zn^{2+} (1.0 ppm); 3 = Co^{2+} (1.0 ppm); 4 = Mn^{2+} (0.2 ppm); 5 = Cd^{2+} (1.0 ppm).

Table 5.3 summarizes the elution order of six transition metal ions on the AUA and Ionpac CS12 columns with different eluents. The pH of the eluent is a key parameter that

controls the cation-exchange properties of our amino acid-modified resorcinarene-based ligand (AUA) and also the Ionpac CS12 column. Adjusting the pH value of the columns before injecting the analyte using a mixed mode acid step gradient greatly affects the separation behavior of the AUA column and the Ionpac CS12 column. A simple oxalic acid gradient can separate the six metal ions effectively in a reasonable time on the AUA column when preceeded by isocratic 10 mM HNO_3 for 10 minutes; in contrast, the separation of six metal ions on the Ionpac CS12 column was achieved within a much shorter time when the same mixed mode acid step was performed using oxalic acid rather than nitric acid before injecting the sample. Yet Ni^{2+} and Zn^{2+} showed much better resolution (1.47) on the AUA column than on the Ionpac CS12 column in which the two ions coeluted. When chelating eluents are used on both columns, the thermodynamic stability differences between the complexes formed between chelating ligands and transition metals result in better ion resolution. Succinic acid and citric acid contain one more carbon than oxalic acid, resulting in a longer distance between the two coordination sites and a weaker chelation effect. When the stronger chelating ligands oxalic acid and PDCA were used as eluents, the elution orders were reversed compared to the stability constants in both columns. The transition metal ion elution order was similar on the Ionpac CS12 column when PDCA was used as eluent.

When the nonchelating acid HNO_3 was used as eluent, the transition metal ions Cu^{2+}, Zn^{2+}, Ni^{2+}, and Co^{2+} coeluted on the Ionpac CS12 column while Cd^{2+} was eluted last (Figure 5.4a). On the silica-based column used by the Sarzanini group, when nonchelating eluent methanesulfonic acid (MSA) was used as eluent, Cd^{2+} was also eluted much later than Cu^{2+}, Ni^{2+},

and Zn^{2+}.[5] The smaller charge to radius ratio and corresponding weaker electrostatic attraction with the anions in the eluent explain the later elution of Cd^{2+}. However, when HNO_3 was used, the AUA column showed selectivity for Cu^{2+} while the other five ions Co^{2+}, Ni^{2+}, Mn^{2+}, Cd^{2+}, and Zn^{2+} coeluted. The AUA structure providing four carboxylic acid groups preorganized on the upper rim of the resorcinarene provides the selectivity for Cu^{2+} when the non-complexing HNO_3 eluent was used. This Cu^{2+} selectivity was neither observed with the Ionpac CS12 column nor with Sarzanini's silica-based column.[5]

Table 5.3 Elution order of transition metal ions with different eluents on the AUA and Ionpac CS12 columns

Eluent	Elution order	
	AUA column	Ionpac CS12
HNO_3	Mn^{2+}, Co^{2+}, Ni^{2+}, Cd^{2+}, Zn^{2+} > Cu^{2+}	Mn^{2+} > Cu^{2+}, Ni^{2+}, Co^{2+}, Zn^{2+} > Cd^{2+}
Oxalic acid	Cu^{2+} > Ni^{2+} > Zn^{2+} > Co^{2+} > Mn^{2+}> Cd^{2+}	Cu^{2+} > Ni^{2+} > Zn^{2+}, Co^{2+} > Mn^{2+} > Cd^{2+}
PDCA	Cu^{2+} > Zn^{2+}, Ni^{2+} > Co^{2+}> Cd^{2+} > Mn^{2+}	Cu^{2+} > Zn^{2+}, Ni^{2+} > Co^{2+}> Cd^{2+} > Mn^{2+}
Succinic acid	Cu^{2+}, Zn^{2+}, Co^{2+} > Mn^{2+}, Cd^{2+} > Ni^{2+}	
Citric acid	Mn^{2+}, Co^{2+}, Zn^{2+} > Cd^{2+}, Ni^{2+} > Cu^{2+}	

4. Conclusions

The AUA ligand was applied as a cation-exchange site in ion chromatography for the separation of transition metal ions. The AUA column yielded good separation of six transition metal ions with a single oxalic acid eluent gradient by adjusting the pH value of the column with

HNO_3 before injecting analyte. The retention time of transition metal ions on the Ionpac CS12 column was greatly reduced by pre-equilibrating the column with 20 mM oxalic acid. Compared with the Ionpac CS12 column, the AUA column showed selectivity for Cu^{2+}, consistent with the optimal coordination environment for Cu^{2+} provided by the preorganized structure of the macrocycle. The resorcinarene class of macrocyclic ligands offers a promising scaffold to generate selective functional groups for liquid chromatographic separations.

References

1. Jackson, P. E.; Thomas, D. H.; Donovan, B.; Pohl, C. A.; Kiser, R. E. New block-grafted anion exchanger for environmental water analysis by ion chromatography. *J. Chromatogr. A* **2001**, *920*, 51-60.
2. Weiss, J.; Jensen, J. D. Modern stationary phases for ion chromatography. *Anal. Bionanal. Chem.* **2003**, *375*, 81-98.
3. Beer, P. D.; Gale, P. A. Anion recognition and sensing: the state of the art and future perspectives. *Angew. Chem. Int. Ed.* **2001**, *40*, 486-516.
4. Evans, N. H.; Rahman, H.; Davis, J. J.; Beer, P. D. Surface-attached sensors for cation and anion recognition. *Anal. Bioanal. Chem.* **2012**, *402*, 1739-1748.
5. Bruzzoniti, M. C.; De Carlo, R. M.; Fiorilli, S.; Onida, B.; Sarzanini, C. Functionalized SBA-15 mesoporous silica in ion chromatography of alkali, alkaline earths, ammonium, and transition metal ions. *J. Chromatogr. A* **2009**, *1216*, 5540-5547.
6. Michalski, R. Applications of ion chromatography for the determination of inorganic

cations. *Crit. Rev. Anal. Chem*. **2009**, *39*, 230-250.

7. Nesterenko, E. P.; Nesterenko, P. N.; Paull, B. Zwitterionic ion-exchangers in ion chromatography: A review of recent developments. *Anal. Chim. Acta* **2009**, *652*, 3-21.

8. Nesterenko, P. N.; Eleferov, A. I.; Tarasenko, D. A.; Shpigun, O. A. Selectivity of chemically bonded zwitterion-exchange stationary phases in ion chromatography. *J. Chromatogr. A* **1995**, *706*, 59-68.

9. Sugrue, E.; Nesterenko, P. N.; Paull, B. Fast ion chromatography of inorganic anions and cations on a lysine bonded porous silica monolith. *J. Chromatogr. A* **2005**, *1075*, 167-175.

10. Elefterov, A. I.; Kolpachnikova, M. G.; Nesterenko, P. N.; *Shpigun,* O. A. Ion-exchange properties of glutamic acid-bonded silica. *J. Chromatogr. A* **1997**, *769*, 179-188.

11. Hoffmann, C.V.; Pell, R.; Lämmerhofer, M.; Lindner, W. Synergistic effects on enantioselectivity of zwitterionic chiral stationary phases for separations of chiral acids, bases, and amino acids by HPLC. *Anal. Chem.* **2008**, *80*, 8780-8789.

12. Kimura, K.; Harino, H.; Hayata, E.; Shono, T. Liquid chromatography of alkali and alkaline-earth metal ions using octadecylsilanized silica columns modified in situ wirh lipophilic crown ethers. *Anal. Chem.* **1986**, *58*, 2233-2237.

13. Lamb, J. D.; Smith, R. G.; Jagodzinski, J. Anion chromatography with a crown ether-based stationary phase and an organic modifier in the eluent. *J. Chromatogr. A*, **1993**, *640*, 33-40.

14. Lamb, J. D.; Drake, P. A.; Woolley, K. E. *Advances in Ion Chromatography*, Vol. 2, Century International, eds P. Jandik, and R.M. Cassidy, Franklin, MA, 1990, pp. 215.

15. Thuaud, N.; Sébille, B.; Deratani, A.; Pöpping, B.; Pellet, C. Enantiomer separations with chromatographic supports based on β-cyclodextrin polymers immobilized on porous silica. Role of the polymer structure in separating ability. *Chromatographia* **1993**, *36*, 373-380.

16. Wang, J.; Harrison, R. G.; Lamb, J. D. Anion separation and preconcentration with cyclen and cyclen-resorcinarene derivatives. *J. Chromatogr. Sci*. **2009**, *47*, 510-515.

17. Li, N.; English, C.; Eaton; A.; Gillespie, A.; Ence, T. C.; Christensen, T. J.; Sego, A.; Harrison, R. G.; Lamb, J. D. Cation separation and preconcentration using columns containing cyclen and cyclen–resorcinarene derivatives. *J. Chromatogr. A* **2012**, *1245*, 83-89.

18. Restorp, P.; Rebek, J. Jr. Reaction of isonitriles with carboxylic acids in a cavitand: observation of elusive isoimide intermediates. *J. Am. Chem. Soc*. **2008**, *130*, 11850-11851.

19. Lamb, J. D.; Morris, C. A.; West, J. N.; K. Morris, T.; Harrison, R. G. Cation effect on anion separations by aza-crown ligands in liquid membranes. *J. Membr. Sci.* **2008**, *321*, 15-21.

20. Jensen, D.; Weiss, J.; Rey, M. A.; Pohl, C. A. Novel weak acid cation-exchange column. *J. Chromatogr. A* **1993**, *640*, 65-71.

21. Gros, N.; Gorenc, B. On chromatographic determination of alkali and alkaline earth metals in mineral waters. *Chromatographia* **1994**, *39*, 448-452.

22. Dionex technical note 10, Determination of transition metals by ion chromatography. Doc. #4691-tn10, Dionex, Sunnyvale, CA, USA.

23. Li, N.; Yang, F.; Stock, H. A.; Dearden, D. V.; Lamb, J. D.; Harrison, R. G. Resorcinarene-based cavitands with chiral amino acid substituents for chiral amine recognition. *Org. Biomol. Chem*. **2012**, *10*, 7392-7401.

24. Jones. P. Major sensitivity improvements in ion chromatography determinations involving post-column spectrophotometric reaction detectors through elimination of pump noise using a dual wavelength monitoring procedure. *Analyst* **2000**, *125*, 803-806.

25. Sillén, L.G.; Martell, A. E. Stability Constants of Metal-ion Complexes, Special Publication No 25, Burlington House, London, 1971.

26. Martell, A. E.; Smith, R. M. Critical stability constants, Plenum press, New York and London, 1974.

Chapter 6 Summary and Perspective

Several resorcinarene-based macrocyclic ligands were designed and synthesized in my research. 2D-NMR, SORI-CID in FTICR-MS, and dynamic light scattering techniques were combined to explore the structure of AUA ligand. The results indicated that AUA has a kite-like structure around the resorcinarene scaffold and that it associates to eight water molecules. Therefore, host-guest interactions were not observed between AUA and the series of amine guests investigated. However, the ^{1}H NMR titration experiments indicated that AUA can bind amine guests through hydrogen bonding. Furthermore, the chiral AUA ligand demonstrated discrimination for chiral secondary amines (S and R-N, α-dimethyl benzyl amine). The factors that affect the binding strength between amines and AUA, including solvent, host and guest molecular size, substituent type, number, and position were investigated. Two ligands, AUA and cyclenbowl, were synthesized and characterized. In addition, they were used as ion-exchangers in ion chromatography for transition metal ion separations. Both columns demonstrated selectivity for Cu^{2+} ion. Preconcentration of Cu^{2+} in parts per billion levels from a high concentration matrix of Mn^{2+}, Co^{2+}, Ni^{2+}, Cd^{2+}, and Zn^{2+} ions was achieved with the cyclenbowl-based column using HNO_3 eluent. Recovery of Cu^{2+} at >98% was obtained. The selectivity of the AUA-based column for Cu^{2+} was not observed in a comparison column containing similar cation-exchangers.

Based on the experimental results that I have obtained, I propose several future research projects which build on these results:

1. Although the AUA ligand had a kite-like structure, the esters AME, AUE, and GUE had well resolved ^{1}H NMR spectra and the H_a protons showed downfield chemical shifts, indicating that these esters have well-defined vase-like structures in solution. It should be possible to introduce small molecules into their hydrophobic cavities. A previous result from Rebek's group[1] showed that the reactivity of small molecules increases when they are locked in a small cavity. The resorcinarene esters should be tested as nanoscale reaction containers.

2. The overcrowding of polar amino acid groups would be one reason for the kite-structure of AUA. Instead of anchoring four substituent groups on the upper rim of resorcinarene, two or three substituent groups on the upper rim should reduce crowding. Recently, a German research group[2] published a paper along these lines, but with different functional groups on the upper rim.

3. In Chapter 2, we reviewed the application of resorcinarenes as pseudo-stationary phases in capillary electrophoresis. The synthesized resorcinarene derivatives in my project could be used in CE to separate neutral species.

4. The AUA column contains chiral alanine groups on the upper rim which provides this molecule stereoselectivity for chiral analytes; therefore, the AUA column should be tested to separate chiral amino acids.

References:

1. Tucci, F. C.; Renslo, A. R.; Rudkevich, D. M.; Rebek, J. Jr. Nanoscale container structures and their host-guest properties. *Angew. Chem. Int. Ed.* **2000**, *39*, 1076-1079.
2. Pochorovski, I.; Boudon, C.; Gisselbrecht, J.; Ebert, M.; Schweizer, W. B.; Diederich, F. Quinone-based, redox-active resorcin[4]arene cavitands. *Angew. Chem. Int. Ed.* **2012**, *51*, 262-266.

Appendix

1. Crystal structure of 5,6-dichloropyrazine-2,3-dicarboxylic acid

All single crystal X-ray experiments were performed on a Bruker FR-591 Dual Source Low Temperature X-ray Diffractometer at 296(2) K. The single crystal structure was solved by direct methods using SHELXS-97. The crystal was obtained by slow evaporation of ethyl acetate solution. The crystal data and structure refinement details for the complex are given in Table 1. Table 2 shows the selected bond lengths /Å and bond angles /º of 5,6-dichloropyrazine-2,3-dicarboxylic acid. The molecular and crystal structure of 5,6-dichloropyrazine-2,3-dicarboxylic acid are shown in Figure 1(a) and (b). Figure 2 shows the three dimensional structure of 5,6-dichloropyrazine-2,3-dicarboxylic acid.

(a)

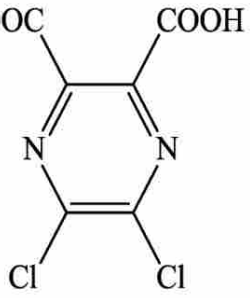

$.H_2O$

Chemical Formula: $C_6H_4Cl_2N_2O_5$

(b)

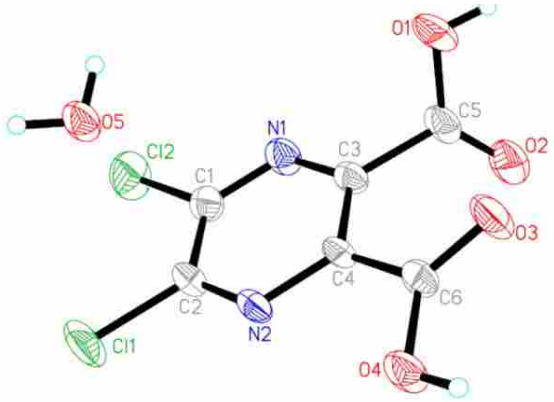

Figure 1 (a) Molecular structure and (b) Crystal structure of 5,6-dichloropyrazine-2,3-dicarboxylic acid.

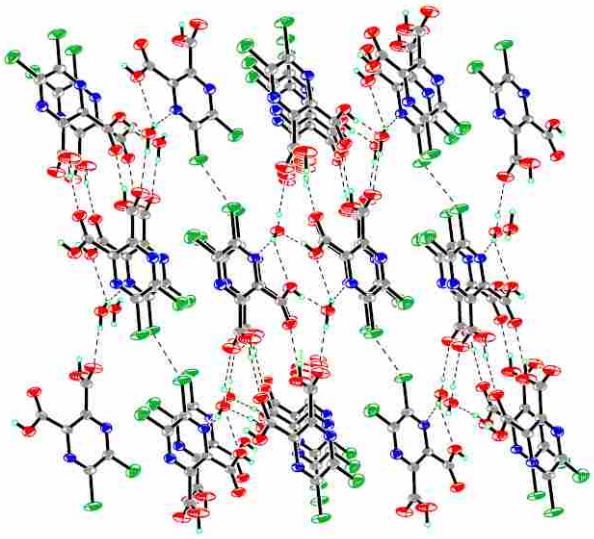

Figure 2 Three dimensional structure of 5,6-dichloropyrazine-2,3-dicarboxylic acid.

Table 1 Crystallographic data for 5,6-dichloropyrazine-2,3-dicarboxylic acid

Empirical formula	$C_2H_{1.33}Cl_{0.67}N_{0.67}O_{1.67}$
Formula weight	85.00
Crystal system, space group	Triclinic, P-1
a (nm)	5.412(2)
b (nm)	8.958(4)
c (nm)	10.906(4)
α(°)	103.179(4)
β(°)	99.397(5)
γ(°)	106.457(5)
V (nm)	478.9(3)
Z	6
D_c (mg.m^{-3})	1.769
F (0 0 0)	256
Absorption coefficient (mm^{-1})	0.681
Limiting indices	$-4 \le h \le 6$, $-10 \le k \le 10$, $-12 \le l \le 12$
Goodness-of-fit on F^2	1.086
R (int)	0.0489
R1, wR2($I>2\sigma$ *(I)*)	0.0355, 0.0903
R1, wR2 (all data)	0.0464, 0.0949
$\Delta\rho_{max}$ and $\Delta\rho_{min}$ (e·nm^{-3})	0.282, -0.216

Table 2 Selected bond lengths /Å and bond angles /º of 5,6-dichloropyrazine-2,3-dicarboxylic acid

Bond	Bond length (Å)	Bond	Bond angle (º)
C(1)-C(2)	1.713(2)	C(2)-N(2)-C(4)	118.10(16)
N(2)-C(2)	1.308(3)	C(1)-N(1)-C(3)	117.70(17)
N(2)-C(4)	1.347(2)	O(3)-C(6)-O(4)	125.76(18)
N(1)-C(1)	1.308(3)	O(3)-C(6)-C(4)	121.01(17)
N(1)-C(3)	1.338(3)	O(4)-C(6)-C(4)	113.19(15)
C(6)-O(3)	1.211(2)	O(2)-C(5)-O(1)	126.28(19)
C(6)-O(4)	1.298(2)	O(2)-C(5)-C(3)	121.7(2)
C(6)-C(4)	1.496(3)	O(1)-C(5)-C(3)	111.97(19)
C(5)-O(2)	1.192(3)	N(1)-C(3)-C(4)	121.34(16)
C(5)-O(1)	1.306(3)	N(1)-C(3)-C(5)	114.90(16)
C(5)-C(3)	1.511(3)	C(4)-C(3)-C(5)	123.63(17)
C(3)-C(4)	1.391(3)	N(2)-C(4)-C(3)	120.22(17)
		C(1)-C(2)-Cl(1)	121.19(16)
		N(2)-C(4)-C(6)	117.35(15)
		C(3)-C(4)-C(6)	122.36(16)
		N(2)-C(2)-C(1)	121.13(17)
		N(1)-C(1)-Cl(2)	117.58(15)
		C(2)-C(1)-Cl(2)	120.96(15)
		N(1)-C(1)-C(2)	121.46(18)

2. Crystal structure of triethylammonium chloride

All single crystal X-ray experiments were performed on a Bruker FR-591 Dual Source Low Temperature X-ray Diffractometer at 296(2) K. The single crystal structure was solved by direct methods using SHELXS-97. The crystal was obtained by slow evaporation of water-methanol solution. The crystal data and structure refinement details for the complex are given in Table 3. Table 4 shows the selected bond lengths /Å and bond angles /º of triethylammonium

chloride. The molecular and crystal structure of triethylammonium chloride are shown in Figure 3(a) and (b). Figure 4 shows the three dimensional structure of triethylammonium chloride.

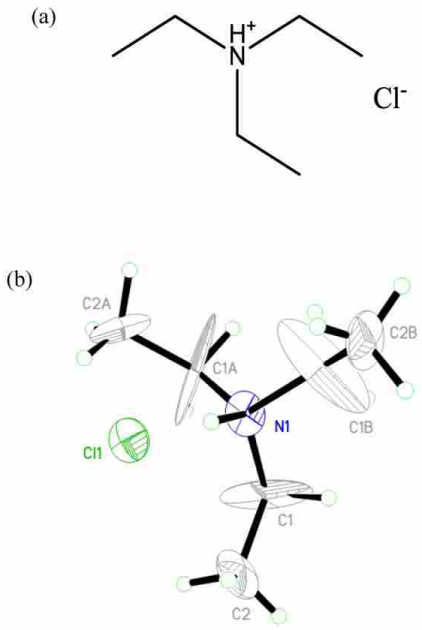

Figure 3 (a) Molecular structure and (b) Crystal structure of triethylammonium chloride.

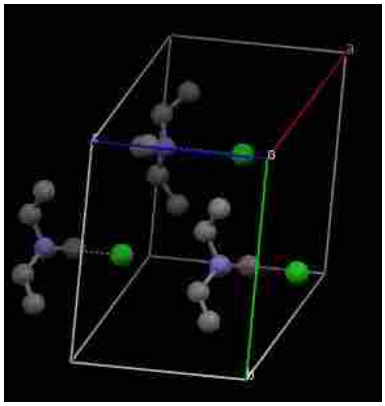

Figure 4 Two triethylammonium chloride molecules in one lattice

Table 3 Crystallographic data for triethylammonium chloride

Empirical formula	$C_6H_{16}Cl_1N_1$
Formula weight	137.65
Crystal system, space group	Trigonal, P31c
a (nm)	8.3565(2)
b (nm)	8.3565(2)
c (nm)	7.0769(4)
α(°)	90
β(°)	90
γ(°)	120
V (nm)	427.98(3)
Z	2
D_c (mg.m^{-3})	1.068
F (0 0 0)	152
Absorption coefficient (mm^{-1})	0.681
Limiting indices	$-4\leq h\leq 4$, $-4\leq k\leq 4$, $-3\leq l\leq 4$
Goodness-of-fit on F^2	1.321
R (int)	0.0308
R1, wR2($I>2\sigma(I)$)	0.0139, 0.0334
R1, wR2 (all data)	0.0193, 0.0350
$\Delta\rho_{max}$ and $\Delta\rho_{min}$ (e·nm^{-3})	0.031, -0.031

Table 4 Selected bond lengths /Å and bond angles /º of triethylammonium chloride

Bond	Bond length (Å)	Bond	Bond angle (º)
N(1)-C(1)	1.41(4)	C(1)-N(1)-C(1)$^{\#1}$	109(3)
N(1)-H(1)	1.0(4)	H(1A)-C(1)-H(1B)	106.1
C(1)-C(2)	1.358(1)	C(1)-N(1)-H(1)	110(3)
C(1)-H(1A)	0.9700	C(2)-C(1)-N(1)	127(4)
		C(1)-C(2)-H(2A)	109.5

3. Characterization of AME, AMNa, and AMA

The NMR and MS experimental conditions are shown in Chapter 3.

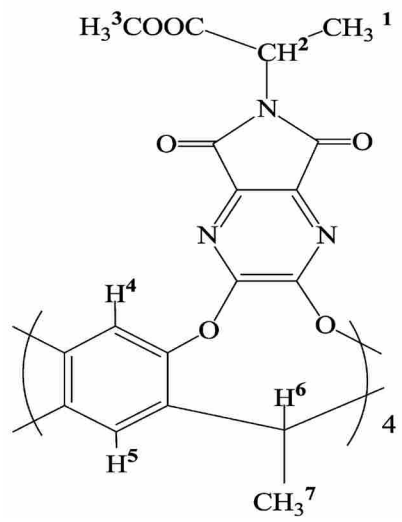

Figure 5 The structure of AME.

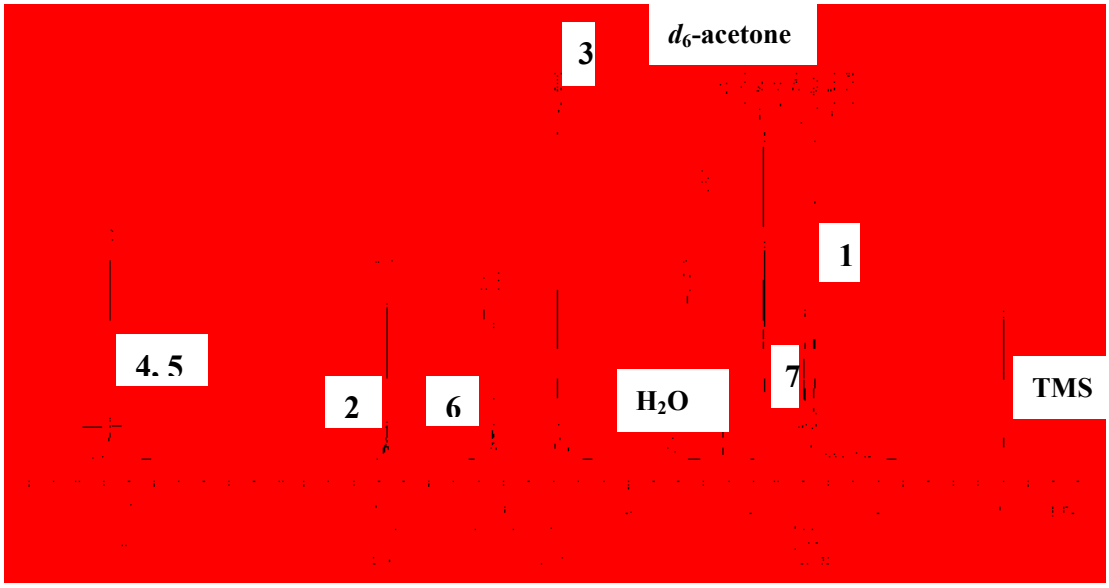

Figure 6 ^{1}H NMR structure of AME in d_6-acetone (peak labels refer protons in Figure 5).

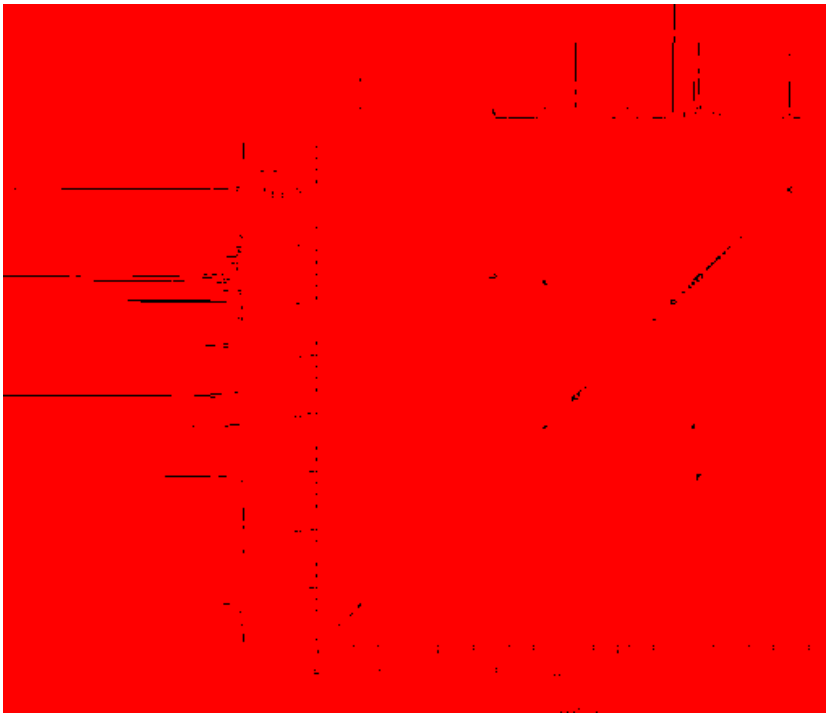

Figure 7 2D COSY of AME in d_6-acetone.

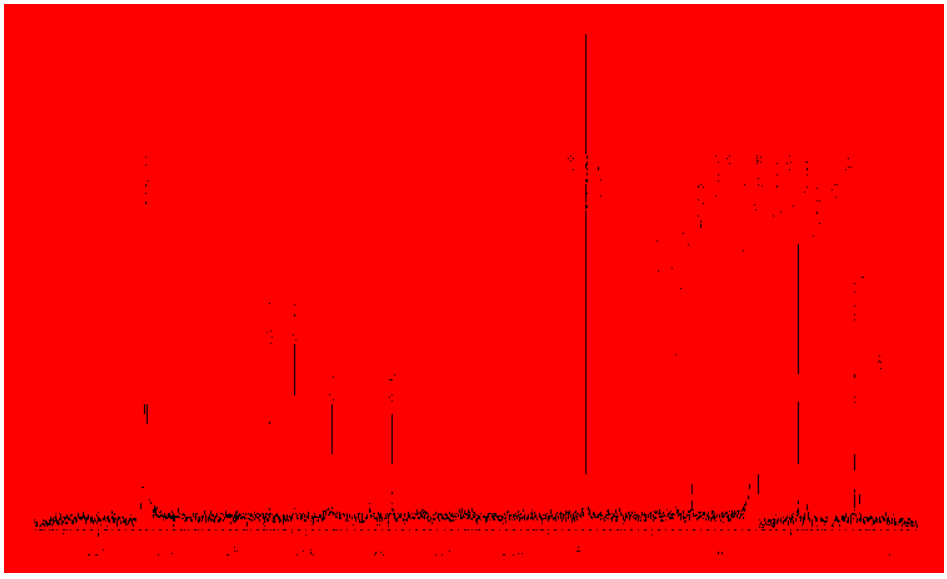

Figure 8 ^{13}C NMR of AME in d_6-acetone.

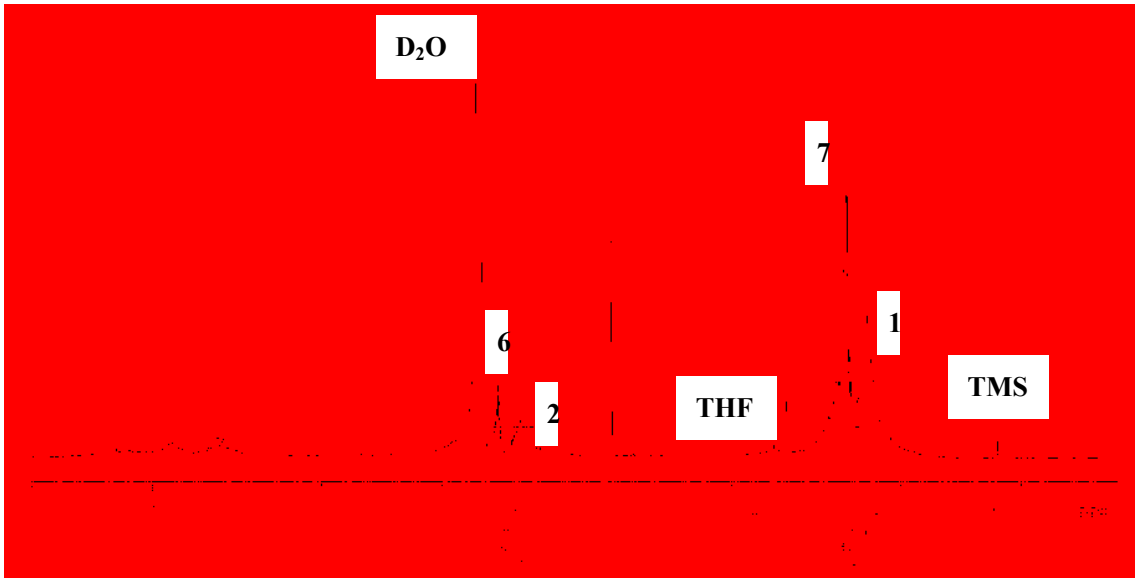

Figure 9 ^{1}H NMR spectrum of AMNa in D_2O at 60 ^{o}C (peak labels refer protons in Figure 5).

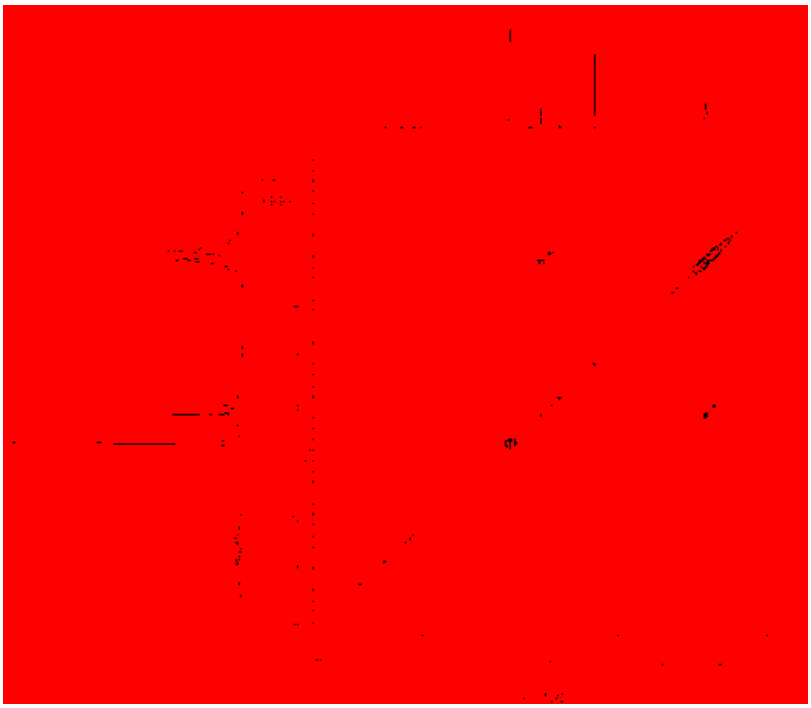

Figure 10 2D COSY of AMNa in D_2O.

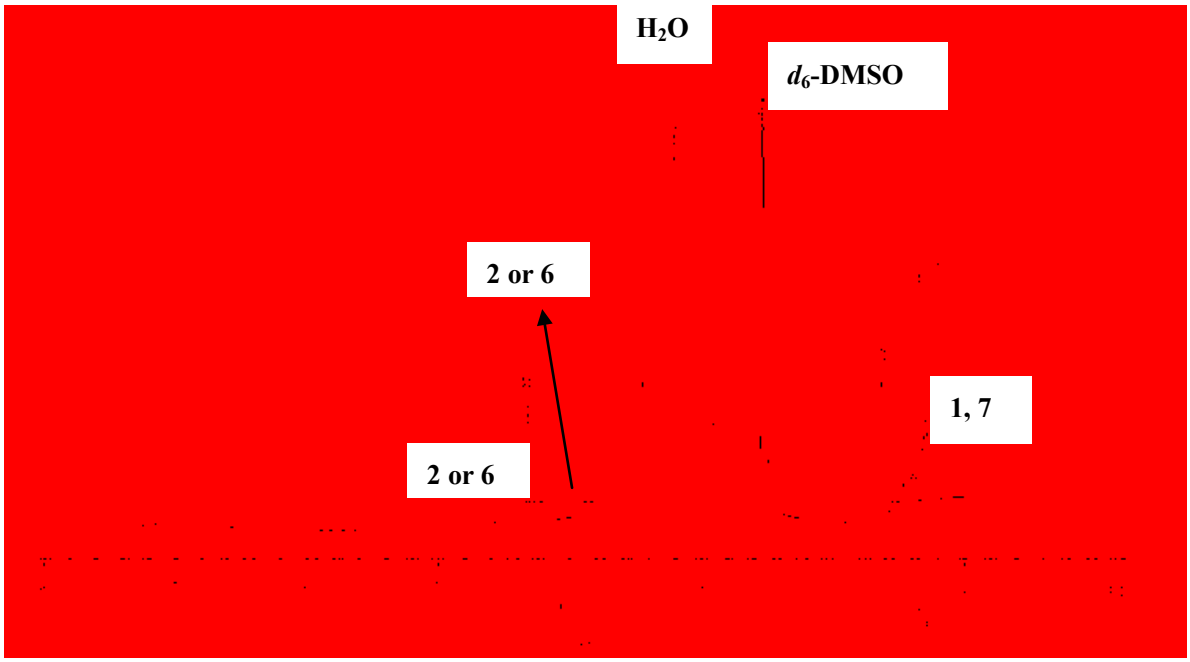

Figure 11 ^{1}H NMR spectrum of AMA in d_6-DMSO at 80 ^{o}C (peak labels refer protons in Figure 5).

Figure 12 2D COSY of AMA in d_6-DMSO.

4. Characterization of GUE, GUNa, and GUA

The NMR and MS experimental conditions are shown in Chapter 3.

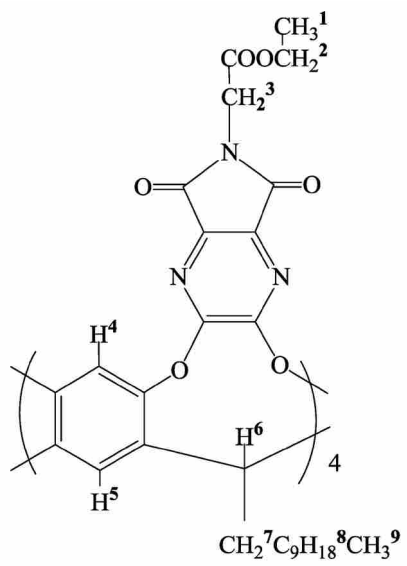

Figure 13 The structure of GUE.

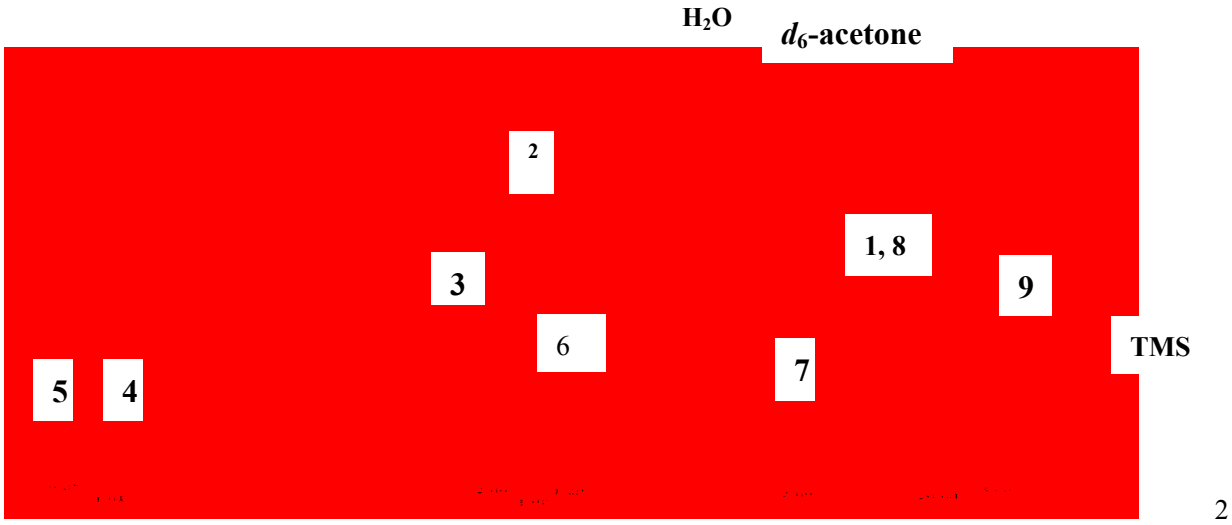

Figure 14 ^{1}H NMR structure of GUE in d_6-acetone (peak labels refer protons in Figure 13).

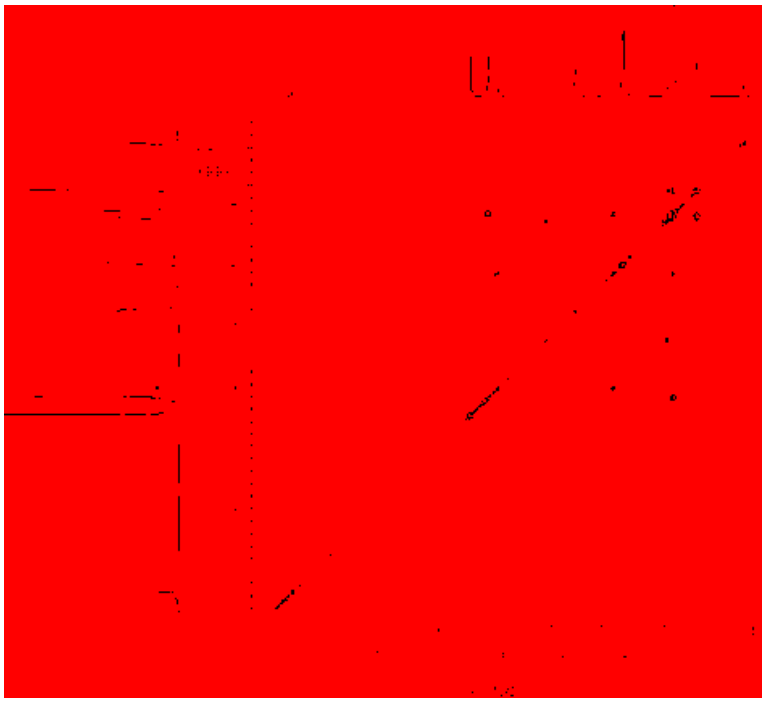

Figure 15 2D COSY of GUE in d_6-acetone.

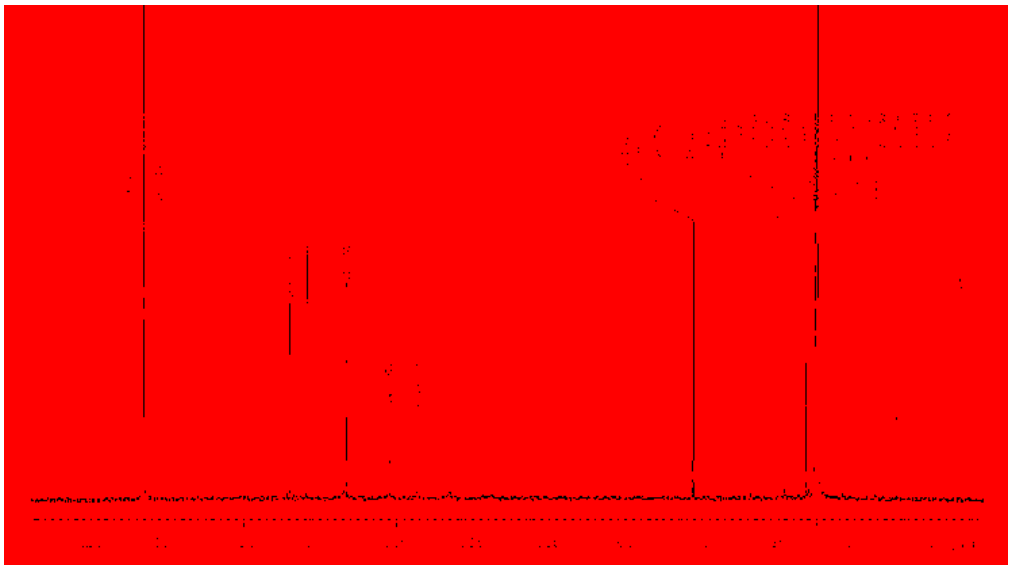

Figure 16 ^{13}C NMR of GUE in d_6-acetone.

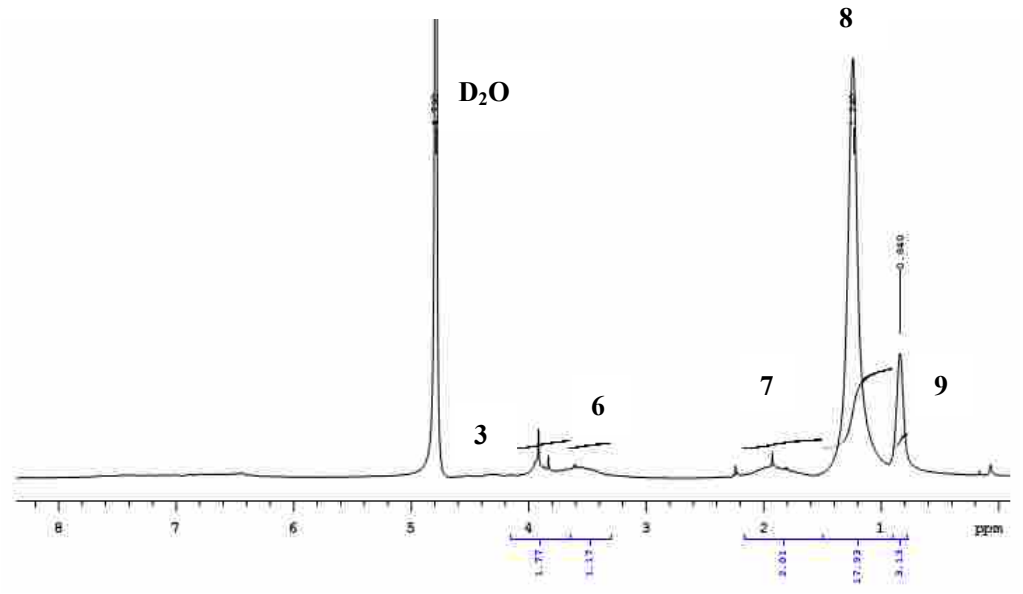

Figure 17 ^{1}H NMR of GUBNa in D_2O (peak labels refer protons in Figure 13).

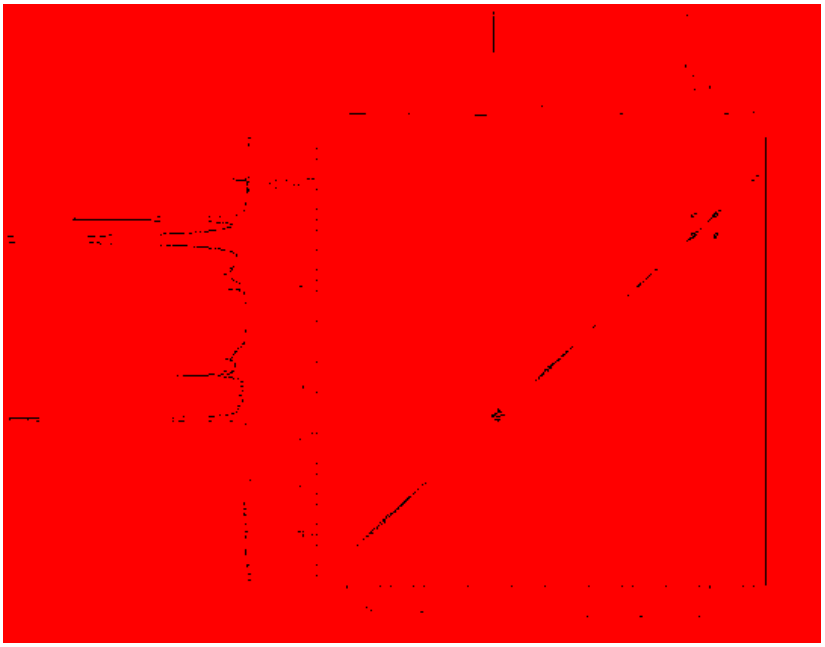

Figure 18 2D COSY of GUNa in D_2O.

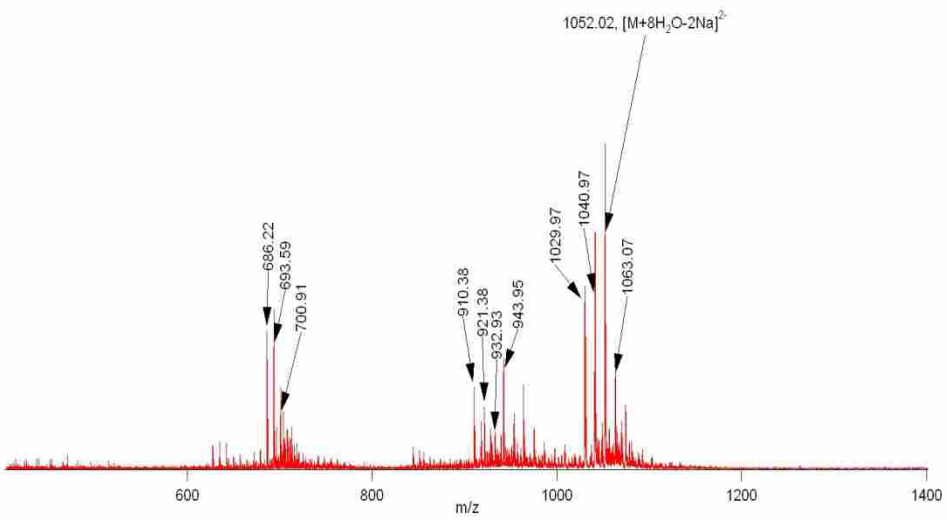

Figure 19 FTICR-MS of GUNa (M = GUNa). M = GUNa; $[M+8H_2O-2Na]^{2-}$ = 1052.02 (calculated: 1052.07); $[M+8H_2O-Na-H]^{2-}$ = 1063.06; $[M+8H_2O-3Na+H]^{2-}$ =1040.97; $[M+8H_2O-4Na+2H]^{2-}$ =1029.97; $[M+8H_2O-3Na-1Arm+H]^{2-}$ =1040.97; $[M+8H_2O-2Na-1Arm]^{2-}$ = 921.38; $[M+8H_2O-Na-1Arm-H]^{2-}$ = 932.93; $[M+8H_2O-1Arm-2H]^{2-}$ = 943.95; $[M+8H_2O-3Na-1Arm+H]^{2-}$ = 910.38; $[M+8H_2O-3Na]^{3-}$ = 693.68; $[M+8H_2O-4Na+H]^{3-}$ =1686.22; $[M+8H_2O-2Na-H]^{3-}$ = 700.91.

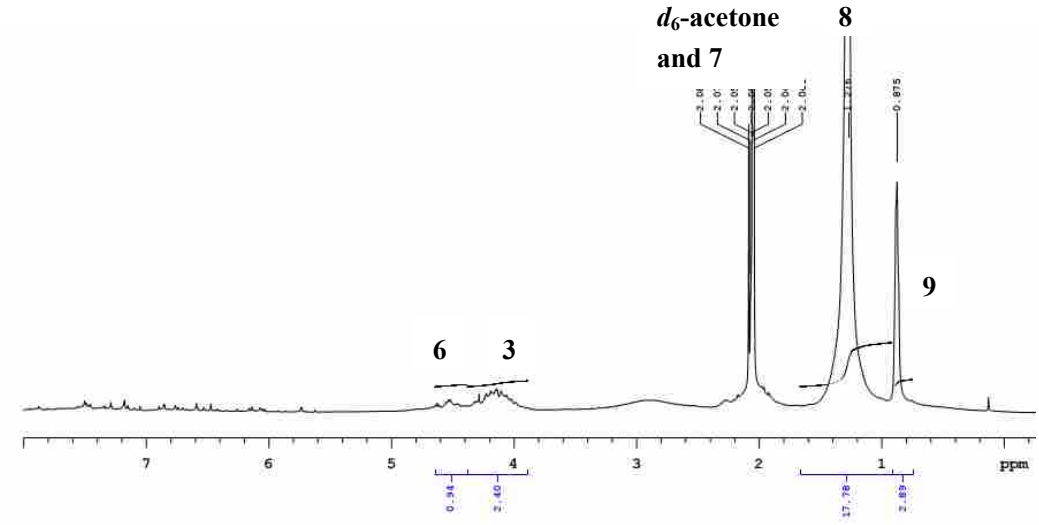

Figure 20 ^{1}H NMR of GUA in d_6-acetone (peak labels refer protons in Figure 13).

Figure 21 2D COSY of GUA in d_6-acetone.

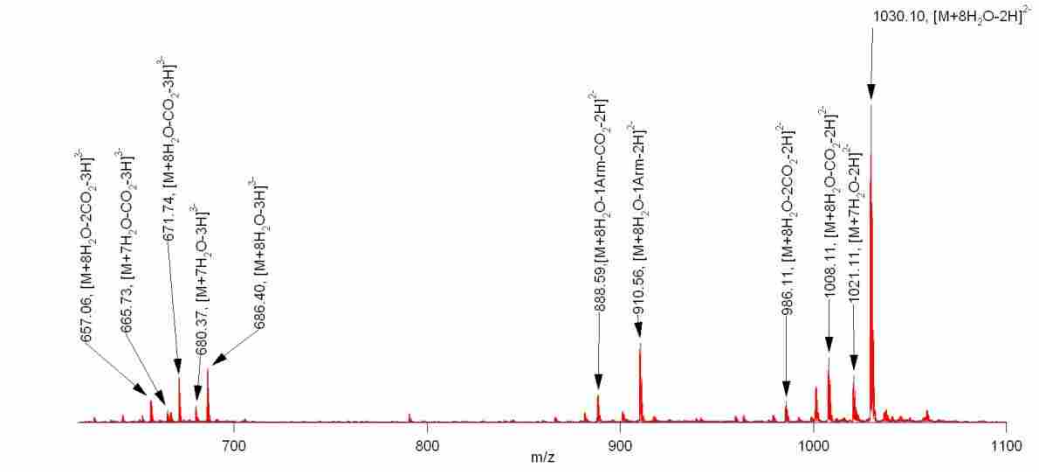

Figure 22 FTICR-MS of GUA (M=GUA).

5. Characterization of AUE, AUNa, and AUA.

The NMR and MS experimental conditions are shown in Chapter 3.

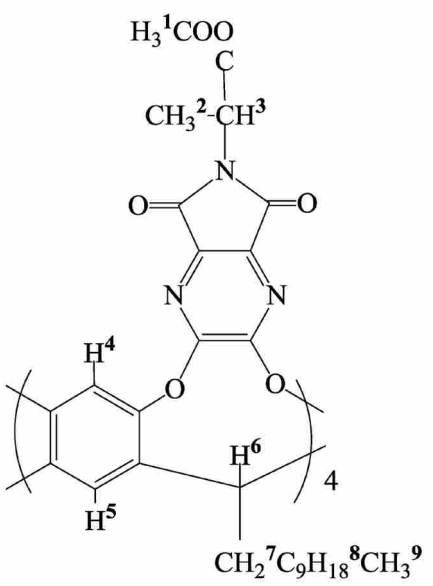

Figure 23 The structure of AUA.

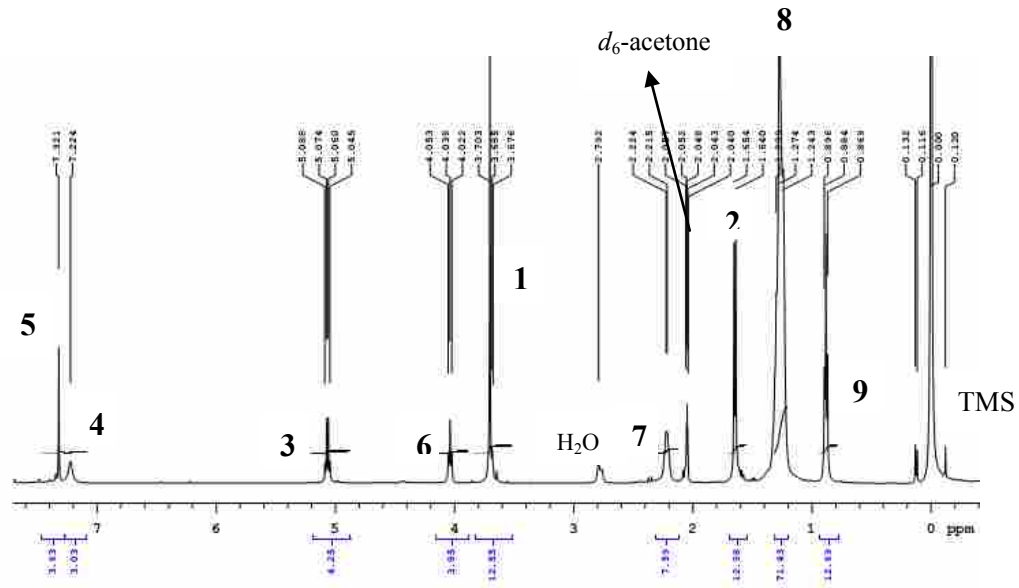

Figure 24 ^{1}H NMR of AUE in d_6-acetone (peak labels refer protons in Figure 23).

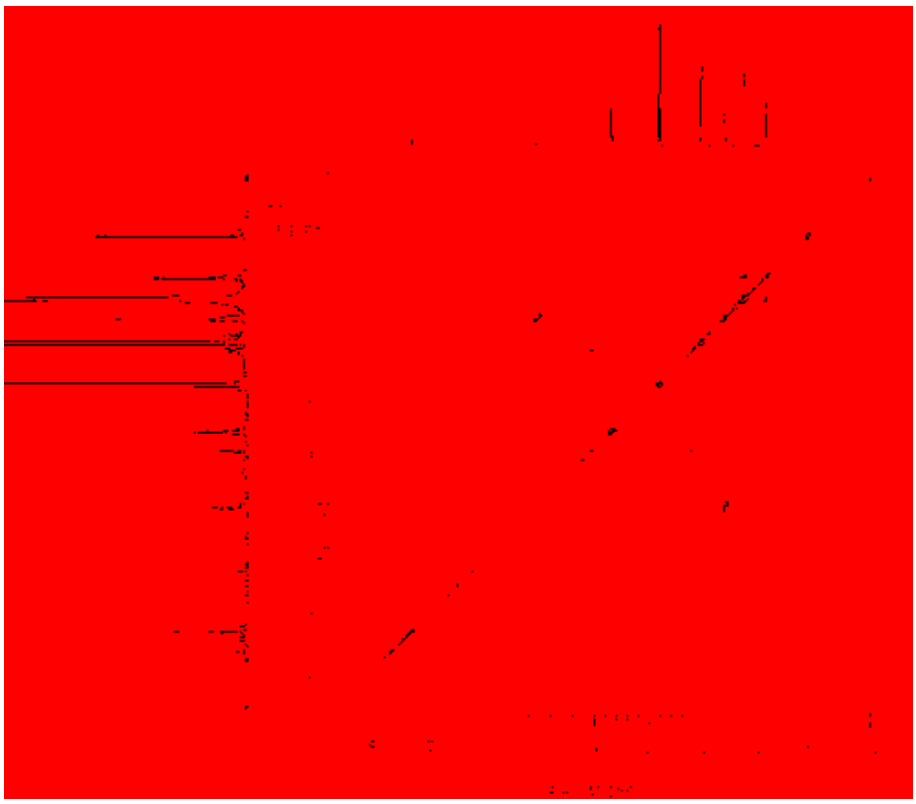

Figure 25 2D COSY of AUE in d_6-acetone.

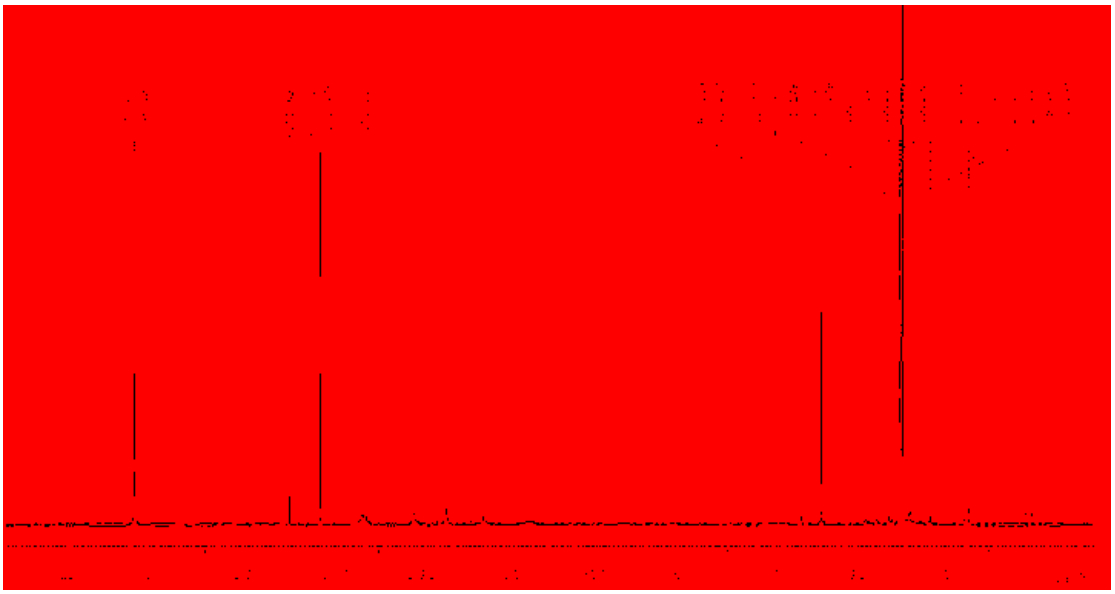

Figure 26 ^{13}C NMR of AUE in d_6-acetone.

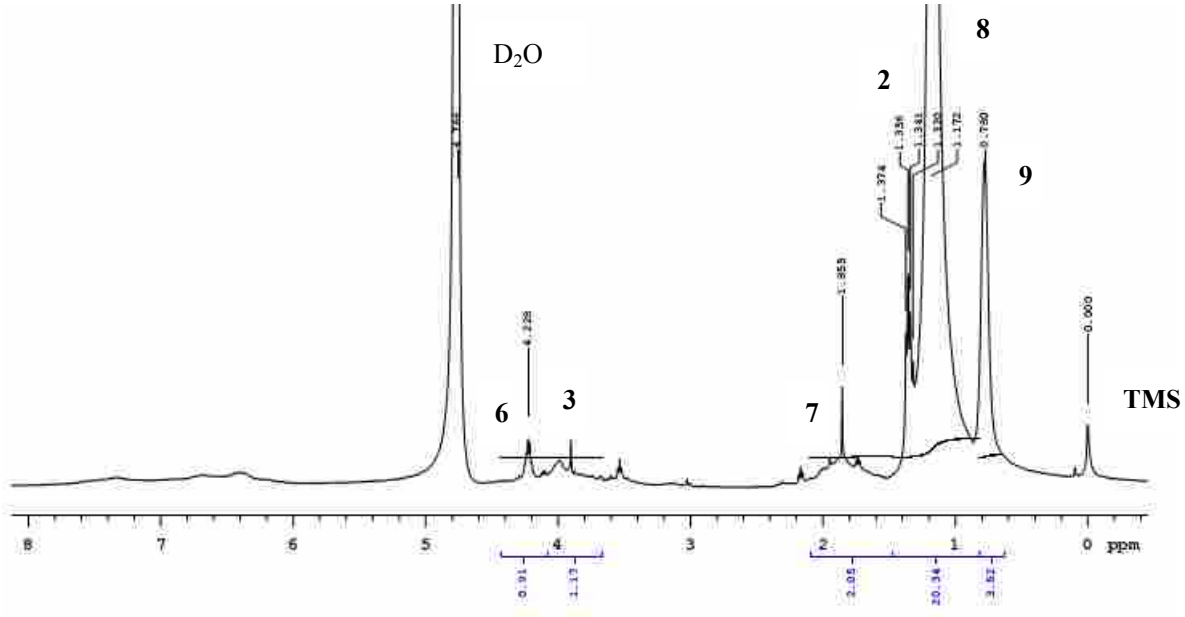

Figure 27 ^{1}H NMR of AUNa in D_2O (peak labels refer protons in Figure 23).

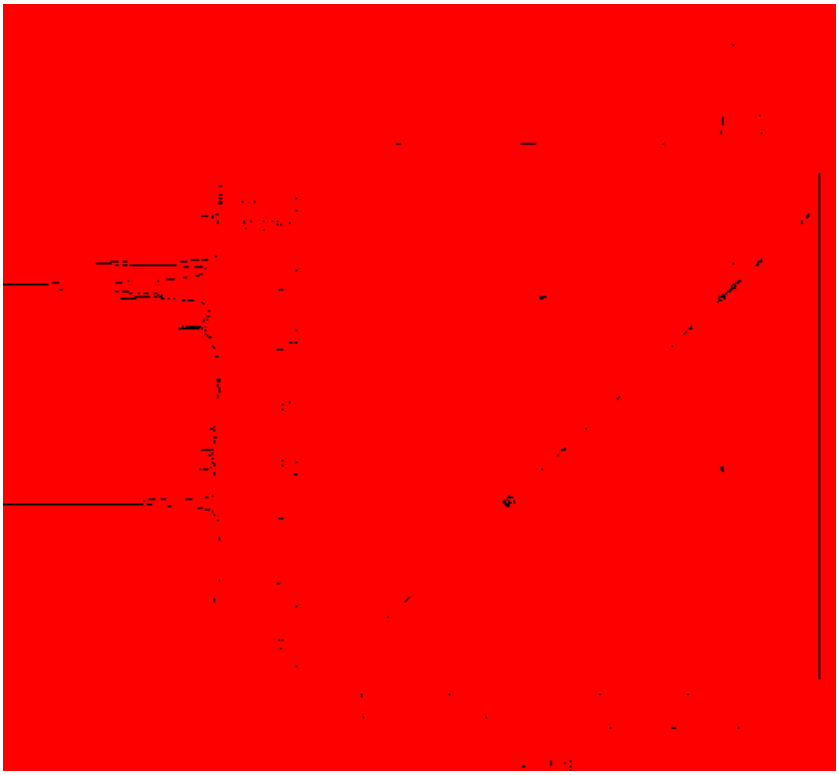

Figure 28 2D COSY AUNa in D_2O.

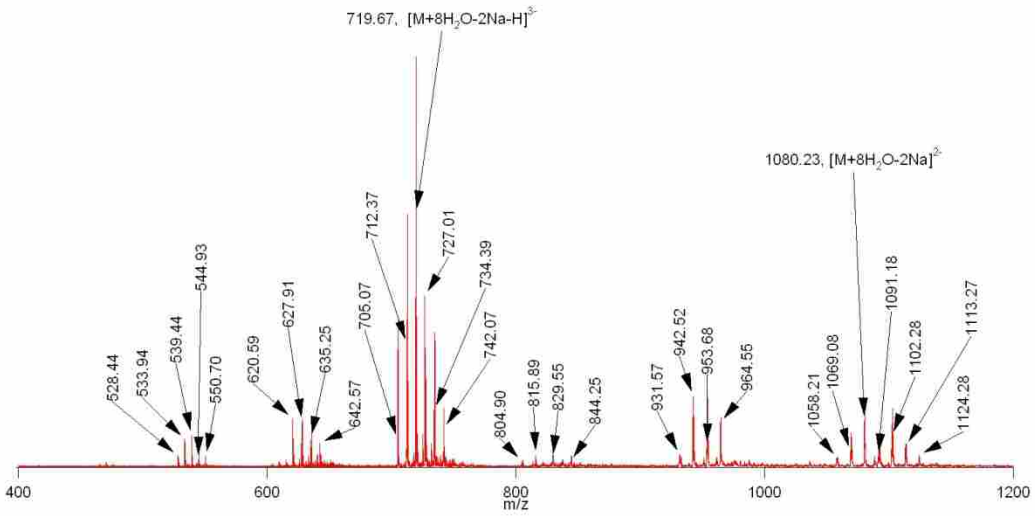

Figure 29 FTICR-MS of AUNa (M = AUNa). $[M+8H_2O-2Na-H]^{3-}$ = 719.67 (Calculated: 719.77); $[M+8H_2O-Na-2H]^{3-}$ = 727.01; $[M+8H_2O-3H]^{3-}$ = 743.39; $[M+8H_2O-3Na]^{3-}$ = 712.37; $[M+8H_2O-3Na]^{3-}$ = 712.37; $[M+8H_2O-4Na]^{4-}$ = 528.44; $[M+8H_2O-3Na-H]^{4-}$ = 533.94; $[M+8H_2O-2Na-2H]^{4-}$ = 539.44; $[M+8H_2O-1Na-3H]^{4-}$ = 544.93; $[M+8H_2O-4H]^{4-}$ = 550.70; $[M+8H_2O-2Na]^{2-}$ = 1080.23; $[M+8H_2O-Na-H]^{2-}$ = 1091.18; $[M+8H_2O-2H]^{2-}$ = 1102.28; $[M+8H_2O+Na-3H]^{2-}$ =113.27; $[M+8H_2O-2Na-1Arm]^{2-}$ = 942.52; $[M+8H_2O-Na-1Arm-H]^{2-}$ =953.68; $[M+8H_2O-2Na-2Arm]^{2-}$ = 804.90; $[M+8H_2O-Na-2Arm-H]^{2-}$ = 815.89; these peaks around 627.91 are the -3 peaks of -2 peaks around 942.52.

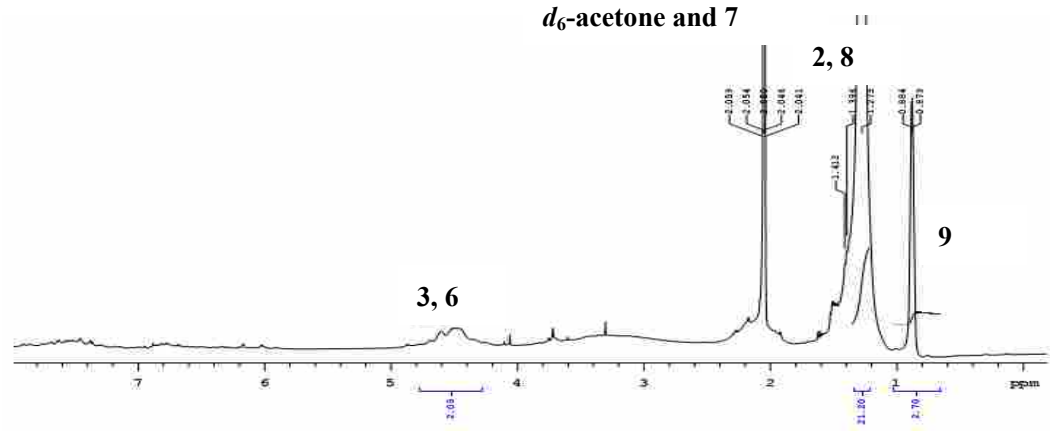

Figure 30 ^{1}H NMR of AUA in d_6-acetone (peak labels refer protons in Figure 23).

Figure 31 2D COSY of AUA in d_6-acetone.

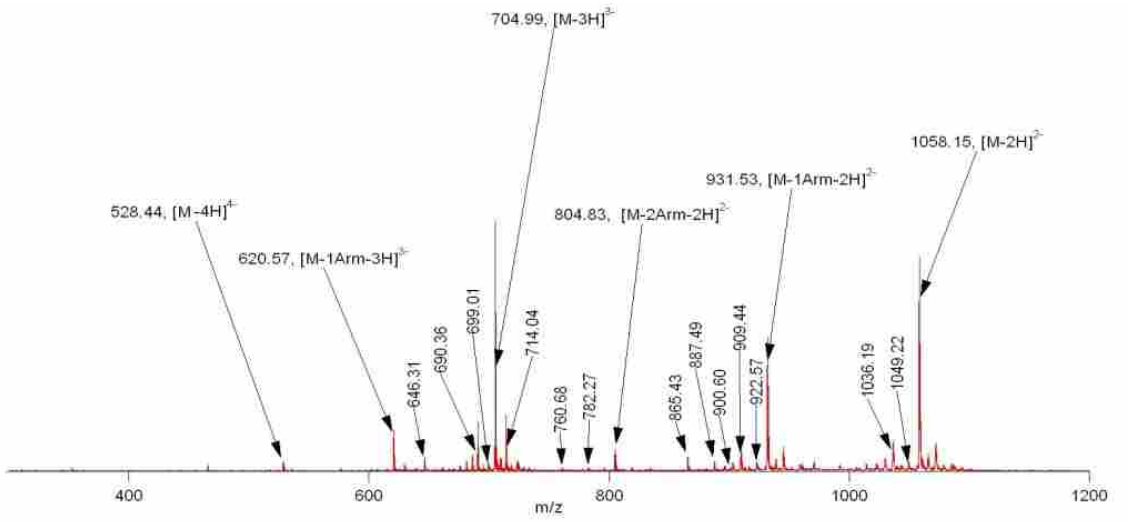

Figure 32 FTICR-MS of AUA (M = AUA+8H_2O). $[M-3H]^{3-}$=704.99 (Calculated: 705.11). $[M-2H-H_2O]^{2-}$ = 1049.22; $[M-2H-CO_2]^{2-}$ = 1036.19; $[M-2H-1Arm-H_2O]^{2-}$ = 922.57; $[M-2H-1Arm-CO_2]^{2-}$ = 909.44; $[M-2H-1Arm-CO_2-H_2O]^{2-}$ = 900.60; $[M-2H-1Arm-2CO_2]^{2-}$ = 987.49; $[M-2H-1Arm-3CO_2]^{2-}$ = 965.43; $[M-2Arm-2H]^{2-}$ = 804.83; $[M-2Arm-2H-CO_2]^{2-}$ = 782.27; $[M-2Arm-2H-2CO_2]^{2-}$ = 760.68; $[M-3H-H_2O]^{3-}$ =699.01; $[M-3H-CO_2]^{3-}$ =690.36; $[M-3H-4CO_2]^{3-}$ =646.31; $[M-3H-1Arm]^{3-}$ =620.57; $[M-4H]^{4-}$ =528.44.